Homo- and heterometallic metal atomic strings

Joona Sahamies

Summary

This thesis concerns about metallophilic interaction in general and especially in metal atomic strings. The theoretical part of this thesis presents the definition, properties and applications of metallopolymers and its subclass extended metal atom chains (EMACs). The concept of metallophilic interaction is discussed. Unclarity between an interaction and a bond is also dissected. Critical view to tabulated values of van der Waals and covalent radii are discussed and emphasized that atoms are not spheres. More advances models like pixel and bond path methods to describe interaction are presented. Classification of EMACs with literature examples is also presented.

Homo- and especially heterometallic EMACs were attempted to crystallize in the experimental part using group 11 metal salts, pyridine-4(1H)-thione (s-pyH) as ambidentate ligand and other metal salts. One heterometallic EMAC, **1**, was been able to crystallize. It was $[Cu_2(s\text{-}pyH)_4]_n^{2n+}$ with n $[ZnCl_4]^{2-}$ counter anions. The metal atom string is pseudolinear. Coordination geometry of copper was twisted tetrahedral. The copper–copper distances were 2.6241(6) and 2.6283(6) Å. Cu–Cu–Cu angles are 156.667(18)° and 157.424(19)°.

Preface

This work containing theoretical and experimental part is performed in University of Jyväskylä. The project is part of research of metallophilic interactions of extended metal atom chains of Doctoral Student Kalle Machal and Professor Matti Haukka. Scientific articles and some of reference books are mainly found using SciFinder® database. Articles are found to lesser extend online portal WebCSD v1.1.1 of Cambridge Crystallographic Data Center. Some books are found using search tool of library of university of Jyväskylä. The theoretical part has been started in September 2014. The experimental part is performed January 2015 to May 2015.

I would like to thank especially my supervisors Kalle Machal and Matti Haukka but also Elina Sievänen who measured solid state NMR for a sample and Elina Hautakangas who measured elemental analysis for my compounds.

I also would like to thank my family and friends who have supported me and given useful advice for my thesis.

In Jyväskylä 7.3.2016

Joona Sahamies

iii

Table of contents

Abbreviations

- ALD   Atomic layer deposition
- ANO-RCC   Atomic natural orbital–relativistic correlation consistent
- AVTZ   Augmented correlation-consistent valence-triple-zeta
- BCP   Bond critical point
- BSSE   Basic set superposition error
- CC   Coupled cluster
- CCSD   Coupled cluster with single and double excitations
- CCSD(T)   Coupled cluster with single and double and perturbative triple excitations
- CN   Coordination number
- CPC   Counterpoise correction
- CSD   Cambridge structural data base
- DCAPS   Dispersion-corrected atom-centered potentials
- DFT   Density functional theory
- DMSO   Dimethyl sulfoxide
- DZP   Double-zeta plus polarization
- E_{int} Interaction energy
- EMAC   Extended metal atom chain
- HF   Hartree-Fock
- LCAO   Linear combination of atomic orbitals
- LC-ωPBE   Long range corrected hybrid of Perdew-Burke-Ernzerhof exchange functional
- LMO   Localized molecular orbital
- LMP2   Local second-order Møller-Plesset perturbation theory
- MC(HF)   Multiconfiguration (Hartree-Fock)
- MIC   Minimum inhibitory concentration
- MP2   Second-order Møller-Plesset perturbation theory
- MBO   Mayer bond order
- NHC   *N*-heterocyclic carbene
- PBE0   A hybrid function, PBE stands for Perdew, Burke and Ernzerhof
- SCDS   Semiclassical density sums
- SIS   Sequential infiltration synthesis
- SRR   Split-ring resonator
- QCISD   Quadratic configuration interaction with single and double excitation excitations
- vdW-DF   Nonlocal van der Waals functional
- VDZP   Valence double-zeta plus polarization
- XDM   Exchange-hole dipole moment

- XRD   X-ray diffraction
- XRPD   X-ray powder diffraction

- 2,2'-bpy   2,2'-bipyridine
- Clterpy   4′-chloro-2,2′:6′,2″-terpyridine
- dpa   anion of *syn,syn*-di-2-pyridylamine i.e. *N*-(2-Pyridinyl)-2-pyridinamine
- dppe   1,2-bis(diphenylphosphano)ethane
- dppy   1,2-bis(di-3-pyridylphosphano)ethane
- h.s.   high spin
- H_2bim   2,2'-biimidazole
- Et   ethyl
- Et_2O diethyl ether
- l.s.   low spin
- Me   methyl
- Me_2bim   1,1'-dimethyl-2,2'-biimidazole
- mes   mesityl i.e. 1,3,5-trimethylfenyl
- ox   oxalate i.e. $(COO)_2^{2-}$.
- *o*-xylylNC   2-isocyano-1,3-dimethylbenzene
- i-mnts   1,1-dicyanoethene-2,2-thioselenolate i.e. $SSeC=C(CN)_2$
- im(CH_2py)$_2$ bis(pyridin-2-ylmethyl)-2,3-dihydro-1*H*-imidazole
- phen   1,10-phenanthroline
- *p*-tolyl-NNNNN-*p*-tolyl   (1*E*,4*E*)-1,5-di-*p*-tolylpentaaza-1,4-dien-3-ide
- pz   anion of pyrazole
- py   pyridine
- solv   unknown solvent
- s-pyH   pyridine-4(1*H*)-thione
- s-py   deprotonated pyridine-4(1*H*)-thione
- py-ss-py   4-(pyridin-4-yldisulfanyl)pyridine
- tpda   tripyridyldiamido dianion

Theoretical part

1 Introduction

This theoretical part concentrates on metallopolymers and metal strings of Cu, Ag, Au, Ru and Rh. However, a few examples of other metals and heterometallic compounds of Cu, Ag, Au, Ru and/or Rh with other metals are discussed in lesser extent. Classification and applications of metallopolymers and extended metal atom chains, (EMAC)s, are presented first. Some examples of lanthanide and metallocene metallopolymers are presented also. It's followed by discussion about metallophilicity, metallophilic interaction and bonding after which different radii used to estimate interactions and the critics using the radii are discussed. More sophisticated models to estimate interactions are followed. Structural classes of EMACs and their properties and applications are presented. Final part of the theoretical part of the thesis concentrates on the most employed ligand of the experimental part, pyridine-4(1H-thione), its different forms and relative stability of the forms.

1.1 Metallopolymers

Metal-containing polymers *i.e.* metallopolymers are polymers which contain metal centers. First metallopolymer, poly(vinyl ferrocene), was reported by Arimoto and Haven[1] in 1955.[2] The field of metallopolymers didn't expand rapidly after the first characterized polymers, because of insolubility problems, synthetic difficulties and characterization problems.[2-4] Increased access to and development of characterization methods (for instance gel permeation chromatography for molecular weight determination, matric-assisted laser desorption/ionization-time of flight spectroscopy (MALDI-TOF), electron spray ionization mass spectrometry (ESI-MS), X-ray photoelectron spectroscopy (XPS), electron microscopy, spatially resolved optical spectroscopy and NMR spectroscopy) have been important to scientists of the field.[2, 4, 5] Rapid progress in the field began in mid-1990s.[2-4]

Early metallopolymers had poor solubility due to for example extensive π–π stacking in conjugated polymers.[6] To increase solubility in toluene and chloroform alkyl groups were attached to them.[7] Also polymers could be insulated by other methods like bearing other bulky side chains than alkyl groups such as dendrons or polymerization of pseudorotaxane ("dumbbell shaped molecule") structures where the conjugated monomer is covered by

cyclic molecules.[6] A very recent review article[6] has been published about insulated π-conjugated metallopolymers. Already monomers have essential to bear insulation in order to prevent insolubilization in π-conjugated polymers.[6]

Development of synthetic methods for metallopolymers has been also vital.[2-4] Many synthetic methods which work well with organic polymers were would to be inefficient or to lead to undesirable side reactions in the presence of metal centres.[4] Those methods largely yielded low-molar-mass metallopolymers and/or materials which were contaminated by structural defects, were insoluble or lacked convincing characterization.[4] New synthetic methods include ring-opening polymerization, electropolymerization, polycondensation, controlled or so called "living" ionic polymerization and controlled radical polymerization.[2, 4]

Metallopolymers have advantages and disadvantages compared to discrete metal complexes and organic polymers. Metal-containing polymers have traditionally inorganic properties like optics, catalysis and electronic properties as well as properties of organic polymers like they are easy to process, flexible and have low density.[5]

Metallopolymers have conductivities commonly in the range of semiconductors ($10^{-8} - 1$ S/cm) but impressive progress has been made to increase conductivity.[2] Conductivities of tethered ferrocene metallopolymers are in the range of $3 \cdot 10^{-3} - 40$ S/cm depending on length and nature of tethering moiety.[8] The reason why metallopolymers are not more commonly conducting materials is that orbital energies of the metal center don't generally match very well with the orbital energies of the organic linker.[3] However, the conductivity can be modulated by multiple ways between states of high and low conductivity which means that they can be used as sensors and switches.[3]

1.1.1 Classification of metallopolymers

Different review articles classify metallopolymers differently. Ho and Wong[9] classify them whether metal is in main chain or side chain and then divided the two classes into conjugated and non-conjugated classes. This classification is done in order to highlight differences between absorption and emission properties of these four classes or metallopolymers. These differences are discussed further hereinafter.

3

Whittell *et al.*[4] classify metal-containing polymers comprehensively first whether the bonding is static (**a**) or dynamic (**b**) (Figure 1). In addition, metal centers can be located either in main chain (**c**) or side chain (**d**). Additionally, they metallopolymers can be classified as linear (**e**), star-shaped (**f**) or dendritic (**g**). Eloi *et al.*[3] and Whittell & Manners[2] have similar classification except without star-shaped class (**f**). Stanley and Holliday[5] have three classes among which Type I contains metal center which is tethered to the polymer backbone by *via* electronically insulating linker. Their Type II has the metal center covalently coupled to the backbone or in Type III directly incorporated into the polymer backbone. Thus division into main chain (**c**) and side chain (**d**) is divided into three groups. Type III has a backbone of alternating metal and organic parts but in Type II the backbone is all organic with metal electronically connected to the backbone. Hardy *et al.*[10] classify metal-containing polymers into four classes: main chain, side chain, star and dendritic but in addition they classify side-chain metallopolymers as shown in Figure 2. It's obvious that this classification is not comprehensive.
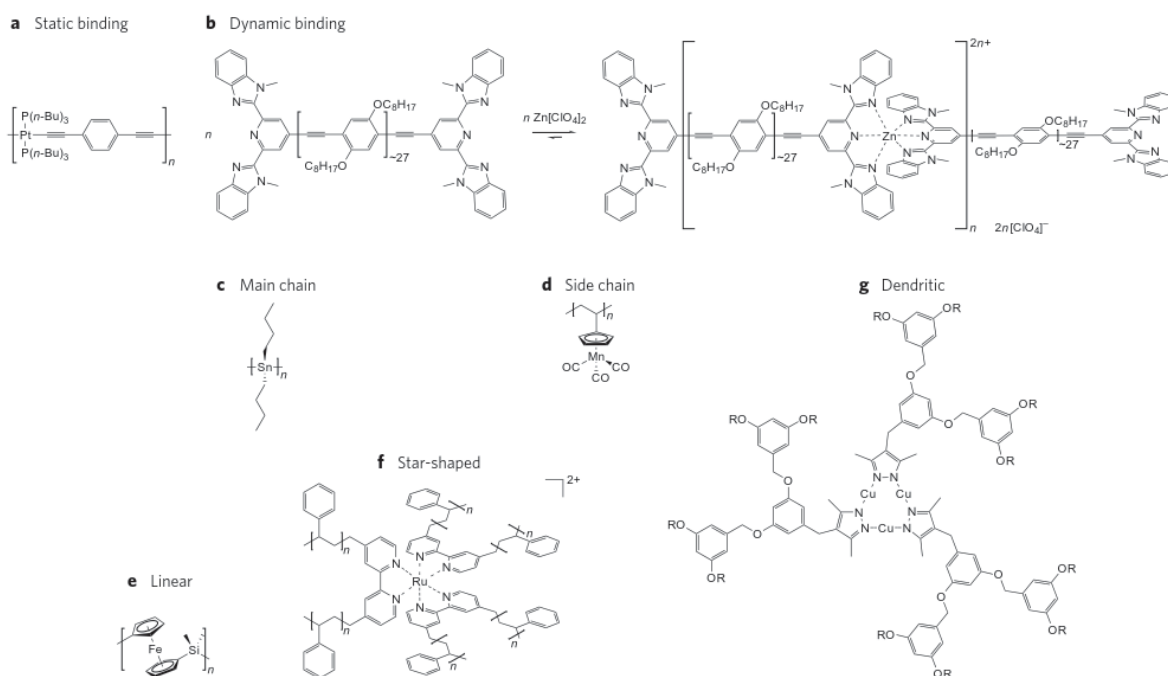
Figure 1. Classification of metal-containing polymers by Whittell *et al.*[4]
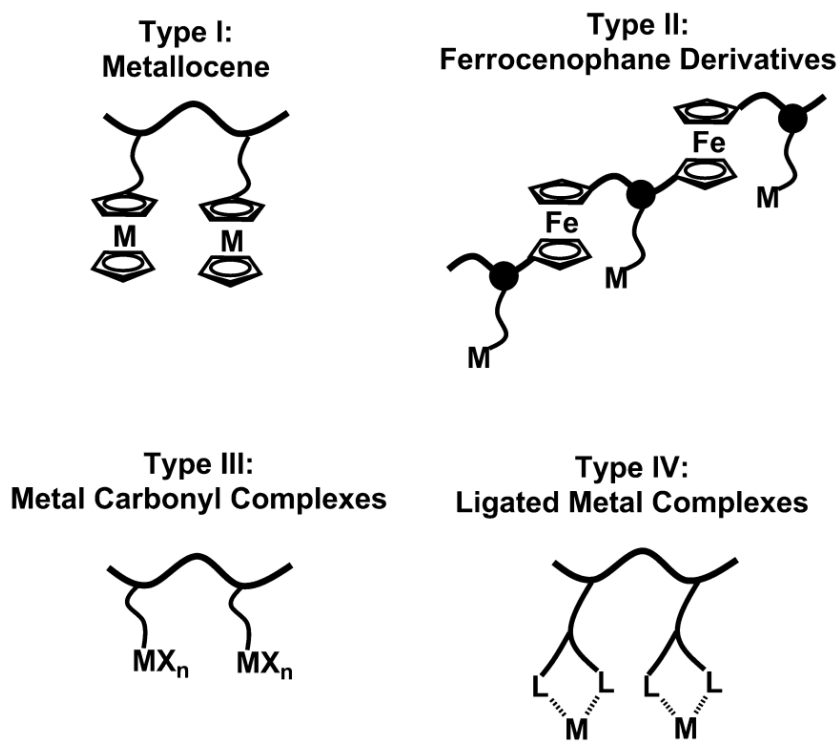
Figure 2. Classification of side-chain metallopolymers according to Hardy *et al.*[10]

Delocalized π-electron system is required for conductive (metallo)polymers. Incorporation of redox-active metal center into polymer can provide an efficient site for redox conductivity but can also trap or localize charges due to energetically low states. Redox active metallopolymers have potential to work for catalytic, photochemical, sensory and photoelectronic applications.[8]

Conductive polymers can be classified into two groups according to the charge transfer mechanism which can occur either via outer or inner sphere mechanism. These two mechanisms are shown in Figure 3 for discrete and polymeric metal systems. In outer sphere mechanism there's no orbital overlap between donating and accepting metal. As a result, even metals would be covalently bound to polymer backbone, their properties are similar to traditional complexes. In contrast, inner sphere mechanism requires conducting and bridging ligand or polymer to transfer the charge. The transfer process is highly dependable on the nature of the ligand or polymer and its orbitals overlap with the orbitals of two metal centers. When orbitals have similar energy and they are strongly coupled to provide additional charge transfer pathways, the resulting material is highly conductive[8]
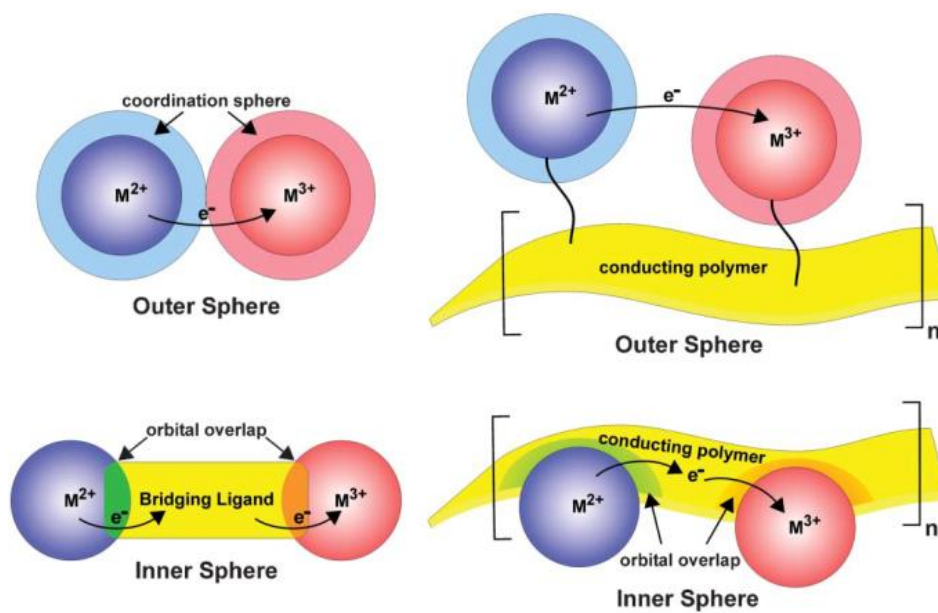
Figure 3. Mechanisms of electron transfer in molecular (left) and conducting polymer (right) systems *via* outer and inner sphere mechanisms.[8]

Some examples of components of conducting of outer and inner sphere metallopolymers are shown in Figure 4 and Figure 5, respectively. Outer sphere systems have been more widely discussed in the literature than inner sphere systems even though both groups are structurally diverse.[8]
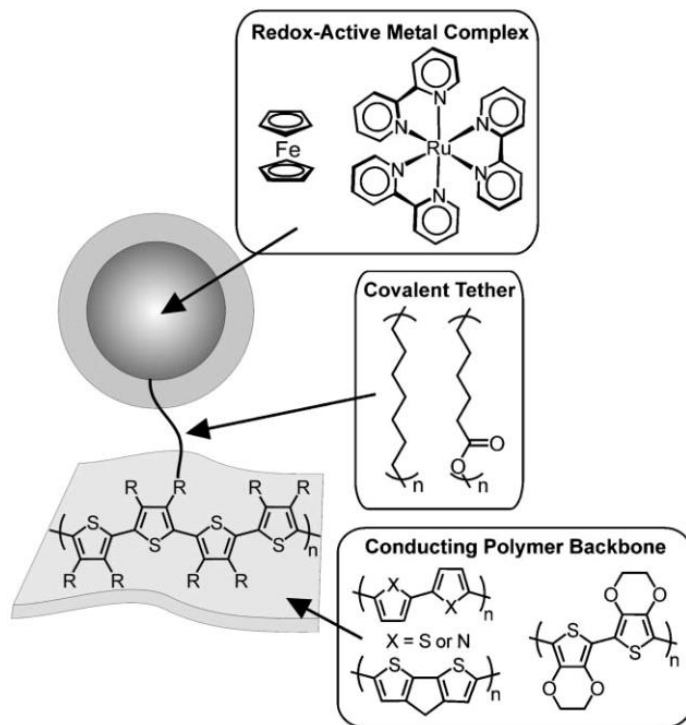
Figure 4. Some examples of molecular components of outer sphere metal-containing polymeric systems.[8]
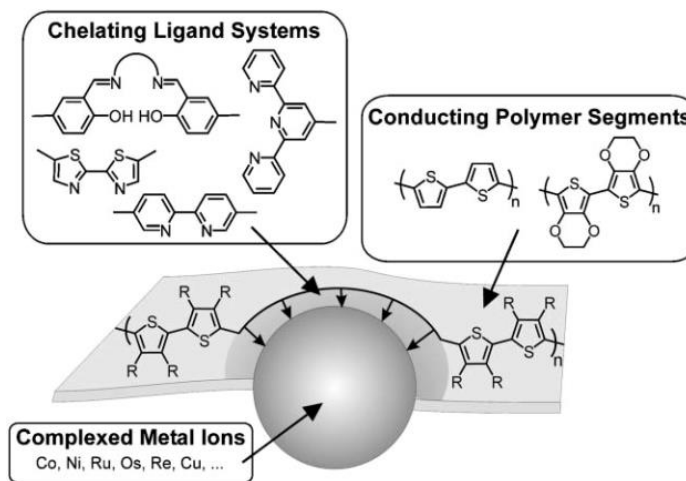
Figure 5. Some examples of molecular components of inner sphere metal-containing polymeric systems.[8]

Because existence of delocalized π-electrons impacts absorption and emission of metallopolymers, similar division can be made. When metal center is attached directly into the conjugated backbone of metallopolymer, there's a direct electronic communication in the structure. The communication is even stronger if the metal is in the core backbone than

if metal center is connected next to the backbone but it has direct communication with the delocalized π-system. The former is type III which was mentioned earlier, *i.e.* the backbone has alternating parts of metal centers and organic parts and the latter is type II which was mentioned earlier. Type III can result in substantial perturbations of the properties of each component and it is synthetically more complicated for lanthanides because they are coordinatively labile. If there's no direct linkage between metal center and delocalized π-electron system or the polymer is not conjugated, the ultraviolet and photoluminescence properties resemble sum of separate species of polymer and metal center.[5, 9]

Metallopolymers based on Ir^{3+} cyclometallates are better for many light-emitting purposes than Zn^{2+} terpyridine chromophores. Metallopolymers based on Ru^{2+} ions are commonly suitable for light-harvesting applications but Pt^{2+} are highly potential for both applications.[9]

1.1.2 Applications of metallopolymers

Metallopolymers have wide range of applications some of which were mentioned before. Polymeric sensors are superior compared to molecular sensors because when only partial binding of analyte is enough to produce a transformation of a property for example quenching of luminescence property of the whole polymer as presented schematically in Scheme 1. Fluorescent chemosensors can be classified into fluorescence "turn-on" and "turn-off" sensors in which binding of analyte either causes chemosensor to fluorescent or quench fluorescence, respectively. Chemosensory systems based on conjugated metallopolymers with transition metals have shown improved sensitivity and selectivity when compared to their pure organic polymer counterparts.[11-13]
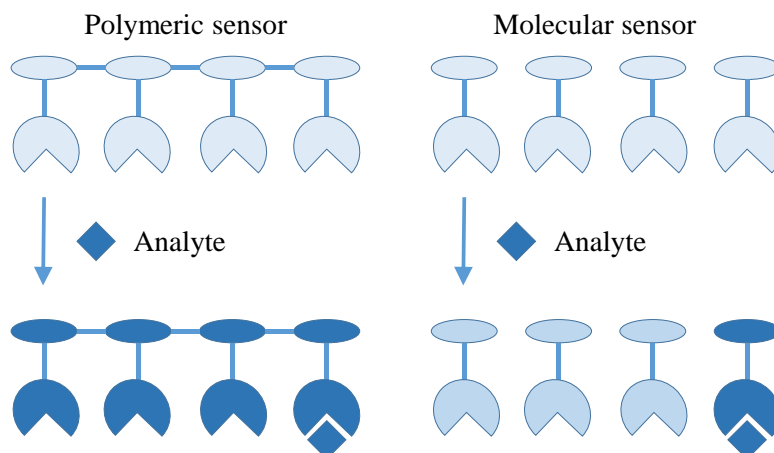
Scheme 1. Schematic presentation of polymeric sensor in fluorescent conjugated polymers and molecular sensor with one active site

Conjugated polymer with coordinated Cu^{2+} to the polymer backbone has been synthesized to detect CN^-.[14] When a cyanide ion complexed, the polymer "turned on" because binding of copper quenched fluorescence of the polymer.[14] A Co^{2+} polymer has been synthesized and observed to detect gaseous NO and NO_2 below 1 ppm.[15] When NO or NO_2 was bound to the metallopolymer, the resistivity of the polymer was changed.[15] The polymer had marvelous selectivity for the two analytes among O_2, NO, NO_2, CO and CO_2.[15] Also a copper based conjugated metallopolymer was synthesized for NO detection.[16] Cu^{2+} was reduced to Cu^+ using an alcohol and NO which "turned on" the metallopolymer.[16]

Multiple other sensor applications have been invented. Ion-imprinted polymers have been studied for detection of radiolanthanides in nuclear power plants, for extraction of medical grade ^{90}Y and for trace analysis of radiolanthanides for food and environment.[17, 18] Luminescent Eu^{3+} or paramagnetic Gd^{3+} complexes has been demonstrated to detect nucleic acids within cells.[19] The polymer consists of alternation of an oligoethylene part which binds to nucleic acids and an octadentate lanthanide chelating part.[19] Redox-active poly(vinylanthracene-*co*-vinylferrocene) is a redox-active polymer for detection of pH.[20] The polymer consists of pH insensitive vinylferrocene moiety which functions as internal standard alongside pH and redox-sensitive vinylanthracene moiety.[20] The pH values were possible to determinate over wide range of temperatures.[20]

Even though sensors contain stimuli-responsive materials, stimuli-responsive gels differ from sensors because their bulk physical property is changed by a stimulus.[4] A

metallopolymer which contains pendant *tris*(2,2´-bipyridine) ruthenium complexes can change its volume between swollen and collapsed state in constant temperature by a change of the oxidation state of Ru.[21]

The combination of a redox-active polyferrocenylsilane gel and a colloidal silica crystal yielded a material which exhibit different colors depending on the potential applied on the material attached to an indium tin oxide electrode.[22] Oxidizing potential yielded cationic ferrocenium moieties which attracted counter-ions and solvent molecules from the electrolyte and caused the gel to swell which increased the spacing between the voids in the photonic crystal and resulted in a redshift of the Bragg peak.[22] The change in color depended on the extent of swelling and thus on oxidizing potential.[22] La^{3+} or Eu^{3+} and Co^{2+} or Zn^{2+} containing metallo-supramolecular gels have been synthesized. Co/La gel is thermoresponsive (reversible gel-sol transitions) and Zn/La gel is thixotropic (mechanical stress like shaking causes physical causes decrease in viscosity).[23]

Multiple photoluminescent and electroluminescent metal-containing polymers have been researched.[2] Photo- and electroluminescent properties of metallopolymers can be tuned by alternating organic backbone or side chain of the polymer.[2] In some photoluminescent polymers the metal center has a solely structural role.[2] Examples include zinc-salen type, polymetallaynes with Pt or Hg and fluorine-*alt*-carbazole with main-chain cyclometallated or N-bound iridium complexes.[2] Wang *et al*.[24] have synthesized thionylphosphazene main chain polymer with aliphatic tether which is bounded to 1,10-phenanthroline (phen) which is bound to [$RuCl_2(phen)_2$] (Figure 6). That compound has been applied for patent to monitor concentration of dissolved oxygen in water for environmental monitoring and air pressure on aircraft wings in wind tunnels by detection of the local phosphorescent intensity of thing films coating the wing using CCD cameras.[2, 24]

10
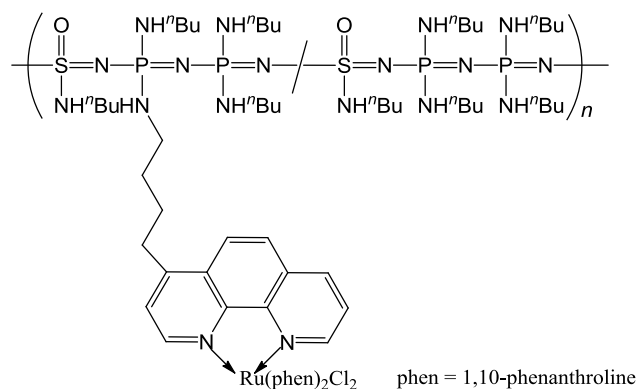
Figure 6. Thionylphosphazene main chain polymer with aliphatic tether which is bounded to 1,10-phenanthroline (phen) which is bound to $[RuCl_2(phen)_2]$ synthesized by Wang *et al.*[24]

Lanthanide light emitting diodes have theoretical efficiency of 100 % by spin statistics which is much higher than it for organic light emitting diodes (only 25 %).[25] This is because energy may be transferred to the metal center from both the singlet (25 %) and triplet (75 %) excitons of the ligands.[25]

Metallopolymers have generally better properties to be used as materials with highly refractive index; organic polymers have narrow range of elements and thus narrow range in refractive index because of they have similar electronic polarization. Blending of organic polymers and inorganic components of high refractive index or using π-conjugate functional groups don't yield as desirable properties as metallopolymers.[2] One example of high refractive index materials is a highly-crosslinked polymer or resin made by copolymerization of lead dimethacrylate, methacrylic acid and styrene.[26]

Chemically modification of soluble transition metal catalysts to be part of metallopolymers facilitates separation of products when catalyst remains in separate phase. Metallopolymers can be used as electrocatalyst as well. Transition metal catalyst can be incorporated into natural protein or the protein can be modified by point mutation to produce artificial metalloenzyme or metallopolymer-biopolymer hybrid. Also *de novo* synthesis of metallopolymer is possible.[2-4]

A single pair mismatch in an 18-base oligonucleotide was possible to detect amperometrically using Os^{2+} containing polymer which coated an electrode and which also was bound to probe oligonucleotides. Target molecules were 18-base oligonucleotides covalently bound to thermostable soy bean peroxidase. Hybridization of the probe and

target oligonucleotides led to an increase in current which depended on the completeness of the hybridization. The current detected resulted from the electrocatalytic reduction of hydrogen peroxide to H_2O.[27]

Different metallopolymers have been developed for memory devices. Those devises need to have two different states which are stabile so the information could be stored as '0' and '1'. Different Eu^{3+} complexes have been researched for memory applications.[28-30] In addition to Eu^{2+} complex attached to the polymer backbone by benzoate, those compounds have fluorene or carbazole moiety. Minor (or greater) changes to the structure of these Eu^{3+} polymer system causes change in memory behavior between flash memory[28] and write-once-read-many-times memory[29, 30].[4] Another flash memory device has been prepared by the random inclusion of ferrocenyl units in PFT2-Fc polymer which structure is shown in Scheme 2.[31] Application of voltage of ±2 V into the system caused change in the oxidation state of iron between (II) and (III) which resulted a large change in resistance of ferrocene moiety in PFT2-Fc polymer (shown in Scheme 2).[31] The device proved robust with on and off current ratios of over 10^3 for more than 100 cycles. Similar logic was in Eu^{3+} flash memory device developed by Ling *et al.*[28]
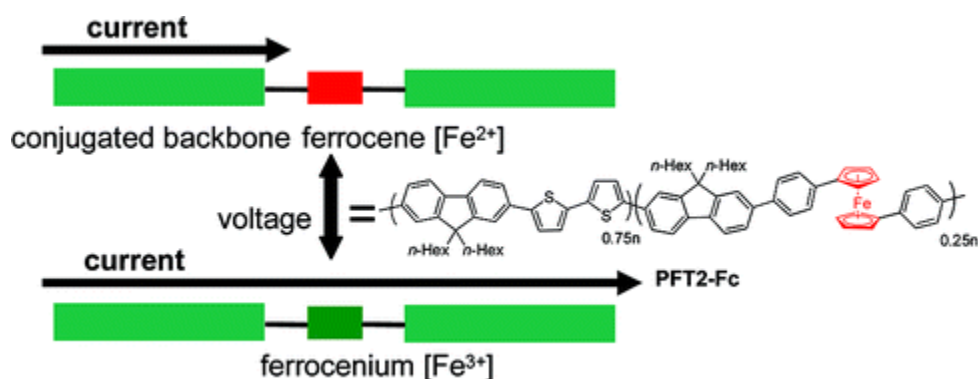
Scheme 2. Structure and high conductive and low conductive states of in PFT2-Fc polymer for flash memory applications.[31]

Metallopolymers have been utilized in nanofabrication and nanomanufacturing and they can be used in synthetization of ceramic or magnetic one-, two- or three dimensional nanomaterials with controlled size and shape. Metal-containing polymers have been used as a lithographic mask in electron-beam lithography and in mask-less inkjet printing. For example poly(ferrocenylsilane)s consist of ferrocenes covalently bound to $-SiR_2-$ unit.

These two groups alter and every cyclopentadienyl is bound to one –SiR$_2$– unit. The structure is shown in Figure 1 (**e**). Block copolymers of poly(ferrocenylsilane)s and an organic block have been used in nanolithography.[32]

The structure of poly(ferrocenylsilane)s upon exposure of oxygen plasma develops robust iron silicon oxide barrier.[33, 34] The robustness is very good property for a polymer to be used as a lithographic mask.[32] Whereas, organic polymers are degraded into volatile compound and evaporated from the surface.[33, 34]

Metal-containing polymers can be pyrolysed to create magnetic ceramic materials. Pyrolysis of polymers is a convenient route for synthesizing ceramic materials.[32] By controlling the experimental conditions of pyrolysis the ceramic material characteristic and magnetic properties can be tuned.[32] Using highly crosslinked metallopolymers very similar bulk properties with up to only minor shape distortions can be obtained.[32] Model for ceramic formation from metal-containing polymer has been suggested but only the schematic part of it has been presented here as Figure 7.[35] Pyrolysis of a crosslinked poly(ferrocenylsilane) created ceramics of α-Fe nanoparticles embedded in a SiC/C/Si$_3$N$_4$ matrix.[35]
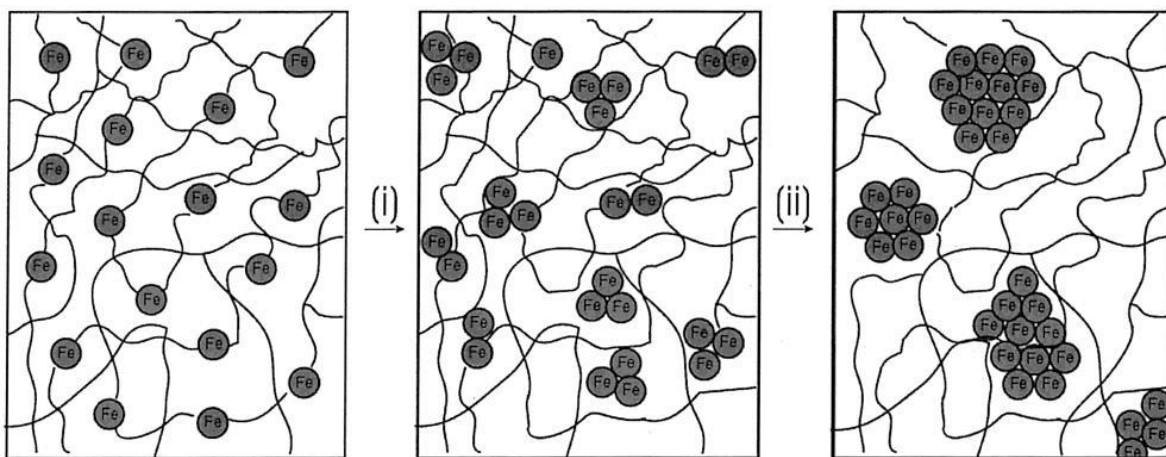
Figure 7. Graphical presentation of a nucleation (i) and growth (ii) of iron nanoparticles and genesis of magnetic ceramics from a crosslinked poly(ferrocenylsilane) using pyrolysis.[35]

Some metallopolymers in solution and thin films have an ability to form self-assembled structures. These self-assembled structures can be infiltrated or deposit a metal within or on the metallopolymer. The calcination of these kinds of structures may lead to magnetic

domains in a form of nanoparticles, nanotubes or nanowires encapsulated by metal-oxide nanotubes. Calcination turns metal into metal oxide at least in some cases. Resulting metal-oxide nanomaterials may have direct applications in photovoltaics and biomedicine because of their biocompatible, dielectric and semiconducting properties.[32]

The infiltration method of metal on metallopolymer is called sequential infiltration synthesis (SIS) and deposition method is called atomic layer deposition (ALD). In SIS organometallic compounds can bind selectively to a certain block in a block copolymer via perfusion the film. For example specific organometallic precursors can bind selectively to poly(methyl metacrylate) part of poly(styrene)-*block*-poly(methyl methacrylate) due to a strong attractive interaction of metal with ester groups. The infiltration changes the properties of the infiltrated block to high etch resistance at least with poly(methyl metacrylate).[32]

Self-assembled metal-containing block copolymers can be used to form nanoporous scaffolds for example by etching less robust block away to obtain interconnected three-dimensional porous morphology from the more robust block like poly(ferrocenylsilane).[32] Nanoporous scaffolds have multiple applications.[32] It's possible to produce variety of ultrathin capsules, vesicles and microspheres from metallopolymers which can be luminescent or permeable in certain conditions.[2]

1.2 Extended metal atom chain compounds

Extended metal atom chain (EMAC) compounds consist of closely spaced metal atoms arranged in a nearly linear fashion.[36-38] There has to be more than two metal atoms in the structure in order the structure to be EMAC. The string is covered by ligands. Different kinds of nature of ligands made up different classes of EMACs. Lengths of designed ligands define the lengths of EMACs in some EMACs. The ligand number four is typical for oligo-α-pyridylamine-based EMACs (Scheme 3) which are one of the most extensively studied classes of EMACs. Other classes are for example metal chains sandwiched within conjugated pπ-extended ligands, trinuclear linear complexes with heterocyclic azole-type ligands, phosphine type ligands, chains with oligo-m-phenyleneoxalamine ligands. The first EMAC founded was [$Ni_3Cl_2(\mu_3$-dpa$)_4$] (dpa is the anion of 2,2'2,2'-dipyridylamine) in 1968.[39]
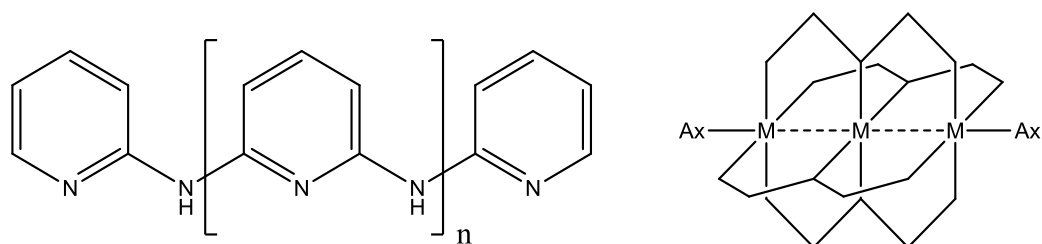
Scheme 3. (Left) general structure of oligo-α-pyridylamine type ligands and (right) schematic structure of $[M_3Ax_2(\mu_3\text{-dpa}_4)]$. Ax is an axial anion and dpa is the anion of 2,2'2,2'-dipyridylamine.

Another class of discrete metallic chains is compounds which contain "unsupported" metal–metal bonds or interactions.[37, 38] It means that metal-metal interactions may be adequate on their own to stabilize molecular chains of metals. These compounds can consist of square planar or linear monometallic complexes which have planar ligands which allow interaction of central metal with central metal of an adjacent unit. One classical example is ruthenium tetracarbonyl polymer $[Ru(CO)_4]_n$ which structure was obtained using X-ray powder diffraction (XRPD) in 1993.[40] $[Ru(CO)_4]_n$ is the first polymeric binary metal carbonyl compound characterized.[40]

Metal atom can have no own ligands but instead it coordinates to adjacent metal atom(s) and their ligand(s) like in the case of polymeric cation $[(\mu\text{-Ag})\{Au_2(\mu\text{-mes})_2(\mu\text{-dppe})\}]_n^{n+}$ in $[Au_2Ag(\mu\text{-mes})_2(\mu\text{-dppe})][SO_3CF_3]$ in which mes is mesityl i.e. 1,3,5-trimesityl group and dppe is 1,2-bis(diphenylphosphano)ethane.[41] Heteroaromatic ligands are common in these compounds because they are flat and in addition π-stacking stabilizes the structure. Also bimetallic ligand supported unit can form "unsupported" molecular chains like in the case of $[\{Rh(\mu\text{-pz})(CN\textit{t}\text{-Bu})_2\}_4]^{2+}$ in $[\{Rh(\mu\text{-pz})(CN\textit{t}\text{-Bu})_2\}_4](PF_6)_2$ (Figure 8).[42] These compounds are discussed more in detail hereinafter.
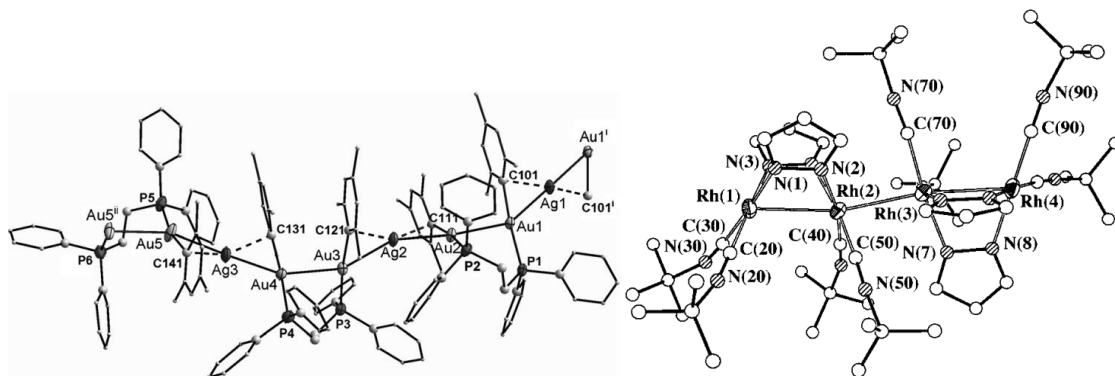
Figure 8. (Left) structure of the polymeric cation $[(\mu\text{-Ag})\{Au_2(\mu\text{-mes})_2(\mu\text{-dppe})\}]_n^{n+}$ in $[Au_2Ag(\mu\text{-mes})_2(\mu\text{-dppe})][SO_3CF_3]$.[41] (Right) structure of pentametallic cation $[\{Rh(\mu\text{-pz})(CNt\text{-Bu})_2\}_4]^{2+}$ of $[\{Rh(\mu\text{-pz})(CNt\text{-Bu})_2\}_4](PF_6)_2$[42].

Structures of one-dimensional metal chains have multiple of interesting properties and applications. They are promising candidates to be the smallest molecular wires because they have an insulating layer of organic ligands around a metal atom string.[43] They have catalytical[44], vapochromic[45], luminescence[41, 46-49], conductivity[50] and magnetic[51] properties.

When axial ligands are changed it may have a major influence on the electronic configuration of the central metal core like $[Ru_3Cl_2(\mu_3\text{-dpa})_4]$ is singlet but $[Ru_3(CN)_2(\mu_3\text{-dpa})_4]$ is triplet.[52] The difference in this case has been tracked down to the electronic state of the central Ru^{2+} unit.[52] In $[Ru_3Cl_2(\mu_3\text{-dpa})_4]$ Ru $3d^6$ electronic configuration is as follows: $d^2_{zy}d^2_{zx}d^2_{xy}$ and in $[Ru_3(CN)_2(\mu_3\text{-dpa})_4]$ it's $d^2_{zy}d^2_{zx}d^1_{xy}d^1_{z^2}$ because Ru–Ru bond is shorter in $[Ru_3Cl_2(\mu_3\text{-dpa})_4]$ which follows that it's Ru–Ru interaction is stronger which destabilizes d_{z^2} orbital more than in $[Ru_3(CN)_2(\mu_3\text{-dpa})_4]$.[52] In addition, the $d_{x^2-y^2}$, is destabilized in both cases because of four nitrogen atoms.[52] Oligo-α-pyridyl EMACs has been shown to be nanoscale molecular split-ring resonators (SRR) that can exhibit concurrent negative magnetic permeability and electric permittivity in UV-VIS region.[53] Some EMACs are paramagnetic like $[Rh_3Cl_2(\mu_3\text{-dpa})_4]$ with one electron and others are not like $[Ru_3Cl_2(\mu_3\text{-dpa})_4]$.[54] Compounds $[Au_2Ag_2(C_6F_5)_4(\mu\text{-N}\equiv CCH_3)_2]_n$ (Figure 15) and $[Au_2Cu_2(C_6F_5)_4(\mu\text{-N}\equiv CCH_3)_2]_n$ are brightly luminescent in solid state at 77 K and room temperature.[47]

Oligo-α-pyridylamine EMACs has been studied for a wide range of metals like Cr, Co, Ni, Cu, Ru, Rh, Pd, Pt. Their amounts of metal atoms range from three to eleven. Complexes with string of three metal atoms represent 71 % of all oligo-α-pyridylamine EMACs.[37]

2 Metallophilicity

The EMACs were defined as compounds consisting of closely spaced metal atoms arranged in a nearly linear fashion.[36-38] The definition evokes a question; how close adjacent metals atoms can locate each other to be considered as 'closely spaced' metal atoms. Comparing the van der Waals radii of the two atoms can be assessed whether there's any kind of bonding interaction between the two atoms. The definition of the van der Waals radius of an atom A is "half of the distance of the closest approach of two non-bonded atoms of A".[55] As a logical result from the definition, when two atoms are closer than their van der Waals radii, they have to have some kind of bonding interactions. This bonding interaction is described as metallophilic interaction and it's considered to be a dispersion interaction between relatively reduced metal centers.[38, 56, 57] However, one has to be careful with van der Waals radii because according to Pyykkö[57] the whole notation of van der Waals radii is rather unclear because nonbonding distances vary substantially. Especially for heavier element and halogens it's not clear which case represents "pure" or "clear" van der Waals distance.[57] There's further criticism about this matter later in this thesis.

Pyykkö[57] represents a presumably better method for measuring the weakness of an interaction than sum of van der Waals radii. It's called the Q ratio (1) where $A \cdots A$ is the intermolecular distance and $A - A$ the intramolecular one.[58, 59] The ratio varies between one and two.[57]

$$Q = \frac{A \cdots A}{A - A} \qquad (1)$$

Metallophilic interaction is typically as the same strength as typical hydrogen bonds.[60] $Au^+ \cdots Au^+$ interaction is the strongest form of metallophilic bonding and its strength can be between the strongest hydrogen bonding and the weakest covalent bonding which makes metallophilic interaction very remarkable.[56, 57] It's especially so because Au^+ nuclei have electrostatic repulsion between one another.[57] It is called as aurophilic interactions. Similar manner, interactions between copper atoms or silver atoms are called cuprophilic or argentophilic interactions, respectively. The $Au^+ \cdots Au^+$ $d^{10} \cdots d^{10}$ interaction is understood as dispersion effect with some virtual charge-transfer contribution.[57] One reason for this

specialty of aurophilic interaction is that gold atoms have high atomic number but another particularly important reason is very large relativistic effects.[57] In fact gold (Z = 80) has greater relativistic effects than any other element with the atomic number smaller than 100.[57] The relativistic effects can considerably strengthen dispersion interaction between closed shell nuclei and for gold the effect is remarkable.[57]

Metallophilic interaction is unique because it can overcome electrostatic interaction and bring together species of same charge like $[M]^+[M]^+$ and $[M]^-[M]^-$ but also neutral species $[M]^0[M]^0$ as well as opposite charged, $[M]^+[M]^-$, ones.[38, 61] (Notation $[M]^{+/-}$ represents a metal containing ion and $[M]^0$ a neutral complex.) Examples of these compounds are given hereinafter. Cationic interactions have been observed also other elements than gold in closed shell systems of s^2, d^8 and d^{10} of inorganic and organometallic compounds.[56] The d^8 system is not strictly speaking closed shell system but it can be considered as one if its crystal field splitting is large.[57] The strength of this interaction is stronger than other van der Waals interaction and its strength is of the same order as typical hydrogen bonds.[56]

Diatomic compounds have been important in the development of bonding theories. That's why also bimetallic model compounds have been important to understand metallophilicity in theoretical level. After that it has been natural to research larger metallic assemblies like metal chains.[62]

3 Metallophilic interactions or metallophilic bond

Can metallophilic interactions be regarded as a metallophilic bond? To answer that question it is first important to recall the exact definition of a bond by IUPAC: "There is a chemical bond between two atoms or groups of atoms in case that the forces acting between them are such as to lead to the formation of an aggregate with sufficient stability to make it convenient for the chemist to consider it as an independent 'molecular species'."[63] This definition leads to another question: how stabile is sufficiently stable? There's no simple answer to this question. Hydrogen bond by its definition is "a form of an association" and "is best considered as electrostatic interaction".[63, 64] However, hydrogen bonding itself is a range of interaction of different strengths; strong hydrogen bonding is classified as mainly covalent, moderate as mainly electrostatic and weak as electrostatic.[65] Metallophilic

interaction is also a form of an association and (as mentioned earlier[56]) closed shell interactions have strengths as strong as hydrogen bond.

Doerrer classifies bonding between metal atoms into three categories: (i) metallic bonding in bulk elemental metal, (ii) open shell interaction between two metal atoms which results sharing of electrons i.e. covalent bonding between metal atoms and (iii) bonding between metals with closed-sub shell dispersion interaction.[61] These three categories as shown in Scheme 4.
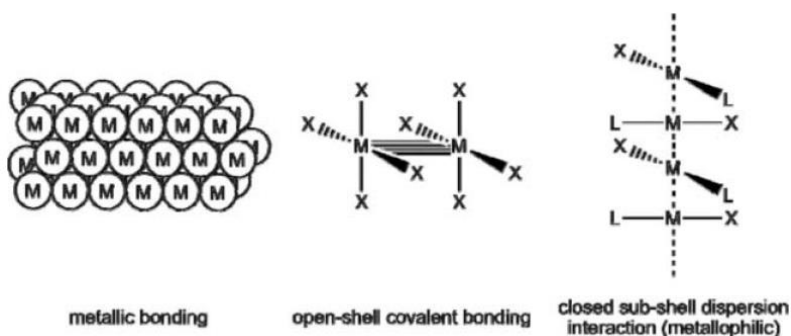
Scheme 4. Three bonding types between metal atoms: (left) metallic bonding, (middle) open-shell covalent bonding and (right) closed sub-shell dispersion interaction i.e. metallophilic bonding.[61]

4 Interatomic distances

Atomic radius was first described by Bragg in 1920.[66] The concept of atomic radius was based on the idea that atoms are hard spheres which touch each other when atoms are bonded to each other. Atoms were assumed not to deform each other nor able to penetrate each other. When more structural data was obtained it was obvious that simply one radius was not enough for one element; universal system of atomic radii was replaced by multiple more specific systems. Each of them meant to describe more specific structural class or particular chemistry. Later on it became clear that single radius for an element even in similar chemical environment is a simplification but this view is discussed hereinafter.[67]

Tables of different radii serve nowadays two main purposes: (1) to make crude estimation of bond distance in unknown structure and (2) to provide standard bond length of an 'ideal' bond and this value can be compared with a specific experimentally obtained value to give

some insight about the bonding or interaction. However, different radii have been quite often used incoherently and misplaced.[67]

All of these radii are used to approximate length of bond or distance in question in additive manner. The length is calculated as sum of individual radii of two atoms:

$$R_{AB} = r_A + r_B .$$ (2).

Schiemenz criticized strongly that the condition of $d(X \cdots Y) < \Sigma r_{vdW}[X,Y]$ would be proof of chemical bonding. He said that criterion 'shorter than the sum of van der Waals radii' should be discarded completely and rely on more reliable methods. His critic is very apposite and it'll be discussed more in detail hereinafter in the discussion of van der Waals radii.[68]

While Schiemenz discussed only about van der Waals radii, Batsanov & Batsanov pointed out generally if a distance between two atoms in a specific structure is close to the sum of tabulated radii, it does not give any sure knowledge about the bonding interaction. Often tabulated values are appropriate for narrow range of compounds with specific interaction and multiple factors affect these radii. For example covalent and ionic radii are not universal.[67]

Initially, atomic radii have been divided into covalent and metallic radii. Latter of which was applied only to all metallic structures and former to all other structures. These radii are practically the same but the differences in these two systems are mainly due to difference in coordination number, bond polarity and oxidation state (valence). Metallic bonds can be thought as nondirectional covalent bonds, which explains the similarities because bonding electrons are shared completely in both bond types. Atomic radius always increases with increasing coordination number.[67]

Bader developed a general theory of atoms in molecules which demonstrates that instead of atoms extended to infinity atoms in solids or molecules can be divided by physically meaningful boundary surfaces. According to Batsanov and Batsanov, even though atoms have not clear-cut boundary surfaces, *ab initio* calculations has proven that equilibrium vdW radii are physically meaningful because they define area which contains 99 % of electron density of an atom.[67] However, the limit of 99 % was arbitrarily chosen and there's no answer which amount of electron density defines atom itself. One could say that 100 %

of the electron density should be included but then the atom would extend to infinity even though the likeliness to find electron very far away from nucleus is extremely unlikely.

4.1 van der Waals radii

van der Waals radii describe the outer size of atoms because it describes distance between atoms with closed shells or nonbonding distances between atoms in different molecules. The vdW forces constitute of both repulsive and attractive interactions. Repulsive interactions are due to Pauli's exclusion rule and attractive interactions are chiefly due to dispersive interactions.[67]

Van der Waals distance between two atoms can be defined as the distance between two atoms when attractive interaction equals to the energy of thermal vibration, kT.[67] Some empirical methods for van der Waals radii takes temperature into account but not every; Badenhoop's and Weinhold's natural steric analysis is one of those methods which do take it into account and it's partially discussed hereinafter in this chapter.[69]

In the solid state the situation is different because the potential energy surface is different. For that reason, also van der Waals radii are different. The sample temperature for X-ray diffraction (XRD) methods is different than for example in gas-phase measurements. van der Waals radii have been tabulated as equilibrium and crystallographic radii. There's only a qualitative agreement between different calculation methods of equilibrium van der Waals radii of elements in second and third row. The accordance is even poorer with van der Waals radii obtained from molecular mechanics calculations by different authors; Batsanov states the differences to be very large because the values were optimized for narrow range of compounds.[67]

There're also different viewpoints for equilibrium radii. Equilibrium radii would correspond to the energy minimum on potential energy surface or then the radii in which attractive interaction energy equals to the energy of thermal vibration, kT. However, according to a different view, the closest atoms are closer than their equilibrium radii so their interaction is repulsive but other more distant atoms have higher distances than their equilibrium radii which have attractive interaction. This would yield neither net attraction nor repulsion. For example when two molecules of three atoms shapes like '>' would approach each other like '> <', the middle atoms would have repulsive interaction between

each other but other two would have attractive interaction. This alternative approach is presented by Allinger among others, which is discussed more in detail hereinafter. Because precise shape of potential energy surface is unknown, direct experimental measurements are only accessible for carbon and rare gases.[67]

Concept of van der Waals radii requires atoms to be hard spheres which is fundamentally an approximation because atoms in molecules are not spheres, neither are orbitals, except *s* orbitals.[70] It's also an approximation because the definition requires two atoms lie as close to each other as possible without deformation or penetration into each other.[67]

It has been observed that Li_2, B_2, C_2, N_2, O_2, and F_2 molecules have shorter van der Waals radii along bond direction than crosswise.[71, 72] Orthorhombic I_2 crystals have two crystallographic van der Waals distances with 0.8 Å difference according to a crystal structure[73] and 0.7 Å difference according to a semiempirical estimation[72].

A Van der Waals radius is smaller along bond axis of diatomic molecules because of increase in bond covalence increases the electron density between two atoms from atomic p_z orbitals to bonding region. (*z* axis is along the bond.) This results a decrease of electron density on the opposite side of the atomic p_z orbitals. Increasing ionic character lessens the covalence of the bond and thus the anisotropy. Thus, there's very small anisotropy in anions. In addition, an increase of bond polarizability and atom polarizability increase anisotropy.[67, 72, 74, 75]

"Hardness" of a radius and thus the polarizability can be measured by gradient of natural bond orbital exchange repulsion potential at steric van der Waals radius in *ab initio* calculations at HF/6-31G* level. The gradient describes the amount of "steric force" needed to push a probe and probed species closer together. Radii of atoms in ionic salts are more sensitive to deformation from spherical shape than neutral atoms and also metals are more sensitive than non-metals in the same row. Radii of atoms in ionic salts are also more dependent on the electronegativity of the other atoms(s).[69]

However, *ab initio* calculations in Hartree-Fock level have shown that it's not always the case that van der Waals radii along bond axis are shorter than perpendicular to it. This 'polar extension' is observed with K and Na in diatomic KH, KF, KCl, KBr, NaF, NaCl and NaBr compounds. The anisotropy was calculated by a simple subtraction of van der Waals radii of along the bond axis and crosswise to it. The remainders were 0.006–0.016 Å for the above-mentioned compounds. 6-311G(2*d,p*) basis set was used for first-row atoms,

MC-311G(2*d,p*) for second-row atoms and DZP for K and Br atoms. MC(HF) stands for multiconfigurational Hartree-Fock and DZP for double-ζ plus polarization. For each halogen atom one diffuse *p* function was added.[75]

The 'polar extension' was investigated using simple model of substitution F^- in NaF for negative point charge. The point charge was set to the optimized bond length (1.885 Å) of NaF molecule. The substitution resulted a small increase in electron density on the opposite side of Na^+ and it thus resulted an extension of Na^+ van der Waals radii in that direction. The reason for this is repulsion between negative point charge and electrons. Thus polar extension functions in real NaF systems as well as model system $(Na^+\cdots 1e^-)$.[75]

Inclusion of electron correlation i.e. electron-electron repulsion increases Hartree-Fock radius of Na^+ and F^- only slightly, by 0.005 Å and 0.016 Å, respectively.[75] Thus naturally, the level of theory has also an effect on calculated van der Waals radii.

Carbon van der Waals radii crosswise bond direction depends on bond order.[76] The van der Waals radii crosswise bond direction is 1.95, 2.01, and 2.17 Å in single, double and triple bond.[76] There's no reason why carbon would be the only element which transverse van der Waals radii depends on bond order so this should be considered possible for each element.

Most widely used van der Waals values were tabulated by Bondi in 1964.[77] The Bondi's article has been cited close to 10,000 times according to SciFinder® research discovery application by late September 2015. This is surprising because Bondi emphasized in this article in 1964 that his values are tentative and his van der Waals radii "are selected for calculation of volumes. They may not always be suitable for the calculation of contact distances in crystals." Bondi used four methods to obtain his values: gas kinetic cross section, liquid state properties, critical densities and most reliable X-ray diffraction data available up to that date.[77]

The reliability of Bondi's values has been questioned and compared with newer results but his values are very reasonable and consistent with later results according to certain authors.[70, 78] Rowland and Taylor calculated and compared accumulated crystallographic data of non-metals to Bondi's values in 1996.[78] Halogens and sulphur values had outstanding congruency. Carbon, nitrogen and oxygen values diverged slightly more but discrepancies were about 0.05 Å.

The single exception to the consistency is hydrogen which radius was obtained to be 0.1 Å smaller than what Bondi[77] tabulated but there's a logical reason for the difference. Hydrogen van der Waals radii was observed to be 1.1 Å in Rowland's and Taylor's article was for every kinds of H···H/X values. However, Rowland and Taylor obtained another H radius which was only for H···H contacts. Its value is 1.19 Å which is almost identical to Bondi's van der Waals radius (1.20 Å) for H. The reason for this why the latter value is so similar to Bondi's values is that Bondi's van der Waals radii for hydrogen was mainly based on H···H contacts of adamantine in a previous study. That's why Bondi's value should be used for H···H contacts and Rowland's and Taylor's values for general H···X case.[78] This is one good example that van der Waals radii are not universal.

According to Rowland and Taylor, the 0.1 Å difference is due to electrostatic reasons; covalently bound hydrogens in organic molecules have partial positive charges which repel each other but X has partial negative charge organic molecules which attracts hydrogen. X was C, N, O, F, S, Cl, Br and I in Rowland's and Taylor's article.[78]

Another reason is peculiar nature of H_2 molecule; it lacks nonbonded electrons so bonding electrons has to take part also in intermolecular interactions both which are attractive and repulsive. The same reasoning applies to –H···H– systems. As a result, electron density is not only located between the atoms. According to exact *ab initio* calculations, only 16 % of the density of electron pair has been concentrated between the atoms in H_2 molecule although H–H bond is one of the strongest simple bonds known! When hydrogen is bonded to another element, its peculiar and intrinsic nature lacking of nonbonded electrons is reduced by existence of nonbonded electrons of another element it's bonded to.[67]

One reason for high strength of H_2 molecule is that because it lacks nonbonded electrons they cannot repel each other. Thus, all the electron density which is between the atoms is attractive to both atoms. This might be one reason to explain why H–H bond is so strong even only so little of the density of the electron pair has been concentrated between the atoms. H_2 molecule and H–H bond has many peculiar properties but they are not discussed further.[67]

Elements O, F, S, Cl, Br, and I had 0.04 Å differences in their van der Waals radii between values of Bondi and Rowland and Taylor. Bondi's van der Waals radius of carbon was 0.05 Å smaller than the one of Rowland and Taylor, which is most likely due to a general phenomenon that carbon van der Waals radius depends on the hybridization of the carbon;

sp hybridized carbons have effectively smaller van der Waals radius than other types of carbons. Bondi used carbon values for *sp* hybridized carbon but Rowland and Taylor for carbon hybridised in all the three ways. That's why the difference is really smaller than the numbers imply.[78] Because of this reason Mantina *et al.* stated van der Waals values for carbon for each hybridization: sp^3, sp^2 and *sp* separately in 2009.[70]

Mantina *et al.* calculated van der Waals distances of main group elements with four probes; Ne, H from HF, F from HF and CH_4. Calculations were performed in CCSD(T) level and ANO-RCC basic set. CCSD(T) stands for coupled cluster with single and double and perturbative triple excitations and ANO-RCC stands for atomic natural orbital–relativistic correlation consistent. Values with Ne as probe differ from Bondi's[77] values (and van der Waals radii of H of Rowland and Taylor[78]) quite a bit. The greatest differences were between H, Si and C which differences were 0.57 Å, 0.48 Å and 0.40 Å, respectively. The average difference between values with Ne as probe and Bondi's values was 0.2 Å.[70]

Results of the other three probes were combined to create a linear combination to minimize root mean square error and van der Waals radii were created but Bondi's values were considered as standard and they were used to form constants for linear combination. This methodology seems very strange because Bondi[77] stated himself that his values are tentative even though Mantina *et al.* cited articles which have obtained similar results to Bondi's values. Not a single set of constants were able to find for the elements which had to divide into four classes: noble gases, open-shell *p*-block non-metals, *p*-block metals, and *s*-block elements. That resulted reproduce the standard van der Waals radii with mean unsigned deviations of 0.01, 0.04, 0.06 and 0.06 Å for these four classes, respectively.[70]

Linear combination method for four groups of main group elements of Mantina *et al.* created van der Waals radii yielded better results. This seems a way to obtain numbers closer in agreement with numbers supposed to standard values in the article. However, this methodology doesn't have any background in theory. It was just a way to create so many parameters which ensured values to have mean unsigned values closer up to 0.06 Å in comparison with Bondi's values. Division of the elements into noble gasses and another group of elements didn't create differences up to 0.06 Å which was their arbitrarily chosen goal so the division of elements had to be continued until 0.06 Å limit vas reached. If 0.06 Å was not arbitrarily chosen, the reasons why it was chosen, were not mentioned.[70]

The probe type in calculations of Mantina *et al.*[70] greatly effects on the van der Waals radii obtained. For example when van der Waals radii of Li is computed from F of HF, the radius is 0.30 Å but when CH_4 or H of HF is used as probe the radius of 2.30 Å and 2.03 Å are obtained.[70] Mantina *et al.*[70] stated that F of HF as a probe results smaller van der Waals than the other three probes "indicates that this kind of probe can lead to a significant covalent interaction". However, this might be a partial reason but better explanation is strong polar dipole of HF which also polarizes the atom under investigation to results partial positive dipole. As discussed more detail later by Schiemenz[68] partial positive charge results smaller van der Waals distances than neutral or anionic species.

Generally speaking, anionic radii are close to van der Waals radii but cationic radii differ greatly from van der Waals radii. For example for ionic radii of Li^+ is 60 pm[79] but van der Waals radii is 260 pm[80]. In less extreme cases when polar bonds results partial charges on atoms, which has to be considered when analyzing interatomic distances. Partial positive charges in organolithium compounds would cause misinterpretations based on van der Waals radii of Y and Li when Y···Li distances are interpreted. Y denotes generally an element.[68]

Ab initio calculations using natural steric analysis have shown clearly that partial charge, especially a positive one affects the radii. For example end-on van der Waals radii for H in LiH, BH_3, C_2H_6, H_2, H_2O and HF are 1.645, 1.461, 1.426, 1.394, 1.200 and 1.103, respectively. Those hydrogens have natural charge of –0.725, –0.128, +0.212, 0.000, +0.477 and +0.520, respectively. Generally speaking the ones which have more positive nature has shorter radii but homonuclear diatomic molecules (H_2, N_2, O_2, F_2, P_2, S_2, Cl_2) have smaller radii than the natural charge would suggest.[69]

Electron withdrawing or donating nature affects the van der Waals radii of metals in organometallic complexes. When electron withdrawing nature of a ligand in a complex decreases, the van der Waals radius of the metal increases because of increased electron density. This has been observed with chlorine, bromine and iodine in $K[AuX_4]$, X = Cl, Br or I, $K_2[PdCl_4]$, $K_2[PdBr_4]$, $Na_2[PdH_4]$, $K_2[PtCl_4]$, $K_2[PtBr_4]$ and $Na_2[PdH_4]$ complexes. The M···M distances in hydride complexes confirm that the increase in metal-metal distances is not due to increase size in ligand; metal-metal distances increase in order of Cl<Br<I<H. Hydride is the smallest but the electron density on the metal is the highest. The hydride Pd and Pt complexes have about 0.7 Å larger intermetallic distance compared to the bromide complexes. The difference between adjacent $K[AuX_4]$, when X = Cl, Br or I, is

about 0.3 Å. The difference between bromide and chloride complexes in Pd and Pt complexes stated above is about 0.2 Å. Each distance has been obtained from separate articles cited in Batsanov's and Batsanov's book[67].

The intermetallic distance also depends on torsion angle between X–M···M–Y.[81] In addition there're not very many crystal structures available which have metal atoms in immediate contact with one another without forming a strong (ionic, metallic or covalent) bond. Some metal van der Waals radii in organometallic compounds have been published but the values differ largely. Those values are obtained from crystal structures from M···M, M···C and M···H distances. Batsanov suggested calculating van der Waals radii from covalent bond distances because covalent bonds are much better defined than contact distances.[67]

The concept of van der Waals radii should be additive so $\frac{1}{2} \cdot d_{vdW}(A \cdots A) + \frac{1}{2} \cdot d_{vdW}(B \cdots B)$ should equal to $d_{vdW}(A \cdots B)$. However, the additivity is not perfect even though it roughly functions. Gas-phase spectroscopic data reveals heteroatomic contacts for noble gases have systematically longer van der Waals distances than homoatomic contacts due to electronic polarizabilities, α, of contacting atoms also the energy is smaller than homoatomic contacts. This is opposite to heteroatomic compounds which have shorter interatomic bond distances and higher energy than corresponding homoatomic compounds. The mutual polarization of two atoms to each other is fundamental nature of van der Waals forces.[82]

Ab initio calculations using natural steric analysis have shown that in certain cases the additivity of van der Waals radii doesn't support. Those cases are in small molecules because the deviation is not observed in larger molecules. Formaldehyde dimer shows that the additivity doesn't fit. O···O contacts in $(H_2CO)_2$ has over 1.0 Å difference from the values predicted values even though CO_2 shows near additivity even though both have –C=O···O=C– contacts. Badenhoop and Weinhold underlines with reason that van der Waals radii are not universally truly additive even with a constant correction.[69]

Polarization corrected gas-phase radius is suggested to call as 'ideal van der Waals radii' because it would tally with the pure van der Waals interaction between two isolated atoms or molecules. If polarization correction is applied to crystallographic van der Waals radii, they will coincide with ideal van der Waals radii. Interatomic distance can be shorter when apparently smaller atom has been replaced by larger one because of certain combinations of atomic polarizabilities.[82]

Molecular substances and rare gases have different polarizabilities in different aggregation state. The relative variation ranges from 0.3 % for Ar to 18 % for I_2.[83] On condensation polarizability can increase or decrease.[67] Because effective molecular volume decreases when substance condenses, this increase of polarizability can be only caused by building-up electron density between molecules.[67] Even noble gas dimers have dipole moments. For example for Ne·Kr it has been estimated to be 0.011 debye.[84]

Because cohesive energy per contact 'bond' in crystalline and molecular state of rare gases are virtually identical and the interatomic distances between atoms are thus also similar, the van der Waals distance is defined only by contacting atoms and depends on other atoms in the crystal or molecular space moderately little. As a result, a contradicting view that the van der Waals contacts in solids are shorter than equilibrium distances because of interactions of multiple particles, should be disputed. The reason for shorter crystallographic radii is increased positive effective charge on atoms. If atoms in gas-phase molecules have charges, their van der Waals radii are smaller than neutral atoms than their van der Waals radii approach crystallographic radii. However, other factors may also operate.[67]

Schiemenz criticized use of sum of van der Waals radii as evaluation of bonding, especially weak bonding. According to him, differences of tables of van der Waals radii are substantial. The criterion 'shorter than sum of van der Waals radii' should be discarded and utilize other safer criteria even though it is widely used. However, if alternative methods are in compliance with conclusions with van der Waals radii, van der Waals radii can be used. If an interatomic distance is less than the sum of van der Waals radii, no conclusion can be drawn about whether bonding interaction exist or not neither the type of possible interaction.[68]

When interatomic distance has been shorter than sum of van der Waals radii in a number of publications, far-reaching conclusions have been made to have bonding interaction. Bonding interaction requires interatomic distance to be shorter than the sum of van der Waals radii but the distance shorter than sum of van der Waals radii doesn't proof that there would be bonding interaction. There's an additional problem that which van der Waals radii are the correct ones. In multiple cases geometry calculations with typical bond lengths and angles results distances in rigid molecular parts to force atoms closer together into a distance which is less than the sum of van der Waals radii. Also in supramolecular systems ion pairing or hydrogen bonding can force atoms to be closer to each other than normally.

In these cases the short interaction destabilizes the system rather than contribute to its bonding energy by additional attractive interaction.[68]

4.2 Covalent radii

Pyykkö has published an article[85] in 2015 which summarized his and other's previous articles of molecular single[86], double[87] and triple[88] bond covalent radii and tetrahedrally bonded crystals[89]. He also compared the values with other data.[85] His key conclusion is that using simple additive formula (2) for one bond one "can get surprisingly far".[85] Predicted R values correspond well with experimental values if bond is not too ionic or the coordination number is close to the values used in original input data for the fit.[85] Bonds between transition metals and halides have been omitted due to partial multiple-bond character.[85] All elements and all data points were treated equally and the radii were self-consistently obtained though least square fit in the four Pyykkö's articles.[86-89]

Cordero *et al*. had a non-self-consistent approach using experimental bond distances from Cambridge Structural Data Base (CSD). Covalent radii were based on experimental bond distances to N, C or O and coordination number (CN) was 6 excluding copper. Copper distances were based on CNs ≤ 4 because of Jahn-Teller distortion in higher coordination numbers. In addition, non-transition elements and Zn, Ag and Au were restricted to coordination numbers 2, 3 and 4 and main group elements were restricted to their typical coordination numbers but also higher coordination numbers up to 4 were allowed. The average standard deviation was 0.06 Å and maximum was 0.12 Å for K. The data was interpolated for few elements which experimental data is lacking.[90]

Whether transition metal complex is high or low spin system, has a significant difference to the covalent radii.[90] High spin systems of Mn, Fe and Co have observed to have higher covalent radii than their low spin analogues.[90] They even have higher covalent radii than third row low spin transition metal compound of the same group.[90] Numerical van der Waals values have been tabulated in Table 1. Pyykkö suggested using additional parameters which might improve fit with experimental data.[85]

4.3 Intermediate cases between covalent and van der Waals radii

Distinction between covalent bond and nonbonded interaction is not always a simple case because interatomic distances vary continuously from van der Waals radii to covalent radii.[72] Multiple tables of van der Waals radii and covalent radii have been published and different methods have been used to obtain van der Waals radii.

Lengthening of intra-molecular bond distance leads to shortening of inter-molecular distance which ultimately leads to the two distances to be same and interchangeable.[91] It's experimentally observed in phase transitions from molecular solid into metal.[67] According to Pauling's famous book, *The nature of the chemical bond*, in 1939, covalent radii are about 0.8 Å shorter than van der Waals radii.[67, 72]

Interdependence of van der Waals radii to covalent radii has been observed in system of $I_1 \cdots I_2 \cdots I_3$. Averaging experimental data shows for the system that intermolecular distance versus intra-molecular distances show hyperbolic behavior and when one of the distances is shortened the other one is lengthened. This means shift of electron density from one side to the other so when van der Waals distance is shortened its covalent nature is increased. When I–I system transforms into symmetric $I_1 \cdots I_2 \cdots I_3$ system the bond order decrease from 1 to 0.5 and coordination number of the central atom changes from 1 to 2. This has been observed also to other systems like Br–Br$\cdots$Br, S–S$\cdots$S, X–Cd$\cdots$X, and Cl–Sb$\cdots$Cl. For example for Cl–Sb$\cdots$Cl the phenomena is clearly visible in values taken from distances between Cl and Sb in *trans* position to each other in only octahedral Sb^{3+} part of one crystal structure of $[Cl_2Sb\{Fe(CO)_2(\eta^5-C_5H_5)\}_2][Sb_2Cl_7]$[92].[67]

When symmetrical trinuclear system is formed from a van der Waals and covalent bond, it equals to transformation of a terminal ligand into bridging ligand. All the changes in bond lengths have similar values: the van der Waals distance is shortened by about 1.35 Å and covalent bond is lengthened by about 0.25 Å.[67]

The shortening of intermolecular distances was assumed to be due to a "secondary", "specific" or "interaction that cannot be described within the framework of the classical theory of chemical bonding" in a number of works. *De facto*, the variations are due to exchange (covalent) forces between molecules located in close vicinity so it can be explained in known concepts and thus it's not a new kind of interaction.[72]

There's no simple answer to the question when one should stop talking about intermolecular bonds and began to talk about short contacts. It might be possible to use certain threshold energy or distance but it's not usually that simple.[93] For hydrogen bond, a crossing point from closed shell interaction to covalent electron sharing seems to occur approximately at 1.33 Å[94] for H⋯O. This value has been reached by using bond path method which is described hereinafter.

4.4 When there's an interactions and when there's not

As mentioned above, there's a continuum between covalent and van der Waals radii, there's also continuum from strong hydrogen bond to weak (or practically non-existing) hydrogen bond. The weak hydrogen bond energies extend all the way to barely above the thermal noise level. The most important question is not whether a hydrogen bond exist or not but to what extend are they relevant in distinguishing one crystal structure from one another. This logic is good also for any kind of interaction.[93]

4.5 More advanced description of intermolecular distances

Mayer bond order (MBO) is a computational method to estimate bond order. It has been extended from Wiberg bond order which is not discussed. MBO is simply a sum of each symmetry component involved and it allows more comprehensive understanding on bonding interactions and variation of bonding interactions within a series of compounds; high-level computational calculations can be understood in terms of LCAO. It takes into considerations of all contributions to bonding instead of only orbitals close to Fermi level and it's computationally efficient. It depends on the basic sets used so only values with same basic set can be compared. Thus, absolute values with finite basic set are not possible to obtain.[95]

Dunitz and Gavezzotti proposed turning from simple scrutiny of atom-atom distances and interactions to more sophisticated interactions like pixel and bond path method in their review.[93] Use of simple localized atom-atom interactions or "bonds" have been widely used because of its simplicity. Inspection of atom-atom interaction is a simplified model which should not be taken too rigorously. However, they are unavoidable and useful to a limited

extend. The interaction between molecules is a complicated matter between molecular charge distribution not simple atom-atom interactions.[93]

Energy difference between different packing modes is not easily partitioned by atom-atom contacts. The packing modes depend on how molecules interact with each other as a whole or how particular areas of them approach and interact with each another. Thus, usage of atom-atom distances to deduce protein folding or crystal packing reasons is close to wishful thinking. Generally, molecular recognition should be performed using more sophisticated methods like pixel which is concentrated on molecule-molecule interactions.[93]

Pixel method is semiclassical and semiempirical method and is also called as semiclassical density sums (SCDS) is developed by Gavezzotti in 2002 and 2003.[96, 97] Electron densities of isolated molecules are calculated by quantum-chemical methods and only four disposable parameters are required for complete evaluation of intermolecular energies for versatile molecular systems. Molecular electric properties are divided into pixels which are further divided into superpixels of an order of magnitude of 10 000 sites rather than a few nuclear positions. Even though the simplifications are at least rough, they produce quite reliable results for molecular dimers and sublimation enthalpies of organic crystals compared to high-level quantum chemical methods. The computation cost is only a fraction of those and it takes 2 h for modern computer time. (The time value was given in 2002.) However, it's less accurate by short intermolecular distances where electron densities overlap significantly which is anticipated because of the molecular electron densities are taken as in static and undeformed free molecules. Very important properties of pixel are superpixel grid includes penetration of partial overlapping molecular densities and many-body effects in polarization energies.[97]

In SCDS method total energy is sum of four energies: electrostatic, polarization, dispersion and repulsion energies. The terms are large but they counterbalance each other. These intermolecular interactions are calculated between superpixels. Repulsion energies are estimated from overlap of electron densities. Dispersion energies are estimated from atomic polarizabilities distributed over the electron density, using an average ionization potential taken as the energy of the highest occupied molecular orbital and the formulation is inverse sixth-power London-type. Pixel method doesn't require burdensome parametrization and it uses readily available wave functions.[97]

Pixel method results that some atom-atom contacts are too close to each other and others are further away than their equilibrium radii which balance each other out. Some atoms are closer and others are further away than their equilibrium van der Waals radii. The phenomenon is called Allinger's effect which is simplifiedly shown in Figure 9. Luckily, the effect is not as widespread as is often surmised.[67]
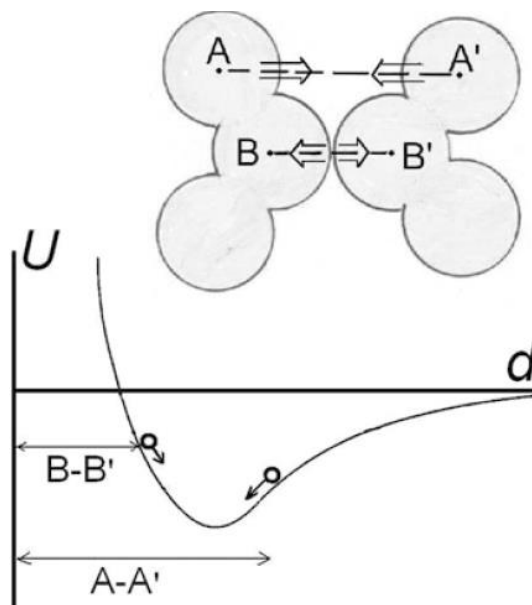
Figure 9. Simplified picture of intermolecular interaction by Allinger when their relative orientation is fixed and only the distance is varied. The attractive and repulsive interactions balance each other to create an equilibrium state. At the equilibrium state, the shortest contacts between B and B' is repulsive but more distant contacts between A and A' are attractive.[67]

Bond path method from electron densities uses Bader's theory of atoms in molecules (AIM). AIM theory provides a punctilious and accurate portioning of energy and space. It qualifies bonds between atoms and atomic basins in terms of the topological properties of charge density $\rho(r)$, its gradient vector $\nabla\rho(r)$ and second derivate $\nabla^2\rho(r)$. A point in which $\nabla\rho(r) = 0$, is a critical point. There're four types of critical points in three dimension space. One of those, $(3, -1)$, has two curvatures negative but one positive which corresponds to a saddle point in the electron-density distribution. This situation takes place between nuclei connected by chemical bond. The three others $(3, 3)$, $(3, 1)$ and $(3, -3)$ are points in nucleus, inside a ring of bonded atoms and local electron minimum, respectively.[98]

Bond path is defined as a path between two (3, 3) critical points in which $\rho(r)$ is higher than in any neighboring line. The two (3, 3) critical points are located at the nuclei of the two atoms. The nature of the bonding interaction depends on electron density ρ_b and its second derivate. If the second derivate, $\nabla^2\rho_b$, is negative, the charge is concentrated on the internuclear region which means that there's covalent bond. If $\nabla^2\rho_b$ is positive, the interaction is closed shell interaction because there's a local deficiency of charge.[98]

Reliable calculations of atomic and bonding properties call for $\rho(r)$ and its space derivate to be accurately known because in intermolecular regions charge densities are low and close to background noise level. Identification and location of critical points and bond paths might thus not to be obvious to detect. There's no unambiguous answer to what significant bond path is and what isn't. Also crystallographic data can be used to deduce bond paths but it has also errors of different kind which makes electron density and especially its space derivatives more unreliable. It's also a problem that in many publications in this area reader is provided not enough information about the experimental details and refinement procedures to make a knowledgeable critical judgement about the reliability of the results.[98]

The intermediate case between covalent and closed shell interaction for H⋯O has been reached by extrapolation of $G(\mathbf{r}_{BCP})$ and $V(\mathbf{r}_{BCP})$ values to the point where $V(\mathbf{r}_{BCP}) = -2G(\mathbf{r}_{BCP})$ and hence $\nabla^2\rho(\mathbf{r}_{BCP}) = 0$. This condition yields a value of 1.33 Å for H⋯O. $G(\mathbf{r}_{BCP})$ and $V(\mathbf{r}_{BCP})$ values stands for local electronic kinetic energy density and corresponding potential energy density, respectively. BCP stands for values at bond critical points. In other words, $V(\mathbf{r}_{BCP})$ is the measure of tendency of electronic charge to concentrate in the elemental volume in question and $G(\mathbf{r}_{BCP})$ is a measure of tendency of electronic charge to leave the elemental volume in question. The condition $\nabla^2\rho(\mathbf{r}_{BCP}) = 0$ is equivalent to the transition from covalent to closed-shell character of the bond under investigation.[93]

Pixel and bond path methods are alternative methods to describe the same matter. Both are used for describing the physical phenomena accompanying of molecules into condensed matter. Bond paths and critical points are used in the bond path method and intermolecular coulombic, dispersion, polarization, or repulsion energies that result from confrontation and overlap of electron densities in relation to nuclear positions are used in the pixel method.[93]

4.6 Numerical values of different radii

Table 1 consists of van der Waals, single bond and double bond radii of different elements. Bondi's values[77] were tentative and they were "observed" mean van der Waals radii according to his article and his van der Waals radii of Cu was based on only one crystal structure. His non-metal values were designed for volume calculations. The values were obtained from critical density, gas kinetic collision cross section, liquid state properties and by selection of most reliable XRD data up to 1964. Those XRD contact distances have been corrected to 0 K. Silver and gold values are from critical volumes. For groups 13–18 elements, van der Waals radii shown in Table 1, "only the most frequently used values for single bonded forms of the elements" are used. No mention about coordination numbers was made in Bondi's article.

Batsanov's values in 2001[72] shown in Table 1 were also isotropic. The values in the third column correspond to recommended crystallographic radii and the values in fourth column correspond to recommended equilibrium radii. Both values are for isotropic atoms. Batsanov's van der Waals radii of metals in 2011[99] were calculated by using Vinet-Ferrante equation of states by estimating when boiled metals will transform into free atoms and the distance supposed to be van der Waals radii of metals. No mention about coordination numbers was made in this Batsanov's article in 2011 nor the anisotropy of the metal atoms.

Single bond covalent radii of Cordero *et al.*[90] were for crystallographic distances of six-coordinated complexes except for Cu, Ag and Au which complexes with coordination number four or less are considered. All non-metallic elements were limited to their typical coordination numbers (for example 2 for S) but allowed for higher coordination numbers but didn't specify that any more in detail. The amount of data used was extensive. For example S single bond radius was based on 10 000 crystal structures and the smallest amount of data of the elements shown in Table 1 was 113 for Au.

Pyykkö's and Atsumi's covalent radii for single[86] and double[87] bond used both experimental and theoretical values with typical coordination numbers as data. All the radii obtained by them were treated equally and then obtained self-consistently through least-squares fit, which was not the case for values of Cordero *et al.*[90]

Pyykkö used following coordination numbers for single bond radii: C (4), N (mainly 3), O (2), S (2), Cl (1), Fe (4), Ru(4), Rh(3), Cu(1), Ag (1) and Au (1).[86] Pyykkö[85] explained that the partially the differences between his and values of Cordero *et al.* are due to differences in coordination number of input data.

Pyykkö's double bond radii were calculated from different systems like from MCH_2^{2-} system for M = Ru; MCH_2^- system for M = Rh; MCH_2^+ system for M = Cu, Ag and Au; $C=CH_2$, H_2EE', E = C–Pb, E' = O–Te for group 14; HE=EH and HN=E'H, E = N–Bi and E' = As–Bi for group 15; $HE=E^+$, E = O–Po for group 16 and $H_2C=E^+$ (E = F–At) for halogens.[87] Batsanov's book[100] was not available but his single and double bond values were taken from Pyykkö's[85] review in 2015.

Table 1. van der Waals, covalent single bond and covalent double bond radii of selected elements in Å. Abbreviations h.s. and l.s. stand for high spin and low spin complexes, respectively. Further details of the radii are given in body text.

	van der Waals radius				single bond radius			double bond radius	
Reference	77	72	72	99	90	86	100	87	100
Year	1964	2001	2001	2011	2008	2009	2008	2009	2008
C	1.70	1.7	1.96	-	-	0.75±3	0.77	0.67±3	0.67
Csp^3	-	-	-	-	0.76±1	-	-	-	-
Csp^2	-	-	-	-	0.73±2	-	-	-	-
N	1.55	1.6	1.79	-	0.71±1	0.71±3	0.73	0.60±3	0.625
O	1.52	1.55	1.71	-	0.66±2	0.63±3	0.72	0.57±3	0.605
S	1.80	1.8	2.06	-	1.05±3	1.03±3	1.03	0.94±3	0.94
Cl	1.75	1.8	2.05	-	1.02±4	0.99±3	0.99	0.95±3	0.89
Fe	-	2.05	2.27	1.86	-	1.16±3	1.31	1.09±3	1.17
Fe h.s.	-	-	-	-	1.32±3	-	-	-	-
Fe l.s.	-	-	-	-	1.52±6	-	-	-	-
Ru	-	2.05	2.37	1.90	1.46±7	1.25±3	1.31	1.14±3	1.17
Rh	-	2.0	2.32	1.93	1.42±7	1.25±3	1.27	1.10±3	1.20
Cu	1.40	2.0	2.27	1.89	1.32±4	1.12±3	1.12	1.15±3	-
Ag	1.72	2.1	2.37	2.05	1.45±5	1.28±3	1.27	1.39±3	-
Au	1.66	2.1	2.41	1.80	1.36±6	1.24±3	1.24	1.21±3	-

Pyridine-4(1*H*)-thione is the most widely used ligand in the experimental part of this thesis. S–C bond distances of it can be used to estimate whether a molecule exists in thiol or thione form which form it's more likely to exist. Electronegativities of S and C are 2.5 in Pauling's scale so the bond is nonpolar and thus 100 % covalent. Even though, electronegativities of elements with different hybridization are different, this effect is assumed to be negligibly small when van der Waals and covalent bond lengths are considered. The carbon is *sp*^{2} hybridized. By using values in Table 1 covalent radii for *sp*^{2} carbon in S–C bond is expected to be 1.76 Å or 1.78 Å. For S=C the distance is 1.61 Å. These values are used in the experimental part for single crystal structures of this thesis.

5 Molecular modelling studies of metallophilicity

Metallophilic interaction has been researched using molecular modelling methods. Especially metallophilicity of group 11 compounds have been investigated with molecular modelling methods. Because dispersion interaction is crucially important in metallophilicity, it's important to choose molecular modeling method which takes dispersion interaction into account. Simple hybridization picture of Hartree-Fock (HF) does not do that and that's why monomer interaction energy curves for example [X–M–PR$_3$]$_2$ are repulsive at HF-level.[56, 101-103] X is variety of groups like halogens, methyl and methanethiolate (H$_3$CS$^-$). Chemists have been aware of this flaw of HF for more than two decades.[56] Another reason for the repulsive interaction is that HF describes electrostatic interaction moderately well.[104] Instead the interaction is attractive in post-HF MP2 level.[56, 101-103] Based on these observations it is concluded that metallophilic interaction (or van der Waals interaction) is dispersive and is also strengthened by relativistic effects.[56, 60, 101-103] For example for [Cl–Au–PH$_3$]$_2$ interaction potential is decreased by 27 % if relativistic effects are omitted at fixed geometry.[60]

Post Hartree-Fock method MP2 has been in almost exclusive used in metallophilicity studies before 2004.[101] However, it has been noticed that MP2 may not be the best method for studies of metallophilicity because the metallophilic interaction of two atoms of a transactinide element Rg (Z = 111, in group 11) in [Cl–Rg–PH$_3$]$_2$ is smaller than other [Cl–M$_{group\ 11\ element}$–PH$_3$]$_2$ compounds when dihedral angle P^1–M^1–M^2–P^2 is fixed to 90°.[101] Application of QCISD (Quadratic configuration interaction with single and double excitations) method, CC (Coupled cluster) method, CCSD (Coupled cluster with single and

double excitations) and CCSD(T) (Coupled cluster with single and double and perturbative triple excitations) for $[Cl–M_{group\ 11\ element}–PH_3]_2$ revealed that metallophilic interaction is actually decreased when going from Ag via Au to Rg which is opposite to MP2 method.[101] As a result silver has the strongest metallophilic attraction in the group 11 among $[Cl–M_{group\ 11\ element}–PH_3]_2$ compounds.[101]

MP2 method has been estimated to result too high energies for metallophilic interaction because it's generally know that MP2 often overestimates van der Waals interactions.[105, 106] For example in MP2 calculations of Magnko *et al.*[105] the interaction energies for $[X–M–PH_3]_2$ compounds between monomers "may well be too large by anything between 0 and 25 %".

In theoretical studies of metallophilicity basic set superposition error (BSSE) is possibly very considerable problem.[101] Basic set superposition error arises when relatively small basis set is used in a quantum mechanical calculation to describe the interaction between two parts of the same molecule or two molecules.[107] When two molecules approach each other from long distance their orbitals begins to overlap.[107] At relatively short distances where overlap is significant, BSSE comes up because when molecule doesn't have enough functions to describe its own molecular orbitals and it delocalizes partially its electron density into a broader area, to empty and diffuse orbitals of other nearby molecules.[107, 108] This is normal behavior to small extend but to further extend it's too much because its own orbital description becomes defective and results overbinding.[105, 107] Overbinding is a problem especially for systems containing weak interactions.[105] For those systems, BSSE might be as great as the interaction energy itself.[109] The choice of basic sets in generally speaking important in all quantum chemistry but because of BSSE it's especially important in the studies of metallophilicity.[101]

To correct BSSE, counterpoise correction (CPC) method has been developed more than 40 years ago by Boys and Bernadi.[110] However, computationally the CPC method at correlated level is costly because instead of a single calculation in the composite basis, the CPC requires (n+1) calculations in the composite basis.[108, 111] (The n is the number of monomers.)[111] CPC often overcorrects superposition error.[108] In the CPC method a low-lying vacant orbital of one molecule is placed into an energy minimum position with respect to another molecule.[107] This is done to the other molecule in a similar manner and CPC method gives the decrease in energy in the system under study with particular combination of basic sets and correlation methods in use as a result.[107]

CPC method is one example of local correlation methods which has advantages over conventional methods and is almost ideally suited for studies of van der Waals interaction.[108, 111, 112] Local treatment of electron correlation results significant computational savings.[108, 111] Local energy gradients are scarcely contaminated by BSSE which results practically speaking BSSE-free geometries.[108, 111, 112] Local treatment of electron correlation enable energy partitioning of intermolecular interaction energy into individual components arising from different excitation classes.[108, 111, 112] It is done by separating the individual localized molecular orbitals into the equivalent orbital domains down to frontiers of the single monomer subunits. The possible double substitutions are classified as shown in Scheme 5.[111, 112]
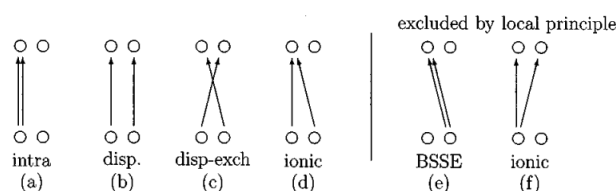
Scheme 5 Schematic presentation of the different double excitation classes of local correlation methods in the context of intermolecular interactions. The upper and lower circles represent different monomers in the ground and excited states, respectively.[111, 112]

Those local contributions have clear physical meanings.[108, 111, 112] Only four of those double excitation classes are included in a local treatment.[111, 112] They are (a) intramolecular correlation, (b) dispersion, (c) dispersion exchange and (d) ionic contribution shown in Scheme 5 and described more in detail in the literature.[111, 112] Two excitation classes are excluded and they are (e) and (f) shown in Scheme 5.[111, 112] (e) is double cross-excitation from one monomer unit to the other virtual space and is mainly responsible for BSSE.[111, 112] (f) is an ionic excitation which contribution to the total energy is assumed to be small and it has noticed to be smaller than basic set truncation error for $(H_2O)_2$.[111]

One example of local correlation methods is local second-order Møller-Plesset perturbation (LMP2) method which offers an efficient way to determine BSSE-free geometries.[111] The reason for developing local correlation method LMP2 was that it has an inherent advantage that its CPCs are small.[105, 108, 111] As an example for $[Cl–Au–PH_3]_2$ system the interaction energies (E_{int}) in calculated equilibrium the energy difference for LMP2 with and without CPC is about 2 kJ/mol and for MP2 8 kJ/mol for a certain basis set.[105] Runeberg *et al.* have

concluded the same for [H–Au–PH$_3$]$_2$ that the energy difference between LMP2/VDZP and LMP2(CP)/VDZP systems is about 2 kJ/mol but for equivalent MP2 system the energy difference is 10 kJ/mol.[112] (VDZP stands for valence double-zeta plus polarization basic set.)

LMP2 has multiple advantages over traditional MP2 in addition that its CPCs are small because BSSE error is substantially decreased into nearly negligible extent.[105, 111] LMP2 enables energy partitioning expressed by localized molecular orbitals (LMO) as described earlier.[105, 111] LMP2 calculations are considerable lighter than the corresponding MP2 calculations which results computational savings.[105, 111]

The energy partitioning of LMP2 has resulted in a better understanding of aurophilic interactions. At long distances for [H–Au–PH$_3$]$_2$ and [Cl–Au–PH$_3$]$_2$ interaction is mainly dispersive (Figure 10). Near the equilibrium distance dispersion and ionic contributions are of similar size (Figure 10). At the equilibrium distance for [H–Au–PH$_3$]$_2$ dispersion and ionic contributions are 126 % and 108 % of the total interaction energy and 133 % and 81 % for [Cl–Au–PH$_3$]$_2$ at MP2/AVTZ level. (AVTZ stands for augmented correlation-consistent valence-triple-zeta.) The great extent of ionic contribution is surprising. The research of Runeberg *et al.* also resulted that dispersion exchange effects to the energy is negligible and intramolecular correlation is repulsive and is 52 % of the total interaction energy of [H–Au–PH$_3$]$_2$ at the equilibrium distance.[112]
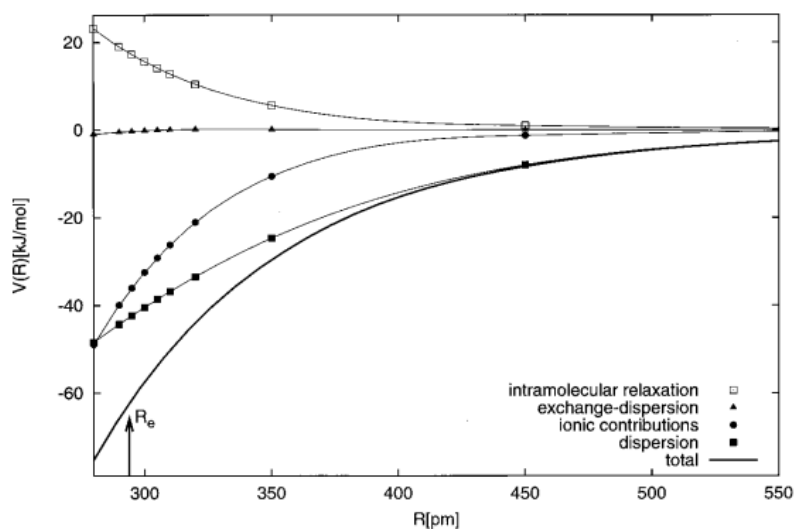
Figure 10. Correlation contributions to the LMP2/AVTZ interaction energy in [H–Au–PH$_3$]$_2$. R$_e$ stands for the equilibrium distance.[112]

It was also concluded that for [H–Au–PH$_3$]$_2$ the ionic attraction decreases exponentially (e^{-R}), while the dispersive interaction decreases asymptotically (R^{-6}).[112] The comparison of quasirelativistic and nonrelativistic pseudopotentials results of [H–Au–PH$_3$]$_2$ for gold at LMP2/AVTZ level ensued that equilibrium distance was shortened by 6 % (19.0 pm) and the interaction energy was increased by 7,5 kJ/mol (28 %) by reason of relativity.

The interaction energy of [H–Au–PH$_3$]$_2$ is dominated by the double excitation from the gold 5d orbitals. However this [5d,5d] pair-excitation does not contribute with 100 % to the attraction but instead 42 %. Also the other significant contributions exist in which one electron is excited from the gold 5d shell into various bonds which totally contribute as much to the attraction as [5d,5d] pair-excitation alone. Those contribution are [5d,Au–H] 21 %, [5d,Au–P] 12 % and [5d,P–H] 11 %. As a result, 86 % of the attraction is from the excitations in which at least one gold 5d orbital is involved. Similar results are found to [Cl–Au–PH$_3$]$_2$; [5d, 5d] contributes with 34 % to the total attraction, [5d,Au–P] with 13 %, [5d,P–H] with 11 %, [5d,Cl(lone pair)] with 11 % and [5d,Au–Cl] with 10 % to the total attraction.[112]

Multiple articles[56, 105, 111] address that density functional theory (DFT) is not suitable for accurate studies of molecular clusters because it cannot describe van der Waals interaction because these interactions are not related in any straightforward way to the electron density. Pyykkö[56] underlines an important point for quasi rectangular compound [Au(i-mnts)]$_2$$^{2-}$.

(The abbreviation i-mnts stands for 1,1-dicyanoethene-2,2-thioselenolate, $(SSeC=C(CN)_2)$.[56]) The point is that even though in two different researches made for two articles failed to find any interatomic electron density between metal atoms of $[Au(i\text{-}mnts)]_2^{2-}$, it does not prove there's no bonding interaction between Au atoms.[56]

However, DFT calculations are used in many articles.[104, 105, 113] In some of them the geometry of monomers like [X–Au–PH$_3$], X = Cl, H, have been optimized using DFT but interaction between monomers are investigated using correlation methods like LMP2.[105]

New DFT methods applicable on investigation of the van der Waals interaction have been developed. A new density functional dispersion corrected (DFT-D) method has been developed for the elements 1–94 and its third version, DFT-D3, published in 2010. It has been compared with three different DFT methods and resulted that the DFT-D method has all the best properties of those three methods. Only two global parameters need to be adjusted for each density functional. One major advantage is that atom connectivity information is not needed instead only the coordinates of atoms in Cartesian coordinates are needed in addition to knowledge of atomic numbers.[114]

Another diffusion corrected DFT method, an exchange-hole dipole moment (XDM) model has been used with the range-separated hybrid functional LC-ωPBE (long range corrected hybrid of Perdew-Burke-Ernzerhof exchange functional).[113] Its binding energies are about 3–4 times more accurate than MP2 achieving error of 6.00 kJ/mol for group 11 [H–M–PH$_3$]$_2$ dimers when the reference has been complete-basis-set extrapolated coupled-cluster (CCSD(T)) method.[113]

5.1 Ligands and metallophilic interaction

Ligands affect the metallophilic interaction energy and the distance between monomers. Increasing softness of X in [X–Au–PH$_3$]$_2$ species increases the interaction energy between monomers in MP2 level.[60] The order is F < H < Cl < Me < CN < Br < HC≡C < I < SMe in which Me stands for methyl.[56, 60] In one article, the position of Me is between F and H.[103] The interaction energy of [I–Au–PH$_3$]$_2$ is 49 % greater than the interaction energy of [F–Au–PH$_3$]$_2$.[60] Also the interaction energy affects to the Au–Au distances but the order seems to be random at the first sight compared to the softness of the ligand.[60] However, within halogen group the greater the interaction, the smaller distance.[60] The same is

observed for hydrocarbon ligands Me and HC≡C.[60] However any general trends of the interaction energy $V(R_e)$ of $[X–Au–PH_3]_2$ has not been able to find for all types of ligands.[60] The $V(R_e)$ has been tried to collate with Au Mulliken charge, charge of natural bond orbital, HOMO and LUMO energies and dipolar moments but the correlation between $V(R_e)$ and those parameters has not been noticed.[60]

For $[Cl–Au–L]_2$ compounds, the nature of the L ligand affects to the $V(R_e)$. The order of increasing interaction energy is $NF_3 < CO < CN–Me < PF_3 < SH_2 < CN_2$ (f–f) $< C_3H_2$ (e–e) $< CN_2$ (e–e) $< NHC–H$ (f–f) $< NH_3 < PH_3 < NHC–Cl$ (f–f) $<$ pyridine (f–f) $<$ triazine (f–f) $< PHC–H$ (f–f) $<$ triazine (e–e) $< PHC–N$(f–f) $< PHC–N$(e–e) $< PHC–H$ (e–e) $< CP_2 < NHC–Me$ (f–f) $< NHC–H$ (e–e) $< NHC–Cl$ (e–e), where PHC means cyclic diphosphinocarbenes and NHC means *N*-heterocyclic carbenes. NHCs are compounds with five membered rings with one C=C and a carbene carbon between two nitrogen atoms. The notation (f-f) means the face-to-face conformation in which plane of ligand is orthogonal to the Au–Au line. The notation (e-e) means the edge-to-edge conformation in which the plane of ligand is collinear with the Au–Au line. The notation after PHC or NHC like N in PHC–N means certain substitution to the basic five membered cyclic diphosphinocarbenes or *N*-heterocyclic carbenes. The N means that one of the double bond carbons have been replaces with nitrogen. H means that both double bond carbons have one H attached to them. Similar way, Cl means that both double bond carbons have one Cl attached to them instead of H. However, Me means that structure similar to H-structure with the exception of there're methyl group on the nitrogen atoms next to the double bond.[115]

6 Structural classes of EMACs

In the introduction part some types of EMACs were shortly presented. In this chapter we will discuss the classes more in detail. EMACs are divided into two groups in respect to covalent bonding between metal atoms in this thesis. Classes A and B are classes of at least partially unsupported and fully supported EMACs, respectively. The class A can be divided further into 3 classes. The classification could be also performed based on the type of ligands used. All four classes are herein:

- Class A1: There's no intramolecular metallophilic interaction, all the metallophilic interaction is intermolecular and the metallic chain is very straight.

- Class A2: There're both intermolecular and intramolecular metallophilic interactions and the metallic chain is very straight.

- Class A3: Like class A1 but the metallic chain is not straight and it may contain clusters like ⌐M◇M⌐ in the chain.

- Class B: There're only intramolecular interactions and the length of scaffold ligands define the length of the chain.

6.1 Class A1

One of the class A subclasses is very linear unsupported EMACs i.e. class A1. There's no intramolecular metallophilic interaction but all the metallophilic interaction is intermolecular. Many rhodium compounds belong to this group and those compounds have infinite linear chains. One of them is $[Rh(2,2'\text{-bpy})(CO)_2][RhCl_2(CO)_2]$ (2,2'-bpy = 2,2'-bipyride) shown in Figure 11.[116] In the structure of another Rh-chain, $[Rh(phen)(CO)_2][RhCl_2(CO)_2]$ (phen = 1,10-phenanthroline), there're two crystallographically distinctive chains.[116] Infinite chains of cationic $[Rh(H_2bim)(CO)_2]^+$ (H_2bim = 2,2'-biimidazole) with counter anion of Cl^-, NO_3^- and PF_4^- has been synthesized.[117] In these compounds hydrogen bonding occurs from one of two nitrogen atoms of the ligands to the anion.[117] $[Rh(Benzoylacetonato-\kappa^2O,O')(CO)_2]$ forms also infinite chains in which has two different $Rh\cdots Rh$ distances 3.308 Å and 3.461 Å.[118] Benzoylacetonato is anion of $PhC(=O)CH=C(OH)CH_3$. The A1 group includes trimeric $[M(NH_3)_6][Ag(CN)_2]_3 \cdot 2H_2O$, M = Ru, Co or Cr in which metal in anion doesn't interact with silver at all so the all the metallophilic interaction is only between three Ag ions.[119] $[NMe_4][Rh(ox)(CO)_2]$ (ox = oxalate, $(COO)_2^{2-}$) is a group A1 compounds which consists of infinite chains.[120] Selected bond distances and angles for these and other compounds are presented in Appendix 1 (Tables A1T1A and B).
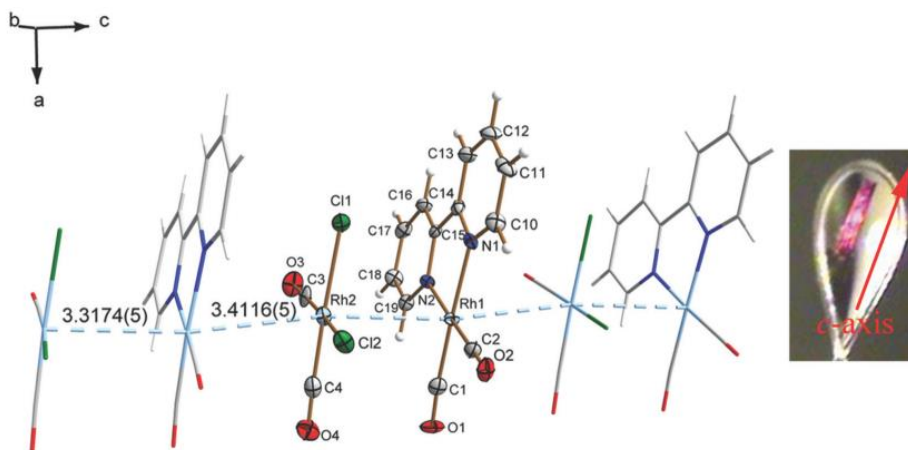
Figure 11 Left: The thermal ellipsoid plot of a type A1 compound: [Rh(2,2'-bpy)(CO)$_2$][RhCl$_2$(CO)$_2$] (at 100 K) at 50 % probability level between adjacent two [Rh(2,2'-bpy)(CO)$_2$][RhCl$_2$(CO)$_2$] complexes. Right: A crystal of the same compound in a cryo-loop with the direction of the c-axis of the unit cell, which shows the lustrous shine of the crystal. [116]

Double salts are one type of A1 compounds which demonstrates metallophilic interaction clearly. In this work term "double salts" means species which anions and cations both contain metal ions and they alternate. Originally the term has been used for species (M)(M')X$_n$.[38]

Here are examples of different kinds of A1 compounds. A compound [methyl violen][AuI$_2$]$_2$ (methyl violen is *N,N'*-dimethylated 4,4'-bipyridine)[121] has anionic [AuI$_2$]$^-$ chains; [AuI(*o*-xylylNC)]$_n$ (*o*-xylylNC = 2-isocyano-1,3-dimethylbenzene)[122] has neutral chains and {[Rh(2,2'-bpy)(CO)$_2$][RhCl$_2$(CO)$_2$]}$_n$ (Figure 11)[116] and {[Au(py)$_2$]$^+$[Au(SCN)$_2$]$^-$}$_n$[123] (py = pyridine) has double salt chains. Selected bond distances and angles for these and other compounds are presented in Appendix 1 (Tables A1T1A and B).

Compounds [Au$_2$Cl$_2$(μ-1,8-di(phospholan-1-yl)octane)]$_n$ and [Au$_2$Cl$_2$(μ-1,8-di(phospholan-1-yl)decane)]$_n$ have bidentate aliphatic ligands with five membered phosphorus containing ring. Phosphorus atoms in each end of the ligand binds to a gold atom. Gold atoms form infinite one-dimensional chains which are separated by the ligand. According to the definition given above for class A1 compound these compounds are A1 compounds. However, the structures can be considered as flattened nanotubes. The structures of these compounds are shown in Figure 12. Selected angles and distances of these two compounds are shown in Appendix 1 (Tables A1T1A and B).[124]

[Au$_2$Cl$_2$(μ-1,8-di(phospholan-1-yl)hexane)]$_n$ has similar structure than the two other compounds but instead of forming flattened nanotubes it forms infinite chains perpendicular to the gold chain. The chains are organized repeating of [-Au-bisphosphine-Au-] units. However, this compound doesn't have a string of gold atoms instead only two gold atoms close to one another locally. The distance between gold atoms is 3.0941(2). Corresponding compounds with odd number of carbons between phosphorus atoms (pentane, heptane, nonane & undecane) formed cycles but there's no intercyclic (neither intracyclic) metallophilic interaction.[124]
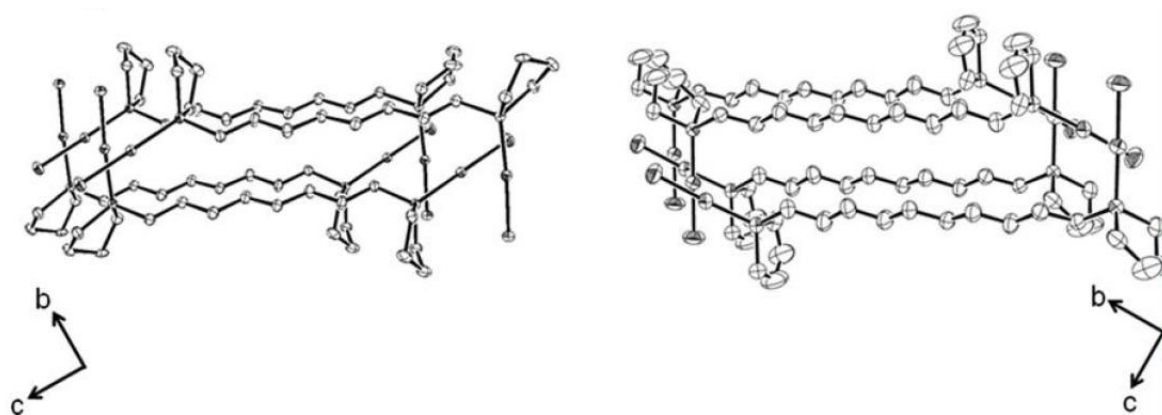
Figure 12. The structures of [Au$_2$Cl$_2$(μ-1,8-di(phospholan-1-yl)octane)]$_n$ (left) and [Au$_2$Cl$_2$(μ-1,8-di(phospholan-1-yl)decane)]$_n$ (right). The nanotubes are along crystallographic *a* axis. Ellipsoids are drawn at the 50% probability level. H atoms are omitted for clarity.[124]

Two different polymorphs of {[Au(py)$_2$][Au(SCN)$_2$]}$_n$ were observed one of which (a) was linear as shown in Figure 13 (left). Another polymorph (b) was less linear with only one of the angles between three gold atoms was reported as 102.44(1)°. The polymorph is shown in Figure 13 (right). The lack of information was probably due to the fact that gold distance was so much longer that no interaction was assumed. Crystals of both polymorphs were colorless, clear and visually nearly identical. Polymorph (a) was produced by dissolving AuSCN to pyridine in annealing tubes and layered *n*-pentane and (b) was AuSCN was dissolved in pyridine in a round-bottomed flask and petroleum ether was adding. During the addition the mixture was stirred and petroleum ether was added until the solution fuzzed permanently. Polymorph (a) was crystallized in refrigerator and (b) in freezer.[123]

Polymorph (b) of $\{[Au(py)_2][Au(SCN)_2]\}_n$ is between polymeric and tetrameric chain because the longest distance between gold atoms is 4.1114(4) Å. Anisotropic crystallographic van der Waals radii is 2.1 Å[72] which makes the van der Waals distance 4.2 Å which is on the edge of whether there's attractive interaction or not. Authors of $\{[Au(py)_2][Au(SCN)_2]\}_n$ concluded that there's no attractive interaction. That is a reasonable conclusion.
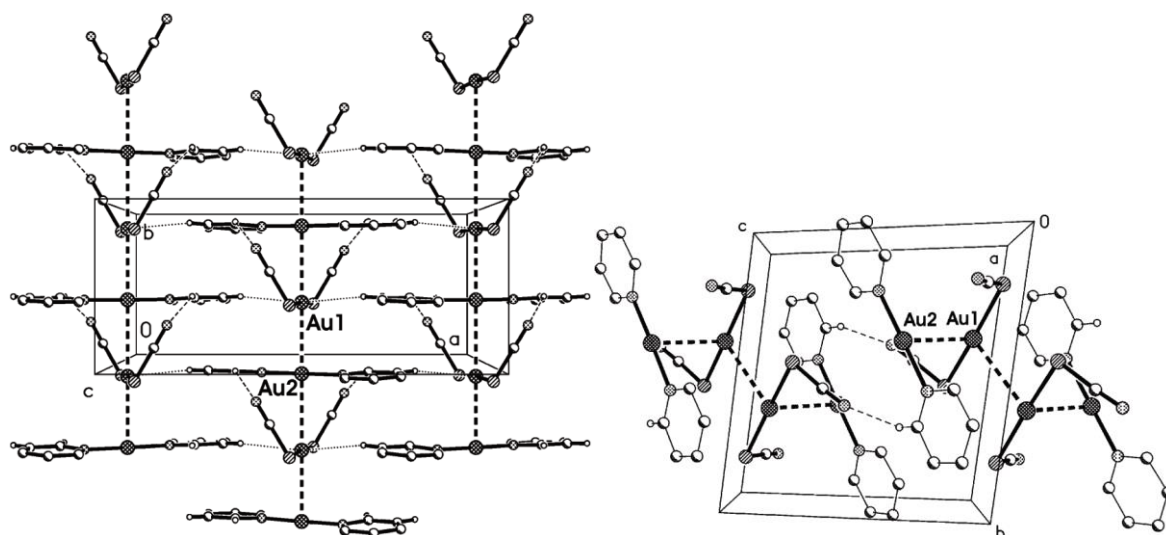
Figure 13. Two polymorphs of $\{[Au(py)_2][Au(SCN)_2]\}_n$ with their unit cell visible. (Left) (a) is linear polymorph with a view along to the c axis and (b) less linear polymorph with a view along the a axis. Dashed lines indicate aurophilic interactions.[123]

6.2 Class A2

Class A2 consists of parts which has covalent binding between metal atoms but these parts are connected with each other noncovalently. An example of the class A2 compound is $[Ru_2\{\mu-O_2C(3,5-CF_3)_2C_6H_3\}_2(CO)_5]_2$ which consists of two covalent $[Ru_2\{\mu-O_2C(3,5-CF_3)_2C_6H_3\}_2(CO)_5]$ units which Ru ions have metallophilic attraction between adjacent $[Ru_2\{\mu-O_2C(3,5-CF_3)_2C_6H_3\}_2(CO)_5]$ units (Figure 14).[125] Many rhodium blue compounds belong to this family. Rhodium blues contain four rhodium atoms in a linear fashion, Rh atoms have metal-metal interactions and Rh atoms have mixed valencies.[42] A rhodium blue compound, $[\{Rh(\mu-pz)(CNt\text{-}Bu)_2\}_4](PF_6)_2$, is shown in the right side of Figure 8.[42] (pz stands for pyrazole anion $C_3H_3N_2$.)

As mentioned before, $[Rh(H_2bim)(CO)_2]^+$ compounds are the A1 compounds but when H_2bim is changed into Me_2bim (Me_2bim = 1,1'-dimethyl-2,2'-biimidazole) the A2 compounds occur. $[Rh_2Cl_2(CO)_2(\mu-Me_2bim)]$ has been observed to form either infinite linear chains or tetranuclear moieties.[117] In both structures Me_2bim is bridging ligands within dimeric Rh_2-unit. Geometry of each rhodium is square planar so no axial ligands observed in these structures. Related $[Rh_2Cl_2(CO)_2(\mu-Et_2bim)]$ and $[Rh_2Cl_2(CO)_2(\mu-Pr_2bim)]$ (Et_2bim = 1,1'-diethyl-2,2'-biimidazole, Pr_2bim = 1,1'-dipropyl-2,2'-biimidazole) has similar infinite chain structure.[126] No metal-metal interaction was found between binuclear $[Rh_2Cl_2(\mu-Bn_2bim)(CO)_2]$, Bn_2bim = 1,1'-dibenzyl-2,2'-biimidazole, motifs.[117] The reason for this was thought to be due to bulkier benzyl substituents compared to metyl or hydrogen group[117] The π-π stacking of benzyl groups and repulsion of CH_2 motifs with each other in Bn most likely prevent planar Rh motifs to be colinear and thus prevents piling up of Rh plane motifs. Selected bond distances and angles for most of these A2 compounds are presented in (Tables A1T2A and B). The intramolecular metal-metal distance in $[Rh_2Cl_2(\mu-Bn_2bim)(CO)_2]$ was notationably larger 3.4720(4) Å than in the other compounds.[117]
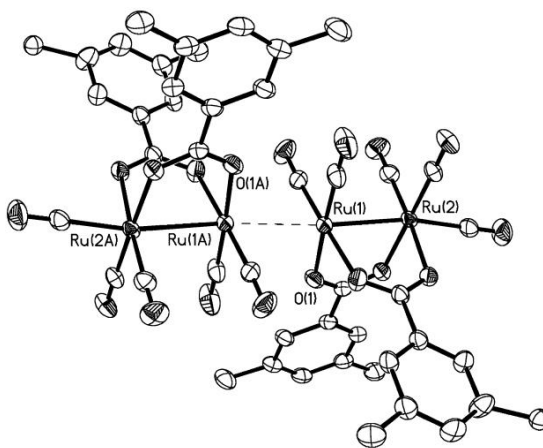
Figure 14. The structure of $[Ru_2\{\mu-O_2C(3,5-CF_3)_2C_6H_3\}_2(CO)_5]_2$ as thermal ellipsoid presentation which has been drawn at 35 % probability level. H and F atoms have been omitted for clarity.[125]

6.3 Class A3

In the class A3 the metal-metal chain is not as linear as in the class A1. The chain it may contain clusters like $[Au_2Ag_2(C_6F_5)_4(\mu-N\equiv CCH_3)_2]_n$ contains.[47] Its structure is shown in

Figure 15. In its structure there is no covalent bonding between metallic units. Similar structures are $[Au_2Cu_2(\mu\text{-}C\equiv C\text{-}R)_4]_n$ type compounds which has extensive metallophilic interaction. They have been synthesized R being 2-hydroxypropan-2-yl, 1-hydroxycyclohexyl, 4-hydroxy-1,7-dimethylheptan-4-yl and hydroxydiphenylmetyl.[46] The starting materials were $[Au(SC_4H_8)Cl]$, $[Cu(NCMe)_4]PF_6$ and the corresponding alkyne in the presence of triethylamine. The ligand SC_4H_8 is tetrahydrothiophene which is a sulphur version of tetrahydrofuran. The generalized reaction has been shown on the left side of Figure 16 and $[Au_2Cu_2(\mu\text{-}C\equiv C\text{-hydroxydiphenylmethyl})_4]_n$ as one example of these compounds is shown on the right side of the same figure. If the R is a rigid bridging moiety like 9-hydroxy-9H-fluoren-9-yl, the polymeric-like formation can be chemically prohibited and discrete $[Au_2Cu_2(\mu\text{-}C\equiv C\text{-}R)_4]$ units will form. If $H\text{-}C\equiv C\text{-}Ph$ was used instead of hydroxyalkynes which were mentioned above, a dodecanuclear molecular cluster, $[Au_6Cu_6(\mu\text{-}C\equiv C\text{-}Ph)_{12}]$, was formed and it was considerably less stable than the compounds mentioned above.
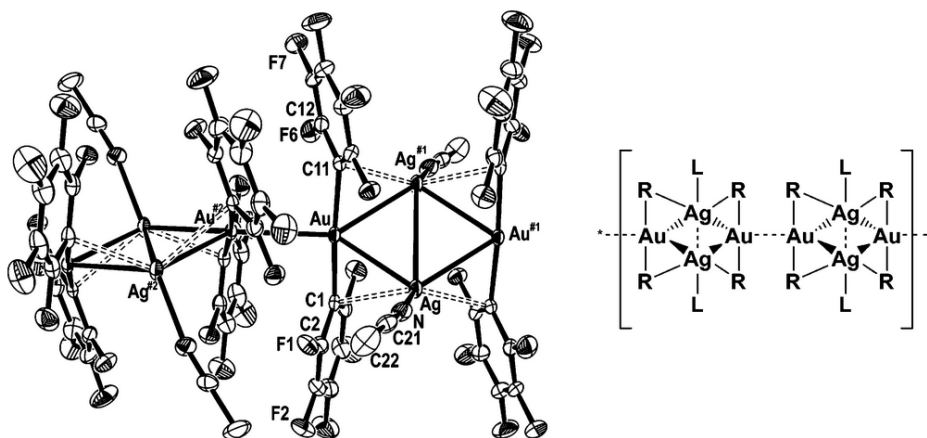
Figure 15 (Left) part of the crystal structure of $[Au_2Ag_2(C_6F_5)_4(\mu\text{-}N\equiv CCH_3)_2]_n$ polymeric chain with labels.[47] Hydrogen atoms have been omitted for clarity. (Right) schematic picture of the structure.
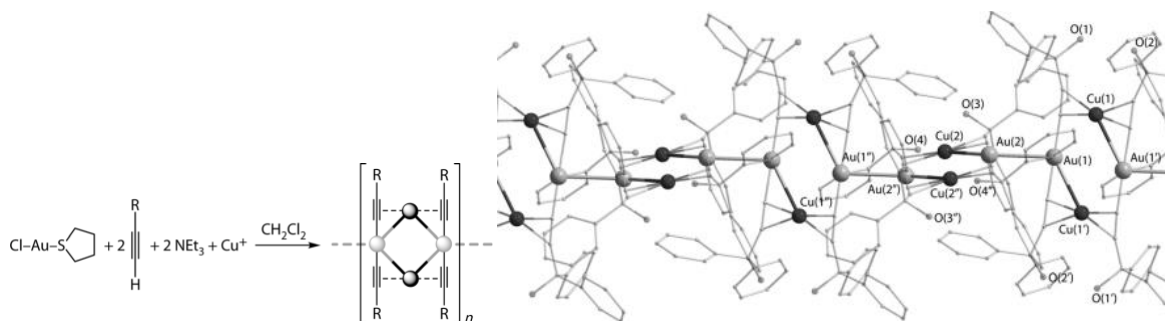
Figure 16. (Right) chemical reaction of making polymeric structures of type of $[Au_2Cu_2(\mu-C{\equiv}C–R)_4]_n$ and (left) example of one structure in which R is hydroxydiphenylmethyl.[46]

The structure of $[Au_2Cu_2(\mu-C{\equiv}C–R)_4]_n$, R = 2-hydroxypropan-2-yl, consists of −Au–Cu–Au–Cu− type helical chains rather than chains containing pentaatomic rings as shown as a product in the schematic picture on the left side of Figure 16. However when R = 1-hydroxycyclohexyl, 4-hydroxy-1,7-dimethylheptan-4-yl and hydroxydiphenylmetyl the structure is like in Figure 16. The intermetallic Cu···Au interactions in complex $[Au_2Cu_2(\mu-C{\equiv}C–R)_4]_n$, R = 2-hydroxypropan-2-yl, range within 2.846–2.955 Å. The distances between golden atoms are 3.401 Å and 3.421 Å which are greater than two van der Waals radii of Au (3.32 Å). When R = 1-hydroxycyclohexyl, the intergold distances are 2.9602(8), 3.4031(6) and 3.3396(8) Å and the Au···Cu distances are 2.9885(12), 3.0085(12), 3.0566(12) and 3.0708(12) Å. When R = 4-hydroxy-1,7-dimethylheptan-4-yl, the Au···Au distances are 2.9982(5) and 3.0045(5) Å and Au···Cu distances 2.8793(11), 2.9251(11), 3.1134(11) and 3.1144(11) Å. The same values when R = hydroxydiphenylmetyl are 2.9916(2), 3.1255(4), 3.9002(2) and 3.9220(2) Å for Au···Au distances and 2.9006(4), 2.9296(4), 3.0946(3) 3.1255(4) Å for Au···Cu distances. On the whole, Au···Au distances for these four $[\{Au_2Cu_2(\mu-C{\equiv}C–R)_4\}_n]$ species are 2.9602(8)–3.9220(2) and Au···Cu distances 2.846–3.1255(4) Å.[46]

Polymeric cation $[(\mu-Ag)\{Au_2(\mu-mes)_2(\mu-dppe)\}]_n^{n+}$ in $[Au_2Ag(\mu-mes)_2(\mu-dppe)][SO_3CF_3]$ is shown in the left side of Figure 8.[41] In its formula mes is mesityl i.e. 1,3,5-trimesityl group and dppe is 1,2-bis(diphenylphosphano)ethane. Intermetallic bond lengths and angles for this compound have been shown in Table 2. As a summary, Au···Au distances are 2.9226(8)–2.9951(12) Å and Au···Ag distances 2.7560(6)–2.8506(13) Å in this compound. The intermetallic Ag···Au···Au angles are really close to 150°.

Atoms	Distance (Å)	Atoms	Angle (°)
Au1···Ag1	2.7560(6)	Ag1···Au1···Au2	150.72(3)
Au1···Au2	2.9228(8)	Ag2···Au2···Au1	149.13(3)
Au2···Ag2	2.7807(12)	Ag2···Au3···Au4	150.49(4)
Au3···Ag2	2.7619(13)		
Au3···Au4	2.9226(8)		
Au4···Ag3	2.8506(13)		
Au5···Ag3	2.8024(13)		
Au5···Au5#1	2.9951(12)		

Table 2. Selected intermetallic of polymeric cation [(μ-Ag){Au$_2$(μ-mes)$_2$(μ-dppe)}]$_n^{n+}$ in [Au$_2$Ag(μ-mes)$_2$(μ-dppe)][SO$_3$CF$_3$]. Atom assignment is shown in Figure 8.[41]

A compound (*o*-xylylNC)AuCl, *o*-xylylNC = 2-isocyano-1,3-dimethylbenzene) has infinite, loose and stepped chain structure which consists of linear interconnected Au···Au···Au···Au moieties. The moiety consists of two more closely spaced Au···Au interactions 3.3570(11) Å which are connected by Au···Au distance of 3.6095(12) Å. The angle within the Au···Au···Au···Au moiety i.e. the angle of Au(1)···Au(2)···Au(2') is 97.67(3)°. This Au···Au···Au···Au moiety is connected to adjacent Au···Au···Au···Au moieties by Au···Au distance of 4.0225(12) Å and angle Au(2)···Au(1)···Au(1') of 123.45(2)°. The labels and the structure are shown in Figure 17.[122]
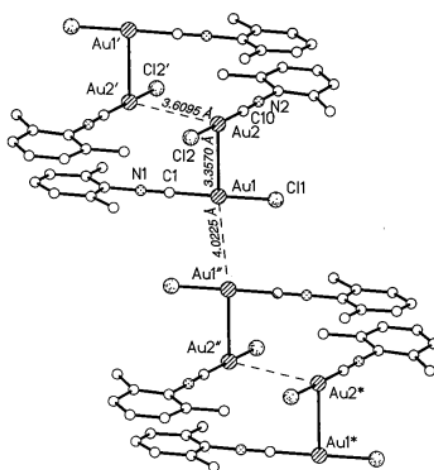
Figure 17 Arrangement of infinite, loose and stepped chain of [AuCl(*o*-xylylNC)]$_n$. Hydrogen atoms have been omitted for clarity.[122]

[AuBr(*o*-xylylNC)]$_n$ has an infinite comb like structure: '_|__|__|__|__|_' in which '|' represents two gold atoms at the top and bottom of the line and '__' contains one gold atom at the center of the line so there're five gold atoms in the unit of '|__|'. The distance between gold atoms in '_' is 3.3480(5) Å and in '|' 3.7071(10) Å. The both horizontal angles ('|__|' and '_|_') are both 170.29(2)°. The angles between horizontal line and rungs i.e. the angles of '|_' and '_|' are 93.50°. [Au(CN)(*o*-xylylNC)]$_n$ has more complicated two-dimensional grid structure and its Au⋯Au connections are shown in Figure 18. The distances of Au(1)⋯Au(2), Au(1)⋯Au(2") and Au(2)⋯Au(3) are 3.4220(6), 3.4615(6) and 3.1706(4) Å, respectively. The angles of Au(1)⋯Au(2)⋯Au(1*), Au(2)⋯Au(1)⋯Au(2"), Au(1)⋯Au(2)⋯Au(3), Au(1')⋯Au(2)⋯Au(3) and Au(2)⋯Au(3)⋯Au(2') are 166.59(1), 169.66(2), 92.38(2), 99.07(2) and 164.97(3)°, respectively.[122]
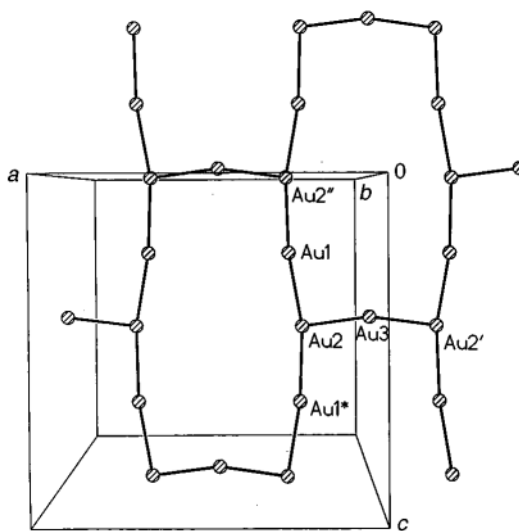
Figure 18. Gold network of [Au(CN)(*o*-xylylNC)]$_n$ in the crystallographic *ac* plane.[122]

6.4 Class B

If all the metal atoms are aided to the closeness of one another by a scaffold ligand and there's no interaction between metals which are bound to neighboring scaffold ligands, the compound is a class B compound. These compounds can be classified according to the scaffold ligand. The most intensively studied and varied class of discrete unidimensional metal arrays is oligo-α-pyridylamine type ligands.[37] For example [Ru$_3$Cl$_2$(μ$_3$-dpa)$_4$] and [Rh$_3$Cl$_2$(μ$_3$-dpa)$_4$] were synthesized in 1996.[54] (dpa is the anion of *syn,syn*-di-2-pyridylamine i.e. *N*-(2-Pyridinyl)-2-pyridinamine.) Oligo-α-pyridylamine-based metal

chains have been prepared at least with Cr, Co, Ni, Cu, Ru, Rh, Pd and Pt.[37] In addition to $[Ru_3Cl_2(\mu_3\text{-dpa})_4]$ and $[Rh_3Cl_2(\mu_3\text{-dpa})_4]$, trinuclear compounds of $[M_3Cl_2(\mu_3\text{-dpa})_4]$ have been also prepared for Cr, Cu, Co and Ni.[127] No $[Ag_3X_2(\mu_3\text{-dpa})_4]$ and $[Au_3X_2(\mu_3\text{-dpa})_4]$ compounds are found in the crystallographic database of Cambridge in January 2016. Aromí estimated in his review article in 2011 that there're around 260 polypyridylamine-based metal chains which nuclearity varies from three to eleven and trinuclear complexes represent 71 % of them.[37]

6.4.1 Heterometallic bis-(2-pyridyl)amine complexes

Also heterometallic oligo-α-pyridylamine complexes have been prepared. The first heterometallic bis(2-pyridyl)amide complex $[CoPdCoCl_2(\mu_3\text{-dpa})_4]$ was published in 2007.[128] Also $[CuPdCuCl_2(\mu_3\text{-dpa})_4]$ and $[CuPtCuCl_2(\mu_3\text{-dpa})_4]$ has been published in 2007.[129] Compounds $[RuRuNiCl_2(\mu_3\text{-dpa})_4]$, $[RuRuCuCl_2(\mu_3\text{-dpa})_4]$ and their monooxidized counterparts $[RuRuNiCl_2(\mu_3\text{-dpa})_4]PF_6$ and $[RuRuCuCl_2(\mu_3\text{-dpa})_4]PF_6$ were prepared in 2008.[130] The structure of $[RuRuCuCl_2(\mu_3\text{-dpa})_4]$ is shown in Figure 19 and the structure of $[RuRuNiCl_2(\mu_3\text{-dpa})_4]$ is isostructural to the former.[130]

The first trimetallic bis-(2-pyridyl)amine complex was $[MoWCrCl_2(\mu_3\text{-dpa})_4]$ and it was printed in 2009.[131] The metal backbone was Mo≡W···Cr but WMoCr chain was unable to synthesize due to polarity of Mo≡W quadrupolar bond to favor MoWCr isomer.[131] Trimetallic $[NiCoRhCl_2(\mu_3\text{-dpa})_4]$ was synthesized in 2013.[132] However, because this thesis concentrates on metals Cu, Ag, Au, Zn, Ru and Rh, no more oligo-α-pyridylamine-based compounds containing other metals than these six mentioned above are given even though far greater deal of articles of oligo-α-pyridylamine based EMACs contains other elements than the six.
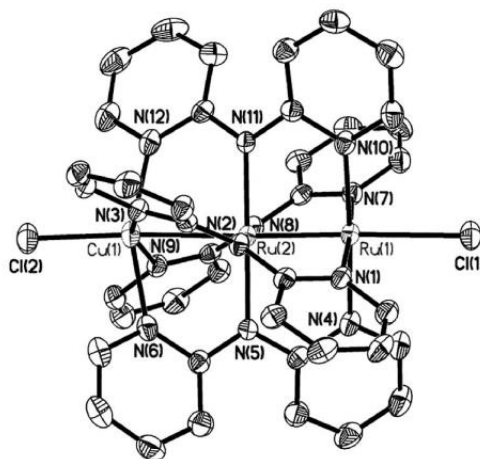
Figure 19. The structure of [CuRuRuCl$_2$(μ_3-dpa)$_4$] which has been drawn at 30 % probability level.[130]

[CuRuRuCl$_2$(μ_3-dpa)$_4$] and [CuRuRuCl$_2$(μ_3-dpa)$_4$]PF$_6$ bond lengths and angles have been determinated by X-ray structures and calculated by spin-unrestricted DFT. Los Alamos core potentials were used to the model 2s2p2d for Cu and 3s3p3d for Ru. The valence shell of Cu and Ru atoms were described at the double zeta level. Also nonmetallic elements were described at double zeta level with one p-type function for atoms coordinating metals. Mayer bond orders have been computed for [CuRuRuCl$_2$(μ_3-dpa)$_4$] and [CuRuRuCl$_2$(μ_3-dpa)$_4$]PF$_6$ and they are 0.986 and 0.934 for Ru–Ru, and 0.235 and 0.016 for Ru···Cu, respectively. Calculations show that metal framework of [CuRuRuCl$_2$(μ_3-dpa)$_4$] consists of two weakly interacting moieties of [Ru$_2$]$^{5+}$ and Cu^{1+}. The electronic structure of the [Ru$_2$]$^{5+}$ moiety resembles the ruthenium core of Ru$_2$Cl(μ-O$_2$CR)$_4$. However, Mayer bond order for Ru···Cu is not negligible because there's a trace of metal-metal bond between Ru and Cu.[130]

6.4.2 Other heterometallic complexes

[Au{μ_3-im(CH$_2$py)$_2$}$_2${Cu(MeCN)$_2$}$_2$](PF$_6$)$_3$ (Figure 20 left) and [Au{μ_3-im(CH$_2$py)$_2$}$_2$ {Cu(MeOH)}$_2$](PF$_6$)$_3$ (Figure 20 right) have interesting vapochromic properties.[133] The ligand im(CH$_2$py)$_2$ is a *N*-heterocyclic carbene: 1,3-bis(pyridin-2-ylmethyl)-2,3-dihydro-1*H*-imidazole. The vapochromic properties have been discussed hereinafter. Intermetallic distances of these two forms are presented in Appendix 1 (Tables A1T2A and A1T2B).
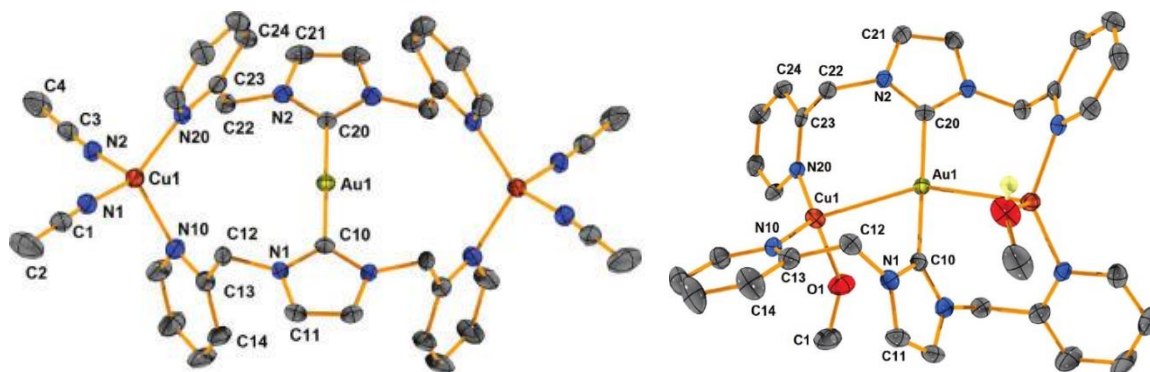
Figure 20. The crystal structure of $[Au\{\mu_3\text{-im}(CH_2py)_2\}_2\{Cu(MeCN)_2\}_2](PF_6)_3 \cdot 2MeCN$ (left) and $[Au\{\mu_3\text{-im}(CH_2py)_2\}_2\{Cu(MeOH)\}_2](PF_6)_3 \cdot 2MeOH \cdot 2Et_2O$ (right) C–H hydrogen bonds , anions and lattice solvents have been omitted.[133]

6.4.3 Homometallic Ru complexes

Synthesis and single crystal structures has been obtained from multiple other trinuclear oligo-α-bipyridylamide ligands with different axial ligand: $[Ru_3Cl_2(\mu_3\text{-dpa})_4]$[54], $[Ru_3(CN)_2(\mu_3\text{-dpa})_4]$[52] and $[Ru_3(NCS)_2(\mu_3\text{-dpa})_4]$[50]. DFT geometry optimization has been executed to $[Ru_3Cl_2(\mu_3\text{-dpa})_4]$, $[Ru_3(CN)_2(\mu_3\text{-dpa})_4]$ and $[Ru_3(NCS)_2(\mu_3\text{-dpa})_4]$ with the PBE0 hybrid density functional.[134] Intermetallic bond distances and angles for $[Ru_3X_2(\mu_3\text{-dpa})_4]$, X = Cl^-, CN^- and NCS^-, $[CuRuRuCl_2(\mu_3\text{-dpa})_4]$ and $[CuRuRuCl_2(\mu_3\text{-dpa})_4]PF_6$ and have been presented in Table 3.

From Table 3 it can be noticed the calculated bond distances are longer than observed ones in $[Ru_3X_2(\mu_3\text{-dpa})_4]$ compounds and Ru–Ru distance increases from X = Cl^- via X = CN^- to X = NCS^- both in theoretical and experimental structures.[134] The discrepancy is probably due to the lattice forces in solid state.[135] Neutral heterotrimetallic compound has shorter inter-ruthenium distance than all neutral homotrimetallic compounds. The angles vary between 165–180°. Two pentaruthenium compounds $[Ru_5Cl_2(\mu_5\text{-tpda})_4]$, (tpda^{2-} tripyridyldiamido dianion, more accurately dianion of N^2,N^6-di(pyridin-2-yl)pyridine-2,6-diamine) and $[Ru_5(NCS)_2(\mu_5\text{-tpda})_4]$ compounds have been synthesized.[51] Their experimental intermetallic distances and angles have been shown in Table 3. R_f-values of crystallographic fitting of $[Ru_5Cl_2(\mu_5\text{-tpda})_4]$ and $[Ru_5(NCS)_2(\mu_5\text{-tpda})_4]$ were 8.08 and 8.38, respectively.

Table 3. Observed and calculated intermetallic distances (Å) and angles (°) of homo- and hetero *syn,syn*-di-2-pyridylamido and tripyridyldiamido compounds of ruthenium. Also temperatures of measured XRD data are shown. In trinuclear compounds notation "Ru–Ru (other)" means that if there're two different distances between ruthenium atoms, the other distance is expressed in this "Ru–Ru (other)" line. [†]The value is an average value. [‡]The article hasn't been available or the value hasn't been mentioned in the article but the value has been obtained from cif-file obtained from the publisher or WebSCD database. *The angle is between Ru_1–Ru_2–Ru_3 in which Ru_3 is the middle one and Ru_1 is at the end of pentaruthenium line. **Structure was optimized based on D_4 symmetry.[50-52, 54, 130, 134]

	$[Ru_2CuCl_2(\mu_3\text{-}dpa)_4]$		$[Ru_2CuCl_2(\mu_3\text{-}dpa)_4][BF_4]$		$[Ru_5Cl_2(\mu_5\text{-}tpda)_4]$	
	Exp.	Calc.	Exp.	Calc.	Exp.	Calc.
Temperature	150(2)		150(2)		150(2)[‡]	
Ru–Ru (inner)	2.246(3)	2.331	2.312(9)	2.308	2.276(1)	2.283
Ru–Ru outer	-	-	-	-	2.283(2)	2.276
Ru–Cu	2.575(3)	2.672	2.510(12)	2.641	-	-
∠ Ru–Ru–Ru/Cu	177.54	-	177.48	-	all 180.00[‡]	~172

	$[Ru_3Cl_2(\mu_3\text{-}dpa)_4]$		$[Ru_3Cl_2(\mu_3\text{-}dpa)_4][BF_4]$	$[Ru_3Cl_2(\mu_3\text{-}dpa)_4][BF_4]_2$	$[Ru_5Cl_2(\mu_5\text{-}tpda)_4]\{[Ru_2Cl(\mu\text{-}OAc)_4]_2Cl\}$	$[Ru_5(NCS)_2(\mu_5\text{-}tpda)_4]$
	Exp.	Calc.	Exp.	Exp.	Exp.	Exp.
Temperature	295[‡]		150(1)	150(1)	150(2)[‡]	150(2)[‡]
Ru–Ru	2.2537(5)[‡]	2.303[†]	2.2939(6)	2.3117(10)	2.2922(8)	2.290(2)[‡]
Ru–Ru (other)	-	-	2.2882(6)	-	2.2832(6)	2.259(1)[‡]
∠ Ru–Ru–Ru	171.17(4)[‡]	165[†]	166.66(3)	172.7(6)	178.77(3)*	all 180.00[‡]

	$[Ru_3(CN)_2(\mu_3\text{-}dpa)_4]$			$[Ru_3(CN)_2(\mu_3\text{-}dpa)_4][BF_4]$
	Exp.	Calc.	Calc.	Exp.
Temperature	150(1)			150(1)
Ru–Ru	2.3738(5)	2.445[†]	2.3943	2.3447(4)
Ru–Ru (other)	2.3794(5)	-	-	2.3487(4)
∠ Ru–Ru–Ru	170.876(19)	172[†]	180.00**	180

	$[Ru_3(NCS)_2(\mu_3\text{-}dpa)_4]$		
	Exp.	Calc.	Calc.
Temperature			
Ru–Ru	2.264(5)	2.314[†]	2.3325
Ru–Ru (other)	2.30(2)	-	-
∠ Ru–Ru–Ru	171	165[†]	180.00**

Also DFT calculations of ruthenium oligo-α-pyridylamide compounds have been performed for tri-, penta-, hepta- and nona-nuclear species. In the absence of symmetry restrictions intermetallic bond angles were shown to deviate from the straight angle as seen in single crystal structures of triruthenium species (see Table 3). The relativistic effects

were also investigated comparing results using nonrelativistic and relativistic basic sets but the relativistic effects didn't have important role in these ruthenium complexes.[134]

[Ru$_5$X$_2$(μ_5-tpda)$_4$], X = Cl$^-$ or SCN$^-$, tpda^{2-} = tripyridyldiamido dianion more exactly the dianion of N^2,N^6-di(pyridin-2-yl)pyridine-2,6-diamine (Figure 21) has been reported in 2008. It was the first pentanuclear EMAC of second row metal published.[51]
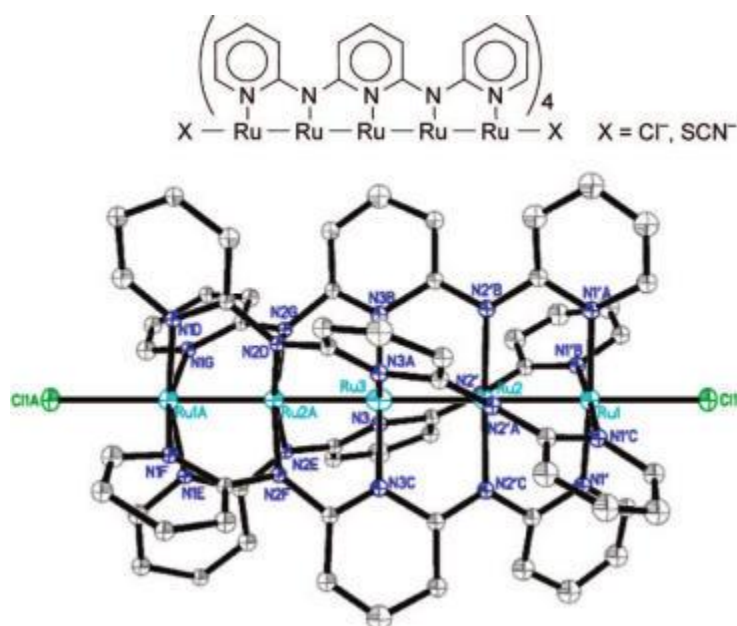
Figure 21. (Top) Schematic presentation of [Ru$_5$X$_2$(μ_5-tpda)$_4$] (Bottom) Crystal structure of [Ru$_5$Cl$_2$(μ_5-tpda)$_4$]. Thermal ellipsoids are drawn at the 30% probability level. Ru, light blue; N, blue; Cl, green; C, gray. The hydrogen atoms are not shown for clarity.[51]

Closely related ligands to oligo-α-pyridylamide ligands are oligo-α-naphthyridylamide type ligands and related compounds to oligo-α-naphthyridylamide. Only Ni containing oligo-α-naphthyridylamide complexes has been published so far with at least three naphtyridine moieties. One example of these is 2-naphthyridylphenylamine, Hnpa, which is shown left in Figure 22. A ruthenium compound which contains the anion of Hnpa ligand is [Ru$_3$(NCS)$_2$(μ_3-npa)$_4$].[136] Intermetallic distances between Ru(1) and Ru(2) is 2.3462(8) Å and between Ru(2) and Ru(3) 2.3646(8) Å. The angle between these ruthenium atoms is 170.26(4)°. The distances are longer than in every ruthenium compound shown in Table 3 except [Ru$_3$(CN)$_2$(dpa)$_4$].
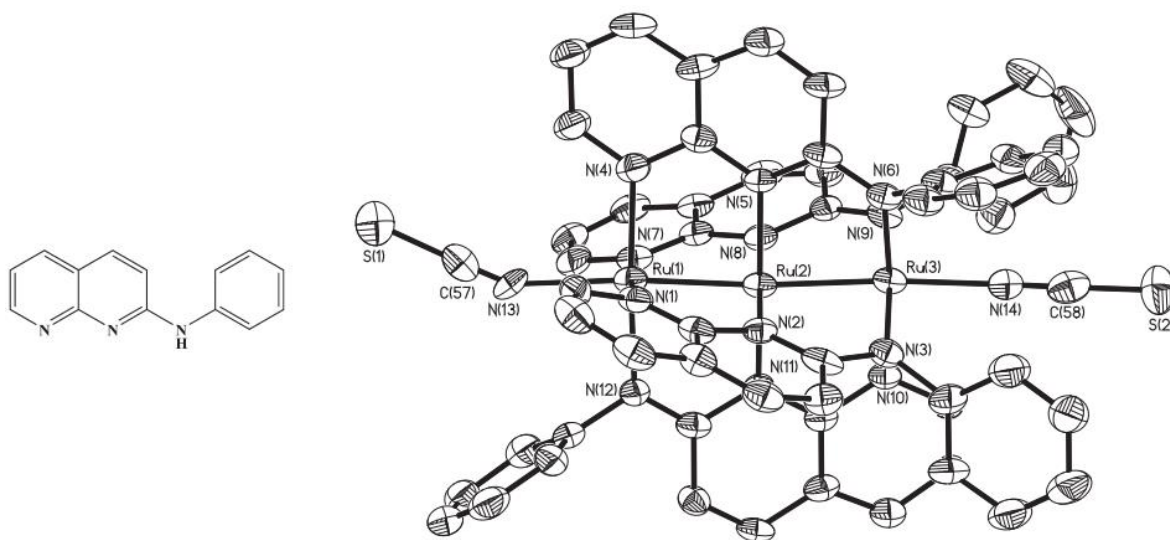
Figure 22. The schematic structure of 2-naphthyridylphenylamine, Hnpa, (left) and ORTEP view of the cationic part of $[Ru_3(NCS)_2(\mu_3\text{-npa})_4][PF_6] \cdot (Me_2CO)_2 \cdot (Et_2O)_2$ (right). Hydrogen atoms have been omitted for clarity and thermal ellipsoids are drawn at 40 % probability level.[136]

Spin unrestricted DFT calculations has been performed for $[Ru_3(NCS)(\mu_3\text{-npa})_4]^+$ and $[Ru_3Cl_2(\mu_3\text{-dpa})_4]^+$. According to the results, $[Ru_3(NCS)_2(\mu_3\text{-npa})_4]^+$ is suggested to have the electronic configuration of $\sigma^2\pi^4\delta^2\pi^4_{nb}\delta^2_{nb}\pi^{*3}$ and $[Ru_3Cl_2(\mu_3\text{-dpa})_4]^+$ the electronic structure of $\sigma^2\pi^4\delta^2\pi^4_{nb}\delta^2_{nb}\delta^{*2}\sigma^1_{nb}$. $[Ru_3(NCS)_2(\mu_3\text{-npa})_4]^+$ has been observed to have more stabilized π^* orbitals compared to $[Ru_3Cl_2(\mu_3\text{-dpa})_4]^+$. Cl^- ligand is a π-base so it destabilizes the π^* orbitals but NCS^- ligand is a π-acid so it's draw electron density away from $[Ru_3]^{7+}$ core which stabilizes the π^* orbitals. This probably results longer interruthenium distances in $[Ru_3(NCS)_2(\mu_3\text{-npa})_4]^+$ compared to $[Ru_3Cl_2(\mu_3\text{-dpa})_4]^+$. As a result, the π^* orbitals are occupied as HOMO in $[Ru_3(NCS)_2(\mu_3\text{-npa})_4]^+$ and unoccupied in $[Ru_3Cl_2(\mu_3\text{-dpa})_4]^+$ as LUMO. The electronic configurations of both of these cations are shown in Scheme 6. Also large bite angle and rigidity of anion of nba^- are other reasons which makes intermetallic distances longer in $[Ru_3(NCS)_2(\mu_3\text{-npa})_4]^+$ than in $[Ru_3Cl_2(\mu_3\text{-dpa})_4]^+$.[136]

σ_nb ———   π* ——— ———

δ* ———   σ_nb ↑
π* ↑↓   ↑   δ* ↑↓

$[Ru_3(npa)_4(NCS)_2]^+$ $[Ru_3(dpa)_4Cl_2]^+$
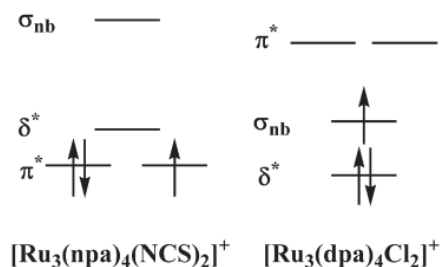
Scheme 6. The qualitative electronic configuration of $[Ru_3(NCS)_2(\mu_3\text{-}npa)_4]^+$ (left) and $[Ru_3Cl_2(\mu_3\text{-}dpa)_4]^+$ (right) near the Fermi level. nb stands for non-bonding.[136]

The uneven distribution of electrons in two π* orbitals in $[Ru_3(NCS)_2(\mu_3\text{-}npa)_4]^+$ has been proposed to be one reason which causes nonlineary.[136] When a compound with uneven distribution (3 electrons in two degenerated orbitals) of electrons of $[Ru_3(CN)_2(\mu_3\text{-}dpa)_4]$ in HOMO−1 is oxidized, the electronic distribution in HOMO−1 becomes even (half-filled) and Ru–Ru–Ru angle changes from 171° to 180°.[52] However, all occupied orbitals are full in $[Ru_3Cl_2(\mu_3\text{-}dpa)_4]$ but the angle between ruthenium atoms is not 180° that's why it's not that simple.[52] HOMO of $[Ru_3Cl_2(\mu_3\text{-}dpa)_4]$, $[Ru_3Cl_2(\mu_3\text{-}dpa)_4][BF_4]$ and $[Ru_3Cl_2(\mu_3\text{-}dpa)_4][BF_4]_2$ is degenerated set of two orbitals. In $[Ru_3Cl_2(\mu_3\text{-}dpa)_4]$ and $[Ru_3Cl_2(\mu_3\text{-}dpa)_4][BF_4]_2$ the electronic distribution is even in all orbitals but in $[Ru_3Cl_2(\mu_3\text{-}dpa)_4][BF_4]$ it's not. This uneven distribution of electrons can be noticed from the angle between ruthenium atoms; It's about 166° for $[Ru_3Cl_2(\mu_3\text{-}dpa)_4][BF_4]$ but for the other two it's 171° or 173° (see Table 3). However, it can be concluded that uneven distribution of electrons in HOMO or HOMO−1 results decreasing of the Ru–Ru–Ru angle in addition other effects which affect the angle.

6.4.4 Homometallic Rh complexes

Lesser amounts of rhodium oligo-α-pyridylamide compounds have been synthesized. $[Rh_3Cl_2(\mu_3\text{-}dpa)_4]$ has Rh–Rh average distances of 2.3920(5) Å[54] and its one electron oxidized form $[Rh_3Cl_2(\mu_3\text{-}dpa)_4][BF_4]$ has Rh–Rh average distances of 2.363 Å[135]. The Rh–Rh–Rh angle is 177.13° for $[Rh_3Cl_2(\mu_3\text{-}dpa)_4]$ and 167.54° for $[Rh_3Cl_2(\mu_3\text{-}dpa)_4][BF_4]$.[54, 135] The decrease in Rh–Rh bond lengths upon oxidation is counterintuitive; increase in positive charge would be expected to increase repulsion between rhodium nuclei.[135] However, the shortening might indicate the enhancement of Rh–Rh bond.[135]

According to the electronic structure of $[Rh_3Cl_2(\mu_3\text{-dpa})_4]$ obtained from DFT calculations with D_4 symmetry, $[Rh_3Cl_2(\mu_3\text{-dpa})_4]$ has one unpaired electron which located on HOMO σ_{nb} (a_2) orbital (see Scheme 7).[135] This orbital and fully occupied σ bonding orbital forms a bond with three centers and three electrons. (This doubly occupied σ bonding orbital is not shown in Scheme 7.) Upon oxidation one electron is removed from doubly occupied δ antibonding orbital (b_2) which results the contradiction of Rh–N bond distances because the orbital has Rh–N antibonding character.
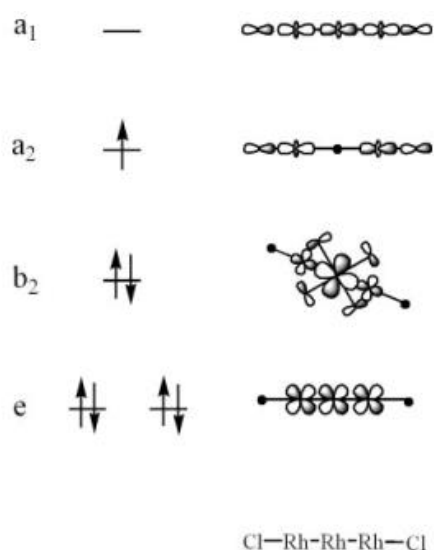
Scheme 7. The qualitative electronic configuration and molecular orbitals of $[Rh_3Cl_2(\mu_3\text{-dpa})_4]$ near the Fermi level.[135]

6.4.5 Homometallic Cu complexes

$[Cu_3Cl_2(\mu_3\text{-dpa})_4]$ and $[Cu_3Br_2(\mu_3\text{-dpa})_4]$ were synthesized and crystallized from water in 1990[137], $[Cu_3(BF_4)_2(\mu_3\text{-dpa})_4]$ in 2003[138] and a oxidation product of $[Cu_3Cl_2(\mu_3\text{-dpa})_4]$: $[Cu_3Cl_2(\mu_3\text{-dpa})_4][SbCl_6]$ in 2003[139]. In $[Cu_3Cl_2(\mu_3\text{-dpa})_4][SbCl_6]$ the Cu_3 unit has formal oxidation state +7 which is the first compound which the Cu_3 unit has formal oxidation state higher than +6.[139] Their intermetallic distances and angles are shown in Appendix 1 in Tables A1T2A and A1T2B, where two different crystal structures of $[Cu_3Cl_2(\mu_3\text{-dpa})_4][SbCl_6]$ have their distinctive values. Multiple crystal structures for $[M_3Cl_2(\mu_3\text{-dpa})_4]$ resulting from different crystallization method is a known phenomenon, thus the same phenomenon for $[Cu_3Cl_2(\mu_3\text{-dpa})_4][SbCl_6]$ is not surprising.[139] The different crystal structures for the same compound are noticed sometimes to affect significantly to

the metal–metal distances.[139] It is commonly noticed that even though the terminal copper atoms are crystallographically independent, copper⋯copper distances are similar.[139] The values in Appendix 1 in Tables A1T2A and A1T2B for these compounds confirm this statement. The angle between metal atoms is closer to the straight angle (178–180°) than in corresponding ruthenium compounds (165–180°).

[$Cu_3(\mu_3$-p-tolyl-NNNNN-p-tolyl$)_3$] (Figure 23) has two different intermetallic distances between adjacent copper atoms: 2.348(2) Å and 2.358(2) Å.[140] The anionic ligand, p-tolyl-NNNNN-p-tolyl is (1E,4E)-1,5-di-p-tolylpentaaza-1,4-dien-3-ide. Intermetallic distances and angles of this and [$Au\{\mu_3$-im$(CH_2py)_2\}_2\{Cu(MeOH)\}_2](PF_6)_3$ have been presented in Tables A1T2A and A1T2B in Appendix 1.
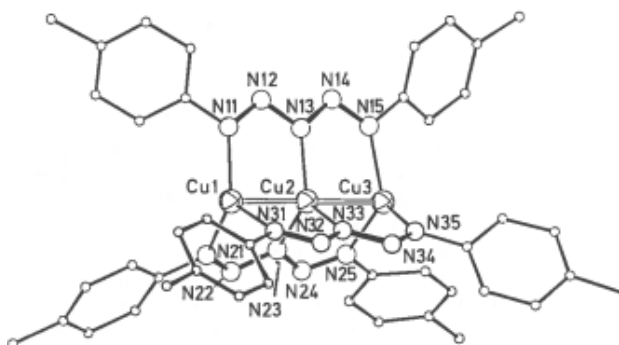
Figure 23. The molecular structure of [$Cu_3(\mu_3$-p-tolyl-NNNNN-p-tolyl$)_3$] in which hydrogens have been obmitted.[140]

7 Applications and properties of EMACs

7.1 Conductivity

The electric conductivity of EMACs has been investigated.[141] Increasing bond order 0→0.5→1 has been shown to indicate increase in conductivity at least in the series of [$M_3(NCS)_2(\mu_3$-dpa$)_2$], M = Cr, Co and Ni, respectively.[141] This is because bond order indicates the degree of electron delocalization and thus efficiency of the electron transfer through metal centers.[141] As a logical result, conductivity increases when electron density along the string increases if it doesn't feature breaks i.e. the density is more evenly distributed.[134] The axial ligands in molecular electronics of EMACs have greater function than only being a contact clip.[50] In fact, it provides a way to modulate electric behavior of

the molecular framework of an EMAC.[50] For example conductivity of $[Ru_3(NCS)_2(\mu_3\text{-dpa})_2]$ is $9.81(\pm2.02) \cdot 10^{-3}$ G_0 and it's higher than the conductivity of $[Ru_3(CN)_2(\mu_3\text{-dpa})_2]$ which is $2.04(\pm0.44) \cdot 10^{-3}$ G_0 ($G_0 = 2e^2/h \approx 77.5$ µS).[50] Also the oxidation state of the metal framework of an EMAC can affect the conductivity like in the case of $[Ru_3(CN)_2(\mu_3\text{-dpa})_2]^0$ and $[Ru_3(CN)_2(\mu_3\text{-dpa})_2]^+$ in which one-electron oxidation doubled the conductivity from $2.04(\pm0.44) \cdot 10^{-3}$ G_0 to $4.17(\pm0.83) \cdot 10^{-3}$ G_0.[50] Whereas in others, like $[Ru_3(NCS)_2(\mu_3\text{-dpa})_2]^{0/+}$, the oxidation state doesn't affect to the conductivity.[50]

DFT calculations for the series of $[Ru_3Cl_2(\mu_3\text{-dpa})_4]$, $[Ru_5Cl_2(\mu_5\text{-tpda})_4]$, $[Ru_7Cl_2(\mu_7\text{-tpta})_4]$ and $[Ru_9Cl_2(\mu_9\text{-ppta})_4]$ complexes (dpa = dipyridylamine$^-$, tpda = tri-α-pyridyldiamine^{2-}, tpta = tetra-α-pyridyltriamine^{3-}, ppta = penta-α-pyridyltetraamine^{4-}) have been performed. They showed that the distribution of electron density is more evenly distributed and chains have higher electron density between metals when the chain length is the longer which suggests higher conductivity.[134]

7.2 Antibacterial activity

Antibacterial activity for Gram-positive, Gram-negative bacteria and yeast has been tested for 10 different organometallic compounds and two silver salts. The structure of cationic chain of one of these compounds, $[Au_2Ag(\mu\text{-mes})_2(\mu\text{-dppe})][SO_3CF_3]$, is shown in Figure 8 (left). Abbreviation dppe means 1,2-bis(diphenylphosphano)ethane and mes means mesityl group (2,4,6-trimethylphenyl). Compounds $[Au_2Ag(\mu\text{-mes})_2(\mu\text{-dppe})][SO_3CF_3]$ and $[Au_2Ag(\mu\text{-mes})_2(\mu\text{-dppe})][ClO_4]$ were the most effective with minimum inhibitory concentration (MIC) of 10 µg/l for Gram-negative (*Salmonella typhimurium* and *Escherichia coli*) bacteria and Gram-positive (*Bacillus cereus* and *Staphyloccocus aureus*) bacteria. MIC for *B. cereus* was only 1 µg/l which is quite impressive. Other complexes were similar to these two with the difference of Cu instead of Au, different anions, different ligands or only with gold. Overall, the toxicity for Au_2Ag compounds was much higher than two silver salts or parent binuclear $[Au_2Ag(mes)_2(\mu\text{-LL})]$ compounds. LL is either dppe which is 1,2-bis(diphenylphosphano)ethane or dppy, which is 1,2-bis(di-3-pyridylphosphano)ethane.[41]

7.3 Catalytical activity

Catalytic activity of $[Ru(CO)_4]_n$ in hydroformulation of 1-hexene has been compared to more conventional catalyst $Ru_3(CO)_{12}$ (3 Ru—Ru). Catalytical activity of ruthenium complexes derived from $[Ru(CO)_4]_n$ is similar to the ruthenium complexes derived from $Ru_3(CO)_{12}$. CO_2 was first reduced to CO with H_2 followed by hydroformulation *in situ*. Direct hydrogenation happened as side reaction and a promoter was used to prevent this reaction. The polymeric catalyst was fragmented into mono- and oligomeric species which were similar but not exactly identical as catalytically active species derived from $Ru_3(CO)_{12}$ according to ESI–MS analysis. Usage of catalytic precursor $[Ru(CO)_4]_n$ favored direct formation of alcohols instead of aldehydes which are found only in some catalytic runs in trace amounts.[44]

7.4 Vapochromic properties

A copper and gold containing *N*-heterocyclic carbene (NHC) has been synthesized which color depends on the distance between copper and gold atoms. $[Au\{\mu_3\text{-im}(CH_2py)_2\}_2\{Cu(MeCN)_2\}_2](PF_6)_3$ (Figure 20 left) can be transformed reversibly into $[Au\{\mu_3\text{-im}(CH_2py)_2\}_2\{Cu(MeOH)\}_2](PF_6)_3$ (Figure 20 right). The ligand $im(CH_2py)_2$ is 1,3-bis(pyridin-2-ylmethyl)-2,3-dihydro-1*H*-imidazole. Au1···Cu1 distances are 4.591 and 2.7915(7) Å, respectively for these two compounds. The former exhibits blue fluorescence ($\lambda_{max} = 462$ nm) with UV-radiation and the latter green fluorescence ($\lambda_{max} = 520$ nm), as shown in Figure 24. Treatment with MeOH vapor into the former compounds produces the latter and vice versa with MeCN.[133]

When the MeOH complex was left to air atmosphere, it partially lost MeOHs and fluorescence maximum changed to faint yellow ($\lambda_{max} = 543$ nm). When the MeOH complex was put into vacuum, MeOH was totally disattached from the complex and fluorescence changed into yellow-orange ($\lambda_{max} = 573$ nm). The MeCN complex treated with Me_2CO and H_2O vapors resulted yellow-orange ($\lambda_{max} = 591$ nm) and green ($\lambda_{max} = 519$) emission, respectively. The excitation wavelength for all the fluorescence emission was 365 nm. The color changes were fast and were supposed to due to the changes of the interaction between gold and silver atoms.[133]
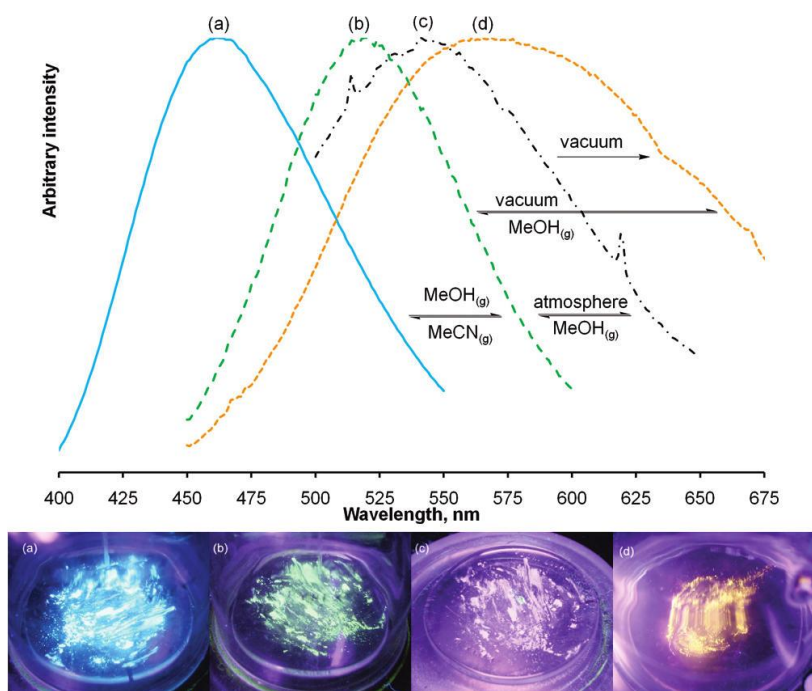
Figure 24. (Top) Normalized solid-state emission spectra with excitation wavelength of 365 nm. Transformations to different forms are also visible. (Bottom) Photographs (a)–(d) shows color differences in different forms. In (a) the complex is $[Au\{\mu_3\text{-im}(CH_2py)_2\}_2\{Cu(MeCN)_2\}_2](PF_6)_3$, in (b) the complex is methanol treated $[Au\{\mu_3\text{-im}(CH_2py)_2\}_2\{Cu(MeCN)_2\}_2](PF_6)_3$ i.e. $[Au\{\mu_3\text{-im}(CH_2py)_2\}_2\{Cu(MeOH)\}_2](PF_6)_3$, in (c) the complex is methanol treated $[Au\{\mu_3\text{-im}(CH_2py)_2\}_2\{Cu(MeCN)_2\}_2](PF_6)_3$ which has been exposed to normal atmosphere, and in (d) the complex is methanol treated $[Au\{\mu_3\text{-im}(CH_2py)_2\}_2\{Cu(MeCN)_2\}_2](PF_6)_3$ which has been exposed to vacuum. The ligand $im(CH_2py)_2$ stands for 1,3-bis(pyridin-2-ylmethyl)-2,3-dihydro-1H-imidazole.[133]

8 Reaching towards experimental section

Nomenclature of tautomeric structures is problematic because each tautomeric structure can be named individually. IUPAC newest nomenclature of organic chemistry in 2013[142] doesn't give any general rule for naming tautomeric compounds and the nomenclature recommendations for tautomeric structures are limited to very few examples none of which are about pyridines, thiols or thiones.

A ligand which was used the most commonly in the experimental section of this thesis exhibits two tautomers: thione and thiol forms shown in Scheme 8. The thione form is pyridine-4(1H)-thione and thiol form is pyridine-4-thiol. The compound has also a zwitterionic form. Only the most stable deprotonated form is shown as the leftmost structure in the figure and it is 4-thioxo-4H-pyridin-1-ide.
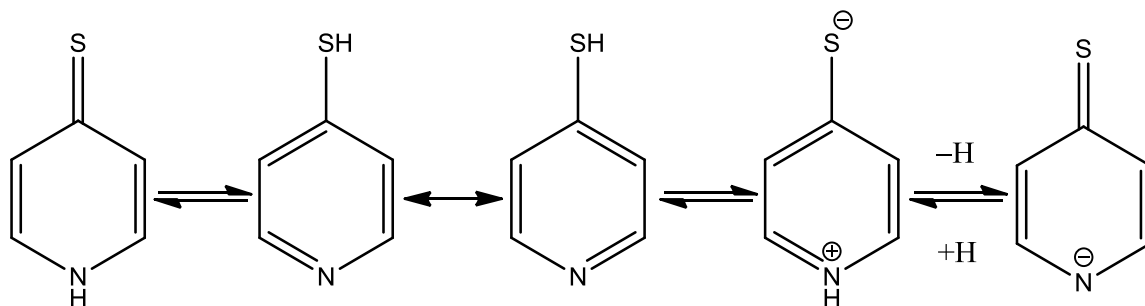
Scheme 8. Tautomeric structures, two resonance structures of thiol form, zwitterionic form and the most stable deprotonated form of pyridine-4(1*H*)-thione.

The natural abundances of the compound has been estimated with a NMR method using combine sets of shielding constants of ^{15}N, ^{14}N, ^{13}C and ^{1}H for a variety of aza-aromatic heterocycles.[143] Thione form was calculated to be present in 99±3 % in 1:1 acetone:dimethyl sulfoxide.[143] Another study[144] using ^{15}N chemical shifts resulted 95±5% of thione form in 4:1 acetone:dimethyl sulfoxide. The latter study emphasizes that "nitrogen NMR is far superior to carbon NMR as far as the investigations of tautomeric equilibria are concerned for nitrogen-containing aromatic systems."

In the article[143], 1:1 acetone:dimethyl sulfoxide was the only mixture in which pyridine-4(1*H*)-thione was measured so exact estimation of the occurrences of thiol and thione form in 1:3 or 2:1 EtOH:MeCN cannot be obtained. The 1:3 and 2:1 EtOH:MeCN mixtures were the most widely used solvent mixtures in the experimental part of this thesis.

In the article[143] 29 different compounds were investigated and 10 was measured in multiple solvents. Some compounds like 3-methyl-2*H*-indazol-2-ol the percentages of tautomeric form of 3-methyl-2*H*-indazol-2-ol varied depending on the solvent from 90±3 % (dimethyl sulfoxide) via 54±2 % (methanol) to 10±3 % (trifluoroacetic acid). Other compound the difference was much lower. A regioisomer of pyridine-4(1*H*)-thione, pyridine-2(1*H*)-thione has similar value of the thione isomer (98±3 %) in acetone. Because thione form of pyridine-4(1*H*)-thione was very close to 100 %, likewise its *ortho*-isomer, it's the most appropriate to call the compound as pyridine-4(1*H*)-thione. The ligand is abbreviated as s-pyH and its deprotonated from as s-py. Commercial name of pyridine-4(1*H*)-thione is 4-mercaptopyrine.[143]

9 Summary

Metallopolymers are metal containing polymers which can be classified numerous ways depending on what is the overall shape of the polymer, where the metal atom is located and whether the binding of monomers is reversible or static. Metallopolymers have many interesting properties which combines properties of organic polymers and coordination complexes. The location of metal and whether the organic part is conjugated or not are crucial to some of its properties like conductivity, luminescence and sensory properties. Metallopolymers have many other applications in addition to be used as sensors. Metallopolymers have potential to function as switches, memory devises, catalysts, artificial metalloenzymes, functional ultrathin films, capsules and vesicles and materials with high refractive index. They can be used in nanofabrication and nanomanufacturing.

Metallophilic interaction is an attractive interaction between two metal ions. The attraction is mainly dispersive and dipole-dipole (ionic) in nature with ionic character as well. Relativistic effects increase metallophilic interaction. Metallophilic interaction has been researched by molecular modelling.

Extended metal atom chains (EMAC) are one group of metallopolymers. EMACs consist of closely spaced metal atoms arranged in a nearly linear fashion. In this thesis, EMACs have been classified into four groups (A1, A2, A3 and B) depending on how to what extend ligands bridge metals and how linear is the metal chain. A1 group compounds have the metallophilic interaction is exclusive intermolecular and the metallophilic chain is very straight. Class B has only intramolecular interactions between metal atoms and the length of the scaffold ligands define the length of the chain. Group A2 is intermediate between A1 and B in the sense that there're both intermolecular and intramolecular interaction between metal atoms and the chain is very straight. Class A3 is like A1 but the metallic chain is not straight and it may contain clusters like ⊦M⟨M⟩M⊦ in the chain. The most famous type of EMACs is oligo-α-pyridylamine-based compounds which are group B compounds.

EMACs have interesting properties. Because they contain metal chain which is surrounded by organic insulating layer they have potential to work as nanoscale wires. However, their conductivities are normally in semiconductor range. For example vapochromic properties of $[Au\{\mu_3\text{-im}(CH_2py)_2\}_2\{Cu(MeCN)_2\}_2](PF_6)_3$ are remarkable and demonstrate that the

distances and thus the amount of interaction between metal atoms affect the greatly the luminescence of the EMAC.[133] Also conductivity of an EMAC is greatly affected by what is the electronic structure of the metal atom string in it. It has been observed for $[M_3(NCS)_2(\mu_3\text{-dpa})_2]$, M = Cr, Co and Ni, that increasing bond order between metal atoms increases conductivity.[141]

Several authors have tabulated different radii like van der Waals, single bond covalent and double bond covalent radii. The sum of two van der Waals radii has been used in literature to figure out whether there's an attractive interaction between two atoms. This kind of method solely based on tabulated values of only two atoms should be completely discarded and utilize safer methods like molecular modelling which has its own uncertainties. For example molecule can have a rigid structure which forces two atoms to closer to themselves than what they normally do and the close distance between two atoms destabilizes the structure rather than stabilizes it. The concept of bond is not simple and for example there is a continuum of interatomic distances from van der Waals to covalent and from weak hydrogen bond to strong hydrogen bond. Thus concept of bond order has been developed to help to explain bonds or interactions with non-integer bond order. However, tables of different radii serve nowadays two main purposes: (1) to make crude estimation of bond distance in unknown structure and (2) to provide standard bond length of an 'ideal' bond and this value can be compared with a specific experimentally obtained value to give some insight about the bonding or interaction.

Experimental part

10 Substances

Substance	Manufacturer and purity
$Ag(CF_3SO_3)$	Sigma-Aldrich 99 %
$AgNO_3$	Sigma-Aldrich 99 %
$AuCl$	Sigma-Aldrich 99.9 %
$AuCl_3$	Brother 99 %
$CrCl_3 \cdot 6\ H_2O$	J. T. Baker 99.9 %
$Cu(OAc)_2 \cdot H_2O$	Merk 99 %
$Cu(OAc)_2 \cdot H_2O$	Fluka Chemie Ag 99 %
$CuCl_2$	Fluka 98 %
$CuCl_2 \cdot 2\ H_2O$	Riedel-de Haën 97 %
$FeCl_3$	Sigma-Aldrich 97 %
$FeCl_3 \cdot 6\ H_2O$	Sigma-Aldrich 99 %
$NaCl$	VWR Prolabro AnalaR NORMAPUR 99.6 %
$NaOEt$	Sigma-Aldrich 95 %
$Ni(CH_3COO)_2 \cdot H_2O$	J. T. Baker 99.7 %
$NiCl_2$	Sigma-Aldrich 98 %
$RuCl_3 \cdot 3\ H_2O$	Sigma-Aldrich (technical)
$Ru_2(CO)_6Cl_2$	Sigma-Aldrich (purity not reported)
$ZnCl_2$	VWR Prolabro AnalaR NORMAPUR 99 %
1,10-phenanthroline monohydrate	Sigma-Aldrich 99.5 %
4′-chloro-2,2′:6′,2″-terpyridine	Sigma-Aldrich 99 %
4-mercaptopyridine, more correctly: pyridine-4(1*H*)-thione, Aldrich 95 %	
2,2´-bipyridine	Sigma-Aldrich, ReagentPlus® 99%
NH_4PH_6	Sigma-Aldrich 95 %
KOH	Sigma-Aldrich 85 %
Et_3N	VWR Prolabro AnalaR NORMAPUR 99 %
Ethyldiisopropylamine, DIPEA	Sigma-Aldrich 99.5 %, redistilled

11 Instruments & programs

Multiple instruments were used; single crystal XRD analysis was performed with Agilent Technologies Supernova using Cu Kα (λ = 1.54184 Å) Mo Kα radiation (λ = 0.70173 Å). The structure refinements from single crystal XRD data were done using Olex2[145]. NMR spectra were recorded with Bruker 500MHz NMR with BBFO probe and Bruker Avance FT 400 MHz. Elemental analyses were performed with VarioEL III V4.01 in CHN mode. Mass spectrometer was ABScienx QSTAR Elite ESI-QTOF with Analyst QS (version 2.0). Rotatory evaporator was Büchi R II Anniversary Edition with Vacuum Controller V-850 and Vacuum Pump V-700. Analytical balances were RADWAG AS 220/X and Denver Instrument APX–200.

12 Reactions

Large amounts of reactions were performed and only highlights and general procedure of them are presented here. Overview of the reactions performed is below (Scheme 9). The main focus was to perform homo- and heterometallic metal atoms chains with metallophilic interactions. Bridging ligand between two metal atoms was pyridine-4(1*H*)-thione (s-pyH) which was aimed to bridge group 11 metals (Ag^+, Au^+ and Cu^{2+}) with other metals in heterometallic complexes. It has soft sulphur end and intermediately hard nitrogen end. Softer metal, usually group 11, was assumed to coordinate to sulphur end and harder to the nitrogen end. Other metal compounds were simple metal salts, 2,2'-bipyridine and 1,10-phenanthroline complexes with a variety of metals (Cr^{3+}, Fe^{3+}, Ni^{2+}, Zn^{2+}, Cu^{2+}, Ru^{3+} and Au^{3+}).

The project was started with monometallic group 11 reactions with s-pyH. Later on, heterometallic reactions were performed with different metal salts and complexes. Target bimetallic compounds are shown in Scheme 10. Monometallic targets were simpler without other metal complexes (M_{other}). Slow diffusion reactions were performed in order to obtain crystals from reactions which originally created precipitate. Table of every reaction performed is located in Appendix 2. The table contains information about starting materials, their ratios, amounts as well as solvents used of each reaction etc.
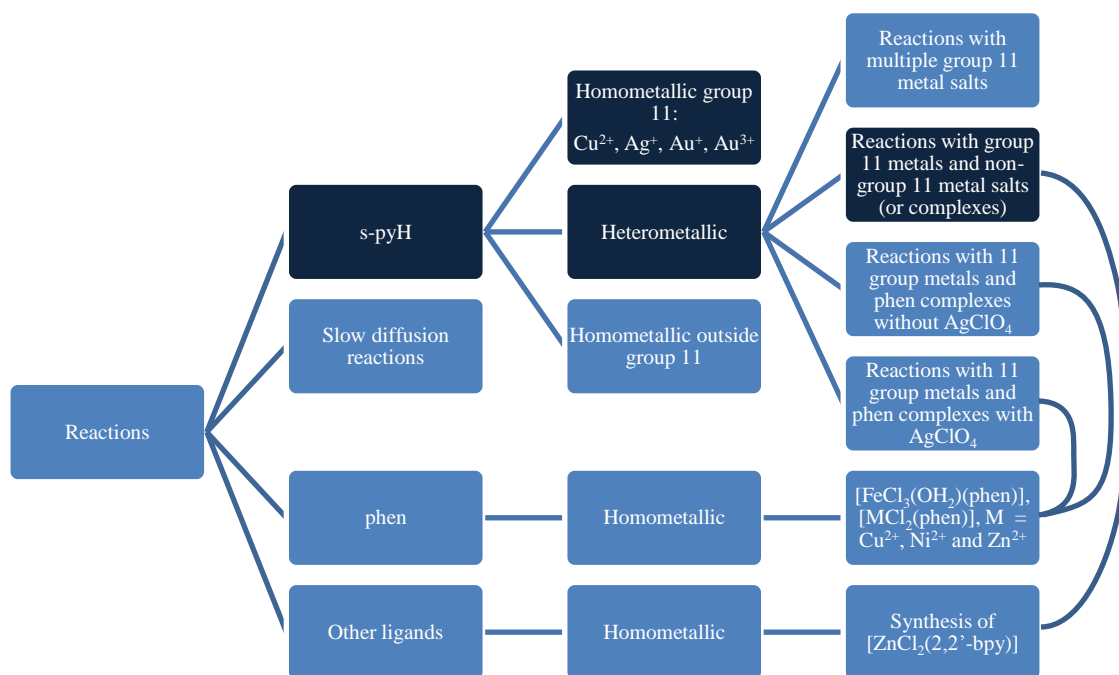
Scheme 9. Overview of performed reactions. An abbreviation s-pyH stands for pyridine-4(1H)-thione, phen stands for 1,10-phenanthroline and 2,2'-bpy stands for 2,2'-bipyridine. Dark blue reactions were the main emphasize of the project. phen and 2,2´-bpy complexes were used in reactions with s-pyH.
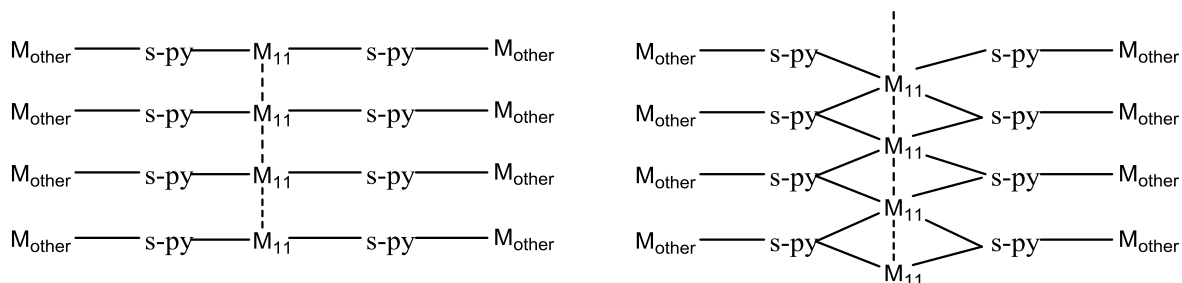
Scheme 10. Synthetical bimetallic targets of the experimental part depending on preferences of group 11 (M_{11}) metal coordination geometry.

12.1 General procedure

General reaction was performed as follows; group 11 metal salt was dissolved in MeCN and pyridine-4(1H)-thione (s-pyH) to EtOH in syntheses at the early stage of the lab work but later 3:1 MeCN:EtOH was used. In gold reactions s-pyH was dissolved either in CH_2Cl_2 or H_2O. If other metal salt was used, it was dissolved in 3:1 or 2:1 MeCN:EtOH with additional water to aid dissolution of the salt.

All starting materials were dissolved separately and pH was lowered in silver reactions with a base. Usually pH was not changed in gold and copper reactions. Group 11 metal solution was added dropwise to the solution of s-pyH meanwhile the mixture was stirred. The reaction was left to stir with short waiting time of 1 to 100 min. Other metal salt was added dropwise and the reaction mixture was left to stir overnight. If very small amount of precipitate was formed by the end of stirring, the precipitate was filtered but the precipitate was thrown away. If there's large enough of amount of precipitate that the precipitate was worth of keeping, it was washed with the same solvents as the reaction was carried at. The filtrate was left to evaporate if it was considered possible to obtain crystals from the filtrate.

Group 11 copper or silver salt was dissolved in 2–5 mL of a solvent. AuCl was dissolved normally in 10–15 mL of a solvent because of poorer solubility. Pyridine-4(1H)-thione (s-pyH) was dissolved in 3–5 mL of a solvent in copper and silver reactions. In gold reactions, s-pyH was dissolved in 10 mL of water. More detailed information about each reaction is tabulated in Appendix 2.

12.2 Homo- and bimetallic Au(I) reactions without other group 11 metals

AuCl was the only starting material for Au(I) reactions used in this project. Solubility of AuCl was checked from couple of literature synthesizes[146-148]. AuCl was attempted to dissolve completely in Et$_2$O, oxolane and MeCN (i.e. tetrahydrofuran) in much smaller gold to solvent ratio than in the literature syntheses. The attempts were unsuccessful but MeCN seemed to be the best solvent among the three so it was used. AuCl didn't dissolve completely in any synthesize. Because gold(I) chloride was been unable to dissolve completely, fewer gold reactions were performed. The amount of dissolved AuCl was not noticed to change when the volume of MeCN was increased from 10 mL to 15 mL so the insoluble part was probably something else. However, AuCl always colored MeCN as light yellow so it was at least partially dissolved unless it was dissolved impurity.

Pyridine-4(1H)-thione (s-pyH) was dissolved mainly in H$_2$O but in some synthesizes in MeCN or in 1:1 mixture of EtOH and H$_2$O. The volume of the solvent of s-pyH was 10–12 mL. Au:s-pyH ratio was 1:6. More detailed information is available in Appendix 2.

Usage of water seems to promote formation of colorless or white crystals on the surface of reaction mixture and on the bottom. Some of these crystals were analyzed with single

crystal XRD and noticed to contain S_8. When more organic solvents were used, formation of S_8 was not always observed. The reason for this is that the solubility of S_8 is assumed to be better in organic solvents than water. Heating of the reaction mixture of AuCl and s-pyH in 55–65 °C didn't change the appearance of the solution. Ammonium hexafluorophospate was used in a few reactions as co-crystallant.

Zinc(II) chloride and nickel(II) chloride were used in an attempt to form bimetallic polymeric structure. They were used in 1:2 or 1:1 ratio, (Au:M). However, the addition of them didn't change the appearance of the crystals formed which indicated that they did not coordinated to s-pyH.

12.2.1 AuCl with 4′-chloro-2,2′:6′,2″-terpyridine

In EAS–235 starting materials were AuCl, s-pyH, $ZnCl_2$, 4′-chloro-2,2′:6′,2″-terpyridine (Clterpy) and DIPEA (ethyldiisopropylamine) with ratios of 1.2:6:2:1:3.3, respectively. An interesting color changes were observed from pastel yellowish orange via reddish orange to red while heating a mixture which contained every starting materials. Cooling down the mixture didn't change its color but slow evaporation of the mixture turned into purple. Colorless and black crystals were observed. The at least one of the former was S_8 and latter $[Zn(Clterpy)_2](NO_3)_2$. The crystal structure of $[Zn(Clterpy)_2](NO_3)_2$ is discussed more in detail in the chapter of crystal structures.

12.3 Ag(I) reactions without other group 11 metals

Two kinds of silver salts were used in Ag(I) reactions without other group 11 metals: $Ag(CF_3SO_3)$ and $AgNO_3$ which were dissolved normally in 5 mL of MeCN. The ligand used was s-pyH which was dissolved normally in 10 mL of EtOH. 0.36 mmol of s-pyH and 0.06 or 0.09 mmol of Ag(I) salts were used. If another metal salt was used, it was dissolved most commonly in 3–5 mL of 1:2 mixture of MeCN and EtOH. Metal salts were iron(III), zinc(II) and copper(II) chlorides, $[ZnCl_2(2,2'-bpy)]$ or 1,10´-phenanthroline complexes of these metal chlorides like $[FeCl_3(OH_2)(phen)]$ and $[CuCl_2(phen)]$. The ligand 2,2'-bpy stands for 2,2'-bipyridine. Twice amount of them was used compared to silver salt. The solvent volumes for these three starting material groups were most commonly 5–10 mL.

One or two bases were mainly used. They were Et$_3$N, KOH and ethyldiisopropylamine a.k.a. DIPEA.

General procedure of Ag$^+$ reactions is as follows: silver salt, s-pyH and another metal compound was each dissolved separately. pH of s-pyH solution was raised with base. Silver solution was added dropwise to the s-pyH solution. Solution of another metal compound was added last. Every solution was stirred. After the last addition, mixture was stirred normally overnight. If precipitate was formed it was filtrated. If the amount of precipitate was considered to be reasonable for storage it was washed with reaction solvent and stored. The filtrate was left to evaporate in aim for crystals if the color of the solution suggested dissolved compounds.

At the beginning of the project non-stoichiometric amounts of either strong KOH(aq) or Et$_3$N(l) was used per reaction. Initially strong KOH(aq) was used which didn't form a precipitate in the solution of s-pyH in which solvents were MeCN and EtOH. However, if pH was tried to rise more than initially to 9–10, white precipitate with slender color differences was formed. The white precipitate began to form already around 8–9. The precipitate was most likely KOH. After these observations solutions of specific amount of base were done in order to avoid formation of KOH. First a solution of KOH in water was used. Later, an interest on practically water-free synthesize resulted preparation of KOH in EtOH. However, because of problems with solubility of KOH in EtOH and uncertainty of the concentration of the solutions, KOH in EtOH wasn't used extensively instead KOH in water. Stoichiometric amounts of DIPEA(l) was used in the end.

When Et$_3$N was used nonstoichiometric amounts, the most commonly 29 or 30 drops of it was used, regardless whether it was the only base or not. That amount of Et$_3$N changed the pH to about 8. If KOH was used afterwards, about 5 drops of unspecified concentration (far less than strong) of it was added. The usage of KOH only as an extra booster after Et$_3$N was done in order to avoid formation of KOH(s).

Concentrated KOH(aq) was used when KOH was used nonstoichiometrically. When KOH was only base used, the color of the solution of Ag(I) and s-pyH was reddish orange or brown. If only slightly amount of KOH was used (pH about 7.4), the color of the solution was reddish orange but if pH was set at least to 8–9 with KOH, the color was brown. In a reaction, reaction mixture didn't change to brown instead was reddish orange even though pH was 9.

When Et_3N was the only base used nonstoichiometric amounts, the counter anion of silver salt (nitrate or triflate) it didn't have an effect on the end product; the color and C, H and N content of products were practically the same. More detailed discussion of elemental analysis is found in Appendix 3. 29–30 drops of Et_3N was used to set pH to 7–8. The product color was orange. When reaction solvent was changed from 1:2 MeCN:EtOH to CH_3NO_2 large amounts of light yellow precipitate was formed instead of orange precipitate.

However, when Et_3N or ethyldiisopropylamine (DIPEA) was used equal amount than s-pyH, the color of the product was yellowish orange or pastel orange in DIPEA version and pastel yellow in Et_3N version. After 10 months the precipitate was heterogenic yellow in Et_3N version and it consisted of two separate species; dark gray and yellow precipitate in DIPEA version. Dark gray color suggests partial reduction of silver.

Ethyldiisopropylamine (DIPEA) didn't seem to be strong enough base alone to create promising color change to the reaction mixture. Even thirteenfold amount of DIPEA compared to the amount of s-pyH wasn't enough to induce promising orange color in a reaction with $AgNO_3$. When 1,25-fold amount (compared to the amount of s-pyH used) of KOH was added after the last addition of DIPEA, the solution was turned from yellow into brownish orange.

If only nitrogenous base, Et_3N or ethyldiisopropylamine (DIPEA), was used, it seemed not to be strong enough base to create the red color. However, orange precipitate had been able to form with Et_3N. Nitrogenous bases were first used in ratio of 1:1 to s-pyH (0.36 mmol), the color of the precipitate stayed yellow and the color of the solution was neither promising red nor orange. Only slight difference in color of the precipitate was noticed with ethyldiisopropylamine with the change from 0.18 mmol to 0.36 mmol of the base; the precipitate became slightly more orange still considered as yellow but the solution stayed the same yellow. This was noticed with ethyldiisopropylamine and Et_3N.

When 2:1 ratio of ligand to KOH was used, the observations were the same as with nitrogenous bases with the same ratio. However, when second 0.18 mmol of KOH was added into the solution of $AgNO_3$ and 0.36 mmol of s-pyH, the precipitate was dissolved and the color of the solution changed from yellow to more brown. Right after the addition of KOH second time the color was temporarily reddish brown. The color of the solution eventually changed into brown after 10 min of the addition of KOH second time. The pH was a bit above 7 right after addition of KOH second time.

In reactions with Et$_3$N and KOH, the addition of couple of drops of diluted KOH (aq) faded precipitate and the solution became red which indicated the formation of polymer or oligomer. When s-pyH was used four times more than silver salt, the color changes seemed to be more promising compared to the reactions in which s-pyH was used six times more than silver salt.

Reaction mixture was very sensitive to temperature. Even very slight amount of warmth was enough to turn solution from red to peculiar brown. Even heating unit of magnetic stirrer was off but friction of old magnetic stirrer caused a very slight increase in energy of the solution. The brown color could've not changed into red or any other color by putting the reaction mixture to ice bath.

If another metal salt was added into the red or brown solution containing Ag(I) salt, Et$_3$N and KOH, precipitate was formed. With FeCl$_3$ the color of solution was reddish brown and there was no difference whether the reaction was made in the room temperature or in ice bath. If ZnCl$_2$ was used, the color was greyish brown. The precipitates were reddish brown with iron and black grey with zinc chloride. Slow diffusion versions of these were tried but no crystals were able to obtain. The precipitate was at least partially AgCl and because of it, these reactions were not tried widely.

It was crucial that base, especially KOH, was added into the solution of the ligand and not the solution of silver(I) salt. If base was added to the solution of silver(I) salt instead of solution of s-pyH or their mixture, relatively large amounts of black precipitate was formed. The precipitate was Ag$_2$O which was formed by commonly known reaction[149] (XXX).

$$AgOH \rightarrow Ag_2O(s) + H_2O \qquad (XXX)$$
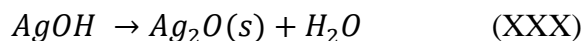
Truly black precipitate was only formed when KOH or NaOEt was added into the solution containing only AgNO$_3$. These bases were used 1:1 ratio to ligand. The reaction solvent was 2:1 MeCN:EtOH. However, the brownish color in other reactions which base was added into the solution of s-pyH instead of silver salt was assumed to indicate partial silver oxide formation possibly with coordination to s-pyH and it was not desirable.

12.4 Cu(II) reactions without other group 11 metals

Copper(II) reactions were mostly commonly used because of the solubility uncertainty of AuCl and basicity problems of silver salts. The most commonly used Cu(II) salt was $CuCl_2 \cdot 2H_2O$. However, before it, $Cu(OAc)_2 \cdot H_2O$ was used. In addition to the two, $[CuCl_2(phen)]$ was used. The abbreviation phen stands for 1,10-phenanthroline.

Wide range of salts was used: $CrCl_3 \cdot 6H_2O$, $FeCl_3$ (anhydr.), $[FeCl_3(OH_2)(phen)]$, $Ni(CH_3COO)_2 \cdot 4H_2O$, $RuCl_3 \cdot 3H_2O$, $ZnCl_2$ (anhydr.) and $[ZnCl_2(phen)]$. Copper(II) salt, s-pyH and other metal salts were used most commonly in 1:6:1 (0.06 mmol : 0.36 mmol : 0.06 mmol). Especially in later reactions double amount of another metal salts was used compared to copper(II) salt and also triple amount was tried. Ammoniumhexafluorophosphate was used in order to aid crystallization but it didn't seem to have an effect. It was always used 0.06 mmol i.e. the equal amount than copper normally.

At the beginning of the project Cu salts were dissolved in MeCN and s-pyH in EtOH. Most commonly 3:1 MeCN:EtOH was used as solvent. Water was used as sole solvent or auxiliary solvent to aid dissolution of $[MCl_x(phen)]$ complexes. Amount of solvents used were as follows: with $CuCl_2 \cdot 2H_2O$ or $Cu(OAc)_2 \cdot H_2O$ 2–12 mL, with s-pyH 3–20 mL and with other metal salts 2–10 mL. In reactions which ammoniumhexafluorophosfate was used, it was dissolved in 5 or 10 mL of 3:1 MeCN:EtOH. $[CuCl_2(phen)]$ was dissolved in a mixture of 2 or 3 mL of either 3:1 MeCN:EtOH or EtOH and 2 or 4 mL of water. Total volume for $[CuCl_2(phen)]$ was 4–7 mL.

Every starting material was dissolved separately to the solvent mentioned in the previous paragraphs. Copper salt was added either dropwise or faster to the solution of s-pyH. If base was used, it was added normally immediately after the addition of copper solution into s-pyH solution. The waiting time was usually less than half an hour, usually only 5 or 15 min or no waiting time at all. If another metal salt was used, its solution was added either dropwise of faster to the mixture. The mixture was left to stir overnight or over weekend.

When Cu(II) solution was added into the solution of s-pyH color transformation from yellow to more orange or orange. The orange color was promising. Small amount of white precipitate or crystals was formed especially in the reactions in water. Some of them were analyzed with single crystal XRD to be S_8. Addition of $CuCl_2 \cdot 2H_2O$ into s-pyH did change color of the solution from yellow to more orange but it was not as orange as when the

reaction was done in water. The solution colors were orange is water, 3:4 MeCN:EtOH and MeOH. Reactions in water didn't create any other precipitate or crystals, whereupon water was not used extensively as solvent. No overnight stirring was attempted with MeOH unlike with water. No immediate precipitate formation was observed in MeOH but MeOH was used only in $AgClO_4$ precipitation reactions which are described hereinafter.

In $CuCl_2 \cdot 2H_2O$ reactions, precipitate was formed immediately in MeCN but not during up to 10 min waiting time in H_2O, MeOH or 3:1 MeCN:EtOH. However, precipitate was formed immediately during the addition of copper chloride solution into s-pyH in MeCN and after overnight stirring in 3:1 MeCN:EtOH. Thus, among these solvents mentioned here, MeCN was required to produce precipitate when concentration of starting materials were kept same. This all is assuming that the reaction volume was 9–15 mL.

Reactions with $Cu(OAc)_2 \cdot H_2O$, s-pyH and KOH are compared in different solutions resulted different colors. The product solution was orange in H_2O but yellow in 1:2 MeCN:EtOH. The pH was set to about 8 in these two reactions. However, the concentration of starting materials was double in H_2O than in 1:2 MeCN:EtOH.

Different stoichiometric amount of Et_3N had an effect whether precipitate was formed or not. If half an amount of Et_3N (0.18 mmol) than s-pyH (0.36 mmol) was used in a reaction with $CuCl_2 \cdot 2H_2O$, large amount of orange precipitate was formed but when the same amount of Et_3N was added again, the precipitate was dissolved and solution turned into yellow.

Observations using KOH in EtOH with $CuCl_2 \cdot 2H_2O$ were similar but more detailed. Precipitate formation started when about 0.07 mmol of KOH was added and the amount of precipitate was increased until about 0.09 mmol of KOH was added. At this point amount of precipitate was so high that further increase in the amount of precipitate weren't able to notice. When more than 0.18 mmol of KOH was added, the amount of precipitate was decreased and when 0.36 mmol was reached, the solution was hazy most likely from insoluble KOH because solubility of KOH is lower in 3:1 MeCN:EtOH than in EtOH. The same or similar hazy yellowish orange color of the solution was observed when double amount (0.12 mmol) of $CuCl_2 \cdot 2H_2O$ was used and 0.36 mmol of KOH(aq) in total of 40 mL of the solvent mixture under argon atmosphere. In another reaction, when 0.36 mmol of KOH(aq) was added into s-pyH solution before the addition of $CuCl_2 \cdot 2H_2O$ solution into s-pyH solution, the solution was yellow. Transitory precipitate was formed

and was visible only during addition to $Cu(OAc)_2 \cdot H_2O$ to the s-pyH solution which was already slightly alkaline (pH 8). Its pH was set to 8 with unspecified amount of diluted KOH(aq).

The same phenomena with half or equal amount of base compared to the amount of s-pyH was observed with $[CuCl_2(phen)]$ and KOH but the color of the halfway precipitate was yellow which is different compared to $CuCl_2 \cdot 2H_2O$ versions in which orange solution resulted orange precipitate.

No reaction with $Cu(OAc)_2 \cdot H_2O$ was performed in 3:1 MeCN:EtOH. When $Cu(OAc)_2 \cdot H_2O$ was used total in 35 mL of 3:4 MeCN:EtOH, orange precipitate was formed immediately during addition of copper solution. The solution remained yellow. In water no precipitate was formed and solution remained orange.

Reactions with $Cu(OAc)_2 \cdot H_2O$ in different solvents and with or without base produced a range of colors: yellowish white, orange yellow, pale brown precipitate colors and brown, orange and yellow solution colors were observed with $Cu(OAc)_2 \cdot H_2O$. All in all, results were motley. Emphasize was changed from $Cu(OAc)_2 \cdot H_2O$ to $CuCl_2 \cdot 2H_2O$ because acetate is a chelating ligand with chelate effect so substitution of it with s-pyH would be harder than chloride. The first attempt with $CuCl_2 \cdot 2H_2O$ created orange precipitate and its slow diffusion reaction created long orange needle shape crystals. In that reaction $ZnCl_2$ was used only but this reaction is discussed more in detail hereinafter in the chapter of Cu^{2+} & Zn^{2+}. Owing to these reasons the chloride seemed to be more auspicious, it was used instead of the acetate.

Reactions with $CuCl_2 \cdot 2H_2O$ were done usually mixing $CuCl_2 \cdot 2H_2O$, s-pyH and another metal with a short waiting time. The length of waiting time within 0–30 min didn't seem to have an effect. When the solvent mixture of MeCN and EtOH was evaporated, red precipitate or more like oily substance was formed during it.

Reaction with $[CuCl_2(phen)]$ and s-pyH created red or reddish orange solution regardless of whether EtOH or 3:1 MeCN:EtOH was used with water to dissolve $[CuCl_2(phen)]$. The color of solution was redder than the corresponding $CuCl_2 \cdot 2H_2O$ version. $[CuCl_2(phen)]$ was heated before and the mixture was heated after the addition of $[CuCl_2(phen)]$ to s-pyH in 65±3 °C. The heating of 6 h changed the color of solution into greenish yellow and remained that during overnight stirring in room temperature. Orange solid matter was

formed close to but beneath the solution surface. The matter consisted of needle-shaped crystals which were separately observed almost colorless.

Interesting color observations were made in this reaction. While observing those slightly orange crystals with a microscope, the reaction mixture was not stirred which resulted color change gradually from yellowish green to green. The solution was filtered and left to evaporate slowly. The next morning the solution changed its color into bluish green but no precipitate was formed. When this solution was evaporated, bluish green crystals were obtained and measured with single crystal XRD. The crystals consisted of polymeric structure of alternating repeating units of $[Cu(OH_2)_2(phen)]^{2+}$ and $[CuCl_4]^{2-}$ with bridging bond between Cu and Cl.

Similar interesting color change than with $[CuCl_2(phen)]$ and s-pyH was also observed in a reaction with $CuCl_2 \cdot 2H_2O$, s-pyH, $[CuCl_2(phen)]$ and KOH in 1:6:1:6 ratio. When every starting material was added, the solution was heated for half an hour in 65 ± 4 °C before and after the addition of $[CuCl_2(phen)]$. The solution was orange red with beige precipitate but next morning, the solution was yellowish orange containing beige precipitate. Color of the solution changed into towards green; it was greenish yellow after two and half days from the addition of phenanthroline salt. Without heating and with the same amount of KOH, the observations differed only slightly; the precipitate was brownish beige instead of beige. Whether the base was added before or after the addition of $CuCl_2 \cdot 2H_2O$, didn't have a difference. This kind of color change from orange or yellow to green or greenish blue was observed other similar reactions. In one of them the color change happened after 1½ h heating in 63 ± 2 °C.

When $[ZnCl_2(phen)]$ was added instead of $[CuCl_2(phen)]$ into the solution of s-pyH and $CuCl_2$ without base, there's no change in the appearance of the solution (i.e. neither color change nor formation of precipitate). The color remained the same regardless of heating of 30 min in 65 ± 3 °C. White and (brownish) red crystals were formed later. There's a big difference in color whether $[ZnCl_2(phen)]$ or $[CuCl_2(phen)]$ is used.

Excluding the reaction mentioned before, reactions with Cu^{2+} and Zn^{2+} were performed exclusively with corresponding chlorides: $ZnCl_2$ (anhydr.) with $CuCl_2 \cdot 2H_2O$. $CuCl_2 \cdot 2H_2O$, s-pyH and $ZnCl_2$ were dissolved in 4–5 mL, 4–10 mL and 3–5 mL of 3:1 MeCN:EtOH, respectively.

Slow diffusion reaction EAS–167 formed orange crystals which were analyzed in the single crystal XRD to be cationic $[Cu_2(s\text{-}py)_2(s\text{-}pyH)_2]_n^{2+}$ with n $[ZnCl_4]^{2-}$ counter anions were orange. The abbreviation s-pyH stands for pyridine-4(1H)-thione and s-py its deprotonated form. Also the precipitate formed in EAS–164 was this same product because the amounts of starting materials were the same. The only differences were minor changes in the solvent conditions between the two reactions. These differences are further discussed in the following section about slow diffusion synthesizes. The differences were assumed to be so small that the product is the same in both reactions except that it's powder in normal version and crystalline in slow diffusion version. Elemental analysis of EAS–164 was performed and it's discussed in Appendix 3. Even the elemental composition of the crystal structure of EAS–167 doesn't result the best possible fit to experimental values.

When H_2O was used as the solvent, the solution was a bit more orange than in 3:1 MeCN:EtOH. No precipitate formation was noticed in water unlike in 3:1 MeCN:EtOH. When only $ZnCl_2$ (anhydr.) was used with s-pyH in 3:1 MeCN:EtOH, no precipitate was formed right after the addition of $ZnCl_2$ which differs from the reaction with $CuCl_2 \cdot 2H_2O$, s-pyH and $ZnCl_2$ in 3:1 MeCN:EtOH in which large amount of precipitate was formed immediate after the addition of $ZnCl_2$. The same amounts of starting materials were used in both reactions in same volume of solvents. Thus the precipitate must be something else than only product of $ZnCl_2$ and s-pyH, which it was, as confirmed with XRD.

Cu+Zn reactions were done in order to get polymeric structures in which copper would coordinate to sulphur end of s-py and Zn would coordinate to the harder nitrogen end of s-py. Copper is classified as intermediate in the principle of hard and soft acids and bases (HSAB) and Zn^{2+} as hard one. However it's obvious that even though they are classified to different groups they are still very similar to each other because both are first row d-block elements with charge +2. Zn^{2+} is slightly harder because it has one more proton in its nucleus which makes it two attract its orbitals a bit closer which increase its charge density a hint. Zn^{2+} has completely filled $3d$ orbitals when Cu^{2+} doesn't. Both ions have equal amounts of orbitals occupied.

Much larger difference in hardness was needed. Fe^{3+} and Cr^{3+} have much higher difference in hardness compared to Cu^{2+} than Zn^{2+} to Cu^{2+}. In addition, Ru^{3+} was used. That's why they were used in further studies in order to coordinate them to the nitrogen end of the ligand. They were also cheap starting materials and easily accessible as chlorides.

12.4.1 Cu^{2+} & Fe^{3+}

Reactions with Fe^{3+} and Cu^{2+}, starting materials were $CuCl_2 \cdot 2H_2O$, s-pyH and anhydrous $FeCl_3$. They were used in 1:6:1 ratio unless otherwise stated. If reaction was not high volume reaction, $CuCl_2 \cdot 2H_2O$, s-pyH and $FeCl_3$ were dissolved in 2–5 mL, 3–7 mL and 4–5 mL of 3:1 MeCN:EtOH, respectively. Ammonium hexafluorophosphate was used in some reactions to aid crystallization, it was used equimolar amount than $CuCl_2 \cdot 2H_2O$ and it was dissolved in 3 or 5 mL of 3:1 MeCN:EtOH. It didn't seem to have any effect.

Obvious color changes were observed when total solvent volume was increased from 20 mL to 50 mL in syntheses with $CuCl_2 \cdot 2H_2O$, s-pyH, $FeCl_3$ (anhydr) and NH_4PF_6. Only differences between the two reactions were the total volume of the reaction mixture and shorter stirring time. In larger version starting materials were dissolved 10 mL of the solvent mixture. An additional 10 mL was added immediately after the addition of the last reactant, $FeCl_3$ in the larger reaction. There's no additional solvent addition in smaller version. Mixing time was only 1 min in the smaller version but overnight in the larger version.

After 7 min from addition of the last reagent solution of the smaller version the solution became slightly turbid. The turbidity increased and the solution was really turbid after 14 min from the last addition. There's plenty of orange precipitate in the solution. The solution itself was orange. Nevertheless, the precipitate changed its color to yellow and the solution was yellow after 24 min. The appearance remained the same to the next morning (right side of Figure 25) when the solution was filtrated.

The goal for the larger version was to avoid precipitate formation by decreasing the concentration by increasing the volume. That's why reactants were dissolved in the double volumes and additional 10 mL was added immediate after the addition of the last reactant. The stirring was kept as short as possible to get crystals rather than precipitate. No solid was formed during 20 min after the addition of the last reactant. The color of the solution was pale orange due to the lower concentrations (left side of Figure 25). In the next morning pale green precipitate had been formed (right side of Figure 25). The color of the precipitate was different than in EAS–197. The solution was so colorless that it was very uncertain to say whether the solution had shade of green or yellow. Green crystals were formed later while pale green precipitate remained. The precipitate or crystal formation was

not due to evaporation of the solvent because the reaction vessel was kept tightly sealed until crystals were measured. Those crystals were measured and the results are discussed hereinafter in the chapter of crystal structures.
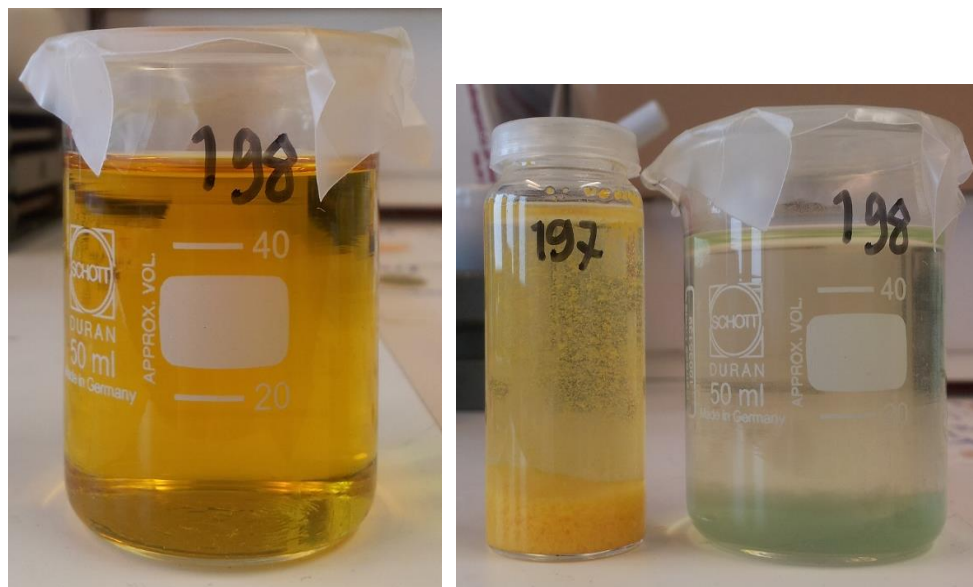
Figure 25. An effect of concentration in reactions with $CuCl_2 \cdot 2H_2O$, s-pyH, $FeCl_3$ and NH_4PF_6 in 1:6:1:1 molar ratio. Left side photograph is from the larger version and is taken about 11 min after addition of the last reagent, $FeCl_3$. Right side photograph shows distinctive change in the appearance of the larger version next morning. The smaller is presented also to demonstrate clear difference of appearance of these two reaction mixtures.

Another reaction was performed in order to investigate whether the addition of 10 mL of solvent before or after the addition of the last reactant ($FeCl_3$) has a difference or not in reactions with 50 mL of solvents. Slightly different color changes were observed after stirring but the observations after first night were the same.

One reaction was performed with $CuCl_2 \cdot 2H_2O$, s-pyH and $FeCl_3$ (anhydr) with double amount of $FeCl_3$ in total reaction volume of 9 mL. $FeCl_3$ was the last added reactant and immediately after its addition the solution became turbid immediately instead of after about 7 min which differs from the observations of reactions with half the amount of $FeCl_3$ which had 15 mL reaction volume. The precipitate was initially very slowly descending but it transformed into larger pieces which descended faster. The solution and precipitate were orange yellow. After overnight stirring the solution was changed its color to greenish

yellow and the precipitate was lime green. The suspension was filtrated and the product was washed with EtOH. Color of the product was changed from lime green into more orange during the wash. Precipitate in the reaction with the same amount of $FeCl_3$ than $CuCl_2 \cdot 2H_2O$ yellow but during wash it was changed slightly into more brown from the edges. The total color of the precipitate remained yellow.

Another reaction was done in argon atmosphere with following substances: $CuCl_2 \cdot 2H_2O$, s--pyH, $FeCl_3$ (anhydr.) and KOH(aq) with ratios of 2:6:1:6 in 40 mL of 3:1 MeCN:EtOH solvent mixture. The solvent mixture was bubbled in argon prior the usage. s-pyH was dissolved in 20 mL and metal salts into 10 mL of the solvent mixture. The reaction was made under argon. KOH was added to the solution of s-pyH which lessens the yellowness of the solution. Dropwise addition of the solution of $CuCl_2 \cdot 2H_2O$ changed the color to dilute yellowish orange and the solution become turbid but not descending precipitate was formed. $FeCl_3$ was added immediately after observations right after the addition of $CuCl_2 \cdot 2H_2O$ solution. Right after the first drop, the solution altered into orange and the color continued to change into dark brownish yellow. There's lots of precipitate in the solution. After half an hour the suspension was brightened into being brownish orange while stirring. The stirring was temporarily stopped to observe the liquid phase to be yellow and the precipitate to be pale brown, in other words beige. The suspension was left to stir until the next morning when the suspension was yellowish orange as stirred which consist of yellow liquid phase and yellowish beige precipitate. The solution was filtrated and washed with 3:1 MeCN:EtOH. The wash solution became yellow and the precipitate was pale brown as dry. Too many parameters were changed in order to compare results to other reactions. Further reactions are needed in order to make definite conclusions.

12.4.2 Cu^{2+} & Cr^{3+}

Reaction with Cu^{2+} and Cr^{3+} were performed with $CuCl_2 \cdot 2H_2O$, s-pyH and $CrCl_3 \cdot 6H_2O$. Copper and chromium were used normally in 1:1 ratio. $CuCl_2 \cdot 2H_2O$, s-pyH and $CrCl_3 \cdot 6H_2O$ were dissolved in 5 mL of 3:1 MeCN:EtOH. If ammonium hexafluorophosphate was used, it was dissolved also in 5 mL of 3:1 MeCN:EtOH. Bases were also used in some reactions. Increase of total volume to 50 mL didn't seem to have any effect unlike in iron reactions in reactions without base and with NH_4PF_6.

When no base was used, there was a difference in the observations regardless of was $CrCl_3\cdot6H_2O$ used in either 2:1 or 1:1 ratio compared to Cu(II) chloride. If they were used in 1:1 ratio, no precipitate was formed by the end of the addition of $CrCl_3\cdot6H_2O$. A bit orange precipitate was formed after half an hour. The color of the liquid phase was not changed. After overnight stirring the precipitate was orange brown. When double the amount of $CrCl_3\cdot6H_2O$ was used, orange precipitate was formed during the addition of $CrCl_3$ solution. The color of the precipitate was changed during the day and continued to change overnight to orange brown. The color of the precipitate was the same regardless of was Cr and Cu used in 2:1 or 1:1 ratio.

Inclusion of NH_4PF_6 to the reactions with $CrCl_3\cdot6H_2O$, s-pyH and $CuCl_2\cdot2H_2O$ seemed to a have a small effect on the color of the precipitate in the products of reactions with 1:6:1 ratios of the starting materials (Cu:s-pyH:Cr). The precipitate was slower descending without NH_4PF_6 than with it. The color of the precipitate was orange brown without NH_4PF_6 and reddish brown with it. There's difference of 5mL in the volume of the reaction because every reactant was dissolved in 5 mL of 3:1 MeCN:EtOH and no additional amounts of solvents were added to either reaction.

Colors of the precipitates initially yellowish color and then they changed towards pastel green; when 0.36 mmol of Et_3N was used, the precipitate was yellowish beige. If 0.36 mmol or 0.18 mmol of KOH in EtOH was used the precipitate was brownish grayish yellow or brownish grayish orange, respectively. Without base and NH_4PF_6 the precipitate was orange brown so lighter than with NH_4PF_6. Without base and with NH_4PF_6 the precipitate was reddish brown. When larger volume was used without base and with NH_4PF_6, the precipitate was (orange) brown. The colors of the precipitates were changed after one year towards pastel green; with 0.36 mmol of Et_3N or KOH, the colors were pastel greenish grayish brown. With only 0.18 mmol of KOH, the precipitate was pastel gray. The precipitate of the reaction of the large volume was pastel green. The pale turquoise grey precipitate was assumed to be some kind of complex of s-pyH and Cr because the product of a reaction with only $CrCl_3\cdot6H_2O$ and s-pyH in 1:3 ratio in oxolane created pale turquoise grey precipitate.

12.4.3 Cu^{2+} & Ru^{3+}

Starting materials of reaction with Cu^{2+} and Ru^{3+} were $CuCl_2 \cdot 2H_2O$, s-pyH and $RuCl_3 \cdot 3H_2O$. No base was used. Ruthenium solution was completely non-transparent. When Cu^{2+}, s-pyH and Ru^{3+} were used in 1:6:2 ratio, the solution of Cu^{2+} and s-pyH was put into a heating bath of 55–65 °C for couple of minutes before the addition of Ru^{3+} during heating. While Ru^{3+} solution was added, black precipitate was formed and color of the solution was changed from orange into brownish orange. There's plenty of black precipitate after the addition. Heating as 2½ h in total but when it was stopped the reaction mixture was left to cool down in the heating bath overnight. The mixture was filtrated next morning. The precipitate was washed and reaction filtrate was black but it was greenish yellowish brown in other words "greenish beer". Because of the very vivid color of Ru^{3+} compounds made it close to impossible to observe precipitate formation, many of these reactions were not performed.

12.5 $AgClO_4$ precipitation reactions

Silver(I)perchlorate was used to remove Cl^- from $[MCl_x(phen)]$ complexes by formation of sparingly soluble AgCl(s) to provide empty coordination site for s-py(H) to coordinate. Abbreviation phen stands for 1,10-phenanthroline. $AgClO_4$ was used with $CuCl_2 \cdot 2H_2O$ or $AgNO_3$ with $[MCl_x(phen)]$ complexes. Zinc was used with $AgNO_3$ and M = Fe^{3+}, Ni^{2+}, Cu^{2+} and Zn^{2+} with $CuCl_2 \cdot 2H_2O$. $AgClO_4$ was used nearly exclusively in 1:1 ratio compared to $[MCl_x(phen)]$.

Generally, $[MCl_x(phen)]$ complexes were dissolved into EtOH if possible if not into MeOH. Water was avoided even though every $[MCl_x(phen)]$ complex used in this project dissolves in water. $AgNO_3$, s-pyH and $[ZnCl_2(phen)]$ were dissolved 5 mL of MeCN, 10 mL of EtOH and 11 mL of MeOH in reactions with $AgNO_3$. In reaction with copper, $CuCl_2 \cdot 2H_2O$, s-pyH, $AgClO_4$, $[FeCl_3(OH_2)(phen)]$, $[NiCl_2(phen)]$, $[ZnCl_2(phen)]$ and $[CuCl_2(phen)]$ were dissolved in 4–5 mL of MeOH, 4–6 mL of MeOH, 4–5 mL of MeOH, 12 mL of EtOH, 12 mL of EtOH, 11 mL of MeOH and 13 mL of 11:2 $MeOH:H_2O$.

Solutions of $AgClO_4$ and $[MCl_x(phen)]$ were mixed with each other. Different reaction times were used. The $AgClO_4+[MCl_x(phen)]$ mixture was filtrated and added directly from filtering funnel into the mixture of pyridine-4(1H)-thione and group 11 metal salts.

Addition of $AgClO_4$ into [$ZnCl_2$(phen)] resulted white precipitate already during the addition. During overnight stirring the color of the precipitate was changed into pastel violet while (top left photograph of Figure 26) the solution remained colorless (in EAS–211). Shorter reaction time, 15 min, resulted different color (EAS–212). On filtration paper overnight reaction had dark purple color while 15 min reaction had much lighter color (Figure 26). Increasing reaction time seems to increase the dark purple color of the precipitate. When reaction time was decreased into 10 min, wet precipitate was nearly colorless (Figure 26) likewise with 2 min reaction time. The color of the precipitate was noticed to change color from white to pastel violet in EAS–215.
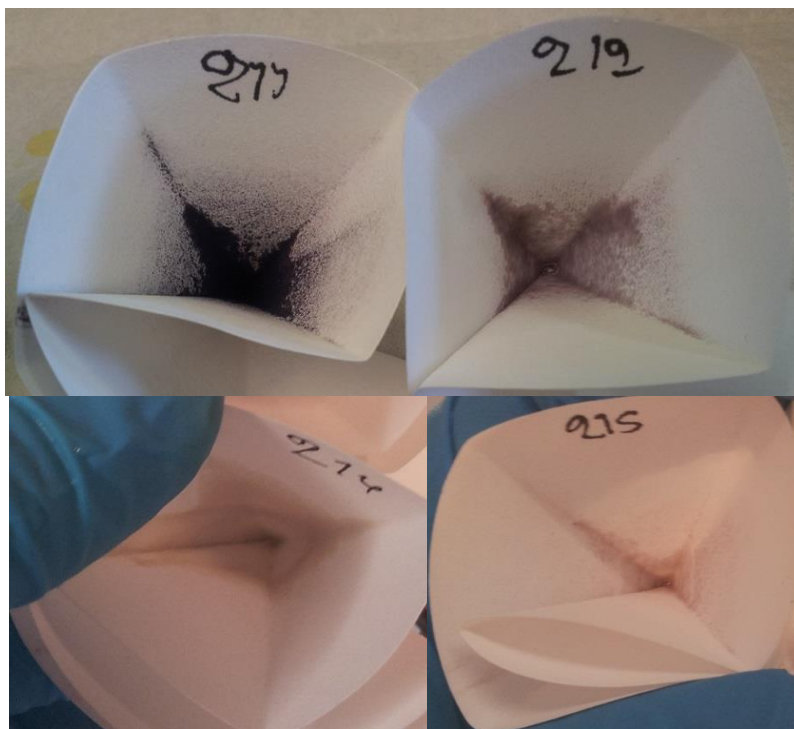
Figure 26. Effect of reaction time in reactions with $AgClO_4$ and Zn(phen)Cl_2. The reaction times were overnight (EAS–211), 15 min (EAS–212), and 2 min (EAS–215). EAS–214 had reaction time of 10 min but it had double the amount of $AgClO_4$ than the other three.

In EAS–215 and EAS−216 [$ZnCl_2$(phen)] was dissolved in EtOH but it was dissolved in MeOH in EAS–211, EAS–212 and EAS−214. This should have not an effect on the formation of AgCl.

The purple color caused confusion because it was not expected. [$ZnCl_2$(phen)] and AgCl are white. Zn could have been replaced by Ag to form [AgCl(phen)] complex. Crystal of

[AgCl(phen)]$_n$ with bridging Cl are red.[150] Crystals of [Ag(phen)]ClO$_4$ are pale yellow.[151] The precipitate cannot be any one of these compounds so it probably is some kind of compound containing silver and zinc.

Reactions of AgClO$_4$ with [FeCl$_2$(OH$_2$)(phen)] with different solvent conditions had interesting observations. Addition of AgClO$_4$ into orange [FeCl$_2$(OH$_2$)(phen)] clouded the solution in EAS–211. Both substances were dissolved in MeOH. 10 min reaction time was used followed by filtration. The precipitate was red on the filtration paper. When MeCN was used instead of MeOH, no precipitate was formed. The solution of AgClO$_4$ and [FeCl$_2$(OH$_2$)(phen)] was yellow not orange in EAS–212. Solid [FeCl$_2$(OH$_2$)(phen)] is orange. The conclusion is that AgCl was not formed instead some other reaction was occurred.

Green [CuCl$_2$(phen)] was dissolved in the mixture of 11 mL of MeOH and 2 mL of H$_2$O (in EAS–219). The solution was dilute blue. AgClO$_4$ and [CuCl$_2$(phen)] were reacted 5 min before filtration which resulted white precipitate in solution. Light green [NiCl$_2$(phen)] was dissolved in 12 mL of EtOH (in EAS–220). The solution was very dilute green. AgClO$_4$ was dissolved in 4 mL of MeOH in EAS–219 and EAS–220.

EAS−215 and EAS–216 were the only reactions with AgClO$_4$ and another silver salt. The problem in these reactions was that also the other silver salt AgNO$_3$ could also remove Cl$^-$ from phen complex. In EAS-215 KOH was added into the solution of s-pyH in 10 mL of EtOH. pH paper had color of pH = 8 immediately after the addition of drop onto the paper. However, while solvent was nearly evaporated the color of the pH paper indicated pH = 10. There're only a few precipitate particles in the yellow solution. AgNO$_3$ in 5 mL of MeCN was added fast and dropwise to s-pyH solution. The solution turned slowly from very dilute yellow into orange at the latter half of the addition of AgNO$_3$ but during 3–10 min after the addition of AgNO$_3$, the solution was turned into orange. Overnight stirring change the color into peculiar yellowish brown with a bit brown precipitate.

Addition of filtrated AgClO$_4$+Zn(phen)Cl$_2$ solution into non-filtrated AgNO$_3$+s-pyH suspension didn't create any visible change in the appearance of the AgNO$_3$+s-pyH solution liquid or solid phase in EAS–215. The same amount of precipitate was in the solution as before the addition of Ag but the amount of precipitate was increased; there're much more precipitate after 3 h of the addition of AgClO$_4$+Zn(phen)Cl$_2$ solution than 15 min after it. During the 3 hour waiting time the solution was evaporated from 30 mL to 25

mL. The solution was evaporated to 20 mL before filtration. The precipitate on filtrating paper was brown and the solution was dilute yellow. Filtrated was left to evaporate but lots of KOH crystals were formed everywhere.

EAS-216 was similar reaction than EAS–215 with the only difference being smaller reaction time of formation of Ag polymer before the addition of zinc containing solution. The reaction time for $AgNO_3$ and s-pyH to react was 2 hours during that time the reaction mixture was not changed into brown instead it remained cloudy orange. The solution was stirred 2 hours but no precipitate was formed. This contradicts to the observation made in EAS–215. It was concluded that EAS–215 favored an undesired reaction bath because of the brown color as other unsuccessful reactions with $AgNO_3$. Remaining orange color was hypothesized to be desirable as mentioned previously. Anyway, the solution was left first not to evaporate but later the solvent was evaporated. When 11 mL of solution was left, lots of solid KOH was around the vessel. KOH in liquid was pastel red and under pastel red KOH it was really dark, nearly black precipitate. EAS–215 and EAS–216 were the only reactions of $AgClO_4$ with another silver salt.

EAS–211, EAS–212, EAS–214, EAS–219, EAS–220, EAS–221 and EAS–222 are the reactions used $AgClO_4$ precipitation with $[MCl_x(phen)]$ followed by addition of this filtrated solution into the solution of $CuCl_2 \cdot 2H_2O$ and s-pyH. No base was used as it was not normally used other copper reactions. The observations of precipitation reactions with $AgClO_4+[MCl_x(phen)]$ were described above. Combination of solutions of $AgClO_4$ & $[MCl_x(phen)]$ and $CuCl_2 \cdot 2H_2O$ & s-pyH are discussed herein.

EAS–221 and EAS–222 are reactions with $[FeCl_2(OH_2)(phen)]$ with the only difference being solvent. MeOH was used in EAS–221 and MeCN in EAS–222. The observations were as follows with MeOH: the solution of $AgClO_4$ and $[FeCl_2(OH_2)(phen)]$ was cloudy orange which was filtrated directly into the orange solution of $CuCl_2 \cdot 2H_2O$ and s-pyH. The solution turned immediately into true red. The solution remained red without precipitate during overnight stirring. The solution was left to evaporate without stirring in the next morning. After one week solution was red and yellow dots were formed on the bottom and sides of the evaporation jar. Red precipitate was formed to the top area of the jar. After three weeks from the reaction solution was red but yellow dots were colored with green layer. Dots turned into black or very intensive brown when the solution was completely evaporated. No red precipitate was formed. Some green crystals existed. MITATTAVA! Most of the precipitates were very intensive brown with the exception of some brown

precipitate midpoint of the evaporation jar and orange yellow precipitate was at the very top of the jar.

Because of the precipitate formed with $CuCl_2 \cdot 2H_2O$ and s-pyH in MeCN in EAS–221, observations were different. The precipitate was orange and the solution was yellow before the addition of filtrated solution of $AgClO_4$ and $[FeCl_2(OH_2)(phen)]$. The latter solution was cloudy yellow before filtration. No precipitate was left on the filtration paper. The addition of the solution of $AgClO_4$ and $[FeCl_2(OH_2)(phen)]$ into the solution of $CuCl_2 \cdot 2H_2O$ and s-pyH the color of the solution turned the (reddish) orange. The precipitate had no or only minor color changes but its amount was increased. The precipitate was also adhered onto sides of the reaction vessel. After two days the precipitate was scraped from the sides and stirring was continued. Stirring was finished on the following day. The solution was red and precipitate was orange.

The solution of EAS–222 was filtrated and filtrate was left to evaporate. During evaporation red layer was adhered onto the sides of evaporation jar. There's also some very dark red or black precipitate or red precipitate with thicker layer in the jar. The lowest part of the red was more orange or brown. Beneath that layer was another layer which was colorless except it contained tiny dark and white precipitate pieces. The bottom of the jar was part of this layer.

Red color of the solution and not having precipitate suggest MeOH to be better solution for the reactions with $AgClO_4$, $[FeCl_2(OH_2)(phen)]$, $CuCl_2 \cdot 2H_2O$ and s-pyH in the future. However, while dried filtrates are compared, the red color in MeCN appeared intuitively more promising.

Only one $AgClO_4$ precipitation reaction with $[NiCl_2(phen)]$ was accomplished and it's EAS–220. One $AgClO_4$ precipitation reactions with $[CuCl_2(phen)]$ was performed and it's EAS–219. Both of these were reacted with $AgClO_4$ followed by filtration which was followed by its reaction with pyridine-4(1H)-thione and $CuCl_2 \cdot 2H_2O$. The reaction with $[MCl_2(phen)]$ and $AgClO_4$ for these two syntheses are described hereinbefore. The latter part of the syntheses is described here.

Solution of $AgClO_4$ with $[CuCl_2(phen)]$ was very dilute blue with white precipitate, presumably AgCl. It was filtered into orange solution of $CuCl_2 \cdot 2H_2O$ and s-pyH. The color of the solution was maybe changed a bit more red but the possible change was so small that it was not completely sure did the color change at all or not. No precipitate was formed

immediately but after 1 h after the end of filtration yellow precipitate was formed. The solution was a bit less red but still orange. The suspension was left to stir overnight. The solution turned into greyish green with plenty of greyish brown precipitate. The solution was filtrated and the filtrate was left to evaporate slowly. Filtrate was cloudy bluish green.

5 mL of the solution of EAS–219 was left after one week of evaporation. There're only blue and light blue precipitates on the lower part of the jar but green precipitate on the higher part. There's white powder on the bottom which maybe was AgCl which has been formed after the filtration. Solution was light blue. Later when only 1 mL of the solution was left, the solution was green or bluish green. Multiple colors of precipitates were observed on the sides of the jar: light blue, pastel green, green, light green. Blue crystals were observed as well as brownish orange. The overall appearance looks similar to EAS–178 and EAS–181T2. EAS–181T2 was a reaction of $CuCl_2 \cdot 2H_2O$, s-pyH and [$CuCl_2$(phen)] in 1:6:1 without base in 3:1 MeCN:EtOH containing 35 % H_2O. Same starting materials were used also in EAS−178 but with ratio of 1:6:2. Solvent composition was the same as in EAS–181T2 but only 22.2 % of H_2O was used. Heating in 63 ± 2 °C was used in EAS–178 for 3 h but neither in EAS–181T2 nor in EAS–219. Because no drastic changes in color were observed, it's impossible to say whether the application of $AgClO_4$ precipitation was useful or not.

EAS–220 was the only $AgClO_4$ precipitation reaction with [$NiCl_2$(phen)]. Mixture of $AgClO_4$ and [$NiCl_2$(phen)] was cloudy and colorless. It was filtrated directly into orange solution of s-pyH and $CuCl_2 \cdot 2H_2O$. The nickel solution caused formation of (yellowish) orange precipitate. The precipitate formation began quite soon after the beginning of addition of the nickel solution. The suspension was left to stir overnight but no change in appearance happened overnight. The precipitate was filtrated and noticed to dissolve in water and MeOH. When concentrated, solution of the product in water was red but more dilute it was orange or yellow.

EAS–211, EAS–212 and EAS–214 were $AgClO_4$ precipitation with [$ZnCl_2$(phen)]. No other this kind of reaction was conducted. Effect of reaction time to AgCl formation was discussed hereinbefore. Addition of filtered colorless solution of $AgClO_4$ and [$ZnCl_2$(phen)] into the orange solution of s-pyH and $CuCl_2 \cdot 2H_2O$. No visible change occurred during the reaction. EAS-214 yielded orange a precipitate by the next morning but that might be the same precipitate with s-pyH and $CuCl_2 \cdot 2H_2O$ only. However, this is assumed to be quite improbable. The biggest difference between EAS–214 and the two

other reactions is the amount of $AgClO_4$ used: $AgClO_4$ was used double the amount in EAS–214 than in EAS–211 or EAS–212. EAS–214 was filtrated and all the three solutions were left to evaporate.

When all the solutions of EAS–211, EAS–212 and EAS–214 were totally evaporated, the colors of the solid matter on the bottom and sides of the jars differed from each other. EAS–211 had greyish brown bottom which was greener on between bottom and sides. EAS–212 was pastel green or pastel turquoise. EAS–214 was black. Sides of the jars had interesting colors. EAS–211 had different green precipitates and reddish brown precipitates. EAS–212 had different mixed colors of green, turquoise, brown and ochre. EAS–214 had black or dark brown area, the previous one but with green, ochre area and brown line. EAS–212 and EAS–214 contained rod shaped colorless or really pale yellow.

In summary of $AgClO_4$ precipitation reactions, removal of chloride with $AgClO_4$ was not as simple as it was thought. The purple change with $ZnCl_2(phen)$ was interesting. Appopriate reaction time with $AgClO_4$ with $[MCl_2(phen)]$ is less than 10 min. Longer waiting time increases the amount of purple precipitate which was undesirable too short waiting time results formation of AgCl into the filtered solution. No great changes in the reactions of $CuCl_2 \cdot 2H_2O$, s-pyH with $[CuCl_2(phen)]$ whether $AgClO_4$ was used or not.

12.6 Cu^{2+} + Ag^+ reactions

Four different reactions with $AgNO_3$ and different Cu^{2+} salts were performed. One of them was slow diffusion reaction which is discussed hereinafter but three are discussed herein (EAS–135, EAS–136 and EAS–180). EAS-135 was only one of these reactions without a base. KOH was used in EAS-180. KOH and acetic acid were used in EAS–136. The copper salt was $Cu(OAc)_2 \cdot H_2O$ in EAS–135 and EAS–136 but $[CuCl_2(phen)]$ in EAS–180. Ag:s-pyH:Cu ratio was 1:6:2.2 in EAS–135 and EAS–136 but 1:4:1 in EAS–180. EAS–135 and EAS–136 were done in water but EAS–180 was done in 5:13:4 $MeCN:EtOH:H_2O$. Total volumes were 22 mL in EAS–180 and 18 mL in other two reactions.

EAS–135 was like EAS–136 but without pH adjustments. Measuring pH in other solvents than water was very challenging and unreliable that's why the reaction was made in water. $AgNO_3$ was dissolved in 4 mL and s-pyH in 10 mL of water. pH of s-pyH solution was set from 6 to 8–9 in EAS–136. $AgNO_3$ was added dropwise into s-pyH solution. Fine

precipitate was formed in EAS–135 and its solution was yellowish orange. EAS–136 contained large and yellow precipitate pieces in yellow solution. pH was set from 6.2 to a bit above 8 in EAS–136. Cu(OAc)$_2$·H$_2$O was dissolved in 10 mL of water and the resulting blue solution was added into the reaction mixture. EAS–135 turned into yellowish orange with blue shade. It also contained fine powder. EAS–136 was not so orange as EAS–135. The color of the solution was yellow with greenish shade. The appearance of EAS–136 didn't change as much as the appearance of EAS–135 in this part.

After addition of Cu(OAc)$_2$·H$_2$O pH of EAS–136 was set from 6 to 10. The precipitate seemed to change into different precipitate of the same color. The amount of precipitate was increased a lot in this step. The precipitate looked like rows of Λ which were on the top of each other. The attempt was not to change pH so much but suspension acted as buffer and pH changed too much after equivalence point of the buffering system. One drop of acetic acid was used to lower pH but it was lowered too much to 6. The precipitate seemed to lower faster after the addition of acetic acid than before and it seemed to fill the vessel but being more airy. More KOH was added and pH settled to 8–10. pH of EAS–135 was about 6 all the time.

The solutions were stirred overnight and left to stay for three days before filtration. EAS–135 smelled acetic acid but EAS–136 didn't. However, the precipitate contained orange precipitate above which was green precipitate. Only the green precipitate was taken and washed. The precipitate of EAS–136 was yellowish beige. The precipitates were filtrated, washed and dried. After that colors of the precipitates were as follows: EAS–135 was greyish brownish green and EAS–136 was light brown with orange shade.

EAS–180 was done similar way than EAS–136. AgNO$_3$ was dissolved in 5 mL of MeCN and s-pyH in 10 mL of EtOH. [CuCl$_2$(phen)] was dissolved in 3 mL of EtOH and 4 mL of water. pH of s-pyH was risen to 10. Addition of KOH into s-pyH demolished yellow color of the solution and further addition created white precipitate which was adhered on the sides of the container. It was most likely KOH with possibly s-pyH. The formation of the precipitate began when pH was about 9–10. AgNO$_3$ solution was added rapidly dropwise which caused the solution to turn into brownish orange with white precipitates prevailing. It was left to mix for 1 h.

[CuCl$_2$(phen)] was added dropwise into the solution of s-pyH and AgNO$_3$. The white precipitate was dissolved most likely because added solution contained water. The solution

became cloudier and its color changed from brownish orange into more brown but the color was still brownish orange. After overnight stirring the solution was filtered and washed. The filtrate was left to evaporate. When almost all of it was evaporated, brownish red precipitate and some green precipitate was formed. Solution was strong green. Most of the precipitate was thought to be impure KOH.

12.7 Cu^{2+} + Au^{3+} reactions

Three reactions with Cu^{2+} and Au^+ or Au^{3+} were performed. They were all done with $AuCl_3$. Two of those reactions were slow diffusion reactions (EAS–189 and EAS–190) and one was not (EAS–187). Only EAS–187 is discussed here. Starting materials were $CuCl_2 \cdot 2H_2O$, s-pyH and $AuCl_3$ in 1:6:1 ratio. Copper salt was dissolved in 4 mL of 3:1 MeCN:EtOH and s-pyH in 7 mL of 3:1 MeCN:EtOH. $AuCl_3$ was dissolved in 7 mL of 9:3:16 MeCN:EtOH:H_2O.

Copper chloride was added into s-pyH solution in EAS–187. The solution was orange without precipitate. The solution was stirred 5 min. Dilute yellow $AuCl_3$ solution was added carefully dropwise into the solution of s-pyH and $CuCl_2$. The drops formed transitory precipitate which was dissolved at the early stage of the addition of gold solution. However, the formed precipitate was permanent. When half of $AuCl_3$ was added the solution was clouded throughout the solution. Orange precipitate was formed while solution was yellow. After 5 min solution was notably brighter and precipitate was yellow or orange yellow. Lots of precipitate was formed. The suspension was left to stir overnight. By the next morning precipitate was change into lime green. Lime green color is promising.

12.8 Slow diffusion reactions

Different slow diffusion reactions were done in order to have higher changes to get crystal structures. Slow diffusion reactions were done especially with similar molar ratios and starting materials than another reaction which yielded a precipitate. However, this was not always the case; slow diffusion reactions were also used without corresponding "normal" reaction. In other words, 0.36 mmol of s-pyH was used in each copper reaction. Molar amounts of starting materials were only ⅔ of the normal in EAS–189 and ⅓ in EAS–190. In slow diffusion silver reactions ratio of starting materials (Ag:s-pyH:M), M stands for

another metal was 1:4:2. The ratio in moles was 0.09 mmol:0.36 mmol:0.12 mmol. In copper reactions the ratio was either 1:6:2 or 1:6:1. The ratio in moles was 0.06 mmol:0.36 mmol:0.12 or 0.06 mmol. In EAS–186 0.06 mmol of ammonium hexafluorophosphate was used. Only 0.090 mmol of s-pyH and 0.017 mmol of $AuCl_3$ were used in every slow diffusion gold reaction with only the two starting materials.

The idea of slow diffusion reaction was obtained in the synthesize of $[ZnCl_2(2,2´-bpy)]$.[152] Abbreviation 2,2'-bpy stands for 2,2'-bipyridine. In that reaction, 2,2'-bpy was dissolved in CH_2Cl_2 which was carefully layered by methanol solution of $ZnCl_2$. This synthesis was performed multiple times with double the amount than in the literature.

In slow diffusion reactions with silver or copper, group 11 salt was added dropwise to the solution of s-pyH like in normal reactions. Reaction time for this was as short as in normal reactions like 15 min or no waiting time at all. Magnetic stirring was used and it was removed before addition of other layers. Other layers were carefully trickled on the top of layer of s-pyH and group 11 salt using Pasteur-pipette followed by adding cap to avoid evaporation of the solvents.

12.8.1 Slow diffusion gold reactions

Gold reactions were slow diffusion reactions with two-layers. Method developed by Kalle Machal was applied. AuCl was dissolved in 10 mL of MeCN and s-pyH in 11 mL of $CHCl_3$ (Scheme 11). Solubility problems with AuCl were similar than in non-layered reactions. 0.017 mmol of AuCl and 0.090 of s-pyH was used in each slow diffusion gold reaction.The separation of the two phases was very clear but no immediate precipitate or crystal formation was observed. Formation of crystals began on the same day but crystals grew overnight larger. Crystals were yellow. Because Kalle Machal had already analyzed the crystal structure of the corresponding reactions before, there's no need to measure the crystal structure again. Its pseudoisomorph has been measured by Räisänen *et al*.[153] The structure is discussed in the chapter of crystallographic data. There's no difference whether the layering was performed in refrigerator or in room temperature.

12.8.2 Slow diffusion silver reactions

Slow diffusion reactions with exclusively three layers were done with silver. They were EAS–155, EAS–156 and EAS–163. The challenge with slow diffusion silver reaction was the usage of base. Only pH of the layer of $AgNO_3$ and s-pyH was risen so when upper layers were added, differences in pH created additional currents between the layers. It would have been hard to estimate the similar amount of bases to the other layers because measuring pH from organic solutions was very untrustworthy. Anyway, schematic pictures of EAS–155 and EAS–156 are shown in Scheme 11. That's why emphasize was on other reactions.
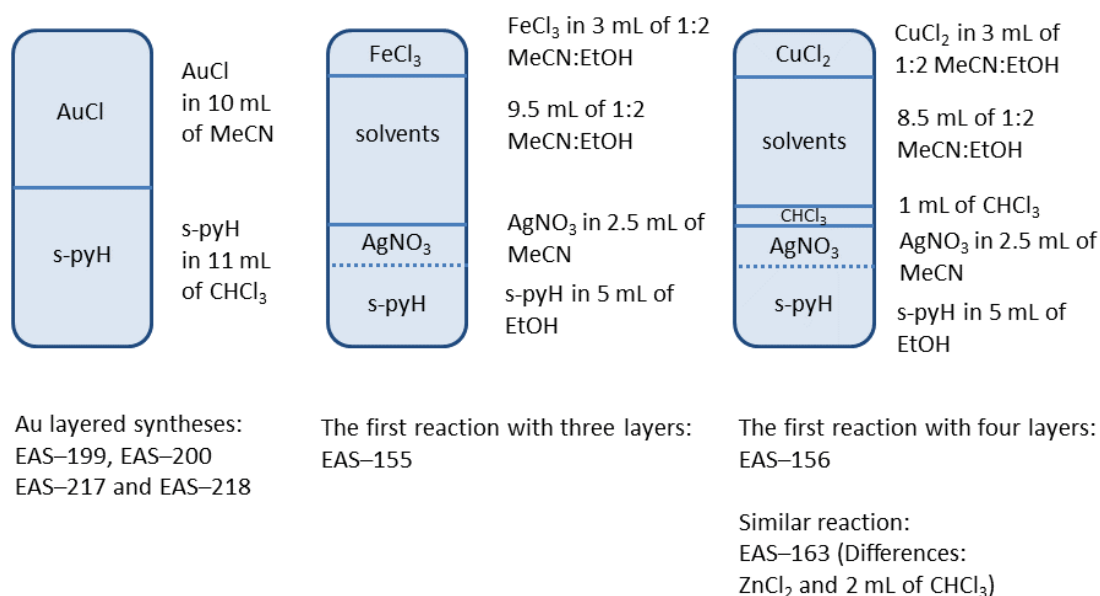
Scheme 11. Different slow diffusion reactions. Leftmost one is general scheme of two-layer reaction with gold and s-pyH. Middle one is scheme of the first three-layer reaction EAS–155 and the rightmost one is the scheme of first four layer reaction EAS–156. Dashed line indicates stirring of s-pyH and group 11 metal solutions before layering.

Anyway, silver reactions were the first multi-layered reactions (i.e. reactions with more than two layers). They had role in developing layered copper reactions because they were done prior to copper reactions. Addition of chloroform layer between stirred solutions of $AgNO_3$ and s-pyH separated better upper layers from the lowest layer in EAS–156 compared to EAS–155. However, because other than group 11 metal salt in this reactions was different, the comparison is harder. EAS–163 was done with third not group 11 metal salt but with double the amount of $CHCl_3$. The separation of the bottommost and $CHCl_3$

layer and other layers was clearly better with EAS−163 than in EAS−155 without $CHCl_3$ layer. The $CHCl_3$ layer mixed with the bottommost layer but this combined layer was clearly separate from the solvent mixture layer in EAS−163. However, most likely layers of $ZnCl_2$ and solvent mixture were combined but it was impossible to notice because the layers were identical with no obvious layer border.

Descending of the uppermost layer was a problem. It was noticed in EAS−155 very clearly with iron chloride and also with copper chloride in EAS−156. Both mixed with pure solvent mixture layer but $CHCl_3$ seemed to prevent or retard mixing of the layers. Without $CHCl_3$ iron chloride seemed to descend into the bottommost layer. Because colorless $ZnCl_2$ was used in EAS−163 it's impossible to say how much the topmost and bottommost layers were mixed soon after addition of the layers. All the layered silver reactions (EAS−155, EAS−156 and EAS−163) created lots of precipitate. Because these reactions were not promising, group 11 element was changed to copper, which functioned better.

12.8.3 Slow diffusion copper reactions

Usage of $CHCl_3$ was promising in slow diffusion silver precipitation reactions so it was used in slow diffusion copper reactions. However, too much chloroform was not wanted to use because it was known that if chloroform or dichloromethane was used as solvent, dimeric structure was formed with Ag.

The first slow diffusion copper reaction was EAS−167 which produced long and orange needle shaped crystals which structure was able to solve. Because of the success of EAS−167, it was most commonly used slow diffusion copper reaction. Schematic picture of its layers is shown on the left in Scheme 12. The biggest difference in EAS−167 type reactions compared to slow diffusion silver reaction with four layers (EAS−156) is the inclusion of chloroform in solvent mixture above the pure chloroform layer. This helped making the solvent mixture layer denser to hinder to retard mixing of solvent layer with the topmost layer. Also the amount of solvent in the topmost layer was increased a bit from 3 mL to 4 mL.

Scheme 12. Slow diffusion reactions of EAS–167 type and EAS–188 type. Left: EAS–167 type, right: EAS–188 type. No other reactions with exactly the same amount of solvents were used that's why EAS–189 and EAS–190 are stated as similar reactions. Dashed line indicates stirring of s-pyH and $CuCl_2 \cdot 2H_2O$ solutions before layering. *Chloroform was used double the amount in EAS–170 than in EAS–167 but other volumes were the same than in EAS–167.

Volume of the uppermost layer was increased further. Likewise, the volume of the bottommost layer was decreased further. The concentration of the metal salts affects to the density of the liquid. Because molar amounts of starting materials were used as constant (or only changed in specific way like metal salt was doubled in some reactions), the concentration was changed by changing the volumes of layers. The volume differences made for EAS–167 resulted layered reaction of EAS–188 type (on the right in Scheme 12). EAS–189 and EAS–190 didn't have exactly the same volumes of all the layers. That's the reason why they are stated as similar reaction to EAS–188 in Scheme 12. Their biggest solvent difference was that their topmost layer had volume of 9.5 mL instead of 7.5 in EAS–188. The nature of the metal of the topmost layer was different: it was $AuCl_3$ in EAS–189 and EAS–190 but $RuCl_3 \cdot 3H_2O$ in EAS–188.

Reactions without $CHCl_3$ were also used. Their volume ratios were similar to EAS–188 type. These reactions EAS–201 type and EAS–205 type which are very similar in volume-wise (Scheme 13). There's one 1 mL difference in $CuCl_2 \cdot 2H_2O$ solution and the topmost layer. Nonetheless, the biggest difference is that the solvent in topmost layer is mainly diethyl ether. Et_2O was used to try different reaction conditions. Its density is also slightly lighter than the densities of ethanol and acetonitrile.
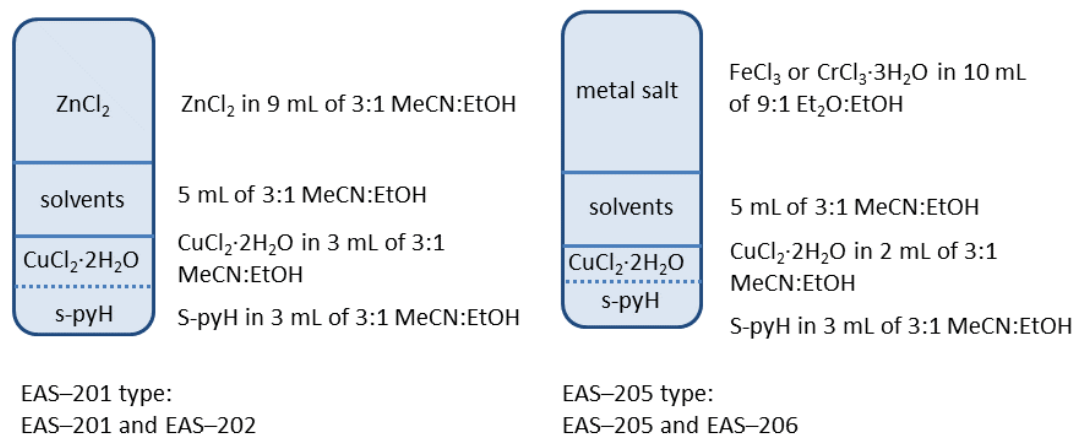
Scheme 13. Slow diffusion reactions of EAS–201 type and EAS–205 type. Left: EAS–201 type, right: EAS–205 type. Dashed line indicates stirring of s-pyH and $CuCl_2 \cdot 2H_2O$ before layering.

EAS–186 was special reaction in which also NH_4PF_6 was used and some chloroform was stirred before layering with pure solvent mixture layer and $[FeCl_3(phen)]$ layer (Scheme 14). Water was used for $[FeCl_3(phen)]$ to dissolve it. EAS–186 is not density-wise as ideal as slow diffusion reactions in Scheme 13. Chloroform was mixed with the bottommost layer in order to increase the density of the lowest layer.
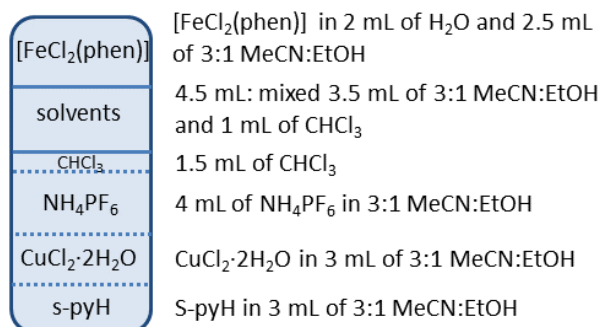
Scheme 14. Slow diffusion reaction of EAS–181. Dashed line indicates stirring of s-pyH, $CuCl_2 \cdot 2H_2O$, NH_4PF_6, and $CHCl_3$ solutions before layering.

Slow diffusion reactions are usually done by having two layers. The lower one is denser and upper one is lighter. In the reactions used, mainly the same solvent was used. The reason for this was to avoid solubility problems of the starting materials i.e. avoid

crystallization of starting material. When the same solvent conditions were used and crystals were formed, it was sure that the crystals were product not starting material because otherwise the starting materials would have not dissolved in the first place.

One problem was that the layer with sole solvent is the lightest one but it was the middle one. That's why the topmost layer was heavier. This problem was observed many times especially with early layered reactions like EAS–155 and EAS–156. To reduce the problem small amount of denser solvent, $CHCl_3$, was added into the solvent mixture layer to make it denser. Another problem was when pure $CHCl_3$ layer was used; it was heavier than bottommost layer of group 11 metal salt and s-pyH. $CHCl_3$ was commonly observed to partially blend into the bottommost layer. Still this was considered better choice than mixing chloroform into the bottommost layer. For example in EAS–167 there was area of stronger color on the on the opposite side of bottom of the layering jar which means that there still were more s-pyH and Cu concentrated area on the very bottom.

The phase border was very clear in EAS–167. However, there's only one clear phase border and it was between $ZnCl_2$ phase and solvent phase in EAS–167. $ZnCl_2$ layer seems to stay well on the top of solvent mixture when it contained $CHCl_3$ at least in EAS–167. However, when double the amount of chloroform was used in EAS–170 than in EAS–167 or EAS–171, other than the topmost layer were blended into each other. The blending was not so fast in EAS–171 than in EAS–170. They were layered immediately after one another.

Crystals were formed in slow diffusion with reaction multiple layers but the crystals were not stable. Crystals were observed in EAS–184 but they were absent later. EAS–184 was attempted to evaporate to get crystals to be measured but it was unable to do so. Same thing happened with EAS–205. Maybe there's certain combination of concentration which created the crystals in the mixture. Transitory crystals spike shape crystals formed in EAS–201 and EAS–202 but they were transformed into precipitate before X-ray measurements. However, it probably was not the exactly the total combination of concentration but rather a local combination of concentrations which was due to lack of stirring. Other possible way is that the crystals were kinetic product but it they were not the thermodynamical product.

Making the bottommost phase smaller i.e. more concentrated seemed to work well in EAS–188. There were two layers separated from one another before the layering the topmost layer in EAS–188. Some diffusion still occurred but lesser amount than in EAS–167. EAS–

189 seemed to work as well as EAS–188 but it wasn't surprising because their layers were nearly identical.

[FeCl$_3$(phen)] was dissolved partially in water in EAS–186 (Scheme 14). The usage of water in the topmost was not optimal because it's denser than EtOH or MeCN. EAS–186 had another problem that it's the most bottom layer was lower in concentration of starting materials than any other reaction which could be a good idea to perform the reaction slower but as the bottommost layer it's not good because its density was low. In EAS–186 chloroform was stirred into the bottommost layer which would afterwards seem better not to do.

12.9 Synthesis of [MCl$_2$(phen)] or [MCl$_3$(OH$_2$)(phen)] complexes

[MCl$_2$(phen)] or [MCl$_3$(OH$_2$)(phen)] complexes were synthesized using different literature routes either directly or applied from similar syntheses. 1,10-phenantholine complexes synthesized were: [NiCl$_2$(phen)], [CuCl$_2$(phen)], [ZnCl$_2$(phen)] and [FeCl$_3$(OH$_2$)(phen)]. Literature[154] synthesis was applied for [NiCl$_2$(phen)]. Yield of the reaction done in this project was 20 % (calc. from NiCl$_2$) but it was 87 % in the literature. However, the molar amounts were ⅓ than in the literature and their ratio was reversed (5:7), (Ni:phen). Literature[155] synthesis for [CuCl$_2$(phen)] was applied with double amount of starting materials. The yield was 79 % (calc. from phen) and the literature yield was 92 %. Literature[154] synthesis for [NiCl$_2$(phen)] was applied for [ZnCl$_2$(phen)]. The yield of [ZnCl$_2$(phen)] was 97 %.

A literature reaction was applied in order to make iron 1,10-phenantholine complex but later an easier literature[156] reaction was used with double amount of starting materials than in the literature. The yield [FeCl$_3$(phen)] for was 87 % in the literature. The product obtained from the literature was [FeCl$_3$(phen)] according to the elemental analysis. The mass percentages of the literature results were indeed closer to [FeCl$_3$(phen)] than [FeCl$_3$(OH$_2$)(phen)] or [FeCl$_3$(OHMe)(phen)]. However, the elemental analysis results of the product of this project (EAS–176) are clearly closer to [FeCl$_3$(OH$_2$)(phen)] than [FeCl$_3$(phen)] or [FeCl$_3$(OHMe)(phen)], as can be seen in Appendix 3. The limiting factor of the reaction was 1,10-phenanthroline with a slight difference. The yield for [FeCl$_3$(OH$_2$)(phen)] calculated from phen is 75 %. (For [FeCl$_3$(phen)] it would be 79 %).

Differences between the literature[156] process and the one exactly executed in this project (EAS–167) were as follows: double the starting materials were used, as mentioned before. Double the solvent volumes were used as well so concentrations of the solutions remained the same. The reaction time was only 15 min in the literature reaction but it was 4 h and the precipitate formed was left to say overnight without stirring before filtration. The suspension was filtrated with Büchner before and after addition of diethyl ether. The amount of diethyl used in the literature is not mentioned in the literature. 30 mL of Et_2O was used in EAS–167. More precipitate was formed when Et_2O was added.

The difference of the product of EAS–167 and literature[156] might be due to different reaction time or addition of diethyl ether after first filtration. These reasons don't seem to be logical, though. Because elemental analysis clearly indicated the product to be $[FeCl_3(OH_2)(phen)]$, it is considered the product of EAS–167.

12.10 Reactions of s-pyH with non-group 11 metals without group 11 metals

Some reactions without group 11 metals but with other metals were performed. The salts were reacted with s-pyH. There were two reasons for making these reactions. One was to see what colors of these products have. The observations would aid interpreting observations from reactions with group 11 metals and non-group 11 metals. Another aim was to complex these metals first with s-pyH and then react them group 11 metals. However, time ran out and these reactions were not able to carry out.

The metals used for these reactions were: $ZnCl_2$, $FeCl_3$, $RuCl_3 \cdot 3H_2O$. Some of these reactions are discussed in the chapter of copper with the corresponding metal. The amount of metal salt was 0.06 mmol in each reaction and the amount of s-pyH was adjusted according to the desired ratio of metal and s-pyH. The salts and s-pyH were normally dissolved in 5 mL of 3:1 MeCN:EtOH. The ratio of metal salts and s-pyH was normally 1:6.

Addition of $FeCl_3$ into the solution of s-pyH created temporary reddish brown color at the beginning of addition of $FeCl_3$. The additions turned solution into orange. When roughly 80–90 % of $FeCl_3$ was added, lots of precipitate was formed. The solution was yellowish orange and the precipitate was yellow. Further addition of $FeCl_3$ created transitory reddish

brown color but the solution and precipitate remained yellow. Overnight stirring didn't change the appearance of the suspension. The precipitate was yellow with green shade as dry and it was soluble in water.

The observations were strictly different in water because the addition of $FeCl_3$ didn't create any changes not even transparent ones in water. After the addition of $FeCl_3$ the solution was weakly yellow with orange shade. No immediate precipitate was formed. Small amount of white precipitate was formed after couple of hours but it was assumed to be S_8. No changes were observed during overnight stirring.

When $FeCl_3$ and s-pyH were used in 1:2 ratio in 3:1 MeCN:EtOH, similar observations were observed in 1:6 than 1:2 ratio of the starting materials in 3:1 MeCN:EtOH. $FeCl_3$ was dissolved in 10 mL of the solvent mixture instead of 5 mL. The reddish brown color was permanent one point but when addition of $FeCl_3$ was continued the solution clouded and became more yellow so much that right after the addition of $FeCl_3$ there's two kinds of precipitate yellow and orange. After 20 min of the addition solution was yellowish orange with yellow precipitate. The solution was left to stir overnight but no change in the appearance was noticed. The dried product was soluble in water but not in MeCN. Wash with MeCN changed the color of the product into more orange to yellowish orange.

The solvent had a great effect on the reaction. Lack of reddish brown color in water seem to suggest that some kind of iron complex was formed in 3:1 MeCN:EtOH which is not formed in water or is formed to much less extend. Sample of 1 mL of the reaction mixture of the water synthesis was evaporated quickly in rotatory evaporator. Heterogenic mixture of yellow and orange precipitate was formed which was only mainly dissolvable in EtOH. Most likely multiple products were formed in all of these reactions. The colors of the product were similar: orange and/or yellow. However, orange color of the product in reactions with $FeCl_3$, s-pyH and group 11 metal salt can be due to a product which doesn't contain group 11 metals as these reactions prove. Further analysis is needed to make further conclusions.

Reactions of $RuCl_3 \cdot 3H_2O$ with s-pyH either in 1:6 ratio in 3:1 MeCN:EtOH or 1:3 ratio in MeOH produced black precipitate. The color of the reaction solution changed from black yellow into orange the reaction with starting material ratio of 1:6 in 3:1 MeCN:EtOH after two and half hours the addition of ruthenium solution into s-pyH solution.

Reaction of $CrCl_3 \cdot 3H_2O$ and s-pyH yielded colorless solution with pastel green precipitate. Starting material $CrCl_3 \cdot 3H_2O$ was true green and s-pyH was yellow. Starting materials were used in 1:3 ratio, respectively. The filtrate was evaporated nearly completely. The color of the solution was turned into violet which is most likely due to colorless anhydrous $CrCl_3$ which is purple as solid.

13 NMR spectroscopy

Some samples were analyzed with NMR spectroscopy but because emphasize was on crystal structures in this project, not very many NMR spectra were measured. One solid state measurement was performed for monometallic silver polymer (EAS–157–160) at 303 K with Elina Sievänen. The spectrum and some parameters are Appendix 1. Three peaks are visible in the spectrum at 173.6731 ppm, 142.7537 ppm and 132.8464 ppm. The last two are close to each other on a hillock. These values correspond to three different carbons on s-py(H) ligand.

14 Crystal structures

14.1 Cu polymer

Crystals of cationic $[Cu_2(s\text{-}py)_2(s\text{-}pyH)_2]_n^{2+}$ with $[ZnCl_4]_n^{2-}$ counter anion (**1**) were obtained in EAS–167 which was a slow diffusion reaction. EAS–167 was slow diffusion reaction of EAS–164. That's why the product of it is also considered as **1**. Repeating cationic $[Au(s\text{-}pyH)_2]^+$ with Cl^- were able to create also in this project but they were not measured because the structure was known by Kalle Machal. Copper polymer (**1**) was pseudolinear. Crystal data for **1** is listed in Table 4.

Table 4. Crystal data for **1**

empirical formula	$C_{20}H_{20}Cl_4Cu_2N_4S_4Zn$
formula mass	778.89
temp (K)	123(2)
λ(Å)	1.54184
crystal system	monoclinic
space group	$P2_1/n$
a (Å)	10.0163(3)
b (Å)	10.0845(3)
c (Å)	29.8809(13)
α(°)	90
β (°)	95.051(3)
γ(°)	90
V (Å^3)	3006.54(19)
Z	4
ρ_{calc} (Mg/m^3)	1.818
μ(Mo Kα) (mm^{-1})	8.656
no. reflections	12623
unique reflections	6128
GOOF (F^2)	1.036
R_{int}	0.0958
$R_1{}^a$ ($I \geq 2\sigma$)	0.0424
$wR_2{}^b$ ($I \geq 2\sigma$)	0.0909

^{a}R1 = $\Sigma||F_o| - |F_c||/\Sigma|F_o|$. ^{b}wR$_2$ = $[\Sigma[w(F_o{}^2 - F_c{}^2)^2]/\Sigma[w(F_o{}^2)^2]]^{1/2}$.

Copper polymer **1** was [Cu(s-pyH)]$_n$[ZnCl$_4$]$_{n/2}$ with crystallized ethanol. The asymmetric unit of **1** is shown in Figure 27. The asymmetric unit consists of [Cu$_2$(s-pyH)$_4$]$^{2+}$, [ZnCl$_4$]$^{2-}$ and EtOH. Copper is roughly tetrahedrally coordinated. Copper and sulphur backbone is not linear but it can be described as pseudolinear. It's shown in Figure 28.
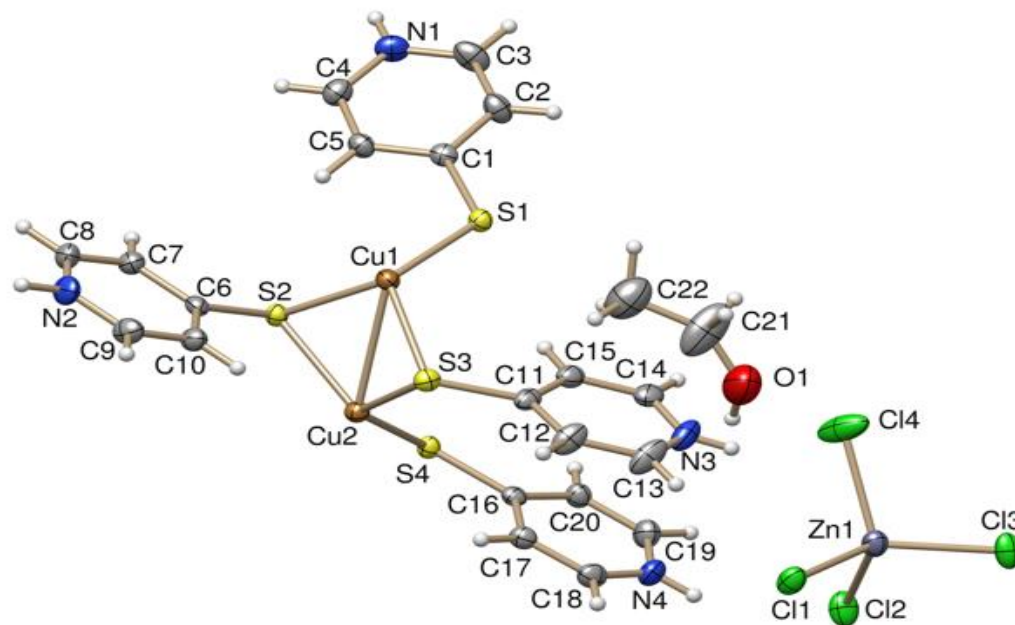
Figure 27. Asymmetric unit of **1**. Color code: dark gray: Zn, green: Cl, white: H, grey: C, blue: N, red: O, yellow: S and brown: Cu.
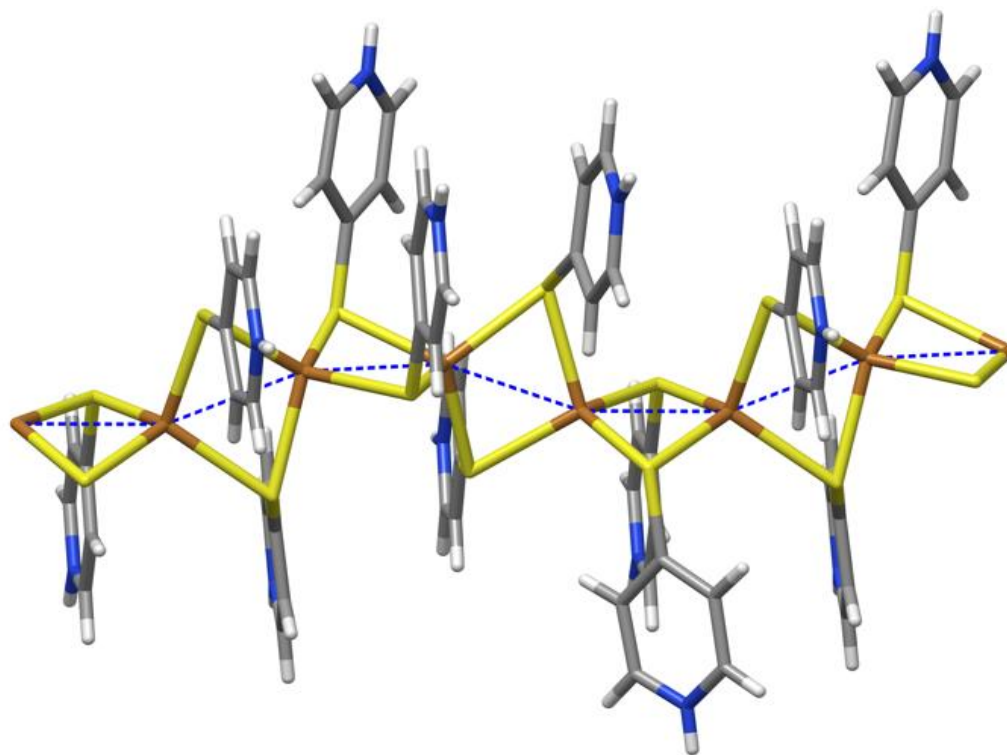
Figure 28. View presenting the polymeric chain of **1**. Color code: white: H, grey: C, blue: N, yellow: S and brown: Cu.

Reasons why the structure is pseudolinear are contemplated to be due to three main reasons: (1) close contacts between $[ZnCl_4]^{2-}$ anions and s-pyH ligands, (2) stacking of aromatic rings and (3) hydrogen bonds between polymeric chains. The hydrogen bonding is N–H⋯S type which is strengthened by interaction of C–H⋯S which can be considered also as hydrogen bonding because of the definition of hydrogen bonding allows the donor to be carbon and acceptor to be sulphur.[157]

$[ZnCl_4]^{2-}$ have short contacts to neighbouring s-py(H)s or EtOH. Every one of these short contacts can also be considered as hydrogen bonding of C–H⋯Cl, N–H⋯Cl or O–H⋯Cl according to the IUPAC's definition of hydrogen bond in theoretical organic chemistry:

"A particular type of multicenter (three center - four electron) X–H …Y in which the central hydrogen atom covalently linked to an electronegative atom X (C, N, O, S..) forms an additional weaker bond with atom Y (N, O, S..) in the direction of its lone electron pair orbital. The energy of hydrogen bonds, which is usually in the range of 3–15 kcal/mol (12–65 kJ/mol), results from the electrostatic interaction and also from the orbital interaction of the antibonding σ*(XH)MO of the molecule acting as the hydrogen donor and the non-bonding lone electron pair MOnY of the hydrogen acceptor molecule."

The definition is not very specific what an electronegative atom is and there's no definition in the same source what is electronegative atom. Because S can be Y, can Cl be Y as well because it's more electronegative than sulphur. Even the electronegativity itself is not totally univocal. That's why the definition is open to interpretations.

Seven of these hydrogen bonds between $[ZnCl_4]^{2-}$ and s-pyHs or EtOH are C–H⋯Cl type, five N–H⋯Cl type and one O–H⋯Cl type. All in all, these interactions connect $[ZnCl_4]^{2-}$ into eight s-pyHs and one EtOH. N–H⋯Cl hydrogen bonds alone connect four different s-pyHs into $[ZnCl_4]^{2-}$.

As mentioned above some of the s-pyHs are not piled up nicely like 'ⅠⅠⅠⅠ' as the rest of the s-pyHs. These are piled up like '/ \ / \'. These s-pyHs have three short contacts. Two with neighboring $[Cu(s-pyH)_2]_n^{n+}$ chain and one with $[ZnCl_4]^{2-}$. This bidentate binding to neighboring chain forms line of chains which are closer to each other than other line of chains. The lines are aligned along *b*-axis. There's empty void between two s-pyHs. There's ethanol molecule next to the void but it's too big to fit there. If it would be between

the two s-pyH's, then similar interchainic connection wouldn't be possible or it would be totally different.

There're one '/ \ / \' type s-pyH per $[CuS_2]_4$ backbone unit which is less than for other s-pyHs in the structure. There're three s-pyHs per $[CuS_2]_4$ backbone unit on both sides because there're 8 s-pyHs per $[CuS_2]_4$ backbone unit. The s-pyH's can be separated into four groups (1+3+1+3=8). As a result, there're two '/ \ / \' type s-pyHs occupy the same space while three normal s-pyHs occupy the same space. This 'space' is considered here only the length along b-axis i.e. along polymer backbone not to other directions. This extra space allows '/ \ / \' type s-pyHs to rotate to optimize interactions with other nearby objects but there's not enough space for EtOH to fit between the ligands. The reason for this is that EtOH is thicker than s-pyH in any directions because the EtOH is not planar.

The interaction between chains by '/ \ / \' type s-pyHs are partially reasoned for creating not strictly linear backbone $[CuS_2]_n$. Another reason is that not every $[CuS_2]$ unit has 'ǀǀǀǀ' type s-pyHs but only ¾ of them has. Regardless of this, every 'ǀǀǀǀ' type s-pyH has piled up by π–π stacking about the same distance from each other along b-axis. To lessen the distances between 'ǀǀǀǀ' type s-pyHs between $[CuS_2]$ unit that doesn't have s-pyH in that pile, the neighboring two s-pyHs are closer to each other because of the twist in the backbone. Due to these reasons the backbone of the polymer has been deviated from linear geometry for better π–π stacking.

The copper–copper distances in **1** are 2.6241(6) and 2.6283(6) Å. Cu–Cu–Cu angles are 156.667(18)° and 157.424(19)°. Cu–S–Cu angles are from 67.34(2)° to 68.08(2)°. One S–Cu–S angle stands outs from the rest; the S(3)–Cu(1)–S(4)#1 angle is 91.19(3)° when the others are between 105.22(3)° and 120.33(3)°.

It seems that $[ZnCl_4]^{2-}$ small structural role not a major one. It's acting as counter anion for the polymer and it fills the empty space. Also EtOH is filling space between lines of chains. $[ZnCl_4]^{2-}$ has many close contacts but none of the geometries of its hydrogen bonds is linear which is the geometry for strongest hydrogen bonds. However, it most likely have had crucial role in the polymer formation by accepting chlorides from copper and possibly aiding the polymer formation otherwise.

14.2 Other crystal structures

Twisted trigonal bipyramidal crystals of [CuCl(phen)$_2$] were obtained by evaporation of filtrate in EAS–181V. The crystals were green and block-shaped. Chlorine occupies in equatorial position and one nitrogen per each phen in equatorial and the other one in axial position. Solvent(s) are disordered in the structure. This is not surprising because the reaction mixture was mainly 3:1 MeCN:EtOH with some water.

EAS–198 yielded an interesting structure. Two ligands have been oxidized to form two 4-(pyridine-4-yldisulfanyl)pyridines (abbr. py-ss-py) in it. The pyridine ends were connected to either iron or copper. Their diffraction difference is small because they have only two electron difference and the quality of the crystal was not very good. Two py-ss-pys form bridge between an adjacent metal atom ◊◊◊◊◊◊-wise. This way one dimensional chain is formed. Nitrogens of py-ss-py coordinates square planar fashion around the metal atom. It's not clear is the geometry of the metal atom square planar or octahedral. It seems that at least one of the axial positions is occupied by chlorine but second one is not sure. Anyway, this crystal structure confines reductions of s-pyH to form py-ss-py in the reaction mixture with copper and iron chlorides.

EAS–181.5 contained cationic [Cu(OH$_2$)$_2$(phen)]$^{2+}$ and anionic [CuCl$_4$]$^{2-}$ units. Copper geometry of the phenanthroline complex of was square planar. Starting materials for this reaction were [CuCl$_2$(phen)] and [CuCl$_2$·2H$_2$O]. The alternating [Cu(OH$_2$)$_2$(phen)]$^{2+}$ units and [CuCl$_4$]$^{2-}$ units are stacked next to another alternating chain which O–H···Cl type hydrogen bonding. The distance between oxygen and chlorine atoms is 2.662 Å which is short end of moderate hydrogen bonding (2.5–3.2 Å).[65] Hydrogen bonding between [Cu(OH$_2$)$_2$(phen)]$^{2+}$ units and [CuCl$_4$]$^{2-}$ units had most likely important structural directing role in crystal formation. Second important matter is the distance between chlorine of tetrachlorocuprate and copper.

There're two chlorine atoms from two different [CuCl$_4$]$^{2-}$ below and above the phenanthroline copper atom. The distance between chlorine and copper atoms is 2.449 Å. According to the literature[86] single bond covalent radii is 99 pm for Cl and 112 pm for Cu which results 2.11 Å for Cu–Cl bond. Crystallographic van der Waals radii of these elements are 1.8 and 2.0 Å, respectively[72]. As a result, the sum is 3.8 Å. The values given above were for elements in oxidation state 0 and other matters were not considered but the values were used as rough estimates. The Cl···Cu distance is between covalent and van der

Waals distance but closer to covalent distance. The bond distance is observed to vary continuously from covalent bond distance to van der Waals distance[72]. Because the distance is less than the sum of van der Waals radii, there's an interaction between chlorine atoms of tetrachlorocuprate and copper atoms.

Because the distance between $[Cu^{II}(OH_2)_2(phen)]^{2+}$ and anionic $[CuCl_4]^{2-}$ units is less than sum of the two van der Waals radii, some kind of interaction between the two units is likely to exist. Thus, the case is a between case of polymeric and monomeric structure. According to IUPAC's definition of polymers, polymer is a structure which consists of macromolecules. The definition of macromolecule requires the entity to be molecule. Definition of molecule is very general; a molecule is an electrically neutral entity which consists of more than one atom. This definition is not accurate. Definition of molecular entity requires the entity to be separately distinguishable. As a result, IUPAC's definitions are not very accurate what kind of interaction between atoms can be when they are considered as one molecule or entity.

Classical definition has been that there has to be covalent bond but van der Waals interaction, dipole-dipole interaction or hydrogen bonding are not strong enough interaction that the both participate sides are included into same molecule (excluding intramolecular interaction). Because of IUPAC's definitions mentioned above as not so specific, the structure of EAS–181.5 is classified as borderline between polymeric and salt structure.

15 Elemental analysis

Elemental analysis was performed to different phenanthroline complexes and products of some other reactions. The elemental analysis confirmed that reactions resulted $[NiCl_2(phen)]$, $[ZnCl_2(phen)]$, $[CuCl_2(phen)]$ and $[FeCl_3(OH_2)(phen)]$. Observations for other compounds were not clear. The discussion and results of these elemental analyses are found in Appendix 3.

16 Conclusions

Reactions to form [CuCl$_2$(phen)], [NiCl$_2$(phen)], [ZnCl$_2$(phen)] and [FeCl$_3$(OH$_2$)(phen)] were successful even though the elemental analysis results were not within the acceptable limits for scientific publications. However, the correct formulas of the complexes were able to deduce from the elemental analysis for example for the iron complex one coordinated water molecule had to be included. Elemental analysis results of other compounds didn't suggest anything clear what would be the elemental composition of the products. The sum of mass ratio of C, H and N of products of silver reactions varied among heterometallic reactions indicating different amounts of inorganic material with s-pyH. Monometallic reactions didn't have that many differences in their elemental composition which suggests that the counter anion in silver reactions (nitrate or triflate) was not included to the product.

Color change from yellow to red or orange was promising. It was observed in copper and silver reactions but not in gold reactions. The color was hypothesized to indicate formation of at least oligomeric structure. Red or orange color was not observed in gold reactions, only yellow or yellowish orange, which suggests that polymeric structure was not formed or it was formed in the lesser extent in solution state than in the reactions with more reddish solutions.

Red or orange color was very hard to obtain and sustain especially in silver reactions. In silver reactions even slight warmth was enough to create undesired brownish color to red solution. The color change could not reversed by putting the reaction vessel into an ice bath. Base was required for creating the red solution in silver reactions. pH of the reaction mixture was very sensitive; the pH should be kept slightly basic. Excess base created undesired brownish color to the solution. The color resulted often grey to brown precipitate which was not been able to dissolve. It was assumed to contain Ag$_2$O or something similar like Ag$_2$OEt with possible coordination to s-py(H). The abbreviation s-pyH stands for pyridine-4(1*H*)-thione and s-py its deprotonated form. Usage of KOH was problematic because of its low solubility in 3:1 MeCN:EtOH and similar solutions and because crystals of polymeric structures were interested not KOH(s). However, Et$_3$N didn't seem to be strong enough base for the reactions alone, thus small amount of KOH was used as an extra booster in silver reaction which was successful in creating red solution. Copper reactions without base seemed to withstand heating better than silver reaction with base.

Precipitate formation when exactly half amount of base was added compared to the amount of s-pyH but no precipitate with equimolar amount of base in copper and silver reactions suggests that when half or less of s-pyH are protonated it forms a stacked structure with every alternating s-pyH and s-py$^-$. Then more base is added it deprotonation of s-pyH is increased and anionic s-py are not so eager to form precipitate with each other because of electrostatic repulsion. Cu^{2+} must also have an effect on the precipitate formation in these reactions. The similar phenomenon was observed with silver salts and KOH.

The usage of base was important in the Ag(I) reactions with s-pyH in order to make possibly polymeric structures because if a base was not used, dimeric $[Ag(s-py)(s-pyH)]_2$ structure was formed. The redest color for silver reactions were observed with 1:4 ratio of $AgNO_3$ and s-pyH with 30 drops of Et_3N and couple drops of dissolved KOH.

$CuCl_2 \cdot 2H_2O$ was more promising starting material than $Cu(OAc)_2 \cdot H_2O$. Oily substance was formed in many copper reactions, which prevented obtainment of crystals. Formation of S_8 crystals and precipitate in many reactions suggests s-pyH to be unstable and degradation of it might be catalyzed by metal complexes.

Slow diffusion reactions created some promising crystals but most of them were unstable. Orange color of crystals of **1** i.e. $[Cu_2(s-pyH)_4]_n$ with n $[ZnCl_4]$ counter anions supports the theory that red or orange color of the solution contained at least oligomeric $[M(s-py(H))_2]_n$ units. The structure of $[Cu_2(s-pyH)_4]_n$ with n $[ZnCl_4]$ counter anions was unexpected because zinc was assumed to coordinate to nitrogen end of s-py(H). Either harder metal ion or more basic conditions were assumed to need in order to coordinate both ends of s-py. No crystals with group 11 metals, s-py(H) and another metal salts were able to obtain except the one mentioned hereinbefore.

Depending on the concentration different precipitates were formed in reactions with $FeCl_3$, s-pyH and $CuCl_2 \cdot 2H_2O$. If reaction volume was 20 mL, precipitate formed was yellow but if it was 50 mL, pale green precipitate was formed as can be seen in Figure 25. However, this kind of difference was not observed in reactions with $CrCl_3 \cdot 6H_2O$. Bluish green crystals were formed later into the reaction vessel of the 50 mL reaction of the iron reaction. Those crystals had coordination of iron or copper to the nitrogen end. The ligand had been reacted with itself during the synthesis to form 4-(pyridin-4-yldisulfanyl)pyridine (py-ss-py). In other words, two s-pyHs were oxidized to form disulfide bridge between two pyridines. Iron or copper was coordinated to both ends of the ligand and formed one

dimensional chain with two py-ss-pys coordinating from one iron or copper to another i.e. between two adjacent atoms there're two bridging 4-(pyridin-4-yldisulfanyl)pyridines. Electron clouds of copper and iron are too similar to identify the metal as copper or iron based on the crystal structure.

The charge of the iron or copper was not totally sure. 4-(pyridin-4-yldisulfanyl)pyridines are most likely neutral ligands. The coordination number of iron or copper seems to be 5 or 6 but it's not totally sure because of the quality of the crystal structure wasn't very good. Four of the coordination sites are occupied by nitrogen atoms from four 4-(pyridine-4-yldisulfanyl)pyridines and one is occupied by Cl^-. There is also lots of solvent disorder in the structure. The charge balance requires another anion. If iron had oxidation state of +3, there would be two anions in addition to one Cl^- which seems even more unlikely. How many hydrogens are located on nitrogen ends of s-py(H)s is hard to tell. Fe^{3+}(aq) is yellow or brown and Fe^{2+}(aq) is pale green which suggest that the iron would be in the oxidation state of +2 if the metal is iron. The other counter anion might be OH^-.

The color changes in multiple reactions from reddish yellow to bluish green or color changes of lesser extend were interesting in the reactions with [CuCl$_2$(phen)] and s-pyH either with or without CuCl$_2$·2H$_2$O either with or without base. It is hypothesized that first s-py(H)s were coordinated to copper to form oligomeric chain but the structure was not stable. It was maybe either because of s-py(H)s were degraded or other discrete copper complexes like [Cu(OH$_2$)$_2$(phen)][CuCl$_4$] were more stable. This hypothesis is supported the fact that [CuCl$_2$(phen)](s) is green and as dissolved into a mixture of MeCN, EtOH and H$_2$O it's blue. Crystals of polymeric structures like the one in **1**, cationic [Cu$_2$(s-pyH)$_4$]$_n^{2+}$ with n [ZnCl$_4$]$^{2-}$ counter anions were orange. Crystals of [Cu(OH$_2$)$_2$(phen)]$^{2+}$ and [CuCl$_4$]$^{2-}$ were bluish green.

Purple precipitate formed in reactions in which AgClO$_4$ in order to open a coordination site to [ZnCl$_2$(phen)] complexes signify that not only AgCl(s) was formed and at least some part of the starting materials were dissolved. Shortened reaction time lessened formation of the undesired purple compound which was preferable.

Reactions in which AuCl was dissolved in MeCN which was layered on the top of a layer of s-pyH in CH$_2$Cl$_2$ crystals were formed and analyzed to contain monomeric [Au(s-pyH)$_2$]Cl units instead of polymeric structure. Chlorinated solvents like

dihloromethane are thought to favor monomeric structures with weaker interaurous interactions than without them. Reactions with AuCl with another metal salt resulted really similar precipitate colors when the other metal containing substance was NaCl, NiCl$_2$ and ZnCl$_2$.

17 Summary

The goal was to produce linear and one dimensional metal atom chains with one or two metals using group 11 metal salts, ambidentate ligand pyridine-4(1*H*)-thione (s-pyH) and other metal salts with harder metal ion. The aims was to coordinate softer ligand to the sulphur end of s-py$^-$ and harder to the nitrogen end. The goal was reached to some extend but not as much as was hoped for. One crystal structure with linear and one dimensional metal atom chains with two metals were able to crystallize and measure. It was [Cu$_2$(s-pyH)$_4$]$_n^{2+}$ with n [ZnCl$_4$]$^{2-}$ counter anions. The zinc didn't coordinate to the nitrogen end as was expected but instead [ZnCl$_4$]$^{2-}$ functioned as counter ion for the copper polymer.

The basicity of the reaction conditions was sensitive and problematic especially in silver reactions but promising red or orange colors were able to form. Reactions with stoichiometric amount of base yielded an hypothesis that anionic s-pys repel reach other and when every other s-py(H) is deprotonated in [M(s-py)(s-pyH)]$_n$, longer chain is formed if every second s-pyH would be deprotonated each side of the chain, which would not cause electrostatic repulsion.

Pyridine-4(1*H*)-thione was sensitive to oxidation and hard and highly oxidized metal was noticed oxidize or catalyze reaction of s-pyH to form disulfide bridged pyridines i.e. 4-(pyridin-4-yldisulfanyl)pyridine (py-ss-py) or S$_8$. Formation of py-ss-py was observed at least in a reaction with copper and iron chlorides.

It's possible to continue project even further. For example reaction with CuCl$_2$·2H$_2$O, s-pyH and NiCl$_2$ is hypothesized to create corresponding structure than [Cu$_2$(s-pyH)$_4$]$_n^{2+}$ with n [ZnCl$_4$]$^{2-}$ counter anions or less likely Ni could coordinate to the nitrogen of s-py. Different reactions conditions could be tested more. Product recrystallization would bring about new structures. Optimization for basicity is also needed further.

18 References

1. F.S. Arimoto and A.C. Haven, Derivatives of Dicyclopentadienyliron, *J. Am. Chem. Soc.* **1955***, 77,* 6295-6297.

2. G.R. Whittell and I. Manners, Metallopolymers: New Multifunctional Materials, *Adv. Mater.* **2007***, 19,* 3439-3468.

3. J.-C. Eloi, L. Chabanne, G.R. Whittell and I. Manners, Metallopolymers with emerging applications, *Mater. Today.* **2008***, 11,* 28-36.

4. G.R. Whittell, M.D. Hager, U.S. Schubert and I. Manners, Functional soft materials from metallopolymers and metallosupramolecular polymers, *Nat. Mater.* **2011***, 10,* 176-188.

5. J.M. Stanley and B.J. Holliday, Luminescent lanthanide-containing metallopolymers, *Coord. Chem. Rev.* **2012***, 256,* 1520-1530.

6. H. Masai, J. Terao and Y. Tsuji, Insulated π-conjugated metallopolymers, *Tetrahedron Lett.* **2014***, 55,* 4035-4043.

7. I.D.W. Samuel, G. Rumbles and C.J. Collison, Efficient interchain photoluminescence in a high-electron-affinity conjugated polymer, *Phys. Rev. B.* **1995***, 52,* R11573-R11576.

8. B.J. Holliday and T.M. Swager, Conducting metallopolymers: the roles of molecular architecture and redox matching, *Chem. Commun.* **2005** 23-36.

9. C.-L. Ho and W.-Y. Wong, Metal-containing polymers: Facile tuning of photophysical traits and emerging applications in organic electronics and photonics, *Coord. Chem. Rev.* **2011***, 255,* 2469-2502.

10. C.G. Hardy, J. Zhang, Y. Yan, L. Ren and C. Tang, Metallopolymers with transition metals in the side-chain by living and controlled polymerization techniques, *Prog. Polym. Sci.* **2014***, 39,* 1742-1796.

11. M.E.A. Fegley, S.S. Pinnock, C.N. Malele and W.E. Jones Jr., Metal-containing conjugated polymers as fluorescent chemosensors in the detection of toxicants, *Inorg. Chim. Acta.* **2012***, 381,* 78-84.

12. T.M. Swager, The Molecular Wire Approach to Sensory Signal Amplification, *Acc. Chem. Res.* **1998***, 31,* 201-207.

13. Q. Zhou and T.M. Swager, Fluorescent Chemosensors Based on Energy Migration in Conjugated Polymers: The Molecular Wire Approach to Increased Sensitivity, *J. Am. Chem. Soc.* **1995***, 117,* 12593-12602.

14. Z. Li, X. Lou, H. Yu, Z. Li and J. Qin, An Imidazole-Functionalized Polyfluorene Derivative as Sensitive Fluorescent Probe for Metal Ions and Cyanide, *Macromolecules.* **2008***, 41,* 7433-7439.

15.   B.J. Holliday, T.B. Stanford and T.M. Swager, Chemoresistive Gas-Phase Nitric Oxide Sensing with Cobalt-Containing Conducting Metallopolymers, *Chem. Mater.* **2006***, 18,* 5649-5651.

16.   R.C. Smith, A.G. Tennyson, A.C. Won and S.J. Lippard, Conjugated Metallopolymers for Fluorescent Turn-On Detection of Nitric Oxide, *Inorg. Chem.* **2006***, 45,* 9367-9373.

17.   A.-S. Chauvin, J.-C.G. Bünzli, F. Bochud, R. Scopelliti and P. Froidevaux, Use of Dipicolinate-Based Complexes for Producing Ion-Imprinted Polystyrene Resins for the Extraction of Yttrium-90 and Heavy Lanthanide Cations, *Chem. - Eur. J.* **2006***, 12,* 6852-6864.

18.   P. Froidevaux, S. Happel and A.-S. Chauvin, Ion-Imprinted Polymer Concept for Selective Extraction of 90Y and 152Eu for Medical Applications and Nuclear Power Plant Monitoring, *Chimia.* **2006***, 60,* 203-206.

19.   J.M. Bryson, K.M. Fichter, W.-J. Chu, J.-H. Lee, J. Li, L. A. Madsen, P. M. McLendon and T. M. Reineke, Polymer beacons for luminescence and magnetic resonance imaging of DNA delivery, *Proc. Natl. Acad. Sci. U. S. A.* **2009***, 106,* 16913-16918.

20.   K.L. Robinson and N.S. Lawrence, Redox-Sensitive Copolymer: A Single-Component pH Sensor, *Anal. Chem.* **2006***, 78,* 2450-2455.

21.   D.Suzuki, T. Sakai and R. Yoshida, Self-Flocculating/Self-Dispersing Oscillation of Microgels, *Angew. Chem. , Int. Ed.* **2008***, 47,* 917-920.

22.   D.P. Puzzo, A.C. Arsenault, I. Manners and G.A. Ozin, Electroactive Inverse Opal: A Single Material for All Colors, *Angew. Chem. , Int. Ed.* **2009***, 48,* 943-947.

23.   J.B. Beck and S.J. Rowan, Multistimuli, Multiresponsive Metallo-Supramolecular Polymers, *J. Am. Chem. Soc.* **2003***, 125,* 13922-13923.

24.   Z. Wang, A.R. McWilliams, C.E.B. Evans, X. Lu, S. Chung, M.A. Winnik and I. Manners, Covalent Attachment of RuII Phenanthroline Complexes to Polythionylphosphazenes: The Development and Evaluation of Single-Component Polymeric Oxygen Sensors, *Adv. Funct. Mater.* **2002***, 12,* 415-419.

25.   K. Binnemans, Lanthanide-Based Luminescent Hybrid Materials, *Chem. Rev.* **2009***, 109,* 4283-4374.

26.   Q. Lin, B. Yang, J. Li, X. Meng and J. Shen, Synthesis, characterization and property studies of Pb^{2+}-containing optical resins, *Polymer.* **2000***, 41,* 8305-8309.

27.   D.J. Caruana and A. Heller, Enzyme-Amplified Amperometric Detection of Hybridization and of a Single Base Pair Mutation in an 18-Base Oligonucleotide on a 7-µm-Diameter Microelectrode, *J. Am. Chem. Soc.* **1999***, 121,* 769-774.

28.   Q. Ling, Y. Song, S. J Ding, C. Zhu, D. S H Chan, D. -L Kwong, E.-T. Kang and K. -G Neoh, Non-Volatile Polymer Memory Device Based on a Novel Copolymer of N-Vinylcarbazole and Eu-Complexed Vinylbenzoate, *Adv. Mater.* **2005***, 17,* 455-459.

29.   Q.-D. Ling, Y. Song, E.Y.H. Teo, S.-L. Lim, C. Zhu, D.S.H. Chan, D.-L. Kwong, E.-T. Kang and K.-G. Neoh, WORM-Type Memory Device Based on a Conjugated Copolymer Containing Europium Complex in the Main Chain, *Electrochem. Solid-State Lett.* **2006***, 9,* G268-G271.

30.   Y. Song, Q.D. Ling, C. Zhu, E.T. Kang, D.S.H. Chan, Y.H. Wang and D.L. Kwong, Memory performance of a thin-film device based on a conjugated copolymer containing fluorene and chelated europium complex, *IEEE Electron Device Lett.* **2006***, 27,* 154-156.

31.   T.-L. Choi, K.-H. Lee, W.-J. Joo, S. Lee, T.-W. Lee and M.Y. Chae, Synthesis and Nonvolatile Memory Behavior of Redox-Active Conjugated Polymer-Containing Ferrocene, *J. Am. Chem. Soc.* **2007***, 129,* 9842-9843.

32.   M. Ramanathan and S.B. Darling, Nanofabrication with metallopolymers - recent developments and future perspectives, *Polym. Int.* **2013***, 62,* 1123-1134.

33.   R.G.H. Lammertink, M.A. Hempenius, J.E. van den Enk, V.Z.-H. Chan, E.L. Thomas and G.J. Vancso, Nanostructured Thin Films of Organic–Organometallic Block Copolymers: One-Step Lithography with Poly(ferrocenylsilanes) by Reactive Ion Etching, *Adv. Mater.* **2000***, 12,* 98-103.

34.   R.G.H. Lammertink, M.A. Hempenius, V.Z.-H. Chan, E.L. Thomas and G.J. Vancso, Poly(ferrocenyldimethylsilanes) for Reactive Ion Etch Barrier Applications, *Chem. Mater.* **2001***, 13,* 429-434.

35.   M. Ginzburg, M.J. MacLachlan, S.M. Yang, N. Coombs, T.W. Coyle, P. Raju, J.E. Greedan, R.H. Herber, G.A. Ozin and I. Manners, Genesis of Nanostructured, Magnetically Tunable Ceramics from the Pyrolysis of Cross-Linked Polyferrocenylsilane Networks and Formation of Shaped Macroscopic Objects and Micron Scale Patterns by Micromolding Inside Silicon Wafers, *J. Am. Chem. Soc.* **2002***, 124,* 2625-2639.

36.   J.F. Berry, *Multiple Bonds Between Metal Atoms,* 3rd Edition, Springer, New York, NY, 2005, ss. 669-706.

37.   G. Aromí, Metal-based molecular chains: Design by coordination chemistry, **2011***, 32,* 163-194.

38.   L.H. Doerrer, Steric and electronic effects in metallophilic double salts, *Dalton Trans.* **2010***, 39,* 3543-3553.

39.   T.J. Hurley and M.A. Robinson, Nickel(II)-2,2'-dipyridylamine system. I. Synthesis and stereochemistry of the complexes, *Inorg. Chem.* **1968***, 7,* 33-38.

40. N. Masciocchi, M. Moret, P. Cairati, F. Ragaini and A. Sironi, Solving simple organometallic structures solely from x-ray powder diffraction data: the case of polymeric [{Ru(CO)$_4$}$_n$], *J. Chem. Soc. , Dalton Trans.* **1993** 471-5.

41. M. Frik, J. Jiménez, I. Gracia, L.R. Falvello, S. Abi-Habib, K. Suriel, T.R. Muth and M. Contel, Luminescent Di- and Polynuclear Organometallic Gold(I)-Metal (Au$_2$, {Au$_2$Ag}n and {Au$_2$Cu}n) Compounds Containing Bidentate Phosphanes as Active Antimicrobial Agents, *Chem. - Eur. J.* **2012**, *18,* 3659-3674.

42. C. Tejel, M.A. Ciriano, J.A. López, F.J. Lahoz and L.A. Oro, Rhodium and Iridium Pyrazolato Blues, *Angew. Chem.* **1998**, *37,* 1542-1545.

43. T.-W. Tsai, Q.-R. Huang, S.-M. Peng and B.-Y. Jin, Smallest Electrical Wire Based on Extended Metal-Atom Chains, *J. Phys. Chem. C.* **2010**, *114,* 3641-3644.

44. M.-L. Kontkanen, L. Oresmaa, M.A. Moreno, J. Jänis, E. Laurila and M. Haukka, One-dimensional metal atom chain [Ru(CO)$_4$]$_n$ as a catalyst precursor—Hydroformylation of 1-hexene using carbon dioxide as a reactant, *Appl. Cat. A.* **2009**, *365,* 130-134.

45. S. Tsukamoto and S. Sakaki, A theoretical study of luminescent vapochromic compounds including an AuCu$_2$(NHC)$_2$ core, *Dalton Trans.* **2013**, *42,* 4809-4821.

46. I.O. Koshevoy, Y.-C.Chang, A.J. Karttunen, J.R. Shakirova, J. Jänis, M. Haukka, T. Pakkanen and P.-T. Chou, Solid-State Luminescence of Au-Cu-Alkynyl Complexes Induced by Metallophilicity-Driven Aggregation, *Chem. - Eur. J.* **2013**, *19,* 5104-5112.

47. E.J. Fernández, A. Laguna, J.M. López-de-Luzuriaga, M. Monge, M. Montiel, M.E. Olmos and M. Rodríguez-Castillo, Photophysical and Theoretical Studies on Luminescent Tetranuclear Coinage Metal Building Blocks, **2006**, *25,* 3639-3646.

48. J.-K. Cheng, Y.-G. Yao, J. Zhang, Z.-J. Li, Z.-W. Cai, X.-Y. Zhang, Z.-N. Chen, Y.-B. Chen, Y. Kang, Y.-Y. Qin and Y.-H. Wen, A Simultaneous Redox, Alkylation, Self-Assembly Reaction under Solvothermal Conditions Afforded a Luminescent Copper(I) Chain Polymer Constructed of Cu$_3$I$_4^-$ and EtS-4-C$_5$H$_4$N$^+$Et Components (Et = CH$_3$CH$_2$), *J. Am. Chem. Soc.* **2004**, *126,* 7796-7797.

49. J. Zhang, J.-K. Cheng, Y.-Y. Qin, Z.-J. Li and Y.-G. Yao, A luminescent Cu(I) complex ligated by 1,3-bis(4-pyridyl)trisulfane generated in situ by the coupling of pyridine-4-thiol, **2008**, *11,* 164-166.

50. K.-N. Shih, M.-J. Huang, H.-C. Lu, M.-D. Fu, C.-K. Kuo, G.-C. Huang, G.-H. Lee, C.-H. Chen and S.-M. Peng, On the tuning of electric conductance of extended metal atom chains via axial ligands for [Ru$_3$(μ_3-dpa)$_4$(X)$_2$]$^{0/+}$ (X = NCS$^-$, CN$^-$), *Chem. Commun.* **2010**, *46,* 1338-1340.

51. C. Yin, G.-C. Huang, C.-K. Kuo, M.-D. Fu, H.-C. Lu, J.-H. Ke, K.-N. Shih, Y.-L. Huang, G.-H. Lee, C.-Y. Yeh, C.-H. Chen and S.-M. Peng, Extended Metal-Atom Chains with an Inert Second Row Transition Metal: Ru$_5$(μ_5-tpda)$_4$X$_2$] (tpda2$^-$ =

tripyridyldiamido dianion, X = Cl and NCS), *J. Am. Chem. Soc.* **2008**, *130,* 10090-10092.

52.   C.-K. Kuo, I.P.-C. Liu, C.-Y. Yeh, C.-H. Chou, T.-B. Tsao, G.-H. Lee and S.-M. Peng, Oxidation of Linear Trinuclear Ruthenium Complexes [Ru$_3$(dpa)$_4$Cl$_2$] and [Ru$_3$(dpa)$_4$(CN)$_2$]: Synthesis, Structures, Electrochemical and Magnetic Properties, *Chem. - Eur. J.* **2007**, *13,* 1442-1451.

53.   Y. Shen, H.-Y. Ko, Q. Ai, S.-M. Peng and B.-Y. Jin, Molecular Split-Ring Resonators Based on Metal String Complexes, *J. Phys. Chem. C.* **2014**, *118,* 3766-3773.

54.   J.-T. Sheu, C.-C. Lin, I. Chao, C.-C. Wang and S.-M. Peng, Linear trinuclear three-centred metal-metal multiple bonds: synthesis and crystal structure of M3(dpa)4Cl2]M = Ru or Rh, dpa = bis(2-pyridyl)amidoanion], *Chem. Commun.* **1996** 315-316.

55.   C.E. Housecroft and A.G. Sharpe, *Inorganic Chemistry,* 3. Painos, Pearson Education Limited, Rotolito Lombarda, Italy, 2008, ss. 31, 740.

56.   P. Pyykkö, Strong Closed-Shell Interactions in Inorganic Chemistry, *Chem. Rev.* **1997**, *97,* 597-636.

57.   P. Pyykkö, Theoretical Chemistry of Gold, **2004**, *43,* 4412-4456.

58.   Krebs, B., Unkonventionelle Wechselwirkungen in der Chemie metallischer Elemente (Unconventional Interactions in the Chemistry of Metallic Elements); VCH: Weinheim, 1992 (in German). 199-217
This book contains the proceedings of the program "Neue Phänomene in der Chemie metallischer Elemente mit abgeschlossenen inneren Elektronenzuständen" of Deutsche Forschungsgemeinschaft. This was reference was not available and it was taken from refence 57.

59.   A.J. Edwards and R.J.C. Sills, Fluoride crystal structures. Part XIII. Difluorochlorine(III) hexafluoroantimonate(V), *J. Chem. Soc. A.* **1970** 2697-2699.

60.   P. Pyykkö, N. Runeberg and F. Mendizabal, Theory of the d10-d10 Closed-Shell Attraction: 1. Dimers Near Equilibrium, *Chem. - Eur. J.* **1997**, *3,* 1451-1457.

61.   L.H. Doerrer, Metallophilic interactions in double salts: Toward 1D metal atom chains, *Comments Inorg. Chem.* **2008**, *29,* 93-127.

62.   J.F. Berry, *Structure and Bonding: Metal-Metal Bonding,* 1st Edition, Springer Berlin Heidelberg, Heidelberg, Germany, 2010, ss. 1-28.

63.   P. Muller, Glossary of terms used in physical organic chemistry (IUPAC Recommendations 1994), *Pure Appl. Chem.* **1994**, *66,* 1077-1184.

64.   A. Elangannan, G.R. Desiraju, R.A. Klein, S. Joanna, S. Steve, A. Ibon, D.C. Clary, R.H. Crabtree, J.J. Dannenberg, H. Pavel, H.G. Kjaergaard, A.C. Legon, M. Benedetta and D.J. Nesbitt, Definition of the hydrogen bond (IUPAC Recommendations 2011), *Pure Appl. Chem.* **2011**, *83,* 1637-1641.

118

65.   G.A. Jeffrey, *An Introduction to Hydrogen Bonding*, Oxford University Press, New York, 1997, ss. 12.

66.   W.L. Bragg, Arrangement of atoms in crystals, *Philos. Mag.* **1920**, *40,* 169-189.

67.   S.S. Batsanov and A.S. Batsanov, *Introduction to Structural Chemistry,* Springer, Dordrecht Heidelberg London New York, 2012.

68.   G.P. Schiemenz, The Sum of van der Waals Radii − A Pitfall in the Search for Bonding, *Z. Naturforsch. B.* **2007**, *62,* 235-243.

69.   J.K. Badenhoop and F. Weinhold, Natural steric analysis: Ab initio van der Waals radii of atoms and ions, *J. Chem. Phys.* **1997**, *107,* 5422-5432.

70.   M. Mantina, A.C. Chamberlin, R. Valero, C.J. Cramer and D.G. Truhlar, Consistent van der Waals Radii for the Whole Main Group, *J. Phys. Chem. A.* **2009**, *113,* 5806-5812.

71.   R.F.W. Bader, W.H. Henneker and P.E. Cade, Molecular Charge Distributions and Chemical Binding, *J. Chem. Phys.* **1967**, *46,* 3341-3363.

72.   S.S. Batsanov, Van der Waals Radii of Elements, *Inorg. Mater.* **2001**, *37,* 871-885.

73.   P.M. Harris, E. Mack and F.C. Blake, The Atomic Arrangement in the Crystals of Orthorhombic Iodine, *J. Am. Chem. Soc.* **1928**, *50,* 1583-1600.

74.   S.S. Batsanov, Anisotropy of Atomic Van der Waals Radii in the Gas-Phase and Condensed Molecules, *Struct. Chem.* **2000**, *11,* 177-183.

75.   M. Ishikawa, S. Ikuta, M. Katada and H. Sano, Anisotropy of van der Waals radii of atoms in molecules: alkali-metal and halogen atoms, *Acta Cryst.* **1990**, *B46,* 592-598.

76.   S.S. Batsanov, Structural features of van der Waals complexes, *Russ. J. Coord. Chem. (Translation of Koord. Khim.).* **1998**, *24,* 453-456.

77.   A. Bondi, van der Waals Volumes and Radii, *J. Phys. Chem.* **1964**, *68,* 441-451.

78.   R.S. Rowland and R. Taylor, Intermolecular Nonbonded Contact Distances in Organic Crystal Structures: Comparison with Distances Expected from van der Waals Radii, *J. Phys. Chem.* **1996**, *100,* 7384-7391.

79.   R.E. Dickerson, H.B. Gray, M.Y. Darensbourg and D.J. Darensbourg, *Prinzipien der Chemie,* 2nd Editon, Walter de Gruyter, Berlin, New York, 1988, ss. 125.

80.   S.S. Batsanov, Experimental determination of covalent radii of elements, *Izv. Akad. Nauk, Ser. Khim.* **1995**, *24,* 2349-2354.

81.   S.S. Pathaneni and G.R. Desiraju, Database analysis of Au···Au interactions, *J. Chem. Soc. , Dalton Trans.* **1993** 319-322.

82.   S.S. Batsanov, On the additivity of van der Waals radii, *J. Chem. Soc. , Dalton Trans.* **1998** 1541-1546.

83.   S.S. Batsanov, *Refractometry and chemical structure,* Painos, Van Nostrand, Princeton, 1966.

84.   Y. Xu, W. Jäger, J. Djauhari and M.C.L. Gerry, Rotational spectra of the mixed rare gas dimers Ne–Kr and Ar–Kr, *J. Chem. Phys.* **1995**, *103,* 2827-2833.

85.   P. Pyykkö, Additive Covalent Radii for Single-, Double-, and Triple-Bonded Molecules and Tetrahedrally Bonded Crystals: A Summary, *J. Phys. Chem. A.* **2015**, *119,* 2326-2337.

86.   P. Pyykkö and M. Atsumi, Molecular Single-Bond Covalent Radii for Elements 1–118, *Chem. - Eur. J.* **2009**, *15,* 186-197.

87.   P. Pyykkö and M. Atsumi, Molecular Double-Bond Covalent Radii for Elements Li–E112, *Chem. - Eur. J.* **2009**, *15,* 12770-12779.

88.   P. Pyykkö, S. Riedel and M. Patzschke, Triple-Bond Covalent Radii, *Chem. - Eur. J.* **2005**, *11,* 3511-3520.

89.   P. Pyykkö, Refitted tetrahedral covalent radii for solids, *Phys. Rev. B.* **2012**, *85,* 024115.

90.   B. Cordero, V. Gómez, A. Platero-Prats, M. Revés, J. Echeverria, E. Cremades, F. Barragán and S. Alvarez, Covalent radii revisited, *Dalton Trans.* **2008** 2832-2838.

91.   H.A. Bent, Structural chemistry of donor-acceptor interactions, *Chem. Rev.* **1968**, *68,* 587-648.

92.   F.W.B. Einstein and R.D.G. Jones, Crystal structure of a complex containing an antimony-iron σ bond $Cl_2Sb\{Fe(CO)_2(h^5-C_5H_5)\}_2]Sb_2Cl_7]$, *Inorg. Chem.* **1973**, *12,* 1690-1696.

93.   J.D. Dunitz and A. Gavezzotti, Molecular Recognition in Organic Crystals: Directed Intermolecular Bonds or Nonlocalized Bonding? *Angew. Chem. , Int. Ed.* **2005**, *44,* 1766-1787.

94.   E. Espinosa, E. Molins and C. Lecomte, Hydrogen bond strengths revealed by topological analyses of experimentally observed electron densities, *Chem. Phys. Lett.* **1998**, *285,* 170-173.

95.   A.J. Bridgeman, G. Cavigliasso, L.R. Ireland and J. Rothery, The Mayer bond order as a tool in inorganic chemistry, *J. Chem. Soc. , Dalton Trans.* **2001** 2095-2108.

96.   A. Gavezzotti, Calculation of Intermolecular Interaction Energies by Direct Numerical Integration over Electron Densities. I. Electrostatic and Polarization Energies in Molecular Crystals, *J. Phys. Chem. B.* **2002**, *106,* 4145-4154.

97.   A. Gavezzotti, Calculation of Intermolecular Interaction Energies by Direct Numerical Integration over Electron Densities. 2. An Improved Polarization Model and the Evaluation of Dispersion and Repulsion Energies, *J. Phys. Chem. B.* **2003**, *107,* 2344-2353.

98.   R.W. F.Bader, *Atoms in Molecules: A Quantum Theory*, Oxford University Press, Oxford, 1990.

99.   S.S. Batsanov, Thermodynamic determination of van der Waals radii of metals, *J. Mol. Struct.* **2011**, *990, 63-66.*

100.   S.S. Batsanov, *Experimental Foundations of Structural Chemistry,* Moscow University Press, Moscow, 2008, ss. 542.

101.   E. O'Grady and N. Kaltsoyannis, Does metallophilicity increase or decrease down group 11? Computational investigations of Cl-M-PH$_3$]$_2$ (M = Cu, Ag, Au, 111]), *Phys. Chem. Chem. Phys.* **2004**, *6, 680-687.*

102.   P. Pyykkö and Y. Zhao, Ab initio Calculations on the (ClAuPH$_3$)$_2$ Dimer with Relativistic Pseudopotential: Is the "Aurophilic Attraction" a Correlation Effect? *Angew. Chem., Int. Ed.* **1991**, *30,* 604-605.

103.   P. Pyykkö, J. Li and N. Runeberg, Predicted ligand dependence of the Au(I)…Au(I) attraction in (XAuPH$_3$)$_2$, *Chem. Phys. Lett.* **1994**, *218,* 133-138.

104.   B. Assadollahzadeh and P. Schwerdtfeger, A comparison of metallophilic interactions in group 11 [X–M–PH$_3$]$_n$ (n = 2–3) complex halides (M = Cu, Ag, Au; X = Cl, Br, I) from density functional theory, *Chem. Phys. Lett.* **2008**, *462,* 222-228.

105.   L. Magnko, M. Schweizer, G. Rauhut, M. Schutz, H. Stoll and H.-J. Werner, A comparison of metallophilic attraction in (X-M-PH$_3$)$_2$ (M = Cu, Ag, Au; X = H, Cl), *Phys. Chem. Chem. Phys.* **2002**, *4,* 1006-1013.

106.   R. Donamaría, V. Lippolis, J.M. López-de-Luzuriaga, M. Monge and M.E. Olmos, Theoretical studies on an unusual [Ag]$^+$···[Au]$^-$···[Au]$^-$···[Ag]$^+$ metallophilic pattern: Dispersive forces vs. classical coulomb forces, *Comput. Theor. Chem.* **2014**, *1030,* 53-58.

107.   N.L. Allinger, *Molecular Structure: Understanding Steric and Electronic Effects from Molecular Mechanics,* Painos, John Wiley & Sons, Incorporated, Hoboken, NJ, USA, 2010.

108.   S. Saebø, W. Tong and P. Pulay, Efficient elimination of basis set superposition errors by the local correlation method: Accurate ab initio studies of the water dimer, *J. Chem. Phys.* **1993**, *98,* 2170-2175.

109.   P. Schwerdtfeger, M. Lein, R.P. Krawczyk and C.R. Jacob, The adsorption of CO on charged and neutral Au and Au$_2$: A comparison between wave-function based and density functional theory, *J. Chem. Phys.* **2008**, *128,* 124302-1-124302-10.

110. S.F. Boys and F. Bernardi, The calculation of small molecular interactions by the differences of separate total energies. Some procedures with reduced errors, *Mol. Phys.* **1970**, *19,* 553-566.

111. M. Schütz, G. Rauhut and H.-J. Werner, Local Treatment of Electron Correlation in Molecular Clusters: Structures and Stabilities of $(H_2O)n$, n = 2-4, *J. Phys. Chem. A.* **1998**, *102,* 5997-6003.

112. N. Runeberg and M. Schütz, The aurophilic attraction as interpreted by local correlation methods, *J. Chem. Phys.* **1999**, *110,* 7210-7215.

113. A. Otero-de-la-Roza, J.D. Mallory and E.R. Johnson, Metallophilic interactions from dispersion-corrected density-functional theory, *J. Chem. Phys.* **2014**, *140,* 18A504-1-18A504-11.

114. S. Grimme, J. Antony, S. Ehrlich and H. Krieg, A consistent and accurate ab initio parametrization of density functional dispersion correction (DFT-D) for the 94 elements H-Pu, *J. Chem. Phys.* **2010**, *132,* 154104-1-154104-19.

115. J. Muñiz, C. Wang and P. Pyykkö, Aurophilicity: The Effect of the Neutral Ligand L on [{ClAuL}$_2$] Systems, *Chem. - Eur. J.* **2011**, *17,* 368-377.

116. E. Laurila, L. Oresmaa, J. Hassinen, P. Hirva and M. Haukka, Neutral one-dimensional metal chains consisting of alternating anionic and cationic rhodium complexes, *Dalton Trans.* **2013**, *42,* 395-398.

117. E. Laurila, L. Oresmaa, M.Niskanen, P. Hirva and M. Haukka, Metal-Metal Interactions in Stacked Mononuclear and Dinuclear Rhodium 2,2'-Biimidazole Carbonyl Complexes, *Cryst. Growth Des.* **2010**, *10,* 3775-3786.

118. C. Pretorius and A. Roodt, (Benzoylacetonato-κ^2O,O')dicarbonylrhodium(I), *ActaCryst.* **2012**, *E68,* m1451-m1452.

119. D.M. Pham, D. Rios, M.M. Olmstead and A.L. Balch, Assisted self-association of dicyanoaurate, [Au(CN)$_2$]$^-$, and dicyanoargentate, [Ag(CN)$_2$]$^-$, through hydrogen bonding to metal ammonia complexes, *Inorg. Chim. Acta.* **2005**, *358,* 4261-4269.

120. J. Real, J.C. Bayon, F.J. Lahoz and J.A. Lopez, Extended linear metal-metal interactions in an anionic rhodium(I) complex. X-Ray structure of NMe$_4$Rh(ox)(CO)$_2$](ox = oxalato), *J. Chem. Soc. , Chem. Commun.* **1989** 1889-1890.

121. Z. Tang, A.P. Litvinchuk, H.-G. Lee and A.M. Guloy, Crystal Structure and Vibrational Spectra of a New Viologen Gold(I) Iodide, *Inorg. Chem.* **1998**, *37,* 4752-4753.

122. H. Ecken, M. Olmstead M., B.C. Noll, S. Attar, B. Schlyer and A.L. Balch, Effects of anions on the solid state structures of linear gold(I) complexes of the type (o-xylyl isocyanide)gold(I) (monoanion), *J. Chem. Soc. , Dalton Trans.* **1998** 3715-3720.

123. C. Döring and P.G. Jones, Amine complexes of gold. Part 8. Two pyridine derivatives of gold(I) thiocyanate, *Z. Naturforsch. B.* **2014**, *69,* 1315-1320.

124. M. Streitberger, A. Schmied and E. Hey-Hawkins, Selective Formation of Gold(I) Bis-Pholane Macrocycles, Polymeric Chains, and Nanotubes, *Inorg. Chem.* **2014**, *53,* 6794-6804.

125. Y. Sevryugina, A.V. Olenev and M.A. Petrukhina, "Dimers of Dimers" of Ruthenium(I): Ru···Ru vs. Ru···O Axial Interactions, *J. Cluster Sci.* **2005**, *16,* 217-229.

126. E. Laurila, R. Tatikonda, L. Oresmaa, P. Hirva and M. Haukka, Metallophilic interactions in stacked dinuclear rhodium 2,2'-biimidazole carbonyl complexes, *CrystEngComm.* **2012**, *14,* 8401-8408.

127. S.-A. Hua, Y.-C. Tsai and S.-M. Peng, A Journey of Metal-metal Bonding beyond Cotton's Quadruple Bonds, *J. Chin. Chem. Soc.* **2014**, *61,* 9-26.

128. M.-M. Rohmer, I. P.-C. Liu, J.-C. Lin, M.-J. Chiu, C.-H. Lee, G.-H. Lee, M. Bénard, X. López and S.-M. Peng, Structural, Magnetic, and Theoretical Characterization of a Heterometallic Polypyridylamide Complex, *Angew. Chem. Int. Ed.* **2007**, *46,* 3533-3536.

129. I. Po-Chun Liu, G.-H. Lee, S.-M. Peng, M. Bénard and M.-M. Rohmer, Cu−Pd−Cu and Cu−Pt−Cu Linear Frameworks: Synthesis, Magnetic Properties, and Theoretical Analysis of Two Mixed-Metal Complexes of Dipyridylamide (dpa), Isostructural, and Isoelectronic with $[Cu_3(dpa)_4Cl_2]^+$, *Inorg. Chem.* **2007**, *46,* 9602-9608.

130. G.-C. Huang, M. Bénard, M.-M. Rohmer, L.-A. Li, M.-J. Chiu, C.-Y. Yeh, G.-H. Lee and S.-M. Peng, $Ru_2M(dpa)_4Cl_2$ (M = Cu, Ni): Synthesis, Characterization, and Theoretical Analysis of Asymmetric Heterometal String Complexes of the Dipyridylamide Family, *Eur. J. Inorg. Chem.* **2008**, *2008,* 1767-1777.

131. M. Nippe, G.H. Timmer and J.F. Berry, Remarkable regioselectivity in the preparation of the first heterotrimetallic Mo≡≡≡W···Cr chain, *Chem. Commun.* **2009** 4357-4359.

132. M.-C. Cheng, C.-L. Mai, C.-Y. Yeh, G.-H. Lee and S.-M. Peng, Facile synthesis of heterotrimetallic metal-string complex NiCoRh(dpa)₄Cl₂] through direct metal replacement, *Chem. Commun.* **2013**, *49,* 7938-7940.

133. C.E. Strasser and V.J. Catalano, "On−Off" Au(I)···Cu(I) Interactions in a Au(NHC)₂ Luminescent Vapochromic Sensor, *J. Am. Chem. Soc.* **2010**, *132,* 10009-10011.

134. M. Niskanen, P. Hirva and M. Haukka, Metal–metal interactions in linear tri-, penta-, hepta-, and nona-nuclear ruthenium string complexes, *J. Mol. Model.* **2012**, *18,* 1961-1968.

135. G.-C. Huang, I. P.-C. Liu, J.-H. Kuo, Y.-L. Huang, C.-Y. Yeh, G.-H. Lee and S.-M. Peng, Further investigations of linear trirhodium complexes: experimental and theoretical studies of Rh₃(dpa)₄Cl₂] and Rh₃(dpa)₄Cl₂](BF₄) dpa = bis(2-pyridyl)amido anion], *Dalton Trans.* **2009** 2623-2629.

136. C.-S. Tsai, I. P.-C. Liu, F.-W. Tien, G.-H. Lee, C.-Y. Yeh, Chun-hsien Chen and Shie-Ming Peng, A novel triruthenium metal string complex with naphthylridylamide ligand: Synthesis, structure, magnetism, and molecular conductance, *Inorg. Chem. Commun.* **2013**, *38,* 152-155.

137. L.-P. Wu, P. Field, T. Morrissey, C. Murphy, P. Nagle, B. Hathaway, C. Simmons and P. Thornton, Crystal structure and electronic properties of dibromo- and dichloro-tetrakis[μ_3-bis(2-pyridyl)amido]tricopper(II) hydrate, *J. Chem. Soc. , Dalton Trans.* **1990** 3835-3840.

138. J.F. Berry, F.A. Cotton, P. Lei and C.A. Murillo, Further Structural and Magnetic Studies of Tricopper Dipyridylamido Complexes, *Inorg. Chem.* **2003***, 42,* 377-382.

139. J.F. Berry, F.A. Cotton, L.M. Daniels, C.A. Murillo and X. Wang, Oxidation of $Ni_3(dpa)_4Cl_2$ and $Cu_3(dpa)_4Cl_2$: Nickel−Nickel Bonding Interaction, but No Copper−Copper Bonds, *Inorg. Chem.* **2003***, 42,* 2418-2427.

140. J. Beck and J. Strähle, Komplexe von 1,5-Di(p-tolyl)-1,4-pentaazadien-3-id, Kristallstrukturen von [Cu(tolylNNNNNtolyl)]$_3$ und [Ni(tolylNNNNNtolyl)$_2$]$_2$, *Angew. Chem.* **1985***, 97,* 419-420.

141. I.-W.P. Chen, M.-D. Fu, W.-H. Tseng, J.-Y. Yu, S.-H. Wu, C.-J. Ku, C.-H. Chen and S.-M. Peng, Conductance and Stochastic Switching of Ligand-Supported Linear Chains of Metal Atoms, **2006***, 45,* 5814-5818.

142. H.A. Favre and W.H. Powell, *Nomenclature of Organic Chemistry: IUPAC Recommendations and Preferred Names 2013,* The Royal Society of Chemistry, Cambridge, UK, 2013.

143. M. Witanowski and L. Stefaniak, Combined approach to tautomerism in azaaromatic heterocycles by means of nitrogen, carbon, and proton NMR shieldings, *Bull. Polish. Acad. Sci. Chem.* **1987***, 35,* 305-320.

144. L. Stefaniak, 14N and 13C NMR of tautomeric systems of mercapto- and amino-pyridines, *Org. Magn. Reson.* **1979***, 12,* 379-382.

145. O.V. Dolomanov, L.J. Bourhis, R.J. Gildea, J.A.K. Howard and H. Puschmann, OLEX2: A complete structure solution, refinement and analysis program, *J. Appl. Cryst.* **2009***, 42,* 339-341.

146. V.Z. Mota, G.S.G. de Carvalho, A.D. da Silva, L.A.S. Costa, P. de Almeida Machado, E.S. Coimbra, C.V. Ferreira, S.M. Shishido and A. Cuin, Gold complexes with benzimidazole derivatives: synthesis, characterization and biological studies, *Biometals.* **2014***, 27,* 183-194.

147. S. González-Gallardo, I. Kuzu, P. Oña-Burgos, T. Wolfer, C. Wang, K.W. Klinkhammer, W. Klopper, S. Bräse and F. Breher, Coinage Metal Complexes of Tris(pyrazolyl)methanide-Based Redox-Active Metalloligands, *Organometallics.* **2014***, 33,* 941-951.

148. M. Guitet, P. Zhang, F. Marcelo, C. Tugny, J. Jiménez-Barbero, O. Buriez, C. Amatore, V. Mouriès-Mansuy, J.-P. Goddard, L. Fensterbank, Y. Zhang, S. Roland, M. Ménand and M. Sollogoub, NHC-Capped Cyclodextrins (ICyDs): Insulated Metal Complexes, Commutable Multicoordination Sphere, and Cavity-Dependent Catalysis, *Angew. Chem. , Int. Ed.* **2013**, *52,* 7213-7218.

149. G. Biedermann and L.G. Sillén, Studies on the Hydrolysis of Metal Ions. Part 30. A Critical Survey of the Solubility Equilibria of Ag_2O, *Acta Chem. Scand.* **1960**, *14,* 717-725.

150. M. Odoko, Y. Wang and N. Okabe, *catena*-Poly[[(1,10-phenanthroline-$^2N,N'$)silver(I)]--chloro], *Acta Cryst.* **2004**, *E60,* m1522-m1524.

151. G.A. Bowmaker, Effendy, S. Marfuah, B.W. Skelton and A.H. White, Syntheses, structures and vibrational spectroscopy of some 1:1 and 1:2 adducts of silver(I) oxyanion salts with 2,2′-bis(pyridine) chelates, *Inorg. Chim. Acta.* **2005**, *358,* 4371-4388.

152. G.H. Eom, H.M. Park, M.Y. Hyun, S.P. Jang, C. Kim, J.H. Lee, S.J. Lee, S.-J. Kim and Y. Kim, Anion effects on the crystal structures of Zn^{II} complexes containing 2,2′-bipyridine: Their photoluminescence and catalytic activities, *Polyhedron.* **2011**, *30,* 1555-1564.

153. M.T. Räisänen, N. Runeberg, M. Klinga, M. Nieger, M. Bolte, P. Pyykkö, M. Leskelä and T. Repo, Coordination of Pyridinethiols in Gold(I) Complexes, *Inorg. Chem.* **2007**, *46,* 9954-9960.

154. B. Brewer, N.R. Brooks, S. Abdul-Halim and A.G. Sykes, Differential metathesis reactions of 2,2'-bipyridine and 1,10-phenanthroline complexes of cobalt(II) and nickel(II): cocrystallization of ionization isomers {cis-Ni(phen)$_2$(H$_2$O)$_2$]cis-Ni(phen)$_2$(H$_2$O)Cl]}(PF$_6$)$_3$·4.5H$_2$O, and a synthetic route to asymmetric tris-substituted complexes, *J. Chem. Cryst.* **2003**, *33,* 651-662.

155. F.L. Yin, J.J. Zhu, J. Hao, J.R. Cui and J.J. Yang, Synthesis, characterization, crystal structure and antitumor activities of a novel demethylcantharidato bridged copper(II) phenanthroline complex, *Sci. China Chem.* **2013**, *56,* 481-489.

156. W.T. Eckenhoff, A.B. Biernesser and T. Pintauer, Structural characterization and investigation of iron(III) complexes with nitrogen and phosphorus based ligands in atom transfer radical addition (ATRA), *Inorg. Chim. Acta.* **2012**, *382,* 84-95.

157. IUPAC. Compendium of Chemical Terminology, 2nd ed. (the "Gold Book"). Compiled by A. D. McNaught and A. Wilkinson. Blackwell Scientific Publications, Oxford (1997). XML on-line corrected version: http://goldbook.iupac.org (2006–) created by M. Nic, J. Jirat, B. Kosata; updates compiled by A. Jenkins. ISBN 0-9678550-9-8. doi:10.1351/goldbook.

158. V. Amani, N. Safari, H.R. Khavasi and P. Mirzaei, Iron(III) mixed-ligand complexes: Synthesis, characterization and crystal structure determination of iron(III) hetero-ligand complexes containing 1,10-phenanthroline, 2,2′-bipyridine, chloride and

dimethyl sulfoxide, [Fe(phen)Cl3(DMSO)] and [Fe(bipy)Cl3(DMSO)], *Polyhedron.* **2007***, 26,* 4908-4914.

159.   M.A. Moreno, M. Haukka, M. Kallinen and T.A. Pakkanen, Reactions of [Ru(CO)$_3$Cl$_2$]$_2$ with aromatic nitrogen donor ligands in alcoholic media, *Appl. Organomet. Chem.* **2006***, 20,* 51-69.

Appendixes

1. Tables of intermetallic distances and angles of selected EMACs

2. Tables of performed reactions in the experimental part

3. Results of elemental analysis

4. Solid state ^{13}C CP NMR spectrum of monometallic silver polymer (EAS–167–160)

Table A1T1A: Table of intermetallic distances of class A1 compounds. *The value is not available because only the abstract of the article is available. Abbreviation na stands for that the information was not available neither in the article itself nor in cif file of supporting info. Abbreviation rt stands for room temperature. ^The value is not published in the article but is taken from cif file with Mercury 3.1 software. Cells with diagonal grid mean that cif file has been checked whether it contains additional values than what is tabulated to previous columns. Cells with diagonal lines but not diagonal grid mean that the article didn't contain information whether there're additional values in addition to the values announced and no cif file was available neither from the published as supporting file nor from WebCSD.

Compound	Temp (K)	Distances (Å) M···M			Ref.
{[Rh(2,2'-bpy)(CO)$_2$]$^+$ [RhCl$_2$(CO)$_2$]$^-$}$_n$	100(2)	3.3174(5)	3.4116(5)		116
{[Rh(phen)(CO)$_2$]$^+$ [RhCl$_2$(CO)$_2$]$^-$}$_n$ chain A	100(2)	3.2734(3)	3.3155(3)		116
{[Rh(phen)(CO)$_2$]$^+$ [RhCl$_2$(CO)$_2$]$^-$}$_n$ chain B	100(2)	3.3211(3)	3.3498(3)		
[Rh^I(H$_2$bim)Cl$_2$(CO)$_2$]$^+$ 1/6 [Rh(CO)$_2$Cl$_2$]$^-$ 5/6 Cl$^-$ · 1/6 [CH$_2$Cl$_2$] · 4/6 H$_2$O	100(2)	3.3878(6)	3.4303(6)	3.4405(6)	117
[Rh(H$_2$bim)(CO)$_2$][NO$_3$]	100(2)	3.2379(9)			117
	297(2)	3.2977(4)			
[Rh(H$_2$bim)(CO)$_2$][BF$_4$]	100(2)	3.2719(2)			117
	220(2)	3.3432(9)			
	297(2)	3.3095(3)			
[Rh(Benzoylacetonato-κ^{2}O,O')(CO)$_2$]	100	3.308(3)	3.461(3)		118
[NMe$_4$][Rh(ox)(CO)$_2$]	*	3.243(1)	*	*	120
[Ru(CO)$_4$]$_n$ (powder XRD used)	r	2.860(1)	*	*	40
[methyl violen][AuI$_2$]$_2$	223	3.3767(3)			121
[AuI(o-xylylNC)]	169(2)	3.4602(3)			122
[Au$_2$Cl$_2$(μ-1,8-di(phospholan-1-yl)octane)]$_n$	130(2)	3.3024(6)	3.5106(1)		124
[Au$_2$Cl$_2$(μ-1,8-di(phospholan-1-yl)decane)]$_n$	293(2)	3.3582(3)	3.5106(1)		124
{[Au(py)$_2$]$^+$[Au(SCN)$_2$]$^-$}$_n$ polymorph a	100(2)	3.1340(2)	3.3652(2)		123
{[Au(py)$_2$]$^+$[Au(SCN)$_2$]$^-$}$_n$ polymorph b	100(2)	3.0572(3)	3.2182(3)	4.1114(4)	123

Table A1T1B: Table of intermetallic angles of class A1 compounds. Explanations for notations are shown in header text of Table A1T1A

Compound	Temp (K)	Angles (°) M⋯M⋅⋅M			Ref.
$\{[Rh(2,2'\text{-bpy})(CO)_2]^+$ $[RhCl_2(CO)_2]^-\}_n$	100(2)	170.927(11)			[116]
$\{[Rh(phen)(CO)_2]^+$ $[RhCl_2(CO)_2]^-\}_n$ chain A	100(2)	170.275(9)			[116]
$\{[Rh(phen)(CO)_2]^+$ $[RhCl_2(CO)_2]^-\}_n$ chain B	100(2)	159.573(9)			
$[Rh^I(H_2bim)Cl_2(CO)_2]^+$ 1/6 $[Rh(CO)_2Cl_2]^-$ 5/6 Cl^- ⋅ 1/6 $[CH_2Cl_2]$ ⋅ 4/6 H_2O	100(2)	156.49(2)	157.080(18)	163.186(17)	[117]
$[Rh(H_2bim)(CO)_2][NO_3]$	100(2)	169.230(17)			[117]
	297(2)	169.367(17)			
$[Rh(H_2bim)(CO)_2][BF_4]$	100(2)	167.283(11)			[117]
	220(2)	166.365(19)			
	297(2)	167.299(11)			
$[Rh(Benzoylacetonato-\kappa^2O,O')(CO)_2]$	100	175.01(3)			[118]
$[NMe_4][Rh(ox)(CO)_2]$	*	175.01(3)	*	*	[120]
$[Ru(CO)_4]_n$ (powder XRD used)	rt	180			[40]
[methyl violen][$AuI_2]_2$	223	180.00			[121]
$[AuI(o\text{-xylylNC})]$	169(2)	164.73(2)			[122]
$[Au_2Cl_2(\mu\text{-1,8-di(phospholan-1-yl)octane})]_n$	130(2)	172.82(1) ^			[124]
$[Au_2Cl_2(\mu\text{-1,8-di(phospholan-1-yl)decane})]_n$	293(2)	176.11(1)^			[124]
$\{[Au(py)_2]^+[Au(SCN)_2]^-\}_n$ polymorph a	100(2)	180.00	180.00		[123]
$\{[Au(py)_2]^+[Au(SCN)_2]^-\}_n$ polymorph b	100(2)	102.44(1)	na		[123]

Table A1T2A. Table of intermetallic distances of other EMAC compounds than group A1. Explanations for notations are shown in header text of Table A1T1A with addition of [†] which stands for that only one value was mentioned in the corresponding article but no mention was made that there're where two different distances which were obtained from the cif file.

Compound	Class	Temp (K)	Distances (Å) M···M intra	intra	inter	Ref.
2 [Rh$_2$Cl$_2$(CO)$_4$(μ-Me$_2$bim)] · EtOH, infinite chain	A2	100(2)	3.2090(12)		3.6341(13)	[117]
[Rh$_2$Cl$_2$(CO)$_4$(μ-Me$_2$bim)], tetrameric	A2	100(2)	3.2327(2)	3.5197(2)	3.4026(2)	[117]
[{Rh(μ-pz)(CNt-Bu)$_2$}$_4$](PF$_6$)$_2$	A2	150.0(2)	2.721(4)	2.723(4)	2.713(4)	[42]
[Rh$_2$(μ-Et$_2$bim)Cl$_2$(CO)$_2$]	A2	100(2)	3.1781(5)		3.4345(6)	[126]
		260(2)	3.2095(5)		3.4990(5)	
[Rh$_2$(μ-Pr$_2$bim)Cl$_2$(CO)$_2$]	A2	100(2)	3.1469(3)		3.4403(3)	[126]
		260(2)	3.1737(5)		3.4944(6)	
		88(2)	3.1426(5)		3.4255(5)	
[Ru$_2${μ-O$_2$C(3,5-CF$_3$)$_2$C$_6$H$_3$}$_2$(CO)$_5$]$_2$	A2	173(2)	2.6859(8)		2.9065(9)	[125]
[Cu$_3$Br$_2$(μ$_3$-dpa)$_4$] ·H$_2$O	B	rt^	2.468(1)			[137]
[Cu$_3$Cl$_2$(μ$_3$-dpa)$_4$] ·H$_2$O	B	rt^	2.471(1)			[137]
[Cu$_3$Cl$_2$(μ$_3$-dpa)$_4$] ·CH$_2$Cl$_2$	B	298	2.492(2)			[138]
		160	2.4769(3)			
[Cu$_3$Cl$_2$(μ$_3$-dpa)$_4$] ·toluene	B	rt^	2.4688(9)	2.4710(9)		[138]
[Cu$_3$Cl$_2$(μ$_3$-dpa)$_4$] ·Et$_2$O	B	rt^	2.4672(8)	2.4735(8)		[138]
[Cu$_3$(BF$_4$)$_2$(μ$_3$-dpa)$_4$]	B	rt^	2.4035(8)	2.4029(8)		[138]
[Cu$_3$Cl$_2$(μ$_3$-dpa)$_4$][SbCl$_6$] · 2.86C$_2$H$_4$Cl$_2$ · 0.792C$_6$H$_{12}$	B	rt^	2.513(1) [†]	2.515(1) [†]		[139]
[Cu$_3$Cl$_2$(μ$_3$-dpa)$_4$][SbCl$_6$] · 2.44Et$_2$O	B	173^	2.505(1) [†]	2.506(1) [†]		[139]
[Cu$_3$(μ$_3$-p-tolyl-NNNNN-p-tolyl)$_3$]	B	rt^	2.348(2)	2.358(2)		[140]
[Au{μ$_3$-im(CH$_2$py)$_2$}$_2${Cu(MeCN)$_2$}$_2$](PF$_6$)$_3$ · 2MeCN	B	100	4.591			[133]
[Au{μ$_3$-im(CH$_2$py)$_2$}$_2${Cu(MeOH)}$_2$](PF$_6$)$_3$ · 2MeOH · 2Et$_2$O	B	100	2.7195(7)			[133]

Table A1T2B. Table of intermetallic angles of other EMAC compounds than group A1.
Explanations for notations are shown in header text of Table A1T1A

Compound	Class	Temp (K)	Angles (°) M···M··M		Ref.
2 [Rh$_2$Cl$_2$(CO)$_4$(μ-Me$_2$bim)] · EtOH, infinite chain	A2	100(2)	163.24(4)		[117]
[Rh$_2$Cl$_2$(CO)$_4$(μ-Me$_2$bim)], tetrameric	A2	100(2)	171.879(6)	155.65(1)^	[117]
[{Rh(μ-pz)(CNt-Bu)$_2$}$_4$](PF$_6$)$_2$	A2	150.0(2)	165.51(14)	167.17(15)	[42]
[Rh$_2$(μ-Et$_2$bim)Cl$_2$(CO)$_2$]	A2	100(2)	174.184(5)		[126]
		260(2)	173.909(9)		
[Rh$_2$(μ-Pr$_2$bim)Cl$_2$(CO)$_2$]	A2	100(2)	179.453(16)		[126]
		260(2)	178.888(10)		
		88(2)	177.352(17)		
[Ru$_2${μ-O$_2$C(3,5-CF$_3$)$_2$C$_6$H$_3$}$_2$(CO)$_5$]$_2$	A2	173(2)	173.961(19)		[125]
[Cu$_3$Br$_2$(μ$_3$-dpa)$_4$] ·H$_2$O	B	rt^	178.12(1)		[137]
[Cu$_3$Cl$_2$(μ$_3$-dpa)$_4$] ·H$_2$O	B	rt^	178.51(2)		[137]
[Cu$_3$Cl$_2$(μ$_3$-dpa)$_4$] ·CH$_2$Cl$_2$	B	298	178.29(3)[†]		[138]
		160	178.30(3)[†]		
[Cu$_3$Cl$_2$(μ$_3$-dpa)$_4$] ·toluene	B	rt^	178.12(4)[†]		[138]
[Cu$_3$Cl$_2$(μ$_3$-dpa)$_4$] ·Et$_2$O	B	rt^	179.01(3)[†]		[138]
[Cu$_3$(BF$_4$)$_2$(μ$_3$-dpa)$_4$]	B	rt^	179.46(3)		[138]
[Cu$_3$Cl$_2$(μ$_3$-dpa)$_4$][SbCl$_6$] · 2.86C$_2$H$_4$Cl$_2$ · 0.792C$_6$H$_{12}$	B	rt^	179.84(5)[†]		[139]
[Cu$_3$Cl$_2$(μ$_3$-dpa)$_4$][SbCl$_6$] · 2.44Et$_2$O	B	173^	177.60(5)[†]		[139]
[Cu$_3$(μ$_3$-p-tolyl-NNNNN-p-tolyl)$_3$]	B	rt^	180.00(1)		[140]
[Au{μ$_3$-im(CH$_2$py)$_2$}$_2${Cu(MeCN)$_2$}$_2$](PF$_6$)$_3$ · 2MeCN	B	100	179.13(1)[†]		[133]
[Au{μ$_3$-im(CH$_2$py)$_2$}$_2${Cu(MeOH)}$_2$](PF$_6$)$_3$ · 2MeOH · 2Et$_2$O	B	100	153.02(2)[†]		[133]

Table of every reaction performed in this thesis

EA	EAS	Lay-ered	G11	G11 anion & rest of the formula (excluding constitutional water)	Li-gand	Base & Acid
YES	135		2: Ag(I)+Cu	NO3	s-pyH	NO
YES	136		2: Ag(I)+Cu	NO3	s-pyH	KOH & AcOH
	156	YES	2: Ag(I)+Cu	NO3	s-pyH	KOH & Et3N
	180		2: Ag(I)+Cu	NO3	s-pyH	KOH
	215		2: Ag(I)+sak(Ag)	NO3	s-pyH	KOH & Et3N
	216		2: Ag(I)+sak(Ag)	NO3	s-pyH	KOH & Et3N
YES	187		2: Cu(II)+Au	Cl	s-pyH	NO
	189	YES	2: Cu(II)+Au	Cl	s-pyH	NO
	190	YES	2: Cu(II)+Au	Cl	s-pyH	NO
	178		2: Cu(II)+Cu	Cl	s-pyH	NO
	181T1		2: Cu(II)+Cu	Cl	s-pyH	KOH
	181T2		2: Cu(II)+Cu	Cl	s-pyH	NO
	181V		2: Cu(II)+Cu	Cl	s-pyH	KOH
	211		2: Cu(II)+sak(Ag)	Cl	s-pyH	NO
	212		2: Cu(II)+sak(Ag)	Cl	s-pyH	NO
	214		2: Cu(II)+sak(Ag)	Cl	s-pyH	NO
YES	220		2: Cu(II)+sak(Ag)	Cl	s-pyH	NO
YES	221		2: Cu(II)+sak(Ag)	Cl	s-pyH	NO
	222		2: Cu(II)+sak(Ag)	Cl	s-pyH	NO
	225		3: Cu(II)+Cu+Zn	polym [ZnCl4] EAS-164	NO	KOH
YES	219		3: Cu(II)+sak(Ag)+Cu	Cl	s-pyH	NO

EA	EAS	Lay-ered	G11	G11 anion & rest of the formula (excluding constitutional water)	Li-gand	Base & Acid
	102		Ag(I)	CF3SO3	s-pyH	KOH
	105		Ag(I)	CF3SO3	s-pyH	NO
	110		Ag(I)	CF3SO3	s-pyH	KOH
	111		Ag(I)	CF3SO3	s-pyH	KOH
	112		Ag(I)	CF3SO3	s-pyH	KOH
	113		Ag(I)	CF3SO3	s-pyH	NO
	115		Ag(I)	NO3	s-pyH	KOH
	116		Ag(I)	CF3SO3	s-pyH	KOH
YES	117		Ag(I)	CF3SO3	s-pyH	Et3N
YES	118		Ag(I)	NO3	s-pyH	Et3N
	121		Ag(I)	(4-mp)2H/117	NO	Et3N
YES	124		Ag(I)	CF3SO3	s-pyH	Et3N
	126		Ag(I)	CF3SO3	s-pyH	Et3N
YES	137		Ag(I)	NO3	s-pyH	KOH & Et3N
YES	138		Ag(I)	NO3	s-pyH	KOH & Et3N
	146		Ag(I)	NO3	s-pyH	KOH & Et3N
	149		Ag(I)	NO3	s-pyH	KOH & Et3N
YES	150		Ag(I)	NO3	s-pyH	KOH & Et3N
YES	151		Ag(I)	NO3	s-pyH	KOH & Et3N
YES	152		Ag(I)	NO3	s-pyH	KOH & Et3N
YES	153		Ag(I)	NO3	s-pyH	KOH & Et3N
YES	154		Ag(I)	NO3	s-pyH	KOH & Et3N

EA	EAS	Lay-ered	G11	G11 anion & rest of the formula (excluding constitutional water)	Li-gand	Base & Acid
	155	YES	Ag(I)	NO3	s-pyH	KOH & Et3N
YES	157		Ag(I)	NO3	s-pyH	Et3N
YES	158		Ag(I)	NO3	s-pyH	Et3N
YES	159		Ag(I)	NO3	s-pyH	Et3N
YES	160		Ag(I)	NO3	s-pyH	Et3N
	163	YES	Ag(I)	NO3	s-pyH	KOH & Et3N
	207		Ag(I)	NO3	s-pyH	DIPEA
	208		Ag(I)	NO3	s-pyH	Et3N
	209		Ag(I)	NO3	s-pyH	KOH
	210		Ag(I)	NO3	s-pyH	DIPEA
	213		Ag(I)	NO3	s-pyH	KOH
	237		Ag(I)	NO3	s-pyH	KOH
	213 B		Ag(I)	NO3	s-pyH	NaOEt
	101		Au(I)	Cl	s-pyH	NO
	119		Au(I)	Cl	s-pyH	NO
	120		Au(I)	Cl	s-pyH	Et3N
	129		Au(I)	Cl	s-pyH	NO
	139		Au(I)	Cl	s-pyH	NO
	140		Au(I)	Cl	s-pyH	NO
	141		Au(I)	Cl	s-pyH	NO
	161		Au(I)	Cl	s-pyH	NO
	162		Au(I)	Cl	s-pyH	NO

EA	EAS	Lay-ered	G11	G11 anion & rest of the formula (excluding constitutional water)	Li-gand	Base & Acid
	172		Au(I)	Cl	s-pyH	NO
	173		Au(I)	Cl	s-pyH	NO
	179		Au(I)	Cl	s-pyH	NO
	199	YES	Au(I)	Cl	s-pyH	NO
YES	200	YES	Au(I)	Cl	s-pyH	NO
YES	217	YES	Au(I)	Cl	s-pyH	NO
	218	YES	Au(I)	Cl	s-pyH	NO
	235		Au(I)	Cl	s-pyH	DIPEA
YES	173B		Au(I)	Cl	s-pyH	Et3N
	143		CANCELLED			
	144		CANCELLED			
	103		Cu(II)	AcO	s-pyH	KOH
	106		Cu(II)	AcO	s-pyH	KOH
	125		Cu(II)	AcO	s-pyH	Et3N
	127		Cu(II)	AcO	s-pyH	Et3N
YES	128		Cu(II)	AcO	s-pyH	NO
	130		Cu(II)	AcO	s-pyH	NO
	131		Cu(II)	AcO	s-pyH	Et3N
	132		Cu(II)	AcO	s-pyH	KOH
	133		Cu(II)	AcO	s-pyH	NO
	134		Cu(II)	AcO	s-pyH	NO
YES	164		Cu(II)	Cl	s-pyH	NO
	165		Cu(II)	Cl	s-pyH	NO

EA	EAS	Lay-ered	G11	G11 anion & rest of the formula (excluding constitutional water)	Li-gand	Base & Acid
	167	YES	Cu(II)	Cl	s-pyH	NO
YES	168		Cu(II)	Cl	s-pyH	NO
YES	169		Cu(II)	Cl	s-pyH	NO
	170	YES	Cu(II)	Cl	s-pyH	NO
	171	YES	Cu(II)	Cl	s-pyH	NO
	174		Cu(II)	Cl	s-pyH	NO
	175	YES	Cu(II)	Cl	s-pyH	NO
	177		Cu(II)	Cl	s-pyH	NO
	182		Cu(II)	phenCl2	s-pyH	KOH
	183		Cu(II)	Cl	s-pyH	NO
	184	YES	Cu(II)	Cl	s-pyH	NO
	185		Cu(II)	Cl	s-pyH	NO
	186	YES	Cu(II)	Cl	s-pyH	NO
	188	YES	Cu(II)	Cl	s-pyH	NO
	191		Cu(II)	Cl	s-pyH	NO
	192		Cu(II)	Cl	s-pyH	KOH
	193		Cu(II)	Cl	s-pyH	KOH(EtOH)
	194		Cu(II)	Cl	s-pyH	NO
	195		Cu(II)	Cl	s-pyH	Et3N
	196		Cu(II)	Cl	s-pyH	NO
	197		Cu(II)	Cl	s-pyH	NO
YES	198		Cu(II)	Cl	s-pyH	NO

EA	EAS	Lay-ered	G11	G11 anion & rest of the formula (excluding constitutional water)	Li-gand	Base & Acid
	201	YES	Cu(II)	Cl	s-pyH	NO
	202	YES	Cu(II)	Cl	s-pyH	NO
YES	203		Cu(II)	Cl	s-pyH	NO
YES	204		Cu(II)	Cl	s-pyH	NO
	205	YES	Cu(II)	Cl	s-pyH	NO
	206	YES	Cu(II)	Cl	s-pyH	NO
	223		Cu(II)	Cl	s-pyH	NO
	224		Cu(II)	Cl	s-pyH	NO
	226		Cu(II)	Cl	s-pyH	NO
	234		Cu(II)	Cl	s-pyH	KOH
	236		Cu(II)	Cl	s-pyH	NO
	181.5		Cu(II)	phenCl2	s-pyH	NO
YES	104		NO	NO	s-pyH	NO
	107		NO	NO	NO	NO
	108	YES	NO	NO	bby	NO
	109	YES	NO	NO	bby	NO
	114	YES	NO	NO	bby	NO
	122	YES	NO	NO	bby	NO
	123	YES	NO	NO	bby	NO
YES	142		NO	NO	phen	HCl
YES	145		NO	NO	phen	NO
YES	147		NO	NO	phen	NO
YES	148		NO	NO	phen	NO
	166		NO	NO	s-pyH	NO
YES	176		NO	NO	phen	NO
	227		NO	NO	s-pyH	NO
	228		NO	NO	s-pyH	NO

EA	EAS	Lay-ered	G11	G11 anion & rest of the formula (excluding constitutional water)	Li-gand	Base & Acid
	229		NO	NO	s-pyH	NO
	230		NO	NO	s-pyH	NO
	231		NO	NO	s-pyH	NO
	232		NO	NO	s-pyH	NO
	233		NO	NO	s-pyH	KOH

EAS	Other metal	M anion & rest of the formula	Other substance(s)	G11:L:M:OS:Base	Amount of ligand if not 0.36 mmol
135	Cu(II)	AcO	NO	1:6:2.2	
136	Cu(II)	AcO	NO	1:6:2.2	
156	Cu(II)	Cl	NO	1:4:2	
180	Cu(II)	phenClx	NO	1:4:1	
215	Zn(II)	phenClx	AgClO4	1:6:1:1	
216	Zn(II)	phenClx	AgClO4	1:6:1:1	
187	Au(III)	Cl	NO	1:6:1	
189	Au(III)	Cl	NO	1:6:1	
190	Au(III)	Cl	NO	1:6:1	
178	Cu(II)	phenClx	NO	1:6:2	
181T1	Cu(II)	phenClx	NO	1:6:1:3	0.18
181T2	Cu(II)	phenClx	NO	1:6:1	0.18
181V	Cu(II)	phenClx	NO	1:6:1:6	
211	Zn(II)	phenClx	AgClO4	1:6:1:1	
212	Zn(II)	phenClx	AgClO4	1:6:1:1	
214	Zn(II)	phenClx	AgClO4	1:6:1:2	
220	Ni(II)	phenClx	AgClO4	1:6:1:1	
221	Fe(III)	phenClx	AgClO4	1:6:1:1	
222	Fe(III)	phenClx	AgClO4	1:6:1:1	
225	Cu(II)	phenClx	NO	1:2.11:1	
219	Cu(II)	phenClx	AgClO4	1:6:1:1	
102	NO	NO	NO	1:6	
105	NO	NO	NO	1:10	0.117
110	NO	NO	NO	1:6	
111	NO	NO	NO	1:6	
112	NO	NO	NO	1:6	
113	NO	NO	NO	4:23	0.23
115	NO	NO	NO	1:6	
116	NO	NO	NO	1:6	
117	NO	NO	NO	1:6	
118	NO	NO	NO	1:6	
121	Zn(II)	bbyCl2	NO	1:2	OTHER
124	NO	NO	NO	1:6	
126	NO	NO	NO	1:6	
137	Zn(II)	Cl	NO	1:6:2	
138	Zn(II)	bbyCl2	NO	279:1670:557	0.167
146	Fe(III)	Cl	NO	1:6:2	

EAS	Other metal	M anion & rest of the formula	Other substance(s)	G11:L:M:OS:Base	Amount of ligand if not 0.36 mmol
149	NO	NO	NO	1:4	
150	Fe(III)	Cl	NO	1:4:2	
151	Zn(II)	Cl	NO	1:4:2	
152	Zn(II)	Cl	NO	1:4:2	
153	Fe(III)	Cl	NO	1:4:2	
154	Fe(III)	Cl	NO	1:4:2	
155	Fe(III)	Cl	NO	1:4:2	
157	NO	NO	NO	1:6	
158	NO	NO	NO	1:6	
159	NO	NO	NO	1:6	
160	NO	NO	NO	1:6	
163	Zn(II)	Cl	NO	1:4:2	
207	NO	NO	NO	1:6:6	
208	NO	NO	NO	1:6:6	
209	NO	NO	NO	1:6:6	
210	NO	NO	KOH	1:4:52:5	
213	NO	NO	NO	1:6:18	
237	NO	NO	NO	1:6	
213 B	NO	NO	NO	1:6:?	
101	NO	NO	NH4PF6	1:6:1	
119	NO	NO	NH4PF6	1:6:1	
120	NO	NO	NH4PF6	1:6:1	
129	NO	NO	NO	1:6	
139	NO	NO	NO	1:6	
140	Ni(II)	Cl	NO	1:6:2	
141	Zn(II)	Cl	NO	1:6:2	
161	NO	NO	NO	1:6	
162	NO	NO	NO	1:6	
172	Zn(II)	Cl	NO	1:6:2	
173	NO	NO	NaCl	1:6:2	
179	Cu(II)	phenClx	NO	1:6:1	
199	NO	NO	NO	17:90	0.090
200	NO	NO	NO	17:90	0.090
217	NO	NO	NO	17:90	0.090
218	NO	NO	NO	17:90	0.090
235	Zn(II)	Cl	Cl-terpy	1.2:6:3.3:2:1	
173B	Zn(II)	Cl	NO	1:6:2	
143					
144					

EAS	Other metal	M anion & rest of the formula	Other substance(s)	G11:L:M:OS:Base	Amount of ligand if not 0.36 mmol
103	NO	NO	NO	1:6	
106	NO	NO	NO	1:6	0.72
125	NO	NO	NO	1:6	
127	NO	NO	NO	1:6	
128	NO	NO	NO	1:6	0.6
130	NO	NO	NO	1:6	
131	NO	NO	NO	1:6	
132	NO	NO	NO	1:6	
133	Fe(III)	Cl	NO	1:6:3	
134	Ni(II)	AcO	NO	1:6:3	
164	Zn(II)	Cl	NO	1:6:2	
165	Zn(II)	Cl	NO	1:6:2	
167	Zn(II)	Cl	NO	1:6:2	
168	Fe(III)	Cl	NO	1:6:2	
169	Cr(III)	Cl	NO	1:6:2	
170	Fe(III)	Cl	NO	1:6:2	
171	Cr(III)	Cl	NO	1:6:2	
174	Ru(III)	Cl	NO	1:6:2	
175	Ru(III)	Cl	NO	1:6:2	
177	Zn(II)	phenClx	NO	1:6:2	
182	NO	NO	NO	1:6:6	
183	Fe(III)	phenClx	NO	1:6:1	
184	Fe(III)	phenClx	NO	1:6:1	
185	Fe(III)	phenClx	ZnCl2	1:6:1:1	
186	Fe(III)	phenClx	NH4PF6	1:6:1:1	
188	Ru(III)	Cl	NO	1:6:1	
191	Cr(III)	Cl	NO	1:6:1	
192	Cr(III)	Cl	NO	1:6:1:3	
193	Cr(III)	Cl	NO	1:6:1:6	
194	Cr(III)	Cl	NH4PF6	1:6:1:1	
195	Cr(III)	Cl	NO	1:6:1:6	
196	Fe(III)	Cl	NO	1:6:1	
197	Fe(III)	Cl	NH4PF6	1:6:1:1	
198	Fe(III)	Cl	NH4PF6	1:6:1:1	
201	Zn(II)	Cl	NO	1:6:2	
202	Zn(II)	Cl	NO	1:6:1	
203	NO	NO	NO	1:6	
204	NO	NO	NO	1:6	
205	Fe(III)	Cl	NO	1:6:1	

EAS	Other metal	M anion & rest of the formula	Other substance(s)	G11:L:M:OS:Base	Amount of ligand if not 0.36 mmol
206	Cr(III)	Cl	NO	1:6:1	
223	Fe(III)	Cl	NH4PF6	1:6:1:1	
224	Cr(III)	Cl	NH4PF6	1:6:1:1	
226	Fe(III)	Cl	NH4PF6	1:6:1:1	
234	Fe(III)	Cl	NO	2:6:1:6	
236	Zn(II)	Cl	NO	1:6:2	
181.5	NO	NO	NO	1:6	
104	Ru2(CO)6Cl4	-	NO	284:39	2.84
107	Ru(III)	Cl	NO	-	solvent
108	Zn(II)	Cl	NO	2:1	0.25
109	Zn(II)	Cl	NO	2:1	0.5
114	Zn(II)	Cl	NO	2:1	0.5
122	Zn(II)	Cl	NO	2:1	0.5
123	Zn(II)	Cl	NO	2:1	0.5
142	Fe(III)	Cl	NO	2:1	2
145	Ni(II)	Cl	NO	257:183	2.57
147	Cu(II)	Cl	NO	1:1	2
148	Zn(II)	Cl	NO	257:183	2.57
166	Zn(II)	Cl	NO	5:2	
176	Fe(III)	Cl	NO	1:1	
227	Fe(III)	Cl	NO	2:1	0.12
228	Fe(III)	Cl	NO	6:1	
229	Fe(III)	Cl	NO	6:1	
230	Ru(III)	Cl	NO	6:1	
231	Ru(III)	Cl	NO	3:1	0.18
232	Cr(III)	Cl	NO	3:1	0.18
233	Fe(III)	Cl	ZnCl2	6:6:1:1	

EAS	G11 solvent	G11 solvent amount (mL)	Ligand solvent	Ligand solvent amount (mL)	M solvent	M solvent amount (mL)
135	H2O	4	H2O	10	H2O	4
136	H2O	4	H2O	10	H2O	4
156	MeCN	2.5	EtOH	5	2:1 EtOH:MeCN	3
180	MeCN	5	EtOH	10	3:4 EtOH:H2O	7
215	MeCN	5	EtOH	10	MeOH	11
216	MeCN	5	EtOH	10	MeOH	11
187	3:1 MeCN:EtOH	4	3:1 MeCN:EtOH	7	9:3:16 MeCN:EtOH:H2O	7
189						
190						
178	3:1 MeCN:EtOH	4	3:1 MeCN:EtOH	7	9:3:16 MeCN:EtOH:H2O	7
181T1	3:1 MeCN:EtOH	2	3:1 MeCN:EtOH	3.5	3:1:4 MeCN:EtOH:H2O	2
181T2	3:1 MeCN:EtOH	2	3:1 MeCN:EtOH	3.5	3:1:4 MeCN:EtOH:H2O	2
181V	3:1 MeCN:EtOH	4	3:1 MeCN:EtOH	7	3:1:4 MeCN:EtOH:H2O	4
211	MeOH	5	MeOH	4	MeOH	11
212	MeOH	5	MeOH	4	MeOH	11
214	MeOH	5	MeOH	4	MeOH	11
220	MeOH	4	MeOH	4	EtOH	12
221	MeOH	4	MeOH	4	EtOH	12
222	MeCN	6	MeCN	6	MeCN	4
225	MeOH	10				
219	MeOH	4	MeOH	4	11:2 MeOH:H2O	13
102	MeCN	5	EtOH	10		
105	MeCN	3	EtOH	4+5		
110	MeCN	5	EtOH	10		
111	MeCN	5	EtOH	10		
112	MeCN	5	EtOH	10		
113	MeCN	25	EtOH	20		
115	MeCN	5	EtOH	10		
116	MeCN	5	EtOH	10		
117	MeCN	5	EtOH	10		
118	MeCN	5	EtOH	10		
121	CH3NO2	10			1:1 EtOH & MeOH	10
124	MeCN	5	EtOH	10		
126	CH3NO2	5	CH3NO2	13		
137	MeCN	5	EtOH	10	EtOH	6
138	MeCN	2.5	EtOH	5	1:1 EtOH & MeCN	6

EAS	G11 solvent	G11 solvent amount (mL)	Ligand solvent	Ligand solvent amount (mL)	M solvent	M solvent amount (mL)
146	MeCN	5	EtOH	10	EtOH	7
149	MeCN	6	EtOH	10		
150	MeCN	5	EtOH	10	2:1 EtOH:MeCN	5
151	MeCN	5	EtOH	10	2:1 EtOH:MeCN	5
152	MeCN	5	EtOH	10	2:1 EtOH:MeCN	5
153	MeCN	5	EtOH	10	2:1 EtOH:MeCN	5
154	MeCN	5	EtOH	10	2:1 EtOH:MeCN	5
155	MeCN	2.5	EtOH	5	2:1 EtOH:MeCN	3
157	MeCN	5	EtOH	10		
158	MeCN	5	EtOH	10		
159	MeCN	5	EtOH	10		
160	MeCN	5	EtOH	10		
163	MeCN	2.5	EtOH	5	2:1 EtOH:MeCN	3
207	MeCN	5	EtOH	10		
208	MeCN	5	EtOH	10		
209	MeCN	5	EtOH	10		
210	MeCN	5	EtOH	10		
213	MeCN	5	EtOH	10		
237	MeCN	5	EtOH	10		
213 B	MeCN	5	EtOH	10		
101	MeCN	10	EtOH & H2O	12		
119	MeCN	10	H2O			
120	MeCN	10	H2O	12		
129	MeCN	15	H2O	10		
139	MeCN	10	MeCN	10		
140	MeCN	15	H2O	10	3:2 MeCN:H2O	5
141	MeCN	15	H2O	10	MeCN	5
161	MeCN	15	H2O	10		
162	MeCN	15	H2O	10		
172	MeCN	15	H2O	10	H2O	5
173	MeCN	15	H2O	10		
179	MeCN	15	H2O	10	H2O	5
199	MeCN	10	CH2Cl2	11		
200	MeCN	10	CH2Cl2	11		
217	MeCN	10	CH2Cl2	11		
218	MeCN	10	CH2Cl2	11		
235	MeCN	5	3:1 MeCN:MeOH	4	MeOH	3
173B	MeCN	15	H2O	10		
143						

EAS	G11 solvent	G11 solvent amount (mL)	Ligand solvent	Ligand solvent amount (mL)	M solvent	M solvent amount (mL)
144						
103	MeCN	5	EtOH	10		
106	MeCN	10	EtOH	20		
125	MeCN	5	EtOH	10		
127	CH3NO2:MeCN 5:3	8	CH3NO2	13		
128	MeCN	15	EtOH	20		
130	H2O	6	H2O	10		
131	H2O	6	H2O	10		
132	H2O	6	H2O	10		
133	H2O	4	H2O	11	H2O	4
134	H2O	4	H2O	11	H2O	4
164	3:1 MeCN:EtOH	4	3:1 MeCN:EtOH	10	3:1 MeCN:EtOH	4
165	H2O	5	H2O	10	H2O	5
167						
168	3:1 MeCN:EtOH	2	3:1 MeCN:EtOH	5	3:1 MeCN:EtOH	2
169	3:1 MeCN:EtOH	2	3:1 MeCN:EtOH	5	3:1 MeCN:EtOH	2
170						
171						
174	3:1 MeCN:EtOH	3	3:1 MeCN:EtOH	5	3:1 MeCN:EtOH	4
175						
177	3:1 MeCN:EtOH	4	3:1 MeCN:EtOH	7	H2O	3
182	9:3:8 MeCN:EtOH:H2O	5	3:1 MeCN:EtOH	7		
183	3:1 MeCN:EtOH	4	3:1 MeCN:EtOH	7	3:1 MeCN:EtOH	4
184						
185	3:1 MeCN:EtOH	3	3:1 MeCN:EtOH	4	15:5:16 MeCN:EtOH:H2O	4.5
186						
188						
191	3:1 MeCN:EtOH	5	3:1 MeCN:EtOH	5	3:1 MeCN:EtOH	5
192	3:1 MeCN:EtOH	5	3:1 MeCN:EtOH	5	3:1 MeCN:EtOH	5
193	3:1 MeCN:EtOH	5	3:1 MeCN:EtOH	5	3:1 MeCN:EtOH	5
194	3:1 MeCN:EtOH	5	3:1 MeCN:EtOH	5	3:1 MeCN:EtOH	5
195	3:1 MeCN:EtOH	5	3:1 MeCN:EtOH	5	3:1 MeCN:EtOH	5
196	3:1 MeCN:EtOH	5	3:1 MeCN:EtOH	5	3:1 MeCN:EtOH	5
197	3:1 MeCN:EtOH	5	3:1 MeCN:EtOH	5	3:1 MeCN:EtOH	5
198	3:1 MeCN:EtOH	10	3:1 MeCN:EtOH	10	3:1 MeCN:EtOH	10
201	3:1 MeCN:EtOH	3	3:1 MeCN:EtOH	3	3:1 MeCN:EtOH	9
202	3:1 MeCN:EtOH	3	3:1 MeCN:EtOH	3	3:1 MeCN:EtOH	9
203	3:1 MeCN:EtOH	2	3:1 MeCN:EtOH	3		

EAS	G11 solvent	G11 solvent amount (mL)	Ligand solvent	Ligand solvent amount (mL)	M solvent	M solvent amount (mL)
204	3:1 MeCN:EtOH	2	3:1 MeCN:EtOH	3		
205	3:1 MeCN:EtOH	2	3:1 MeCN:EtOH	3	9:1 Et2O:EtOH	10
206	3:1 MeCN:EtOH	2	3:1 MeCN:EtOH	3	8:2 Et2O:EtOH	10
223	3:1 MeCN:EtOH	10	3:1 MeCN:EtOH	10	3:1 MeCN:EtOH	10
224	3:1 MeCN:EtOH	10	3:1 MeCN:EtOH	10	3:1 MeCN:EtOH	10
226	3:1 MeCN:EtOH	10	3:1 MeCN:EtOH	10	3:1 MeCN:EtOH	10
234	3:1 MeCN:EtOH	10	3:1 MeCN:EtOH	20	3:1 MeCN:EtOH	10
236	3:1 MeCN:EtOH	4	3:1 MeCN:EtOH	4	3:1 MeCN:EtOH	4
181.5	3:2 EtOH:H20	5	3:1 MeCN:EtOH	7		
104			EtOH	14	EtOH	7
107						
108						
109						
114						
122						
123						
142						
145						
147						
148						
166						
176						
227			3:1 MeCN:EtOH	5	3:1 MeCN:EtOH	5
228			3:1 MeCN:EtOH	5	3:1 MeCN:EtOH	10
229			H2O	5	H2O	5
230			3:1 MeCN:EtOH	5	3:1 MeCN:EtOH	5
231			MeOH	5	MeOH	5
232			Oxolane		Oxolane	
233			3:1 MeCN:EtOH	10	3:1 MeCN:EtOH	10

EAS	Other s. solvent	Other s. solvent amount (mL)	Additional solvents and amounts
135			
136			
156			
180			
215	MeOH	5	
216	MeOH	5	
187			
189			
190			
178			
181T1			
181T2			H2O
181V			
211	MeOH	5	MeOH 1
212	MeOH	5	MeOH 1
214	MeOH		
220	MeOH	4	
221	MeOH	4	
222	MeCN	4	
225			
219	MeOH	4	
102			
105			
110			
111			
112			
113			
115			
116			
117			
118			
121			
124			
126			
137			EtOH 10
138			EtOH 10
146			

EAS	Other s. solvent	Other s. solvent amount (mL)	Additional solvents and amounts
149			
150			
151			
152			
153			
154			
155			
157			
158			
159			
160			
163			
207			
208			
209			
210			
213			
237			
213 B			
101			
119			CH2Cl2 2+0.5
120			
129			
139			
140			
141			
161			
162			
172			
173	H2O		
179			
199			
200			
217		5	
218			
235	MeOH	7	
173B	H2O		
143			
144			

APPENDIX 2

EAS	Other s. solvent	Other s. solvent amount (mL)	Additional solvents and amounts
103			
106			
125			
127			
128			
130			
131			
132			
133			
134			
164			
165			
167			
168			
169			
170			
171			
174			
175			
177			
182			
183			
184			
185	3:1 MeCN:EtOH	3	
186			
188			
191			
192			
193			
194	3:1 MeCN:EtOH	5	
195			
196			
197	3:1 MeCN:EtOH	5	
198	3:1 MeCN:EtOH	10	3:1 MeCN:EtOH 10
201			3:1 MeCN:EtOH 5
202			3:1 MeCN:EtOH 5

EAS	Other s. solvent	Other s. solvent amount (mL)	Additional solvents and amounts
203			
204			
205			3:1 MeCN:EtOH 5
206			3:1 MeCN:EtOH 5
223	3:1 MeCN:EtOH	10	3:1 MeCN:EtOH 10
224	3:1 MeCN:EtOH	10	3:1 MeCN:EtOH 10
226	3:1 MeCN:EtOH	10	3:1 MeCN:EtOH 10
234			
236			
181.5			
104			After evaporation EtOH
107			
108			
109			
114			
122			
123			
142			
145			
147			
148			
166			
176			
227			
228			
229			
230			
231			
232			
233	3:1 MeCN:EtOH	10	

Elemental analysis of selected compounds

Acceptable limit for elemental analysis in many scientific articles is 0.4 percentage. Every sample was measured twice and the average was used as the experimental value. The experimental values of 1,10-phenanthroline (phen) complexes are shown in Table 5. Calculated values for the compounds and the difference between calculated and experimental values in percentage and percentage point (pp) are shown in Table 6. The negative sign in the difference indicates an experimental value to be greater than the corresponding calculated value.

The differences of mass percentages of duplicate samples were much higher than the acceptable limit of many scientific articles (0.4 %). The average differences of all elemental analysis between parallel samples were 0.3±0.5 pp for C, 0.07±0.04 pp for H and 0.10±0.7 pp for N. The errors in % were 0.8±0.6 %, 3±2 % and 1.4±1.1 %, respectively. These errors are much higher than the acceptable limit; hence it's not expected that many of the products will fall within the limit.

The high differences between parallel samples can be explained in multiple reasons: samples might have had different solvent or moisture content of the samples even though (nearly) all the samples were dried in the vacuum overnight. Reactions didn't yield one product but mixture of multiple products. The washing of the product was insufficient so some unreacted starting materials and by-products were remained in the dried product. These reasons gave rise to the mixture of substances and their possible uneven distribution among the duplicate samples induced differences of elemental mass percentages.

The elemental analyzer used was based on combustion of the product. If the products were slow-burning, the combustion was not complete and some of C, H and N might have remained in the combustion pocket. This would have caused differences in the amounts of CO_2, H_2O and nitrogen oxides of which amount were measured to determine the mass ratio of C, H and N. The accuracy of the instrument was unknown. The last reason is there's another error consequent upon the elemental analyzer.

The most likely reasons or errors were assumed to be due to insufficient combustion of the products, the accuracy of the instrument itself and different solvent or water content of the products. The amount of solvent crystallized into the product also affects the elemental composition of the products but not to the difference between parallel samples because

compounds were assumed to crystallize only in a crystal form even if polymorphism might happen.

Elemental analysis of phenanthroline compounds

Elemental analysis of EAS-142 [phen•H][FeCl$_4$(phen)]

EAS-142 was made according to the literature[158]. The calculated values for [phen•H][FeCl$_4$(phen)] i.e. $C_{24}H_{17}Cl_4FeN_4$ are C: 51.56 %, H: 3.06 and N: 10.02 %. Experimental values are 49.57 %, 3.23 %, 9.72 % of which H and N are within the 0.4 percentage point (pp). However, the difference in C is 1.69 percentage point (Table 6). The difference between experimental and calculated values in percentage vary being 3–5.6 % too large or small. For [FeCl$_3$(phen)] i.e. $C_{12}H_8Cl_3FeN_3$ the calculated values are C: 42.09 %, H: 2.35 % and N: 8.18 %. These values are much more different than the ones for [phen•H][FeCl$_4$(phen)]. The reaction was made in water so the inclusion of water to the product would only decrease the percentage value of carbon not to include which would make the difference between experimental and calculated value even greater.

The molar ratio of carbon, hydrogen and nitrogen is 6.80:5.28:1 i.e. 27.18:21.13:4 which is about 27:21:4. However the theoretical ratio was 24:17:4 which means that there would be additional C_3H_3. However, this doesn't correspond to any possible compound in the reaction mixture. It can be concluded that the product is most likely [phen•H][FeCl$_4$(phen)] even the percentage value of carbon differs from the calculated value.

Elemental analysis of EAS-145 [NiCl$_2$(phen)]

For [NiCl$_2$(phen)] i.e. $C_{12}H_8Cl_2NiN_3$ the calculated values are C: 46.52 %, H: 2.60 % and N: 9.04 % and experimental values are: 46.60 %, 2.78 % and 9.03 %, respectively. The difference between experimental and calculated values of C and N is less than 0.4 % but for H it's 7.1 %. Even if the nearer value of the parallel samples were used (2.895 %), the difference is still 5.4 %. If the sample would have been wet, the the mass percentage of H would be higher but percentage of C and N would be lower. As a result, the fit would not be any better that way. It can be resulted that the product was clearly [NiCl$_2$(phen)] regardless of the difference in H values.

Elemental analysis of EAS-147 [CuCl$_2$(phen)]

For [CuCl$_2$(phen)] i.e. C$_{12}$H$_8$Cl$_2$CuN$_3$ the calculated values are C: 45.80 %, H: 2.56 % and N: 8.90 % and experimental values are: 44.83 %, 2.45 % and 8.86 %, respectively. However, only N percentage is within the limit of 0.4 %. The reaction was made in ethanol and water so they might be as included to the compound but the fit with water or ethanol in the formula creates only greater difference between experimental and calculated values as can be seen in Table 5 and Table 6. There's too much hydrogen percentage-wise and inclusion of water or ethanol only increases its ratio and decreases nitrogen ratio which is already within the limit of 0.4 %. There's no other compound except the 1,10-phenantholine which could increase the percentage of nitrogen so it concluded that the product is [CuCl$_2$(phen)] even if there is about 1 % difference between calculated and experimental values of carbon and smaller one in the values of hydrogen.

Elemental analysis of EAS-148 [ZnCl$_2$(phen)]

For [ZnCl$_2$(phen)] i.e. C$_{12}$H$_8$Cl$_2$ZnN$_3$ the calculated values are C: 45.54 %, H: 2.55 % and N: 8.85 %. The experimental values are 44.52 %, 2.50 % and 8.65 %, respectively. The H and N values differs only 0.05 pp and 0.20 pp but 1.8 % and 2.3 % respectively. The difference in carbon is greater (1.02 pp and 2.24 %). Addition of water or ethanol would only result greater difference between calculated and experimental values. The product is [ZnCl$_2$(phen)] regardless of deviations between values.

Elemental analysis of EAS-176 [FeCl$_3$(OH$_2$)(phen)]

Iron(III) chloride 1,10-phenanthroline complex of EAS-176 was done with different procedure than EAS-142 [phen•H][FeCl$_4$(phen)]. The starting iron compound was iron(III)chloride hexahydrate so the product most likely also contains coordinated water. The reaction was done in methanol that's why also methanol adduct should be considered as possible product. The calculated elemental analysis values for [FeCl$_3$(phen)], [FeCl$_3$(MeOH)(phen)] and [FeCl$_3$(OH$_2$)(phen)] are shown in Table 5 and Table 6. The monohydrate is by far the best choice among these three options. The H and N values differ less than 0.1 pp, respectively but carbon has a considerably greater difference, 0.72 ppm. These values are still small so the product of EAS-176 is [FeCl$_3$(OH$_2$)(phen)].

Table 5. Experimental and calculated mass percentages of C, H and N for synthesized 1,10-phenantholine complexes. Multiple possible product choices have been presented for multiple reactions. Left percentages are experimental data and right percentages are calculated data.

Synthesis code EAS–	C (%)	H (%)	N (%)	Calculated compound	Elemental composition	C (%)	H (%)	N (%)
142	49.565	3.234	9.716	[phen•H][FeCl$_4$(phen)]	C$_{24}$H$_{17}$N$_4$Cl$_4$Fe	51.56	3.06	10.02
				[FeCl$_3$(phen)]	C$_{12}$H$_8$N$_3$Cl$_3$Fe	42.09	2.35	8.18
145	46.595	2.785	9.032	[NiCl$_2$(phen)]	C$_{12}$H$_8$N$_3$Cl$_2$Ni	46.52	2.60	9.04
147	44.825	2.447	8.858	[CuCl$_2$(phen)]	C$_{12}$H$_8$N$_3$Cl$_2$Cu	45.80	2.56	8.90
				[CuCl$_2$(OH$_2$)(phen)]	C$_{12}$H$_{10}$N$_3$Cl$_2$OCu	43.32	3.03	8.42
				[CuCl$_2$(EtOH)(phen)]	C$_{14}$H$_{14}$N$_3$Cl$_2$OCu	46.61	3.91	7.71
148	44.520	2.505	8.646	[ZnCl$_2$(phen)]	C$_{12}$H$_8$N$_3$Cl$_2$Zn	45.54	2.55	8.85
176	39.27	2.730	7.777	[FeCl$_3$(phen)]	C$_{12}$H$_8$N$_3$Cl$_3$Fe	42.09	2.35	8.18
				[FeCl$_3$(MeOH)(phen)]	C$_{13}$H$_{12}$N$_3$Cl$_3$OFe	41.70	3.23	7.48
				[FeCl$_3$(OH$_2$)(phen)]	C$_{12}$H$_{10}$N$_3$Cl$_3$OFe	39.99	2.80	7.77

Table 6. Comparison between experimental and calculated values presented in Table 5. Both differences in % and percentage point (pp) are presented. Negative sign denotes an experimental value being greater than the theoretical value.

Synthesis code EAS–	Calculated compound	Elemental composition	Difference C (%)	Difference H (%)	Difference N (%)	Difference C (pp)	Difference H (pp)	Difference N (pp)
142	[phen•H][FeCl$_4$(phen)]	C$_{24}$H$_{17}$N$_4$Cl$_4$Fe	3.87	-5.69	3.03	2.00	-0.17	0.30
	[FeCl$_3$(phen)]	C$_{12}$H$_8$N$_3$Cl$_3$Fe	-17.8	-37.6	-18.8	-7.47	-0.88	-1.54
145	[NiCl$_2$(phen)]	C$_{12}$H$_8$N$_3$Cl$_2$Ni	-0.16	-7.10	0.09	-0.07	-0.18	0.01
147	[CuCl$_2$(phen)]	C$_{12}$H$_8$N$_3$Cl$_2$Cu	2.13	4.41	0.48	0.97	0.11	0.04
	[CuCl$_2$(OH$_2$)(phen)]	C$_{12}$H$_{10}$N$_3$Cl$_2$OCu	-3.47	19.24	-5.20	-1.51	0.58	-0.44
	[CuCl$_2$(EtOH)(phen)]	C$_{14}$H$_{14}$N$_3$Cl$_2$OCu	3.83	37.42	-14.88	1.79	1.46	-1.15
148	[ZnCl$_2$(phen)]	C$_{12}$H$_8$N$_3$Cl$_2$Zn	2.24	1.78	2.31	1.02	0.05	0.20
176	[FeCl$_3$(phen)]	C$_{12}$H$_8$N$_3$Cl$_3$Fe	6.70	-16.2	4.93	2.82	-0.38	0.40
	[FeCl$_3$(MeOH)(phen)]	C$_{13}$H$_{12}$N$_3$Cl$_3$OFe	5.83	15.5	-3.97	2.43	0.50	-0.30
	[FeCl$_3$(OH$_2$)(phen)]	C$_{12}$H$_{10}$N$_3$Cl$_3$OFe	1.80	2.52	-0.09	0.72	0.07	-0.01

Elemental analysis of nonphenanthroline compounds

Elemental analysis was performed to many other products than simple phenanthroline complexes.

Elemental analysis of EAS-104

The reaction was made by breaking a ruthenium dimer [RuCl$_2$(CO)$_3$]$_2$ i.e. [Ru$_2$Cl$_2$(μ-Cl)$_2$(CO)$_6$] in ethanol. Molar ratio of starting materials [RuCl$_2$(CO)$_3$]$_2$ and s-pyH is 1:7.28 so the molar ratio of Ru and s-pyH is 1:3.64. The reaction was done identical way than the literature[159] in EtOH. In the literature ligand was either pyridine (py) or pyrazine which brought [RuCl$_2$(CO)$_3$(py)] and [RuCl$_2$(CO)$_3$(pyrazine)]. However, the product of EAS-104 was not [RuCl$_2$(CO)$_3$(s-pyH)] as expected. It was not sure what the product was but it contained mainly two pyridine-4(1H)-thione ligands per ruthenium center. Many different product alternatives were considered also with solvent as impurity and their theoretical values were compared to experimental ones. None of them was not close to experimental values. Experimental values were C: 37.25 %, H: 3.207 % and N: 6.756 %. The values between parallel samples differences from each other moderately, especially with H. Most likely the product is mixture of multiple products and/or contaminated by moisture or solvents.

Elemental analyses of syntheses of Au(I) compounds

Elemental analyses of syntheses with Au(I) compounds were executed in a few reactions (EAS–173B and EAS–200&217). Products of EAS–200 and EAS–217 were combined because they were done identically. In EAS–173B, experimental results were 37.45 % for C, 2.674 % for H and 8.758 % for N. It was calculated that molar C:H:N ratio would be 4.99:4.24:1 i.e. 20:17:4. It corresponds to gold with four s-pyH ligands of which three is deprotonated and one neutral. If all of the ligands would be coordinated to Au^{3+}, the product would be [Au(s-pyH)(s-py)$_3$] which has elemental composition of C$_{20}$H$_{17}$N$_4$AuS$_4$. The complex is reasonable because coordination number 4 is typical for Au^{3+} complexes. The calculated values for this elemental composition is C 37.62 %, H 2.68 % and N 8.77 %. The difference between experimental and calculated values is hence 0.45 %, 0.22 % and 0.14 % and 0.17 pp, 0.01 pp and 0.01 pp, respectively. The product of EAS–173B is thus [Au(s-pyH)(s-py)$_3$] or at least it contains the same elemental composition.

The parallel samples of EAS–200&217 differ notably from each other. Hydrogen and nitrogen have greater than 6 % difference which is considerably greater than the average difference between parallel samples of all samples measured in this project. Carbon has considerably less (1.3 %) difference but it's also greater than the average difference between parallel samples of all samples measured in this project. The differences reflect to the molar ratio as well which varies from 4.92:4.92:1 to 5.17:5.56:1 for C:H:N. The average is 5.04:5.23:1. The average suggests the ratio is 20.16:20.93:4 ≈ 20:21:4. The H:N ratio suggests one additional H per four s-pyHs. Because of the ratio, gold is Au^+ and its normal coordination number is 2, it means that the product should be $2Au^++4s\text{-pyH}+H^++3Cl^-$ i.e. $C_{20}H_{21}N_4Au_2Cl_3S_4$.

Mass percentages of C, H and N of this compound are close to experimental values as shown in Table 7 and Table 8. Experimental values are very close to theoretical combination of $2Au^++4s\text{-pyH}+H^++3Cl^-$. Another product choice is presented in Table 7 and Table 8. It is $[AuCl(s\text{-pyH})_2]$ or $[Au(s\text{-pyH})_2]Cl$ with elemental composition of $C_{10}H_{10}N_2AuClS_2$ which is the same as former candidate but without additional HCl per four s-pyHs. This candidate's values differ from experimental values much more than $C_{20}H_{21}N_4Au_2Cl_3S_4$ does. The difference in carbon and nitrogen of $C_{10}H_{10}N_2AuClS_2$ is so high (Table 8) that the product isn't $[AuCl(s\text{-pyH})_2]$ or $[Au(s\text{-pyH})_2]Cl$ with elemental composition of $C_{10}H_{10}N_2AuClS_2$.

Table 7. Experimental and calculated mass percentages of C, H and N for EAS-200&217 sample. Two possible product choices have been presented for the reactions. Left percentages are experimental data and right percentages are calculated data.

Synthesis code EAS-	C (%)	H (%)	N (%)	Calculated compound	Elemental composition	C (%)	H (%)	N (%)
200&217	25.655	2.235	5.937	$2Au^++4s\text{-pyH}+H^++3Cl^-$	$C_{20}H_{21}N_4Au_2Cl_3S_4$	25.39	2.24	5.92
				$[Au(s\text{-pyH})_2]Cl$	$C_{10}H_{10}N_2AuClS_2$	26.41	2.22	6.16

Table 8. Comparison between experimental and calculated values presented in Table 7. Both differences in % and percentage point (pp) are presented. Negative sign denotes an experimental value being greater than the theoretical value.

Synthesis code EAS-	Calculated compound	Elemental composition	Difference C (%)	Difference H (%)	Difference N (%)	Difference C (pp)	Difference H (pp)	Difference N (pp)
200& 217	$2Au^+ + 4s\text{-pyH} + H^+ + 3Cl^-$	$C_{20}H_{21}N_4Au_2Cl_3S_4$	1.03	-0.11	0.21	0.26	-0.002	0.013
	$[Au(s\text{-pyH})_2]Cl$	$C_{10}H_{10}N_2AuClS_2$	-2.87	0.84	-3.65	-0.76	0.019	-0.23

Based on elemental analysis the products elemental composition corresponds very closely to $C_{20}H_{21}N_4Au_2Cl_3S_4$. However, the chemical interpretation of this elemental composition is not very logical. $[Au(s\text{-pyH})_2]Cl$ units are logical but then having H^+ and Cl^- per two $[Au(s\text{-pyH})_2]Cl$ unit is not intuitively very logical. There're already hydrogens everywhere and there seems to be no good place for H^+. Only possible place would be somehow close to multiple Cl^-s but it doesn't sound appropriate. $[Au(s\text{-pyH})_2]Cl$ sounds much better but experimental values differ greatly from theoretical values for this compound.

The product was dried with argon flow which seems to be inadequate because of notable differences in mass percentages of duplicate samples. Vacuum drying was avoided because of possible structural deterioration but in further studies it should be tried or longer argon drying should be applied.

Although the elemental analysis correspond very well with elemental composition of $C_{20}H_{21}N_4Au_2Cl_3S_4$ of $2Au^+ + 4s\text{-pyH} + H^+ + 3Cl^-$ than $[Au(s\text{-pyH})_2]Cl$, the single crystal XRD structure confirms the structure to be $[Au(s\text{-pyH})_2]Cl$.

Elemental analysis of monometallic silver reactions

EAS-117 reaction with $AgSO_3CF_3$ and s-pyH in 2:1 EtOH and MeCN with Et_3N resulted orange powder with mass ratios of C: 36.22 %, H: 3.142 % and N 8.660%. The molar ratio of the three elements is 4.88:5.04:1, respectively. The mass ratio of the ligand is 5:1 for C:N. If the effect of the solution mixture is considered, it only lowers the ratio of C

compared to N. The product was washed with EtOH so inclusion of only EtOH would only lower the ratio of C compared to N when only the product part of the possible mixture is considered. Inclusion of 1/8–1 Et_3N for every two s-pyHs would much higher differences than without it. If the compound would contain anion of $CF_3SO_3^-$, the C:N ratio would change into the wrong direction.

The mass ratios of the average of two duplicate samples with errors between parallel samples are shown in the first row of Table 9. Some calculated compounds are shown in second (and third) rows of each section with elemental composition in Table 9. Elemental composition of $C_{10}H_9N_2AgS_2$ has better equivalence with experimental values than $C_{10}H_{10}N_2AgClS_2$. [Ag(s-py)(s-pyH)] has elemental composition of $C_{10}H_9N_2AgS_2$. $C_{10}H_{10}N_2AgClS_2$ would corresponds to [Ag(s-pyH)$_2$]Cl. The differences between experimental and calculated values for $C_{10}H_9N_2AgS_2$ are high especially for H because there should be more hydrogen because the calculated molar ratio was 4.88:5.04:1 not 5:4.5:1. As result, the elemental analysis suggests that the elemental composition might be $C_{10}H_9N_2AgS$.

EAS–118 was made identical way than EAS–117 with the exception of silver salt being $AgNO_3$ EAS–124 was done like EAS–117 but using 30 drops of Et_3N. Reactions EAS–157–160 were made exactly like EAS–124 i.e. like EAS–117 but with 30 drops of Et_3N that's why their products were combined and elemental analysis was performed for this combined product. The results of EAS–157–160 are similar to the corresponding values of EAS–117, EAS–118 and EAS–124. The comparison of experimental values for these products with calculated values for $C_{10}H_9N_2AgS_2$ has shown in Table 9. All in all, the mass percentages are very similar to each other especially sum of C, H and N mass percentages are 47.45–48.02 % within sum of C, H and N mass percentages of $C_{10}H_9N_2AgS_2$ lies.

Table 9. Comparison between experimental and calculated values of monometallic silver reactions. Both differences in % and percentage point (pp) are presented. The mass ratios of the average of two duplicate samples with differences between parallel samples of each sample are shown in the first row of each section. Some calculated compounds are shown in second and third rows of each section with elemental composition. Their theoretical mass percentages are shown followed by differences between experimental values and theoretical values. Because $C_{10}H_9N_2AgS_2$ has better correspondence to experimental results in each case than $C_{10}H_{10}N_2AgClS_2$. That's why its mass percentages and differences between EAS−117 is shown only in the first section. Negative sign denotes an experimental value being greater than the theoretical value. The fifth column is sum of mass percentages of C, H and N.

Reaction or composition	C (%)	H (%)	N (%)	Σ CHN (%)	Diff. C (pp)	Diff. H (pp)	Diff. N (pp)	Diff. C (%)	Diff. H (%)	Diff. N (%)
EAS−117	36.22	3.142	8.660	48.02	0.02	0.032	0.049	0.06	1.02	0.57
$C_{10}H_9N_2AgS_2$	36.49	2.756	8.512	47.75	0.27	−0.387	−0.147	0.73	−14.03	−1.73
$C_{10}H_{10}N_2AgClS_2$	32.85	2.756	7.663	43.27	−3.37	−0.386	−0.996	−10.27	−13.99	−13.00
EAS−118	36.45	2.970	8.645	48.06	0.52	0.103	0.173	1.437	3.53	2.02
$C_{10}H_9N_2AgS_2$	36.49	2.756	8.512	47.75	−0.04	−0.214	−0.132	−0.10	−7.78	−1.56
EAS−124	36.02	2.898	8.532	47.45	0.12	0.028	0.030	0.33	0.97	0.35
$C_{10}H_9N_2AgS_2$	36.49	2.756	8.512	47.75	−0.47	−0.143	−0.020	−1.27	−5.17	−0.23
EAS−157−160	36.21	2.858	8.572	47.63	0.19	0.101	0.016	0.53	3.60	0.19
$C_{10}H_9N_2AgS_2$	36.49	2.756	8.512	47.75	0.28	−0.102	−0.060	0.77	−3.70	−0.70

Experimental molar masses of monometallic reactions of Ag(I) are shown in Table 10. The molar masses vary from 324 g/mol to 333 g/mol and molar mass of the assumed elemental composition $C_{10}H_9N_2AgS_2$ is 329.19 g/mol which is close to calculated values. The molar masses calculated from mass ratios of C are greater than N due to most likely solvent impurities. For example molar mass of EAS−117 calculated from mass percentage of C has been calculated as follows:

$$M_{product\ from\ C} = \frac{m_{product}}{m_{C\ of\ the\ product}} \cdot M_{C\ of\ the\ product} = \frac{100\%}{36.22\%} \cdot 10 \cdot 12.011 g/mol = 332 g/mol$$

Also the molar ratios of these monometallic reaction products of Ag(I) have been summarized in Table 10. In other words, the three last columns of Table 10 corresponds to molar ratio of C:H:N, respectively. None of them correspond very well with 10:9:2 ratio, respectively

Table 10. Experimental molar masses of monometallic reactions of Ag(I) and molar ratios of C, H and N. The molar masses are calculated from the experimental mass ratios of C and N with the assumption of 10 moles of carbon and 2 moles of nitrogen per one mole of the product. This corresponds to two s-py(H) ligands. The effect of solvents or moisture hasn't been included to the calculations. The last two rows are theoretical values for two elemental compositions.

Reaction or composition	Calc. from C (g/mol)	Calc. from N (g/mol)	Ratio of C (mol)	Ratio of H (mol)	Ratio of N (mol)
EAS–117	332	323	9.76	10.08	2
EAS–118	330	324	9.83	9.55	2
EAS–124	333	328	9.85	9.44	2
EAS–157–160	332	327	9.85	9.27	2
$C_{10}H_9N_2AgS_2$	329.20	329.20	10	9	2
$C_{10}H_{10}N_2AgClS_2$	365.66	365.66	10	10	2

As conclusions and a summary, monometallic silver reactions had C:N ratios 5:1 but the molar ratio of hydrogen differed more than the molar ratio of C compared to molar ratio of N. Calculated molar masses for theoretical elemental composition $C_{10}H_9N_2AgS_2$ corresponded moderately well to calculated molar masses from experimental mass ratios of carbon and nitrogen. One additional HCl unit per two Ag and four s-py(H)s is possible but not very likely because it would make the molar mass higher by ½·36.46 g/mol. (This is because the molar masses calculated in Table 10 were per one Ag and two s-py(H)s). If it would be so, then the calculated experimental and calculated theoretical molar masses would differs more greatly than without the additional HCl per two Ag and four s-py(H)s. Inclusion of 30 drops of Et_3N didn't have any notable difference in the elemental composition of the products. (Base was used in EAS–124 and EAS–157–160 but not in EAS–117 and EAS–118. The ratio is a bit lower in the reactions with base but loss of H would require counter anion which would increase the molar mass.) The product is most likely at least mainly $C_{10}H_9N_2AgS_2$ which corresponds to [Ag(s-py)(s-pyH)].

Elemental analysis of dimetallic silver reactions with second metal salt outside group 11

Elemental analysis was conducted from seven different reaction product in which synthesis second metal was used. The second metals were outside group 11. Reactions with two group 11 metal salts are discussed in another chapter. Three of these seven reactions were made using $FeCl_3$, two with $ZnCl_2$ and one with $[ZnCl_2(2,2'-bpy)]$. Abbreviation 2,2'-bpy stands for 2,2´-bipyridine. The mass percentages are shown in Table 11 for these seven products. The C:H:N molar ratios of the products are shown in Table 12.

Table 11. Elemental analysis of dimetallic silver reactions with second metal salt outside group 11. The differences in percentage point (pp) and percentages (%) are presented. In the left side of the table are differences between parallel samples and the mass percentages in the right side are average values for two parallel samples. The sixth column is sum of mass percentages of C, H and N.

Reaction	Second metal salt	C (%)	H (%)	N (%)	Σ CHN (%)	Diff. C (pp)	Diff. H (pp)	Diff. N (pp)	Diff. C (%)	Diff. H (%)	Diff. N (%)
EAS–137	$ZnCl_2$	37.17	2.609	8.787	42.57	0.14	0.028	0.052	0.38	1.08	0.59
EAS–138	$[ZnCl_2(2,2'-bpy)]$	37.66	2.754	8.767	49.18	0.10	0.037	0.005	0.27	1.35	0.06
EAS–151	$ZnCl_2$	25.15	1.966	5.845	32.96	0.53	0.017	0.000	2.13	0.87	0.00
EAS–152	$ZnCl_2$	31.19	2.397	7.037	40.62	0.61	0.140	0.104	1.98	6.02	1.49
EAS–150	$FeCl_3$	14.88	1.773	3.221	19.87	0.05	0.033	0.058	0.34	1.88	1.82
EAS–153	$FeCl_3$	18.00	2.132	3.837	23.97	0.09	0.081	0.089	0.50	3.87	2.35
EAS–154	$FeCl_3$	16.93	1.951	3.724	22.61	0.13	0.019	0.026	0.77	0.98	0.70

Table 12. Molar ratios of carbon, hydrogen and nitrogen of the products in dimetallic silver reactions with second metal salt outside group 11.

Reaction	Ratio of C (mol)	Ratio of H (mol)	Ratio of N (mol)
EAS–137	9.87	8.25	2
EAS–138	10.02	8.73	2
EAS–151	10.03	9.35	2
EAS–152	10.34	9.47	2
EAS–150	10.80	15.34	2
EAS–153	10.94	15.44	2
EAS–154	10.60	14.56	2

Reactions EAS–137 and EAS–138 were done using either Et_3N, KOH and either $ZnCl_2$ or [$ZnCl_2$(2,2'-bpy)]. The conditions were the same with the exception of the starting materials of EAS–138 were dissolved in half the amount used in EAS–137 except [$ZnCl_2$(2,2'-bpy)] was dissolved in 6 ml of 1:1 MeCN:EtOH. As result, the conditions were practically speaking the same.

Interesting is that elemental analysis suggest the two products to be the same because they differ only slightly from each other. Inclusion of 2,2'-bpy would have to create greater difference between mass percentages of C, H and N so EAS–138 doesn't contain 2,2'-bpy. Because 2,2'-bpy is chelating ligand it's unlike to be replaced by solvent or s-py(H)s, that's why if there's no 2,2´-bpy, can be concluded that there's no Zn either. According to HSAB (hard and soft acids and bases) principle, 2,2'-bpy prefers Zn^{2+} over Ag^+. This suggests that the product of EAS–138 doesn't contain zinc at all which suggest that the product of EAS–137 doesn't contain zinc either. However, the color of the products is brownish grey not orange like in EAS–117, EAS–118, EAS–124 and EAS–157–160. This means the structure has to be different but it doesn't mean that the elemental composition has to be different. The product might contain AgCl(s) or something similar as undesired side product. However, it's impossible to say sure what the product was in EAS–137 and EAS–138.

EAS–151 and EAS–152 differ greatly from mass ratios of EAS–137 and EAS–138 and each other. This is very interesting because the only difference between EAS–151 and EAS–152 was the addition of 30 ml of 2:1 EtOH:MeCN in EAS–152. All the four reactions had 1:4:2 ratio of $AgNO_3$, s-pyH and Zn(II) salt. The molar ratios of EAS–151 and EAS–

152 are 10.03:9.35:2 and 10.34:9.47:2, respectively. Molar ratios of hydrogen are higher than in EAS–137 and EAS–138 and EAS–152 has higher carbon ratio than the other three products. Their colors are similar yet EAS–151 and 152 are dark grey i.e. darker than EAS–137 and EAS–138. Most likely products are mixtures of multiple compounds.

Products of Ag(I) and Fe(III) reactions have distinctive difference in elemental analysis results than products of Ag(I) and Zn(II) reactions; sum of molar ratios with Fe(III) is much lower 20–24 % than with Zn(II) 33–49 % (Table 11). In addition, molar hydrogen content is much higher in Fe(III) reactions than in Zn(II) reactions (Table 12). In fact carbon content is too high to originate from s-py(H)s alone, because the ratio should be 10:2 but it's closer to 11:2 which suggest inclusion of impurities or by-products. Anyhow, the hydrogen content is relatively very high and it's very hard to think any logical theoretical product which would fit to the experimental values.

Elemental analysis of homo- and heterometallic Cu(II) products without other group 11 metals

Elemental analyses were done to products of two reactions with only one metal salt which was either $Cu(OAc)_2$ (EAS–128) or $CuCl_2 \cdot 2H_2O$ (EAS–203 & 204). Products of EAS–203 and 204 were combined because their experimental procedures were identical and they are counted as one reaction. Elemental analyses of four heterometallic reaction with $CuCl_2 \cdot 2H_2O$ were executed also. Two of these reactions contained $FeCl_3$ (anhydrous), one $ZnCl_2$ (anhydrous) and another $CrCl_3 \cdot 6H_2O$. Their experimental elemental analysis results are shown in Table 13. Also molar ratios were calculated but they are not presented because interpretation of the results didn't ensue any clear answers to any of these six reactions.

Table 13. Elemental analysis results of homo- and heterometallic Cu(II) products without other group 11 metals. Second column tells the metal salt used. If it's copper salt, it's the only metal salt used. If it's not, $CuCl_2 \cdot 2H_2O$ has been used with the metal salt presented in the column. Leftmost 6 columns are differences between parallel samples and columns three to five tells the average elemental analysis result of two parallel samples. Sigma CHN stands for sum of mass percentages of C, H and N.

Reaction	Metal salt	C (%)	H (%)	N (%)	Σ CHN (%)	Diff. C (pp)	Diff. H (pp)	Diff. N (pp)	Diff. C (%)	Diff. H (%)	Diff. N (%)
EAS–128	Cu(OAc)$_2$	33.25	2.658	7.741	43.64	0.55	0.081	0.153	1.67	3.10	2.00
EAS–203 & EAS –204	CuCl$_2$ ·2H$_2$O	35.82	2.951	8.672	47.44	0.22	0.044	0.089	0.62	1.50	1.03
EAS–164	ZnCl$_2$	31.08	3.050	7.371	41.50	0.47	0.124	0.445	1.52	4.15	6.23
EAS–168	FeCl$_3$	36.03	2.638	8.622	47.29	0.17	0.076	0.072	0.47	2.92	0.84
EAS–169	CrCl$_3$·6H$_2$O	32.05	3.031	7.341	42.42	0.40	0.030	0.106	1.26	0.99	1.45
EAS–198	FeCl$_3$	34.46	2.556	8.899	45.91	0.47	0.018	0.061	1.37	0.71	0.69

Nonetheless, two example of the closest theoretical product is presented here. EAS–203&204 is closest to $C_{20}H_{19}N_2Cl_3CuS_2$ which equals to three s-pyHs one s-py$^-$, two Cu^{2+} and three Cl$^-$. The mass percentages are 35.48 %, 2.828 % and 8.277 % with errors 0.97 %, 4.34 % and 4.77 % for C, H and N, respectively. These values are far away from 0.4 %. However, EAS–128 doesn't have as good results as EAS–203&204 because of when the total charge of the compound has been balanced, the differences between experimental and theoretical value for product candidate are high and vice versa. Possibility to have more than one metal with unknown first coordination sphere makes the interpretation even harder.

Comparison of selected theoretical candidates for EAS–164 is presented in Table 14. As be seen, there's no one clear candidate which is better than the others. Composition of $2Cu^+ + 4spyH + ZnCl_4^{2-} + EtOH$ is the correct composition according to the crystal structure but only the sum of C, H and N percentage values are the closest to the experimental values among the candidates presented in the table. Thus, it's not certain, which is the correct elemental composition of EAS–164 according to the elemental analysis.

Table 14. Comparison of experimental results of EAS–164 with possible theoretical compositions. Values with green background are closest values among these candidates to experimental values. Sigma CHN stands for sum of mass percentages of C, H and N.

Theoretical composition	Theoretical elemental composition	C (%)	H (%)	N (%)	Σ CHN (%)
Experimental values		31.08	3.050	7.371	41.50
$2Cu^+ + 4spyH + ZnCl_4^{2-} + EtOH$	$C_{22}H_{26}Cl_4Cu_2N_4OS_4Zn$	32.03	3.18	6.79	42.00
$2Cu^+ + 4spyH + ZnCl_4^{2-}$	$C_{20}H_{20}Cl_4Cu_2N_4S_4Zn$	30.84	2.59	7.19	40.62
$2Cu^+ + 2spyH + 2spyH + ZnCl_4^{2-} + EtOH$	$C_{22}H_{24}Cl_4Cu_2N_4OS_4Zn$	32.11	2.94	6.81	41.86
$2Cu^+ + 2spyH + 2spyH + ZnCl_4^{2-}$	$C_{20}H_{18}Cl_4Cu_2N_4S_4Zn$	30.92	2.34	7.21	40.47
$2Cu^+ + 4spyH + ZnCl_4^{2-} + 1/4EtOH + 3/4MeCN$	$\frac{1}{4}(C_{88}H_{95}Cl_{16}Cu_8N_{19}OS_{26}Zn_4)$	32.18	2.92	8.10	43.20

Elemental analysis of heterometallic reactions with two group 11 metals

Elemental analysis results of six different products from six reactions of heterometallic reactions with two group 11 metals have been analyzed here. Starting materials of the reactions excluding pyridine-4(1H)-thione are presented in Table 15. The elemental analysis results are shown in Table 16. Molar ratios of C, H and N are presented in Table 17.

Table 15. Starting materials of the reactions excluding pyridine-4(1H)-thione of heterometallic reactions with two group 11 metals. The molar ratio of metal salts and additional substances as well are presented. AgClO$_4$ is presented as additional substance because it was used to remove chlorides from 1,10-phenanthroline complexes in order to create a coordination place for pyridine-4(1H)-thione and resulting AgCl(s) was removed by filtration (or at least attempted to remove). AS stands for additional substance. Leftmost column shows the molar ratio of starting materials excluding s-pyH. The amount of KOH and CH$_3$COOH are not shown in the leftmost column in EAS–136 because their molar amount was unknown.

Reaction	Metal salt 1	Metal salt 2	Additional substance	Molar ratio of metal 1:metal 2:AS
EAS–135	$AgNO_3$	$Cu(OAc)_2 \cdot H_2O$	–	1:2.2
EAS–136	$AgNO_3$	$Cu(OAc)_2 \cdot H_2O$	KOH & CH$_3$COOH	1:2.2
EAS–187	$CuCl_2 \cdot 2H_2O$	$AuCl_3$	–	1:1
EAS–219	$CuCl_2 \cdot 2H_2O$	$[CuCl_2(phen)]$	$AgClO_4$	1:1:1
EAS–220	$CuCl_2 \cdot 2H_2O$	$[NiCl_2(phen)]$	$AgClO_4$	1:1:1
EAS–222	$CuCl_2 \cdot 2H_2O$	$[FeCl_3(phen)]$	$AgClO_4$	1:1:1

Table 16. Elemental analysis results of heterometallic reactions with two group 11 metals. Leftmost 6 columns are differences between parallel samples and columns two to four tells the average elemental analysis result of two parallel samples. Sigma CHN stands for sum of mass percentages of C, H and N.

Reaction	C (%)	H (%)	N (%)	∑ CHN (%)	Diff. C (pp)	Diff. H (pp)	Diff. N (pp)	Diff. C (%)	Diff. H (%)	Diff. N (%)
EAS–135	35.74	2.652	9.962	48.35	0.27	0.046	0.077	0.76	1.75	0.78
EAS–136	34.92	2.557	8.211	45.69	0.16	0.008	0.070	0.46	0.31	0.86
EAS–187	29.17	2.349	6.931	38.45	0.15	0.020	0.018	0.52	0.86	0.26
EAS–219	36.75	2.586	8.734	48.07	0.04	0.029	0.155	0.11	1.13	1.79
EAS–220	35.52	3.051	8.369	46.94	0.00	0.054	0.225	0.00	1.79	2.73
EAS–222	28.76	2.530	7.058	38.35	0.08	0.119	0.150	0.28	4.82	2.15

Table 17. Molar ratios of heterometallic reactions with two group 11 metals based on the elemental analysis results. Some multipliers of molar ratios are shown also which would be the ratio the closest to integers.

Reaction or composition	Ratio of C (mol)	Ratio of H (mol)	Ratio of N (mol)
EAS–135	4.18	3.70	1
EAS–136	4.96	4.33	1
EAS–136	14.88	12.98	3
EAS–187	4.91	4.71	1
EAS–187	19.63	18.84	4
EAS–219	4.91	4.11	1
EAS–220	4.95	5.07	1
EAS–222	4.75	4.98	1
EAS–222	19.01	19.92	4

Interpretation of these results is complicated but some conclusions can be drawn: EAS–136 has close correspondence to $K^+Cu^+Cu^{+2}(s\text{-py})^-_3OH^-$ i.e. $C_{15}H_{13}N_3Cu_2OS_3K$ which has mass percentages of 35.07 %, 2.551 % and 8.183 % for C, H and N, respectively. The difference between experimental and calculated values for this elemental composition was –0.44 %, 0.25 % and 0.35 %, respectively. Negative sign indicates the experimental value to be greater than theoretical value and vice versa. However, the ratio and kind of metals and ligands seems improper chemically.

Solid state ^{13}C CP NMR spectrum of monometallic silver polymer (EAS–167-160)